論文 / 著書情報
Article / Book Information

題目(和文)	
Title(English)	Fatigue Load Carrying Mechanism of Reinforced Concrete Beams with Corrosion Cracks Along Tensile Rebar
著者(和文)	山田雄太
Author(English)	Yuta Yamada
出典(和文)	学位:博士(工学), 学位授与機関:東京工業大学, 報告番号:甲第10963号, 授与年月日:2018年9月20日, 学位の種別:課程博士, 審査員:岩波 光保,二羽 淳一郎,廣瀬 壮一,佐々木 栄一,千々和 伸浩
Citation(English)	Degree:Doctor (Engineering), Conferring organization: Tokyo Institute of Technology, Report number:甲第10963号, Conferred date:2018/9/20, Degree Type:Course doctor, Examiner:,,,,
学位種別(和文)	博士論文
Type(English)	Doctoral Thesis

FATIGUE LOAD CARRYING MECHANISM OF REINFORCED CONCRETE BEAMS WITH CORROSION CRACKS ALONG TENSILE REBAR

Yuta Yamada

Supervisor: Professor Mitsuyasu Iwanami

Tokyo Institute of Technology

This dissertation was submitted as a partial fulfillment of the requirements for the degree of Doctor of Engineering.

CONTENTS

NOTATION AND TERMINOLOGY

The general notation and terminology in this study are defined as follows.

Terminology	*Description*	*Notation*
Load carrying mechanism:	The classified stress and strain distribution caused by applied load in the beams	-
Load:	The applied load on the beam	P, V
Static strength:	The load when the applied load reaches maximum load of the beams	P_f, V_f
Displacement:	The mid span displacement of beam caused by applied load	u
Failure displacement:	The displacement when the applied load reaches static strength	u_f
Fatigue of the beam:	The phenomenon that the beam resists applied cyclic load	-
Failure of the beam:	The phenomenon that the displacement of the beam reaches at the failure displacement	-
Upper limit load:	The applied maximum load under cyclic load	$P_{\max}$
Lower limit load:	The applied minimum load under cyclic load	$P_{\min}$
Upper limit load ratio:	The ratio of upper limit load against static strength	S
Number of cycles:	The applied acting number of the cyclic loads	N
Number of cycles at failure:	The number of acting cycles when the displacement reaches failure displacement	N_f
Fatigue strength:	The applied upper limit load until the failure of beams (When the lower limit load is constant in each beam, the fatigue strength have a same meaning with stress range.)	$P_{f\max}$
Arch mechanism:	A load carrying mechanism of the beam that the position resultant force in cross section is changed in vertical direction	-
Beam mechanism:	A load carrying mechanism of the beam that the magnitude of resultant force in cross section is changed in vertical direction	-
Contributed load of arch mechanism:	A part of applied load which is contributed in arch mechanism	V_a
Contributed load of beam mechanism:	A part of applied load which is contributed in beam mechanism	V_b
Absorbing energy:	An closure area in the load deflection curve	U
Absorbing energy of arch mechanism:	A part of absorbed energy which is contributed in arch mechanism	U_a
Absorbing energy of beam mechanism:	A part of absorbed energy which is contributed in beam mechanism	U_b
Averaged absorbing energy of arch mechanism:	A part of absorbed energy which is contributed in arch mechanism per one cycle under cyclic loading	U_a^*

Terminology	*Description*	*Notation*
Averaged absorbing energy of beam mechanism:	A part of absorbed energy which is contributed in beam mechanism per one cycle under cyclic loading	U_b^*
Normal stress:	The stress acting on the infinitesimal elements in the continuous bodies in normal direction	σ_{ii}
Shear stress:	The stress acting on the infinitesimal elements in the continuous bodies in tangential direction	τ,σ_{ij}
Normal strain:	The strain generating on the infinitesimal elements in the continuous bodies in normal direction	ε_{ii}
Shear strain:	The strain generating on the infinitesimal elements in the continuous bodies in tangential direction	γ,ε_{ij}
Elastic modulus in normal direction:	Elastic modulus in normal direction of infinitesimal element surface of the materials	E_{ii}
Elastic modulus in tangential direction:	Elastic modulus in tangential direction of infinitesimal element surface of the materials	G,E_{ij}
Stiffness of the beam:	The ratio between load and mid span displacement of the beam	K
Stress function in Cartesian coordinate:	The function related to the integral of each stress tensor in Cartesian coordinate	$U_{(x,y)}$
Stress function in polar coordinate:	The function related to the integral of each stress tensor in polar coordinate	$U_{(r,\theta)}$
Stress intensity factor in mode *I* and *II*:	The factor to represent singular stress field near the crack tip which give one to one relationship between stress and coordinate function in each deforming mode of crack mouth	K_I, K_{II}

*Suffix takes permutations of *i*=1,2,3 and *j*=1,2,3 in 3 dimensional problem.

CHAPTER 1
INTRODUCTION

This chapter explains the background, objective and methodology of this research based on previous reviews. Also, this chapter mentions a necessity to make clear the shear fatigue load carrying mechanism of RC beam with corrosion cracks due to increase in the number of deteriorated infrastructures. To make clear the mechanism, this research focuses on the corrosion cracks along tensile rebar in shear span and the effect of stirrup in the RC beams of a/d =1.0, 1.6 and 2.9. For this purpose, cyclic loading experiments and FE analysis are conducted.

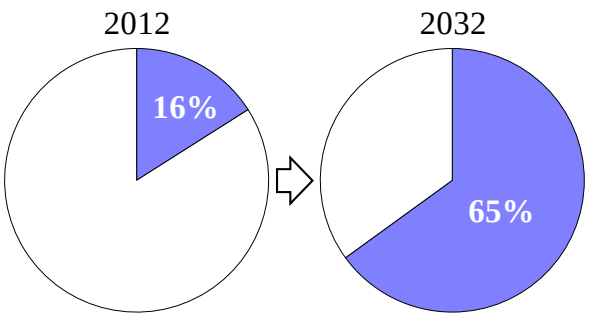

Figure 1.1 Change in percentage of more than 50 years old bridge

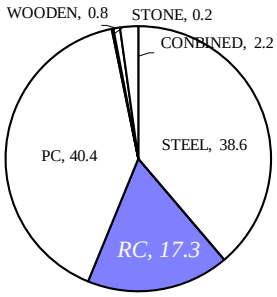

Figure 1.2 Percentage of structural types of infrastructures

1.1 Backgrounds

The number of deteriorated infrastructures which were constructed in the period of high economic growth has been increased in Japan. The damage caused by the deteriorated infrastructure has been reported frequently. Figure 1.1 shows the change in the percentage of more than 50 years old bridge[1]. From Figure 1.1, it is expected that the number of deteriorated infrastructures will increase. There is a necessity to make clear the deterioration mechanism to predict the failure position and remaining life of the deteriorated infrastructure.

From Figure 1.2 [1], it is found that the RC (reinforced concrete) and PC (pre-stressed concrete) are main structural types of concrete bridge as a representative infrastructure. Thus, focused on the deterioration mechanism of RC which is a main structural member, single deterioration mechanism (such as, carbonization, alkali silicate reaction, chloride attack and fatigue) has been investigated by previous researches. The progress of deterioration can be measurable expected. However, the number of researches regarding combined deterioration is few. In addition, it is expected that the combined deterioration of fatigue and rebar corrosion will be remarkable because the accumulation of fatigue damage is difficult to remove from the RC structure and the rebar corrosion is one of the main cause of aging deterioration. It could be deduced that the structure which has corrosion might be under the repeated loading because of long time service condition. Especially, it can be considered that the combine deterioration is distinguished in harbor structure.

1.2 Review of Previous Researches

There are mainly two types of fatigue phenomena of RC beams. One is flexural fatigue and another is shear fatigue. It is known that flexural fatigue is governed by flexural theorem. Thus, it can be said that the flexural behavior of RC beams under static and cyclic loading was made clear. The shear behavior of RC beam under static loading was governed by truss theory even though it is difficult to treat the contribution of concrete and angle of compressive member in

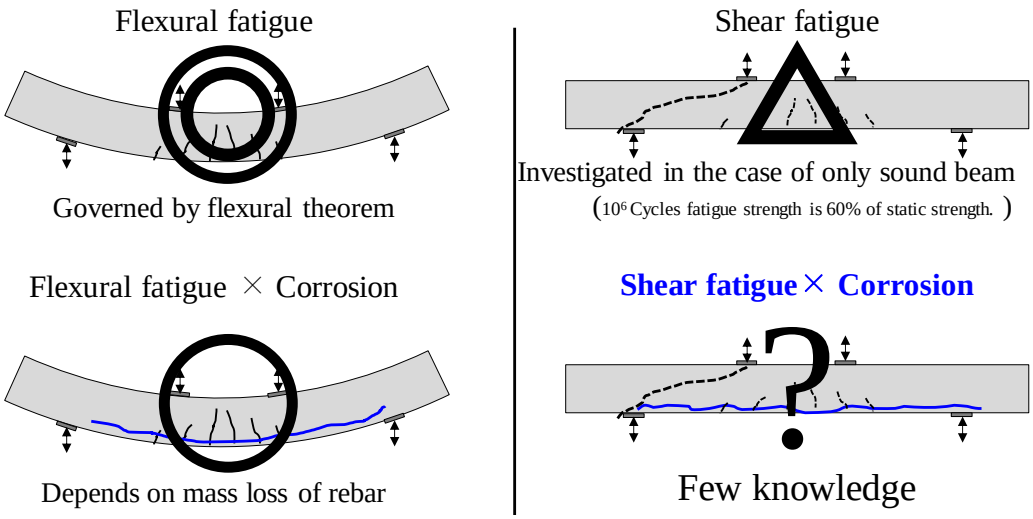

Figure 1.3 Investigating and research fields

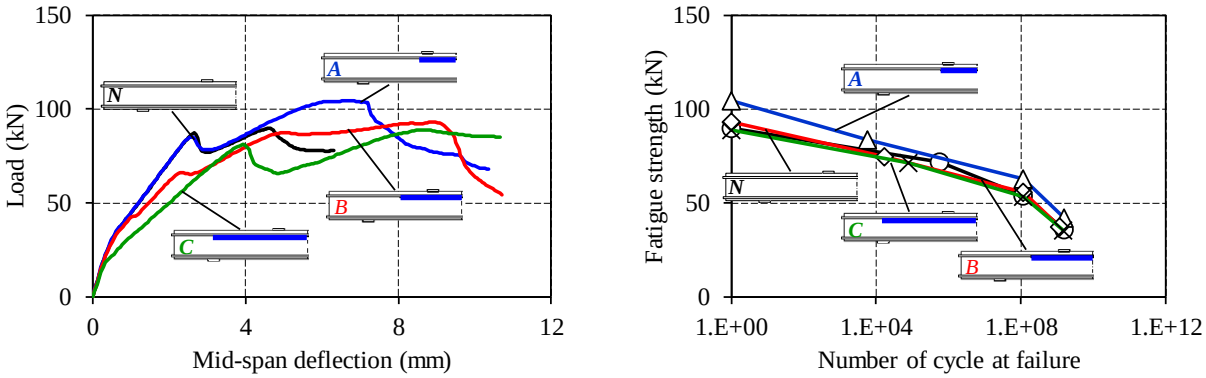

(a) Load deflection curve under static loading *(b) Tendency of fatigue strength*

Figure 1.4 Effect of rebar corrosion cracks along compressive rebar[19]

this theory. Some research gives the important knowledge about size effect of the RC beams under static loading[2]. Moreover, several researches regarding shear fatigue of sound structure[3]-[9] were conducted. A important result that the shear fatigue strength of sound beams without stirrup at the 1000000 cycles was 60 % of static strength regardless of failure mode was derived[3].

Focused on the research field regarding to the combined deterioration, some research could be confirmed even though the number is few. From the research about flexural static loading and rebar corrosion, it is indicated that the failure mode was changed by uniform and pitting corrosion[10],[11]. Moreover, from the research about shear static loading and rebar corrosion, it is indicated that the shear strength was enhanced by the corrosion crack inside of shear span along tensile rebar, and that the anchorage crack decreased the strength, and that effect of corrosion along stirrup was relatively small[12]-[15].

There are several researches regarding the combined deterioration of fatigue and material

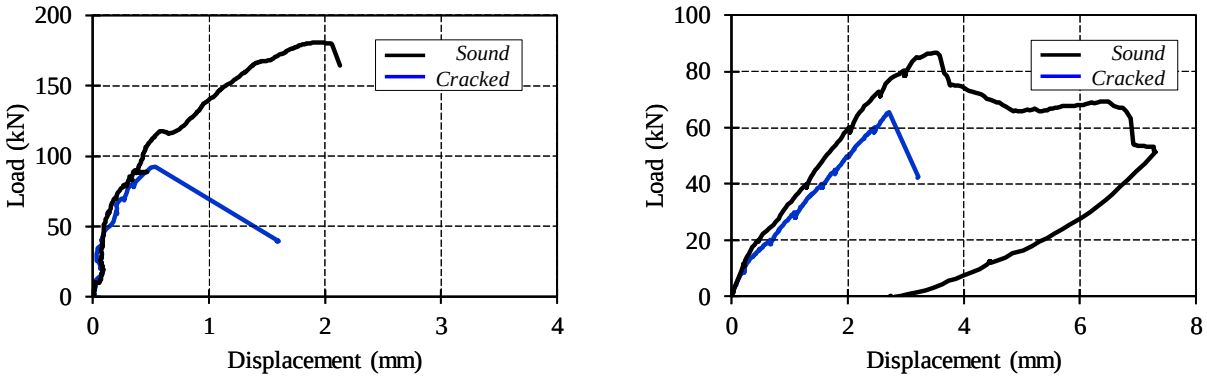

(a) a/d=1.6 *(b) a/d=2.9*

Figure 1.5 Load deflection curve of cracked beams at the anchorages[20]

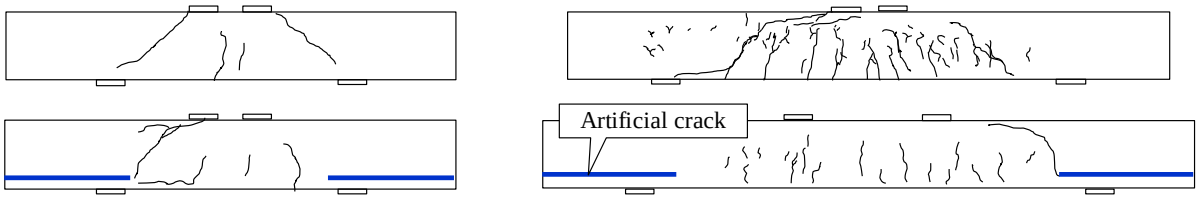

(a) a/d=1.6 *(b) a/d=2.9*

Figure 1.6 Failure mode of cracked beams at the anchorages[20]

deterioration[16]-[21]. According to the previous research regarding RC beams with rebar corrosion under flexural fatigue [16], it was explained that the fatigue behavior could be estimated by mass loss of tensile rebar. In addition, from the previous research which treated RC columns (a/d > 4.0) with rebar corrosion under cyclic loading[17], it mentioned that decrease in the ductility was mainly affected by corrosion of stirrups and localized corrosion.

According to the previous research which treated RC slabs with rebar corrosion due to chloride attack[18], it was reported that corrosion of compressive rebar affected compared with the tensile rebar for the fatigue behavior of the slab, and that the fatigue durability decreased under 5 % mass loss of rebar.

However, there was no research except authors study regarding shear fatigue of RC beam with rebar corrosion (Figure 1.3). So far, the problem of shear was difficult to treat, because the phenomenon did not depend on the beam theorem and because fatigue experiment including large scatter spends long time to conduct. On the other hand, the analytical system which could treat fatigue problem of concrete was developed by recent research. The analytical approach was effective to neglect the scatter and time spending. From this research background, the way to make clear shear fatigue problem was opened.

Moreover, normally, the RC beams as the structural members are designed as fail in flexural. However, when the beam had corrosive rebar, the load carrying behavior might be changed.

There is necessity to make clear the load carrying mechanism of the beam which fail in shear.

Therefore, this research focuses on the combined deterioration of shear fatigue and rebar corrosion of RC beams. The review of previous researches regarding the combined deterioration and the objective of this research are explained in the following sections.

1.2.1. Effects of shear span ratio

The effect of *a/d* (shear span ratio) is one of the important parameters to discuss the shear fatigue behavior of RC beams. According to the previous research[2], the size effect of RC beam was mentioned. The paper explained that the shear stress at the failure against *a/d* showed constant value in the region of $a/d > 3.0$, and minimum point of relative strength of the beam were $a/d=3.0$ regardless of beam height. From this fact, it is expected that the load carrying mechanism of RC beam is considerably changed in $a/d < 3.0$. In the fundamental beam theory which neglects the contribution of vertical stress, the shear stress at the failure should be constant regardless of *a/d*. This fact represents the load carrying mechanism is changed by *a/d*. It is considered that this tendency can be described by contribution of vertical stress near the loading points which will be mentioned in **Chapter 3**.

There is a possibility that the beam fail in flexure in the case $a/d > 3.0$. Therefore, this research discusses the load carrying mechanism of slender beam ($a/d < 3.0$), short beam ($a/d < 2.5$) and deep beam ($a/d < 1.0$) as the research targets.

1.2.2. Effects of position and length of rebar corrosion cracks

Effects of position and length of rebar corrosion cracks under static loading were explained by previous researches. According to the previous research[12], it was mentioned that the strength of the beams which had corrosion cracks inside of shear span increased compared with that of sound beam due to tied arch mechanism. In addition, from the analytical knowledge of previous research[19], it was showed that the existence of corrosion cracks along compressive rebar did not affect the behavior of load deflection curves remarkably.

The load deflection curve and the magnitude of fatigue strength versus number of cycles at failure of the beam which has different length of artificial crack along compressive rebar are shown in Figure 1.4. It was confirmed that the contribution of the crack length along compressive rebar was not remarkable. Moreover, from the experimental knowledge of the previous researches [14], [20], it was made clear that the behavior of beams which had corrosion cracks at the position of anchorages was governed by the diagonal crack which propagated from the position of crack tip.

The load deflection curve and crack distribution at the failure of the beams which had artificial cracks at the position of anchorages in case of $a/d = 1.6$ and $a/d = 2.9$ are shown in Figure 1.5

and Figure 1.6 [20]. It was confirmed that the strengths of cracked beams decreased because the failure of each beams were caused by occurrence of the diagonal crack under static and cyclic loading.

From the results of previous researches, it can be considered that the fatigue load carrying mechanism of the beams which have the corrosion cracks along compressive rebar and at the position of anchorages are not changed remarkably. Therefore, this research focuses on the beams which have the corrosion cracks along tensile rebar inside of shear span.

1.2.3. Effect of stirrups

According to the previous research which treated sound beams with stirrups, it was made clear that the fatigue strength of stirrup was remarkably low compared with the strength of steel due to opening of localized cracks across the stirrup[4]. Other research mentioned that the existence of stirrup affected the restriction of concrete in short beams[9].

It can be considered that the effect of stirrup gives important effect for the load carrying mechanism of cracked RC beams. Therefore, this research investigates the behavior of cracked RC beams with and without stirrup.

1.3 Objective

From the knowledge of previous researches, it can be deduced that the corrosion cracks along tensile rebar in shear span are most influenced on the load carrying mechanism compared with the beams which has the cracks other positions, and that the beams of $a/d < 3.0$ are subjected by shear fatigue load. Moreover, there is high possibility that if the behavior of the beam is investigated while corrosion environment, the behavior is completely deferent with the case with separating the effect of corrosion and fatigue. However, to make clear the effect of each factor of corrosion and fatigue, the loading experiments and analyses were conducted with separating the two processes in this study as a first step.

Therefore, to make clear the shear fatigue load carrying mechanism of RC beams, this study investigates the following items.

i) the effect of shear span ratio (a/d =1.0, 1.6, 2.9)

ii) the effect of difference in the length of corrosion cracks along tensile rebar

iii) the effect of existence of stirrup

iv) the validity of reproducing method of load carrying mechanism by artificial crack

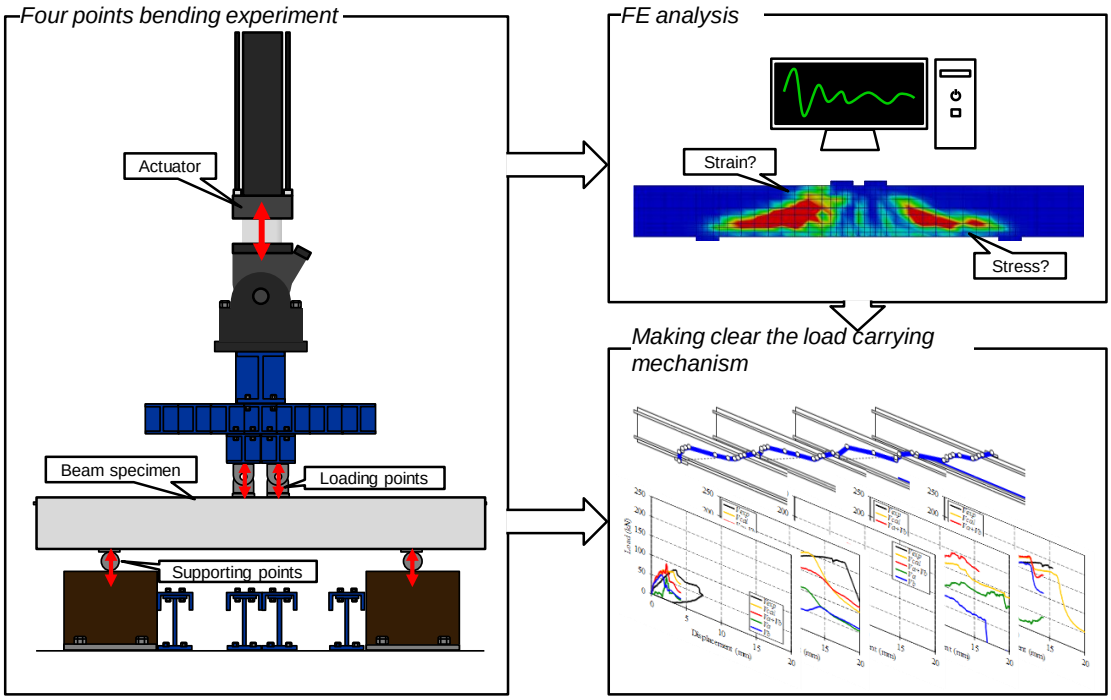

Figure 1.7 Main research scheme

1.4 Methodology

To make clear the shear fatigue load carrying mechanism of RC beams, cyclic loading experiment and FE (finite element) analysis were conducted. The load carrying mechanism is deduced and calculated based on the results of experiments and analysis (Figure 1.7) in each chapter of research flow. The research flow of this research is shown in Figure 1.8.

In **Chapter 1**, introduction and objective of this research based on previous reviews is mentioned.

In **Chapter 2**, methods to describe the load carrying mechanism of cracked RC beams are explained. Each method is derived from the result of FE analysis. Thus, the constitutive law of FE analysis and the previous researches are also explained.

In **Chapter 3**, the load carrying mechanism of cracked RC beams without stirrups is described by using the description methods as mentioned in **Chapter 2**. The artificial crack which make the uniform surface is installed in the specimens and FE models to simulate severe state of corrosion cracks.

In **Chapter 4**, the load carrying mechanism of cracked RC beams with stirrups is described by using the description methods as mentioned in **Chapter 2**. The effect of stirrup is discussed by comparison with the results of **Chapter 3**. The artificial crack is also introduced in the beams.

In **Chapter 5**, validity of the artificial cracks which are introduced in **Chapter 3** and **Chapter**

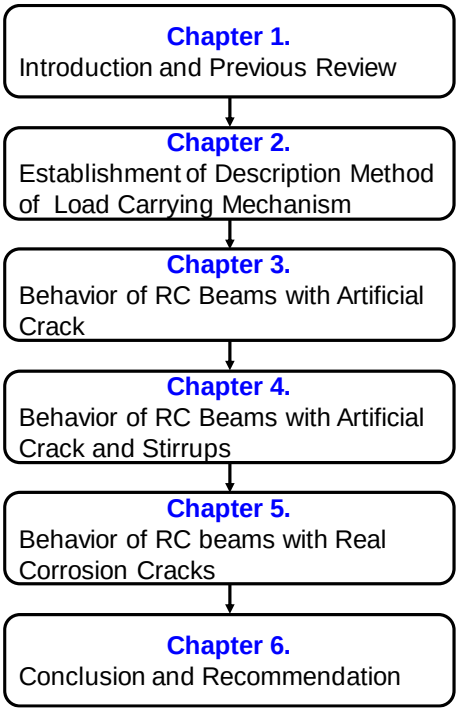

Figure 1.8 Research flow

4 is discussed. To confirm the validity, RC beam which has corrosion crack with and without stirrups are made, and cyclic loading experiment are conducted. The behaviors are compared with the results of **Chapter 3** and **Chapter 4**.

Finally, in **Chapter 6**, the conclusions and recommendations are obtained from the results of **Chapters 2 - 5**.

1.5 Summary of Chapter 1

This chapter explained the background, objective and methodology of this research based on previous reviews. Also, this chapter mentioned a necessity to make clear the shear fatigue load carrying mechanism of RC beam with corrosion cracks due to increase in the deteriorated infrastructures.

As a result of the previous research survey, it was found that the effect of shear span ratio, the effect of corrosion cracks along tensile rebar, and the effect of stirrup were main influential factors for the load carrying mechanism.

This research treats the beams which have the artificial cracks to neglect the effect of actual corrosion crack surface. To make clear the load carrying mechanism, this research investigates the effect of shear span ratio (a/d=1.0, 1.6, 2.9), the effect of difference in the length of corrosion cracks along tensile rebar, the effect of existence of stirrup, and the validity of artificial crack.

References in Chapter 1

[1] Ministry of Land, Infrastructure, Transport and Tourism: Annual Statistics Report of Road, 2015.

[2] Kani, G. N. J.: How safe are our large reinforced concrete beams?, *ACI Journal Proceedings*, Vol.64, No.3, pp.128-141, 1967.3.

[3] Higai, T.: Fundamental Study on Shear Failure of Reinforced Concrete Beams, *Proceedings of the Japan Society of Civil Engineers*, Vol.279, pp.113-126, 1978.11. (in Japanese)

[4] Okamura, H., Farghaly, A.S. and Ueda, T.: Behaviors of Reinforced Concrete Beams with Stirrups failing in Shear under Fatigue Loading, *Proceedings of Japan Society of Civil Engineers*, No.308, pp.109-122, 1981.4.

[5] Forrest, R. W. B., Higgins, C., Senturk, E.: Experimental and Analytical Evaluation of Reinforced Concrete Girders under Low-Cycle Shear Fatigue, *ACI Structural Journal*, Vol.107, No.2, pp.199-207, 2010.4-5.

[6] Graddy, C. J., Kim, J., Whitt, H. J., Burns, H. N., Klingner, E. R.: Punching-Shear Behavior of Bridge Decks under Fatigue Loading, *ACI Structural Journal*, Vol.99, No.3, pp.257-266, 2002.5-6.

[7] Kwak, H. K., Suh, J., Hsu, T. T. C.: Shear-Fatigue Behavior of Steel Fiber Reinforced Concrete Beams, *ACI Structural Journal*, Vol.88, No.2, pp.155-160, 1991.3-4.

[8] Ou, C. Y., Chen, H. H.: Cyclic Behavior of Reinforced Concrete Beams with Corroded Transverse Steel Reinforcement, *Journal of American Society of Civil Engineers, Journal of Structural Engineering*, 140(9), 2014.

[9] Teng, S., Ma, W., Wang, F.: Shear Strength of Concrete Deep Beams under Fatigue Loading, *ACI Structural Journal*, Vol.97, No.4, pp.572-580, 2000.8.

[10] Zhu, W., Francois, R., Coronelli, D., Cleland, C.: Effect of corrosion of reinforcement on the mechanical behavior of highly corroded RC beams, *ELSEVIER Science Direct, Engineering Structures*, 56, pp.544-554, 2013.

[11] Hanjari, Z. K., Kettil, P., Lundgren, K.: Analysis of Mechanical Behavior of Corroded Reinforced Concrete Structures, *ACI Structural Journal*, Vol.108, No.5, pp.532-541, 2011.9-10.

[12] Tsunoda, M., Watanabe, K., et al.: The Study Regarding Shear Load Carrying Behavior of RC Beams with Localized Rebar Corrosion, *Proceedings of the Japan Concrete Institute*, Vol.30, No.3, pp.1705-1710, 2008. (in Japanese)

[13] Pimanmas, A. and Maekawa, K.: Control of Crack Localization and Formation of Failure Path in RC Members Containing Artificial Crack Device, *Journal of Materials, Conc. Struct., Pavements, JSCE*, V-52, No.683, pp. 173-186, 2001.8.

[14] Chijiwa, N., Kawanaka, I. and Maekawa, K.: The Effect of Strengthening the Damage Expected Zone in a RC Member with Damaged Anchorage, *Journal of Japan Society of Civil Engineers*, E, Vol.66, No.2, pp.179-192, 2010.5.

[15] Ith, V., Matsumoto, K., Niwa, J.: Mechanical Characteristics of RC Beams with Corroded Stirrups or Main Reinforcements, *Proceedings of the Japan Concrete Institute*, Vol.36, No.1, pp.1288-1293, 2014.

[16] Nishiwaki, K., Ooyado, M., et al.: Fatigue Behavior of RC Beam with Corroded Rebar, *Proceedings of the Japan Concrete Institute*, Vol.24, No.1, pp.783-788, 2002. (in Japanese)

[17] Kato, E., Iwanami, M., et al.: Effect of Rebar Corrosion in RC Column Subjected Repeated Load, *Proceedings of the Japan Concrete Institute*, Vol.27, No.2, pp.1489-1494, 2005. (in Japanese)

[18] Maeshima, T., Koda, Y., Tsuchiya, S. and Iwaki, I.,: Influence of Corrosion of Rebars Caused by Chloride Induced Deterioration on Fatigue Resistance in RC Road Bridge Deck, *Journal of Japan Society of Civil Engineers*, E2, Vol.70, No.2, pp.208-225, 2014.

[19] Yamada, Y., Chijiwa, N. and Iwanami, M.: Effect of Corrosion along Compressive Rebar in Shear Fatigue Mechanism of Reinforced Concrete Beams without Stirrups, *Proceedings of Japan Society of Civil Engineers 2015 Annual Meeting*, No.V, pp.1299-1300, 2015.9. (in Japanese)

[20] Yamada, Y., Chijiwa, N. and Iwanami, M.: Shear Fatigue Mechanism of Reinforced Concrete Beams with Cracks due to Rebar Corrosion, *Proceedings of the Fourth International Symposium on Life-Cycle Civil Engineering*, pp.1491-1499, 2014.11.

[21] Ahmed, T., Burley, E., Rigden, S.: The Static and Fatigue Strength of Reinforced Concrete Beams Affected by Alkali-Silica Reaction, *ACI Materials Journal*, Vol.95, No.4, pp.356-368, 1998.7-8.

CHAPTER 2
EXPLANATION METHODS OF THE LOAD CARRYING MECHANISM

This chapter explains the description methods of the load carrying mechanism of cracked RC beams. The methods which is proposed in this study are obtained from mainly numerical analysis. At first, constitutive laws of the analysis which is proposed by previous researches to explain the fatigue behaviors of cracked RC beams are explained. After that, to categorize the load carrying mechanism of cracked RC beams reasonably a calculating method which decompose the mechanisms to *Arch* and *Beam* mechanisms is developed in this research based on the traditional concept. Next, a method to visualize the mechanisms is proposed in this research. Finally, a method to express the effect of cyclic loading and existence of corrosion cracks as an effective strength coefficient is proposed in this research.

2.1 Constitutive Law of Numerical Models

2.1.1. Outline of the law in the finite elements

This research used the finite element (FE) analysis to explain the load carrying mechanisms of cracked RC beams. The load carrying mechanism was explained based on the result of analysis by *COM3* which was developed for concrete structures as a FE analytical system [1]. *COM3* can reproduce the fatigue behavior of RC beams. The smeared crack model which treats stress strain relationships averagely is applied to *COM3* and the models are suitable to express the whole behavior of RC structures after cracking.

The fatigue damage in concrete can be expressed as elastic stiffness reduction caused by the progress of plastic deformation and propagation of micro-cracks. In *COM3*, propagation of the non-linearity can be considered by formulation of plastic strain and fracture parameters in the fundamental constitutive laws of concrete which is subjected to cyclic compressive and tensile stress. In addition, infinitesimal damage factors are introduced to represent the reduction of shear transfer due to smoothing of the crack surfaces.

a) Time-space averaging model in concrete element

In microscopic focuses, RC structure is a discontinuous body because the structural system functions after crack occurrence in tensile side. However, the macroscopic behavior of the discontinuous body can be treated by averaging the stress-strain relationship of the FEs in suitable size. The smeared crack model is an averaging method of the stress-strain relationship of finite region to grasp the behaviors of whole region (Figure 2.1). The analytical scale of this model can be reduced relatively, because of less modeling cost of each crack.

On the other hand, the dispersive crack model which can simulate occurrence of each crack in finite region is an efficient model to grasp the phenomenon regarding the bonding effect and stress transfer on interfacial zone between each structural component. In general, if the dispersive crack model is applied, expectation of crack position is needed. It is difficult to apply the model in the case that the occurrence and propagation positions of the crack are unknown. In this case, the analytical scale becomes large. *COM3* can apply such a dispersive method by arrangement of bond elements in the interfacial zone of discontinuous surfaces.

Rotating crack model and fixed crack model are ones of the common models as the smeared crack model. In the case of the rotating crack model, principal axis of stress-strain is rotated to correspond the crack direction with principal strain direction constantly. The fixed crack model is the model which fixes the crack direction and consider the shear transfer on the crack surfaces. The initial constitutive model of *COM3* is the fixed crack model, and *COM3* can apply the rotating crack model as well. Normal and shear stresses are treated as an

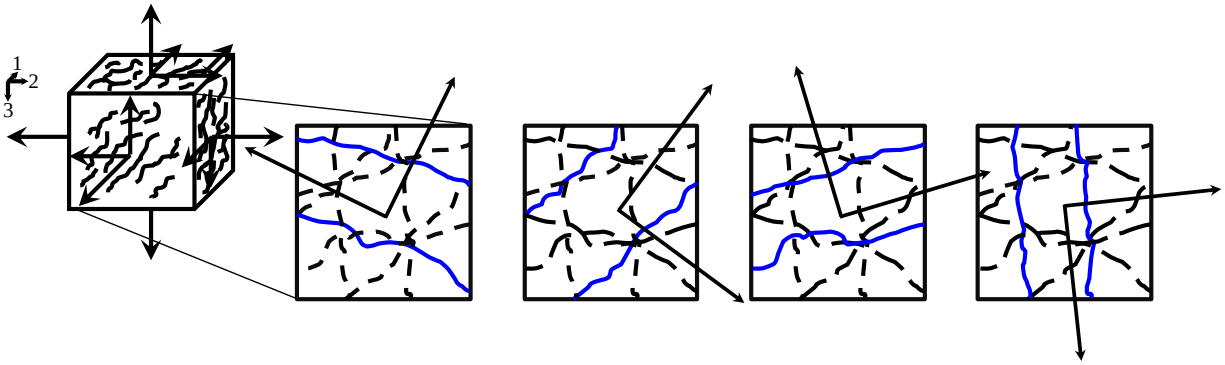

Figure 2.1 Concept of smeared crack model and active cracks

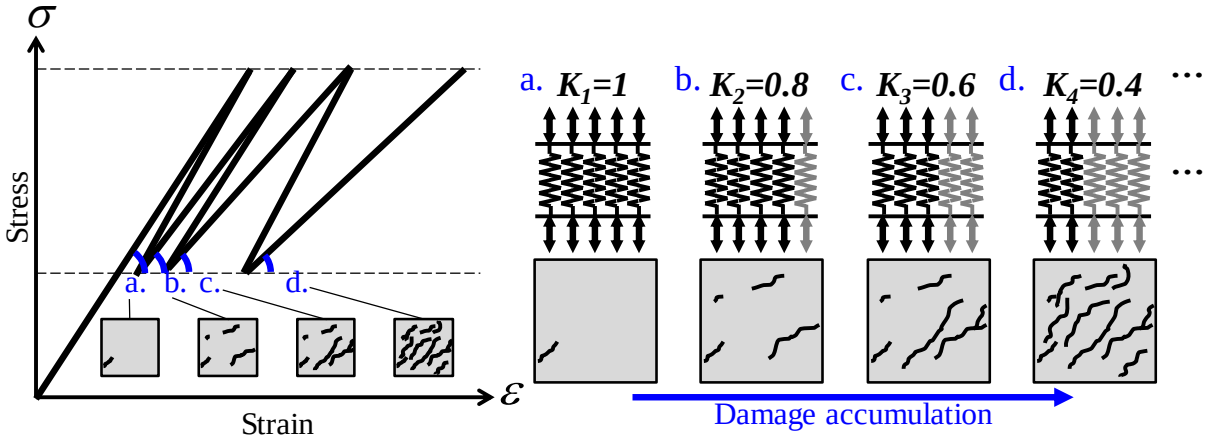

Figure 2.2 Concept of elasto-plastic fracture model

independent model in the fixed crack model by preserving nonlinearity. The models become relatively complex. However, the cracks which occur in multi directions can be modeled directly. Thus, this model is an efficient model to treat the phenomena of shear fracture which occurs by change in the direction of principal stress caused by cyclic loading.

b) Multi directional nonlinear fixed crack model

In the cracked elements which have high nonlinearity, all cracks do not contribute to this nonlinearity at the same time. Several opening cracks which show strong non-linearity govern nonlinear behavior of cracked elements. These cracks are called “Active cracks”. Deformation on the closing crack surfaces except for active cracks can be neglected. It is possible that analytical region can be expanded from two directions to multi directions by introducing the concept of active cracks. The multi directional nonlinear fixed crack model which can treat the behavior of RC element in maximum four directions of cracks in two dimensional plane stress condition was proposed (Figure 2.1).

In this model, “imitating orthogonal cracks” whose magnitude of cross angles with initial cracks are $\pi/2 \pm \pi/8$, and “non-orthogonal cracks” whose magnitude of cross angles with initial

cracks are less than $\pi/2$-$\pi/8$, are defined. By using the definitions, four independent directional cracks can be dealt in imitating orthogonal and non-orthogonal systems of crack.

2.1.2. Models under cyclic loading

a) The law in compressive side

The EPF (elasto-plastic fracture) model[2] which was obtained from results of uniaxial compressive test was applied as a fundamental constitutive law in compressive side. In the EPF model, the compressive stiffness of concrete is expressed by multiple springs (Figure 2.2). The total stiffness is reduced by failure or collapse of the springs.

Averaged stress-strain relationships are formulated as the following equations.

$$\varepsilon = \varepsilon_e + \varepsilon_p \tag{2.1}$$

$$\sigma = E_0 \varepsilon_e K_c \tag{2.2}$$

Where, ε: total strain, ε_e: elastic strain, ε_p: plastic strain, σ: compressive stress, E_0: initial stiffness, K_c: failure parameter. K_c represents survival ratio of the springs. When $K_c = 1$, no damage occurs in the element. The reduction of K_c represents propagation of micro-cracks under cyclic stresses. ε_p and K_c are function of time (t) and plastic strain (ε_p), thus, increment of ε_p and K_c can be denoted as follows.

$$\delta\varepsilon_p = \frac{\partial \varepsilon_p}{\partial t}\delta t + \frac{\partial \varepsilon_p}{\partial \varepsilon_e}\delta\varepsilon_e \tag{2.3}$$

$$\delta K_c = \frac{\partial K_c}{\partial t}\delta t + \frac{\partial K_c}{\partial \varepsilon_e}\delta\varepsilon_e \tag{2.4}$$

To express the time dependency, damage potentials are introduced considering the phenomenon that nonlinearity of the concrete is affected by restriction of surrounding materials and load applying time. The potentials are obtained as follows.

$$F_k = F_{k_{(K_c,\varepsilon_e)}} = K_c - \exp[-0.73\beta\{1 - \exp(-1.25\beta)\}] \tag{2.5}$$

$$F_p = F_{p_{(\varepsilon_p,\varepsilon_e)}} = \varepsilon_p - 0.038\left\{\exp\left(\frac{\varepsilon_e}{0.55}\right) - 1\right\} \tag{2.6}$$

$$\beta = \frac{-1}{0.35}\left\{\mathrm{In}\left(1 - \frac{7\varepsilon_{ec}}{20}\right)\right\} \tag{2.7}$$

Where, F_k: elastic damage potential, F_p: plastic damage potential, ε_{ec}: elastic strain regarding the confinement ratio. If there is no confinement, $\varepsilon_{ec} = \varepsilon_e$is satisfied.

F_k is function of K_c, ε_e. F_p is function of $\varepsilon_p, \varepsilon_e$. Elastic strain depending the term of *(2.3)* and *(2.4)* can be derived as follows.

$$\frac{\partial \varepsilon_p}{\partial \varepsilon_e} = \begin{cases} 0 & F_p > 0 \\ -\dfrac{\partial F_p / \partial \varepsilon_e}{\partial F_p / \partial \varepsilon_p} & F_p = 0 \end{cases} \tag{2.8}$$

$$\frac{\partial K_c}{\partial \varepsilon_e} = \begin{cases} 0 & F_k > 0 \\ -\dfrac{\partial F_k / \partial \varepsilon_e}{\partial F_k / \partial K_c} & F_k = 0 \end{cases} \tag{2.9}$$

When the damage potential is positive value, the time dependent term is remained. In this case, the damage progresses under applied constant stress. The time dependent term in *(2.3)* and *(2.4)*, are called "Plastic ratio function" and "Damage ratio function", respectively. The plastic ratio function can be expressed as the following equations.

$$\frac{\partial \varepsilon_p}{\partial t} = \varphi \left(\frac{\partial \varepsilon_p}{\partial t} \right)_b \tag{2.10}$$

$$\left(\frac{\partial \varepsilon_p}{\partial t} \right)_b = 0.034 \left\{ \exp\left(\frac{\varepsilon_{ep}}{4} \right) - 1 \right\} \tag{2.11}$$

$$\varphi = exp\left(-6 \frac{F_p^{0.6}}{\varepsilon_e^{1.2}} \right) \tag{2.12}$$

$$\varepsilon_{ep} = \gamma \varepsilon_e \tag{2.13}$$

Where, φ: plastic damage reduction factor, γ: confinement factor.

The damage ratio function can be expressed as the following equations.

$$\frac{\partial K_c}{\partial t} = exp\left\{ \xi \left(\frac{K_c}{K_c - F_k} - 1 \right) \right\} \left(\frac{\partial K_c}{\partial t} \right)_b \tag{2.14}$$

$$\left(\frac{\partial K_c}{\partial t} \right)_b = (K_c - F_k) \left(\frac{\partial K_c}{\partial t} \right)_n \tag{2.15}$$

$$\left(\frac{\partial K_c}{\partial t} \right)_n = 0.015 \log(K_c - F_k) \tag{2.16}$$

$$\xi = 45 \Psi^{-0.5(1-\exp(-5\varepsilon_e))} \tag{2.17}$$

Where, Ψ is a function of γ. *(2.14)* -(2.*17)* represents time dependent fracture of relatively weak springs in EPF models. This time dependent fracture represents damage progress which causes delayed fracture. In addition, to consider reduction of K_c due to occurrence of micro-cracks, *(2.16)* is introduced with $K_c - F_k$.

The reduction of elastic stiffness by cyclic compressive stress should be treated as another problem against time dependency. From this view point, the term to represent damage progress in *(2.3)* can be written as follows.

$$\frac{\partial K_c}{\partial \varepsilon_e} = \begin{cases} -\dfrac{\partial F_k / \partial \varepsilon_e}{\partial F_k / \partial K_c} + \lambda & F_k = 0 \\ \lambda & F_k < 0 \end{cases} \tag{2.18}$$

Where, λ: micro-crack propagation ratio. The effect is changed by micro-crack generating ratio (K_c). In the region where $K_c \in (0.5 \quad 1.0]$, effect of λ becomes large because micro-crack propagates remarkable, and in the region where $K_c \in [0.0 \quad 0.5]$, effect of λ becomes small. It is expected that in the region where $K_c \in [0.0 \quad 0.5]$, elastic stiffness does not reduce remarkably because local brittle failure progresses. From this expectation, λ is defined as follows.

$$\lambda = K_c^3(1 - K_c)^4 g \tag{2.19}$$

$$g = 0.6\left(\frac{9\gamma_n^8}{1 + 10^{30K_c - 22}}\right) \tag{2.20}$$

$$\gamma_n = \frac{\varepsilon - \varepsilon_{e,tp}}{\varepsilon_{emax}} \tag{2.21}$$

Where, $\varepsilon_{e,tp}$: turning point of compressive elastic strain. g is defined from experimental results to represent phenomena of high cycle fatigue under low level stress. γ_n is normalizing factor of maximum stress amplitude under cyclic compressive stress.

b) The law in tensile side

The softening behaviors of RC elements under averaged tensile stress are caused by reduction of bonding between concrete and rebar. The bonding which depends on time is caused by secondary cracks which propagate from ribs of rebar after occurrence of preliminary cracks. The secondary cracks distribute inside of concrete averagely[3]. Thus, averaged stress-strain relationships are suitable for the cracked RC elements.

The averaged stress-strain relationships are defined as follows.

$$\sigma = E_0 \varepsilon K_T \tag{2.22}$$

Where, σ: tensile stress, E_0: initial stiffness, ε: tensile strain K_T: failure parameter. K_T is scalar parameter which depends on failure condition changed by loading path, tensile creep and damage accumulation by cyclic stress. The nonlinearity of concrete under cyclic tensile stress is given as follows.

$$\delta K_T = H\delta\varepsilon + F\delta t + G\delta\varepsilon \tag{2.23}$$

The term including H means renewal of tensile fracture in each numerical step as follows.

$$H = \begin{cases} -(1+\alpha)\left(\dfrac{f_t}{E_0}\right)\varepsilon_{cr}^{\alpha}\varepsilon_{max}^{-(2+\alpha)} & \delta\varepsilon > 0 \wedge \varepsilon = \varepsilon_{max} \\ 0 & \delta\varepsilon \le 0 \vee \varepsilon < \varepsilon_{max} \end{cases} \tag{2.24}$$

Where, ε_{cr}: tensile strain as a criterion of crack occurrence, ε_{max}: historical maximum strain, f_t: uni-axial tensile strength, α: factor which depends on bonding. α takes 0.4 in the case of normal deformed rebar.

The term F in *(2.23)* represents stiffness reduction which is obtained by tensile creep test under 20°C and 60%RH. This term can be expressed as follows.

$$F = \begin{cases} 10^{-5}S^3(K_T - 0.5)^2 & \varepsilon_{max} < \varepsilon_{cr} \\ 10^{-6}S^6 & \varepsilon_{max} \geq \varepsilon_{cr} \end{cases} \quad (2.25)$$

$$S = \frac{E_0 \varepsilon K_T}{f_t} \quad (2.26)$$

S represents magnitude of acting stress. The nonlinearity after cracking depends on bond reduction caused by time and delayed cracks in the direction of cross section.

The term G in *(2.23)* represents damage which is accumulated by cyclic loading. This is expressed as follows.

$$G\delta\varepsilon = K_T \left(\frac{\sigma_{tp}}{\sigma_{env}}\right)^{20} \delta\tilde{\varepsilon} \quad (2.27)$$

$$\sigma_{env} = f_t \left(\frac{\varepsilon_{cr}}{\varepsilon_{tp}}\right)^{\alpha} \quad (2.28)$$

$$\delta\tilde{\varepsilon} = \begin{cases} 0 & \delta\varepsilon \geq 0 \\ 9\gamma_n^m \dfrac{\delta\varepsilon}{\varepsilon_0} & \delta\varepsilon < 0 \end{cases} \quad (2.29)$$

$$\gamma_n = -\frac{\varepsilon - \varepsilon_{tp}}{\varepsilon_{max}} \quad (2.30)$$

Even if constant stress amplitude is acting on the element, the strain increases by numerical renewal of fracture parameter in *(2.27)*. Damage progress by cyclic stress is governed by propagation of bonding crack and occurrence of new cracks in cross sectional direction. Thus, increase in the plastic stress is neglected in this modeling. The condition of before cracking can be simulated by applying of $m = 20 \wedge \sigma_{tp}/\sigma_{env} = 1.0$.

2.1.3. Stress transfer on crack surfaces

a) Contact density function

The contact density model which was proposed by Maekawa and Li et.al [1],[4]. was introduced in *COM3* to formulate the shear transfer model on crack surfaces against various loading path. In this model, crack surface as shown in Figure 2.3 is divided by infinitesimal element which is called "unit contact" to model the shapes of crack surfaces. The contact density function is applied to express the distribution of the unit contact in normal direction of crack surfaces. The contact density function is not affected by the maximum size of coarse aggregate, and the assumptions of the function coincide with the measured value of surface area of cracks. From this fact, the function is given as follows.

$$\Omega_{(\theta)} = 0.5\cos\theta \quad (2.31)$$

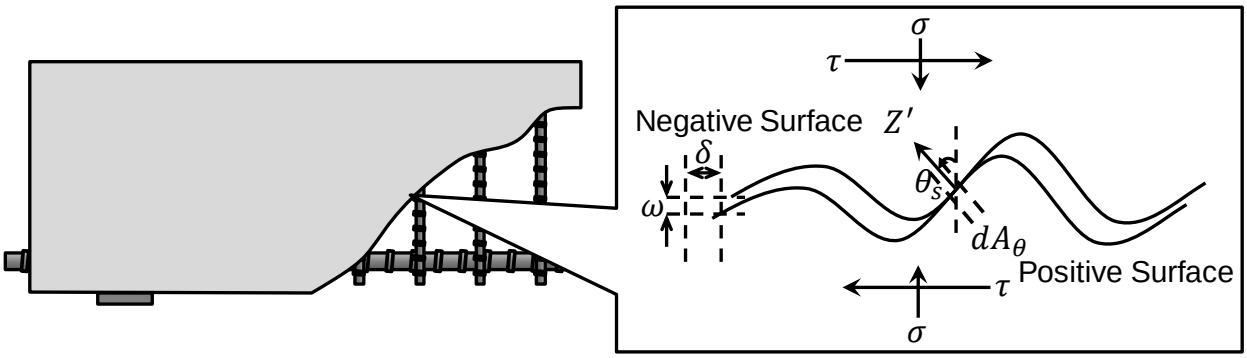

Figure 2.3 Concept of crack surface in contact density model

$$\int_{-\pi/2}^{\pi/2} \Omega_{(\theta)} d\theta = 1 \tag{2.32}$$

Where, $\Omega_{(\theta)}$: contact density function. The function is related to the ratio of shear stress versus transferred compressive stress. However, when the concrete has less than 50 MPa of compressive strength, this ratio is not related to compressive stress. Thus, the assumption is applied that the function does not depend on type of concrete and coarse aggregate.

b) Elasto plastic model of contacting stress on crack surfaces

The stress condition at the contact point is not governed by uni-axial compressive condition. The displacement in the normal direction on the crack surfaces is governed by the normal stress. The failure strength in normal direction is given as the following equations because stress transfer becomes low due to plasticity at the contact position.

$$\sigma'_{con} = \begin{cases} R_s(\omega'_\theta - \omega'_{\theta p}) & \omega'_\theta \geq \omega'_{\theta p} \\ 0 & \omega'_\theta < \omega'_{\theta p} \end{cases} \tag{2.33}$$

$$\omega'_{\theta p} = \begin{cases} \omega'_{max} - \omega'_{lim} & \omega'_{max} > \omega'_{lim} \\ 0 & \omega'_{max} \leq \omega'_{lim} \end{cases} \tag{2.34}$$

$$f'_y = R_s \omega'_{lim} \tag{2.35}$$

Where, σ'_{con}: normal stress on the unit contact, ω'_θ: displacement in the normal direction, $\omega'_{\theta p}$: plastic displacement in the normal direction, ω'_{max}: maximum displacement in the normal direction, ω'_{lim}: elastic limit displacement in the normal direction, f'_y: failure strength of unit contact, R_s: elastic stiffness per unit crack length.

c) Modeling of contacting area

The stress transfer on the crack surfaces is related to the contacting area which is generated by the opening of crack width. The height of crack surface is almost less than the maximum size of coarse aggregate. Consequently, the contact occurs in the range that the height of crack surfaces is higher than that of crack width. From this fact, an effective ratio of contacting area is introduced as a function of crack width. The ratio is given as follows.

$$K = 1 - \exp\left(1 - 0.5\frac{G_{max}}{\omega}\right) \tag{2.36}$$

Where, K: effective ratio of contacting area, G_{max}: maximum size of coarse aggregate, ω: crack width.

d) Formulation of constitutive equation

In the infinitesimal area, the external force in each coordinate on crack surfaces should be balanced with integration values of shear stress and normal stress that is transferred on the crack surfaces. Thus, the shear stress and normal stress can be written as follows.

$$\tau = \int_{-\pi/2}^{\pi/2} Z' \sin\theta d\theta \tag{2.37}$$

$$\sigma' = \int_{-\pi/2}^{\pi/2} Z' \cos\theta d\theta \tag{2.38}$$

$$Z' = \sigma'_{con} K A_t \Omega_{(\theta)} \tag{2.39}$$

$$A_t = \left(\int_{-\pi/2}^{\pi/2} \Omega_{(\theta)} \cos\theta d\theta\right)^{-1} \tag{2.40}$$

Where, τ: shear stress, σ': normal stress, δ_θ: displacement in normal direction, Z': compressive force acting on the contact unit, A_t: total surface area on unit crack surface. Coordinate transformation from local coordinate system $(\delta_\theta, \omega'_\theta)$ to the crack surface coordinate system (δ, ω) is expressed as follows.

$$\omega'_\theta = \delta sin\theta - \omega cos\theta \tag{2.41}$$

$$\delta_\theta = \delta cos\theta + \omega sin\theta \tag{2.42}$$

When iterated integral method is used as the solution method of nonlinear problem, the stiffness matrix is obtained by partial differentiation of constitutive equation *(2.37)* - (2.*38)*.

$$\begin{bmatrix} d\tau \\ d\sigma' \end{bmatrix} = \begin{bmatrix} D_{11} & D_{12} \\ D_{21} & D_{22} \end{bmatrix} \begin{bmatrix} d\delta \\ d\omega \end{bmatrix} \tag{2.43}$$

$$\begin{bmatrix} D_{11} & D_{12} \\ D_{21} & D_{22} \end{bmatrix} = \begin{bmatrix} \int \frac{\partial Z'}{\partial \delta} sin\theta d\theta & \int \frac{\partial Z'}{\partial \omega} sin\theta d\theta \\ \int \frac{\partial Z'}{\partial \delta} cos\theta d\theta & \int \frac{\partial Z'}{\partial \omega} cos\theta d\theta \end{bmatrix} \tag{2.44}$$

e) Modeling of damage due to cyclic loading

The reduction of shear stress can be expressed as the following equations by considering stress reduction by cyclic loading[4]-[5].

$$\tau = X\tau_{or(\delta,\omega)} \tag{2.45}$$

$$X = 1 - \frac{1}{10}\log_{10}\left(1 + \int \left| d\frac{\delta}{\omega} \right|\right) \geq 0.1 \qquad (2.46)$$

Where, $\tau_{or(\delta,\omega)}$: shear stress in *(2.37)*. This equation was obtained from experimental results.

2.1.4. Logarithmic loading method

In the fatigue analysis, logarithmic loading method that can obtain the equivalent solution against the solution of normal method is applied to reduce the analytical time cost. This method can reduce the analytical time cost by introducing logarithmical time term. The constitutive law in the case of logarithmic loading method can be expressed as follows.

$$\delta\varepsilon_p = \zeta \frac{\partial \varepsilon_p}{\partial t}\delta t + \frac{\partial \varepsilon_p}{\partial \varepsilon_e}\delta\varepsilon_e \qquad (2.47)$$

$$\delta K_c = \zeta \frac{\partial K_c}{\partial t}\delta t + \frac{\partial K_c}{\partial \varepsilon_e}\delta\varepsilon_e \qquad (2.48)$$

$$\frac{\partial K_c}{\partial \varepsilon_e} = \left[-\frac{\partial F_k/\partial \varepsilon_e}{\partial F_k/\partial K_c} + \zeta\lambda \right] \qquad (2.49)$$

$$X = 1 - \frac{1}{10}\log_{10}\left(1 + \int \zeta \left| d\frac{\gamma}{\varepsilon} \right|\right) \geq 0.1 \qquad (2.50)$$

The coefficient ζ is applied to reproduce the cyclic damage mathematically. When ζ is multiplied as in *(2.47)-(2.50)*, the equations can consider progress of nonlinearity. In general, cyclic damage becomes remarkable in the initial phase of loading, and after this phase, the damage does not progress remarkably. From this fact, in the initial analytical step, ζ is equals to 1, and ζ increases with increase in the analytical step.

2.2 Decomposition of Load Carrying Mechanism

2.2.1. Outline of decomposition method

If the contributed load against external force in each mechanism could be calculated, the systematic explanation could be derived for cracked RC beams. To categorize the load carrying mechanism of cracked RC beams, this research applied the decomposition of the mechanisms. In general, from the equilibrium condition of the forces in the free body, the shear strength (V) is obtained as the liner summation of contributed load of concrete (V_C) and stirrup (V_S) (Figure 2.4). It is known that the contributed load of stirrup can be obtained based on traditional truss theory, modified truss theory and so on. In addition, the shear strength (V) can be separated to the contributed load of arch (V_a) and beam (V_b) mechanisms [6]. The arch mechanism appears when the acting position of resultant compressive (tensile) force is changed in the direction of cross sectional height. The mechanism is caused by formation of compressive strut. The beam

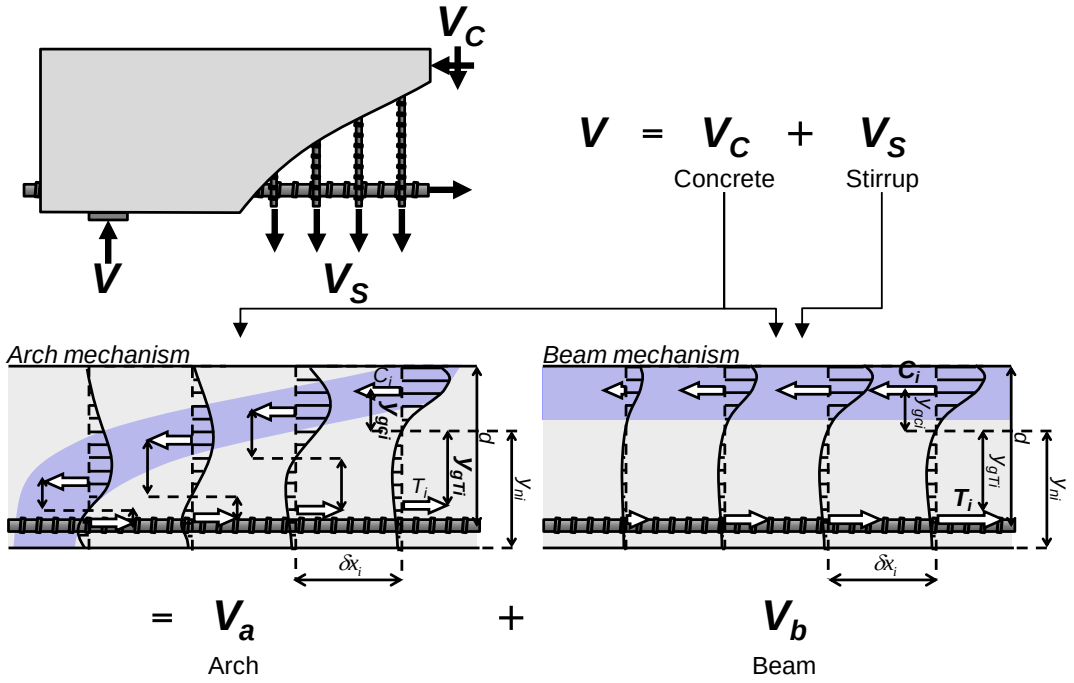

Figure 2.4 Concept of decomposition of load carrying mechanism

mechanism appears when the magnitude of the resultant compressive (tensile) force is changed in the member axis direction. The mechanism is mainly caused by truss mechanism. If the beam has stirrups, tensile force is transferred by stirrups, and the stresses flow as a "Howe truss". Thus, the shear strength (V) can be expressed as follows.

$$V = V_C + V_S = V_a + V_b = V_{Ca} + V_{Cb} + V_S \tag{2.51}$$

Where, V: shear strength, V_C: contributed load by concrete, V_S: contributed load by stirrup, V_a: contributed load by arch mechanism, V_b: contributed load by beam mechanism, V_{Ca}: contributed load by arch mechanism in concrete, V_{Cb}: contributed load by beam mechanism in concrete. V_S is included in V_b. Thus,

$$V_a = V_{Ca} \tag{2.52}$$

$$V_b = V_{Cb} + V_S \tag{2.53}$$

V_a and V_b were obtained from the longitudinal stress in the results of FE analysis which was mentioned in the previous section. Mainly two types of the derivation method in V_a and V_b will be described in this section. The *Visual Basic* (*VB*) was used as a calculation programming code. The actual code is shown in **Appendix. A**.

2.2.2. Derivation of arch and beam mechanisms

a) Derivation based on chain law of differential coefficient

In the analysis, a bond element which is mentioned in the following chapter was inserted in the analytical models to reproduce existence of corrosion crack. The stress distribution

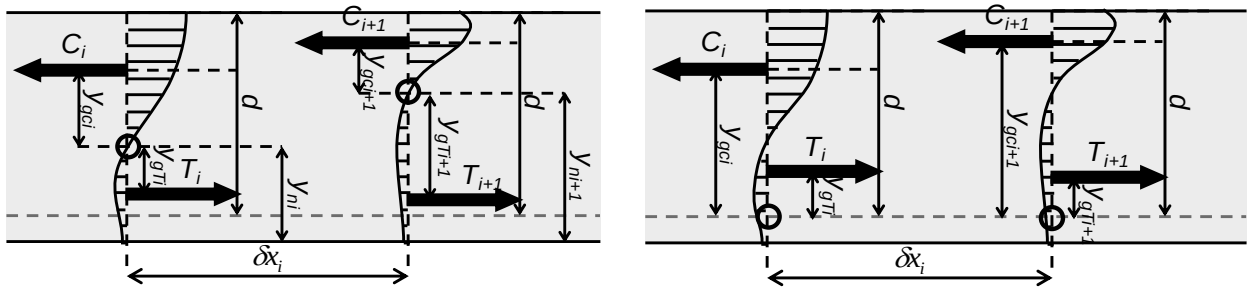

(a) Without bond element *(b) With bond element*

Figure 2.5 Equilibrium condition of cross sectional forces

around bond elements is disturbed due to discretization of continuous body. To eliminate the disturbance, two types of calculating methods were proposed in this research. Consider the equilibrium condition of cross sectional forces (Figure 2.5), a moment in a cross section is given in the following equation.

$$\begin{pmatrix} M_{(x,t)} \\ \widehat{M}_{(x,t)} \end{pmatrix} = \begin{pmatrix} 1 & 1 \\ 1 & -1 \end{pmatrix} \begin{pmatrix} C_{(x,t)} y_{gC(x,t)} \\ T_{(x,t)} y_{gT(x,t)} \end{pmatrix} \tag{2.54}$$

Where, $M_{(x,t)}$: cross sectional moment without bond element, $\widehat{M}_{(x,t)}$: cross sectional moment with bond element, $C_{(x,t)}$: resultant compressive force, $T_{(x,t)}$: resultant tensile force, $y_{gC(x,t)}$: acting position of resultant compressive force, $y_{gT(x,t)}$: acting position of resultant tensile force.

The shear force is given as the first derivative in longitudinal coordinate of cross sectional moment as follows.

$$\begin{pmatrix} V_{(x,t)} \\ \widehat{V}_{(x,t)} \end{pmatrix} = \frac{\partial}{\partial x} \begin{pmatrix} M_{(x,t)} \\ \widehat{M}_{(x,t)} \end{pmatrix} \tag{2.55}$$

Where, $V_{(x,t)}$: cross sectional shear force without bond element, $\widehat{V}_{(x,t)}$: cross sectional shear force with bond element. The moment vector $\boldsymbol{M}$, can be regarded as a functional of $C_{(x,t)}$, $y_{gC(x,t)}$, $T_{(x,t)}$, $y_{gT(x,t)}$. Thus,

$$\boldsymbol{V} = \frac{\partial}{\partial x}\boldsymbol{M}_{[C,T,y_{gC},y_{gT}]} = \frac{\partial \boldsymbol{M}}{\partial C}\frac{\partial C}{\partial x} + \frac{\partial \boldsymbol{M}}{\partial y_{gC}}\frac{\partial y_{gC}}{\partial x} + \frac{\partial \boldsymbol{M}}{\partial T}\frac{\partial T}{\partial x} + \frac{\partial \boldsymbol{M}}{\partial y_{gT}}\frac{\partial y_{gT}}{\partial x} \tag{2.56}$$

Where, $\boldsymbol{V}=\begin{pmatrix} V_{(x,t)} & \widehat{V}_{(x,t)} \end{pmatrix}^T$. From *(2.56)*, $\boldsymbol{V}$ is obtained as follows.

$$\boldsymbol{V} = \begin{pmatrix} 1 & 1 & 1 & 1 \\ 1 & -1 & 1 & -1 \end{pmatrix} \begin{pmatrix} C\dfrac{\partial y_{gC}}{\partial x} & T\dfrac{\partial y_{gT}}{\partial x} & y_{gC}\dfrac{\partial C}{\partial x} & y_{gT}\dfrac{\partial T}{\partial x} \end{pmatrix}^T \tag{2.57}$$

The arch mechanism appears when the acting position of resultant force is changed. The beam mechanism appears when the magnitude of resultant force is changed. Thus,

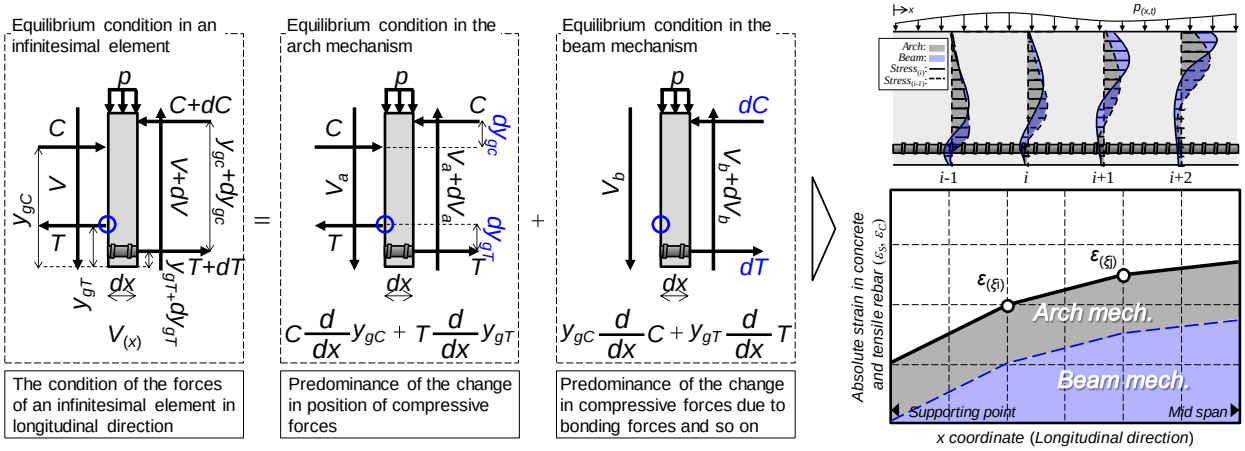

Figure 2.6 Equilibrium condition of cross sectional forces in geometrical consideration

$$\boldsymbol{V_a} = \begin{pmatrix} 1 & 1 & 0 & 0 \\ 1 & -1 & 0 & 0 \end{pmatrix} \left(C\frac{\partial y_{gC}}{\partial x} \quad T\frac{\partial y_{gT}}{\partial x} \quad y_{gC}\frac{\partial C}{\partial x} \quad y_{gT}\frac{\partial T}{\partial x} \right)^T \tag{2.58}$$

$$\boldsymbol{V_b} = \begin{pmatrix} 0 & 0 & 1 & 1 \\ 0 & 0 & 1 & -1 \end{pmatrix} \left(C\frac{\partial y_{gC}}{\partial x} \quad T\frac{\partial y_{gT}}{\partial x} \quad y_{gC}\frac{\partial C}{\partial x} \quad y_{gT}\frac{\partial T}{\partial x} \right)^T \tag{2.59}$$

Where, $\boldsymbol{V_a} = \left(V_{a(x,t)} \quad \hat{V}_{a(x,t)}\right)^T$, $\boldsymbol{V_b} = \left(V_{b(x,t)} \quad \hat{V}_{b(x,t)}\right)^T$, $V_{a(x,t)}$: contributed load of arch mechanism without bond element, $\hat{V}_{a(x,t)}$: contributed load of arch mechanism with bond element, $V_{b(x,t)}$: contributed load of beam mechanism without bond element, $\hat{V}_{b(x,t)}$: contributed load of beam mechanism with bond element.

b) Derivation based on mechanical equilibrium condition of cross sectional forces

(2.58) and *(2.59)* can be derived geometrically. Physical meaning of arch and beam mechanisms can be grasped by geometrical consideration.

Consider the infinitesimal element of the beam as shown in Figure 2.6. The equilibrium condition of moment around Point O in infinitesimal deformation theory is,

$$\begin{aligned} &C\left(y_{gC} - y_{gT}\right) - (C + dC)\left(y_{gC} + dy_{gC} - y_{gT}\right) \\ &+(T + dT)\left(y_{gT} + dy_{gT} - y_{gT}\right) - (V + dV)dx + \frac{1}{2}pdx^2 = 0 \end{aligned} \tag{2.60}$$

In the infinitesimal deformation theory, the second order differential terms can be neglected.

$$V = -C\frac{\partial y_{gC}}{\partial x} + T\frac{\partial y_{gT}}{\partial x} - y_{gC}\frac{\partial C}{\partial x} + y_{gT}\frac{\partial T}{\partial x} \tag{2.61}$$
$$(\because dC = dT)$$

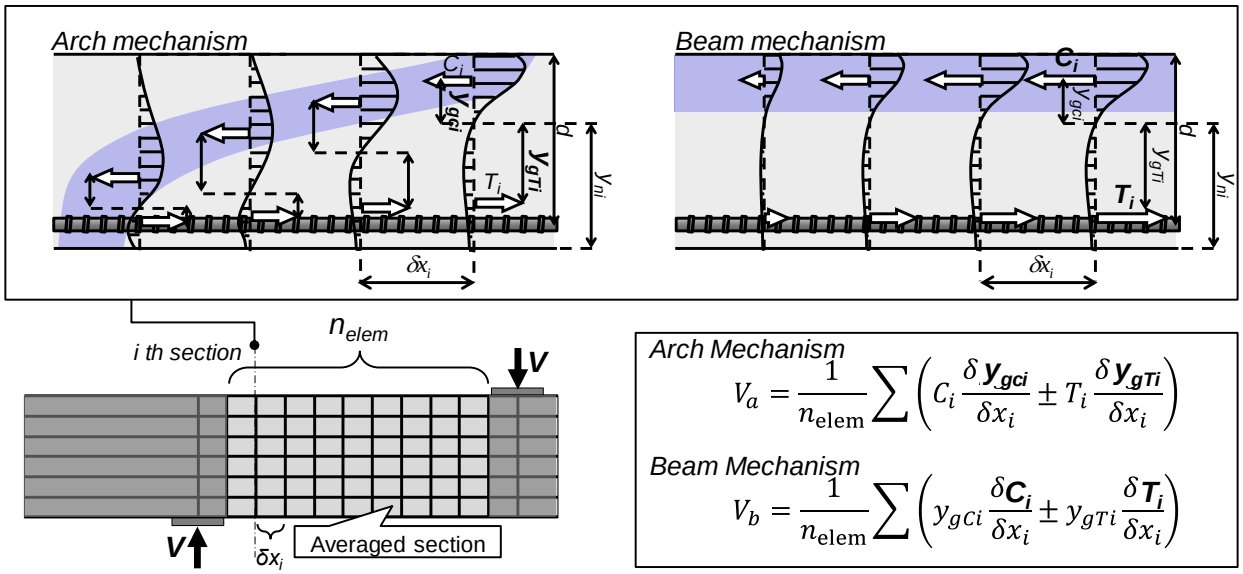

Figure 2.7 Concept of numerical expansion in decomposition of the load carrying mechanism

From the definitions of load carrying mechanism,

$$V_a = -C\frac{\partial y_{gC}}{\partial x} + T\frac{\partial y_{gT}}{\partial x} \tag{2.62}$$

$$V_b = -y_{gC}\frac{\partial C}{\partial x} + y_{gT}\frac{\partial T}{\partial x} \tag{2.63}$$

(2.62) and *(2.63)* are corresponding to *(2.58)* and *(2.59)* respectively. Plus or minus sign of the equations is changed by the definition.

The equations *(2.62)* and *(2.63)* can be derived by considering the parts of the equilibrium condition of resultant forces shown in Figure 2.6. It is confirmed that the beam mechanism depends on the differences of compressive force (*dC*) and tensile force (*dT*), and that the arch mechanism is derived from constant resultant forces (*C* and *T*) between considering cross section and next cross section. Thus, it was understood that the arch mechanism is obtained by the constant part of the stresses in that of next cross section, and that beam mechanism is obtained by the differences of stresses in that of next cross section (Figure 2.6).

The conceptual figure of contribution of arch and beam mechanism on the rebar and concrete after the appearance of arch mechanism is also illustrated in Figure 2.6. The contribution of arch and beam mechanism on the stress distribution of concrete and rebar can be regarded as follows; the arch mechanism is caused by the stress which differed from the stress at the supporting point and distributed constantly in longitudinal direction, and the beam mechanism is caused by the stress which is changed in longitudinal direction as the difference part between the contributed stress in arch mechanism and actual stress.

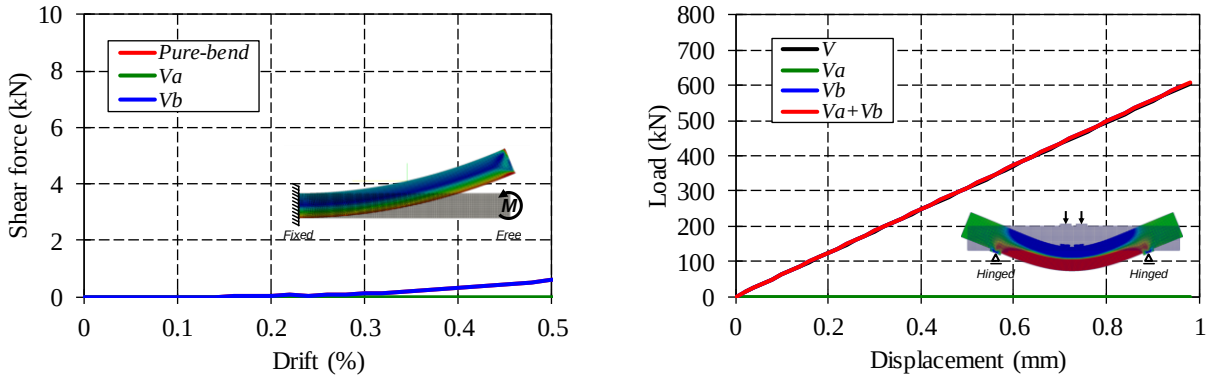

(a) Pure bending condition *(b) Four points bending condition*

Figure 2.8 Validity of decomposition method

2.2.3. Numerical expansion for calculation

In the numerical expansion, $\boldsymbol{V_a}$ and $\boldsymbol{V_b}$ were averaged in the shear span except for the position of loading plates where the internal shear force of the beam was not equal to the external shear force due to distributed loads on the loading plates (Figure 2.7). Discretizating formula of *(2.58)* and *(2.59)* are,

$$\boldsymbol{V_a} = \frac{1}{n_{elem}} \sum_i \begin{pmatrix} 1 & 1 & 0 & 0 \\ 1 & -1 & 0 & 0 \end{pmatrix} \left(C_i \frac{\delta y_{gCi}}{\delta x_i} \quad T_i \frac{\delta y_{gTi}}{\delta x_i} \quad y_{gCi} \frac{\delta C_i}{\delta x_i} \quad y_{gTi} \frac{\delta T_i}{\delta x_i} \right)^T \qquad (2.64)$$

$$\boldsymbol{V_b} = \frac{1}{n_{elem}} \sum_i \begin{pmatrix} 0 & 0 & 1 & 1 \\ 0 & 0 & 1 & -1 \end{pmatrix} \left(C_i \frac{\delta y_{gCi}}{\delta x_i} \quad T_i \frac{\delta y_{gTi}}{\delta x_i} \quad y_{gCi} \frac{\delta C_i}{\delta x_i} \quad y_{gTi} \frac{\delta T_i}{\delta x_i} \right)^T \qquad (2.65)$$

Where, n_{elem}: number of element in averaged span, δx_i: length of FEs.

By using *(2.64)* and *(2.65)* for calculating, the solutions which neglect the effect of disturbance of stress fields can be obtained.

2.2.4. Validity of decomposition method

To confirm the validity of the calculation, the calculation for elastic FE model made by steel (elastic modulus: 205800 N/mm^2) was conducted under following two conditions: pure bending condition and four points bending condition. In case of pure bending condition, the cross sectional shear force should be zero, and in case of four points bending condition, the contributed load of arch mechanism should be zero because position of resultant force in longitudinal direction is not changed in elastic beam. The shape of target beam was 2010 mm in longitudinal direction and 230 mm in vertical direction and 150 mm in perpendicular to the longitudinal direction. The pure bending condition was produced by application of the

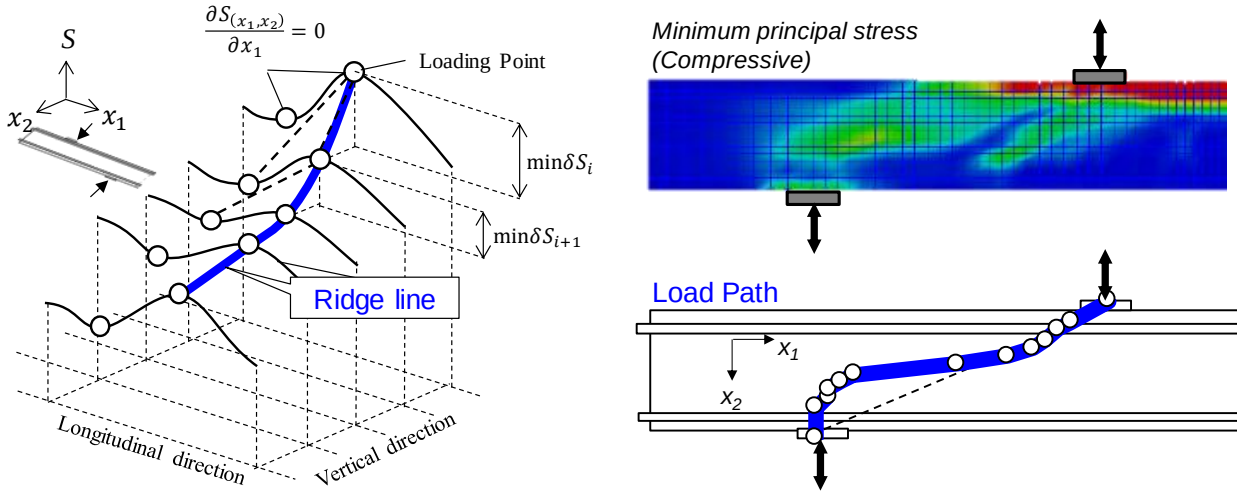

(a) Concept of ridge line in stress distribution *(b) Calculating example*

Figure 2.9 Concept of load path

concentrating moments at the edge part of the beams. The shear span of the beam was 600 mm in the four points bending condition.

The results of calculations are shown in Figure 2.8. It was confirmed that the shearing forces in arch and beam mechanism were almost zero against increase in the drift of the beam under pure bending condition (Figure 2.8 *(a)*), and that the beam resisted the load by only beam mechanism under four points bending condition (Figure 2.8 *(b)*). Therefore, the validity of calculating method was confirmed.

2.3 Load Path

To visualize the load carrying mechanism which was shown in the previous section, the load path was proposed in this study. The load path was defined as the ridge line of minimum (compressive) principal stress which was obtained from the results of FE analysis as shown in Figure 2.9. By introducing the concept of load path, the stress flow can be represented obviously. To calculate the ridge line, a special set of points was required. The set of points was determined as the gradient between the special points against member axis direction was equal to zero. The ridge line was given when the stress difference took the minimum value in the set of points and the ridge line was started from the loading point (Figure 2.9 *(a)*). That is,

$$(LP_1, LP_2) = \left\{ (x_1, x_2) \;\middle|\; (x_1, x_2) \in \mathbb{R}^2, \left(\frac{\partial S_{(x_1,x_2)}}{\partial x_j} = 0 \;\wedge\; \delta S_i = |\min\delta S_i| \right) \right\} \qquad (2.66)$$

Where, LP_1: coordinate of load path in x_1 direction, LP_2: coordinate of load path in x_2 direction, $x_j = (x_1, x_2)$, $S_{(x_1,x_2)}$: minimum principal stress, $\delta S_i = S_i - S_{i+1}$ $(i = 1,2,3,\ldots,n_{nod})$. The Visual Basic (*VB*) was used as a calculation programming code. The actual code is shown in

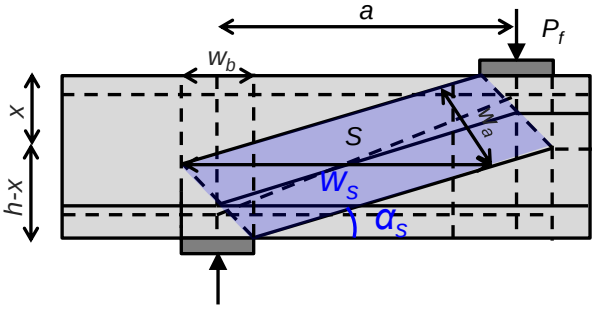

Figure 2.10 Basic model

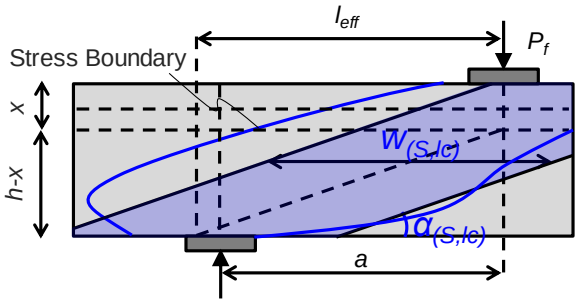

Figure 2.11 Concept of derivation in effective strut width and angle

Appendix. B.

The calculating results of the load path is shown in Figure 2.9 *(b)*. It is confirmed that the stress flow can be represented more clearly compared with the stress distribution map by introducing the concept of load path.

2.4 Equivalent Effective Strength Coefficient based on Strut and Tie Model

2.4.1. Outline of equivalent effective strength coefficient

The load carrying mechanism of cracked RC beam can be described qualitatively by using the decomposition method and concept of load path. For the quantitative description, the method that difference of load carrying mechanism is expressed as a change in the coefficient of concrete strength in strut and tied model was proposed.

In the cracked RC beams, it is expected that the load carrying mechanism is changed by propagation of micro-cracks in the sound concrete and shear transfer on the corrosion cracks. Focusing on strut and tie model which can express the load carrying mechanism simply, it is regarded that stress transfer area is changed by the strut width and strut angle. In the recent design code[7]-[9], effective strength which can be obtained by multiplying effective compressive coefficient to design strength is used. In general, the coefficient takes 0.4-1.0 by considering of condition of strut. If the strut width and angle is changed, ultimate load of strut is also changed. Thus, there is a possibility that the effect of corrosion crack can be explained as a change in the "equivalent effective compressive coefficient". This section describes the derivation method of equivalent effective compressive coefficient to express the effect of change in the load carrying mechanism due to existence of corrosion cracks as a concept for design code.

2.4.2. Derivation of equivalent effective strength coefficient

In RC beams which have corrosion cracks in member axis direction, compressive strut is

formed across the crack surface. In this case, there is a possibility that change in the strut angle caused by shear stress transfer on the crack surfaces occurs in the direction of principal stress in the continuous body with cracks. On the other hand, there is a possibility that propagation of micro-cracks due to cyclic stress changes the microscopic compressive stress transfer area. It is expected that the change in microscopic compressive stress transfer area appears as the change in compressive strut width. These changes in the strut angle and width change the fatigue strength. Therefore, this research proposed the method to replace the change in strut angle and width as the equivalent effective strength coefficient.

Assumed that strut is compressive stress transferring member, strut width is decided by height of neutral axis and loading plate width as shown in Figure 2.10. When this model is used, failure load of strut can be expressed as follows.

$$P_{fS} = -\upsilon f_c' b w_s \sin^2 \alpha_s \qquad (2.67)$$

Where, P_{fS}: failure load of strut, υ: effective strength coefficient, f_c': compressive strength of concrete, b: beam width, w_s: strut width, α_s: strut angle. In this derivation, it is assumed that cross sectional shape of beam is rectangular shape.

The failure load of strut can be expressed as another form by using effective strut width and angle which includes effect of corrosion cracks.

$$P_{fS} = -f_c' b w_{(S,l_c)} \sin^2 \alpha_{(S,l_c)} \qquad (2.68)$$

Where, S: upper limit load ratio, l_c: corrosion crack length, $w_{(S,l_c)}$: effective strut width, $\alpha_{(S,l_c)}$: effective strut angle.

From *(2.67)* and *(2.68)*, equivalent effective strength coefficient is derived as,

$$\nu_{s(S,l_c)} = \frac{w_{(S,l_c)} \sin^2 \alpha_{(S,l_c)}}{w_s \sin^2 \alpha_s} \qquad (2.69)$$

$w_{(S,l_c)}$ and $\sin \alpha_{(S,l_c)}$ were calculated by minimum (compressive) principal stress which was obtained from the result of FE analysis. The concept regarding the calculation is shown in Figure 2.11.

$w_{(S,l_c)}$ was sum of averaged size of FE which existed inside of stress boundary determined from geometrical condition of beams.

$$w_{(S,l_c)} = \frac{1}{h} \sum_i \sum_j \left\{ 1 - H_{(\sigma_{ij} - \sigma_{3min})} \right\} w_{ij}^{x_2} \qquad (2.70)$$

Where, h: height of beam, i, j: index regarding inner surface coordinate, $w_{ij}^{x_2}$: finite element size in longitudinal coordinate, $H_{(\sigma_{ij} - \sigma_{3min})}$: *Heaviside* function.

The threshold of stress boundary was given as constant multiplication of transferred stress in compressive strut.

$$\sigma_{3min} = -n\frac{P_{max}}{bw_s \sin\alpha_s} \tag{2.71}$$

Where, n: scale factor, P_{max}: upper limit load. In the case of static loading, $\nu_{s(S,l_c)} = 0$ should be satisfied. n was given to satisfy this condition. By this modification, cyclic damage and position of corrosion cracks can be represented as change in effective strut angle and width compared with sound state.

$\sin\alpha_{(S,l_c)}$ was given from the middle point of stress boundary and neutral axis in the following equation.

$$\sin\alpha_{(S,l_c)} = \frac{h-x}{\left\{{l_{eff}^{\alpha}}^2 + (h-x)^2\right\}^{0.5}} \tag{2.72}$$

Where, l_{eff}^{α}: distance between loading point and middle point of stress boundary. x : height of neutral axis calculated by equivalent stress block in ultimate state.

2.5 Summary of Chapter 2

This chapter described description methods of the load carrying mechanism. The methods were obtained from FE analysis. The decomposition method of load carrying mechanism could express the mechanism systematically. Arch and beam mechanisms which represented the contribution of compressive strut and contribution of truss mechanism respectively were calculated from the minimum principal stress in member axis direction. Concept of the load path which was defined as ridge line of minimum principal stress was suitable to visualize these mechanisms. By using this concept, the stress flow became more obvious than the flow deduced by stress distribution directly. The equivalent effective strength coefficient was introduced to express change in the load carrying mechanism due to corrosion cracks quantitatively. The coefficient could be calculated by change in effective strut width and effective strut angle in the strut and tie model. These concepts were applied to describe the load carrying mechanisms in the following chapters.

References in Chapter 2

[1] Maekawa, K., Pimanmas, A., Okamura, H.: Nonlinear mechanics of reinforced concrete, *Spon, London*, 2003.

[2] Maekawa, K., Toongoenthong, K., Gebreyouhannes, E., Kishi, T.: Direct Path-Integral Scheme for Fatigue Simulation of Reinforced Concrete in Shear, *Journal of Advanced Concrete Technology*, Vol.4, No.1, pp.159-177, 2006.2.

[3] Goto, Y.: Cracks Formed in Concrete Around Deformed Tension Bars, *ACI Journal, Proceedings*, Vol.68, No.4, pp.244-251, 1971.

[4] Gebreyouhannes, E., Maekawa, K.: Numerical Simulation on Shear Capacity and Post-Peak Ductility of Reinforced High-Strength Concrete Coupled with Autogenous Shrinkage, *Journal of Advanced Concrete Technology*, Vol.9, No.1, pp.73-88, 2011.2.

[5] Gebreyouhannes, E., Kishi, T., Maekawa, K.: Shear Fatigue Response of Cracked Concrete Interface, *Journal of Advanced Concrete Technology*, Vol.6, No.2, pp.365-376, 2008.6.

[6] Park, R., Paulay, T.: *Reinforced Concrete Structures*, John Wiley & Sons, New York, 1975.

[7] ACI Committee 318: Building Code Requirements for Structural Concrete and Commentary ACI 318-08, pp.379-393, 2008.2.

[8] Schlaich, J., Schafer, K., Jennewein, M. : Toward a Consistent Design of Structural Concrete, *PCI Journal*, Vol.32, pp.74-150, 1987.5-6.

[9] Yun, Y., M., Ramirez, A., J.: Strength of Struts and Nodes in Strut-Tie Model, *Journal of Structural Engineering*, 1996.1.

CHAPTER 3
BEHAVIOR OF RC BEAMS MODELED BY ARTIFICIAL CRACK WITHOUT STIRRUPS

This chapter describes an effect of artificial crack length on fatigue load carrying mechanism of cracked RC beams without stirrups. To make clear the mechanism, cyclic loading experiments and FE analyses were conducted by using the specimens which had different length of artificial cracks. The results indicated that the number of cycles at failure was almost the same as the sound beam under the cyclic load of 40% upper limit load ratio in case of the beams whose static strength was enhanced due to tied arch mechanism. It was demonstrated that the reason was localization of relative damage accumulation area due to linearization of the load path. As a result of calculation of equivalent effective strength coefficient, it was confirmed that the calculated values of the coefficient were higher than the value of most dangerous side in the present design code. It was also described that the calculating methods of the crack starting position and the fatigue life based on strut and tie model were available by application of the theory of elasticity.

3.1 Outline of Cyclic Loading Experiments and FE Analyses

In this section, the outline of cyclic loading experiments and FE analyses to grasp the macroscopic behavior of cracked RC beams without stirrups is explained.

When the position of crack tip changes, the stress distribution which characterize the load carrying mechanism is also changed. Thus, it is expected that the load carrying mechanism of cracked beams is mainly governed by position and width of corrosion cracks. The corrosion cracks occur mainly along tensile rebars in RC beams under corrosion environment. It can be considered that investigation of the load carrying mechanism of the beams which have the corrosion cracks along tensile rebars is important to understand the behavior of cracked RC beams. To grasp the load carrying mechanism of cracked RC beams, the behavior of the RC beams without stirrups should be investigated as the first step because it is expected that the beam mechanism is affected by existence of stirrups.

Moreover, it can be considered that effect of the opening width and non-uniformly shape of corrosion cracks can be regarded as the magnitude of shear transfer in averaged area including corrosion cracks. The effect of the width and the non-uniformity of corrosion cracks can be neglected to investigate the effect of corrosion crack position as main experimental and analytical parameters. Thus, an artificial crack is inserted in the specimens and analytical models to control the effect of the shear transfer on the corrosion cracks in this study. The magnitude of shear transfer on the artificial cracks can be regarded as the shear transfer which is caused by crack width and aggregate interlocking effect on corrosion crack surfaces. From these viewpoints, this study treats the RC beams which have artificial crack instead of corrosion crack.

Consequently, as the first step, the behavior of RC beams which have artificial crack along tensile rebars without stirrups is investigated.

3.1.1. Definition of D and B regions

It is expected that the behavior of cracked RC beams is mainly affected by the position of crack tip which generates stress concentration. The stress concentration is one of the causes of change in the load carrying mechanism. In addition, the magnitude of stress concentration is changed by difference in the stress fields where the crack tip exists in the beam. *D* and *B* regions were focused as the stress fields where the magnitude of stress concentration was different. *D* region is where the stress field is disturbed, that is, *Bernoulli* and *Euler's* assumption cannot be applied. *B* region is where the *Bernoulli* and *Euler's* assumption can be applied. In beam theory based on *Bernoulli* and *Euler's* assumption, contribution of vertical stress is neglected (Figure 3.1). Thus, it is considered that definition of *D* region should be based on the contribution of vertical stress, and *D* region can be redefined as where the contribution of vertical stress cannot be neglected.

If this assumption is true, in the *D* region, shear stress decreases compared with that in the *B*

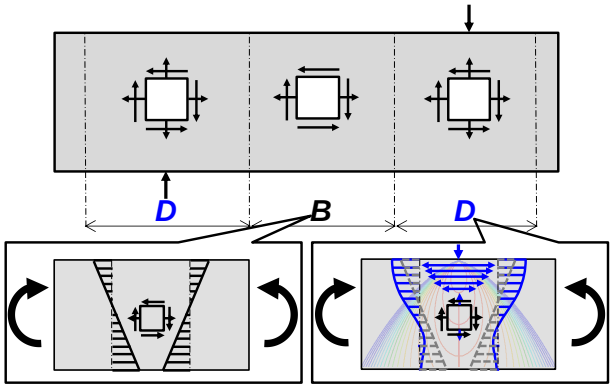

Figure 3.1 Concept of stress disturbance in D region

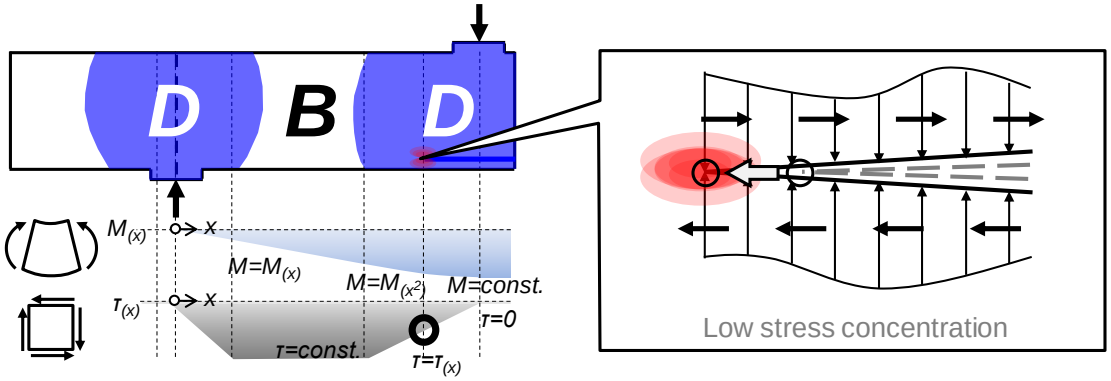

(a) Case that crack tip exists inside of D region

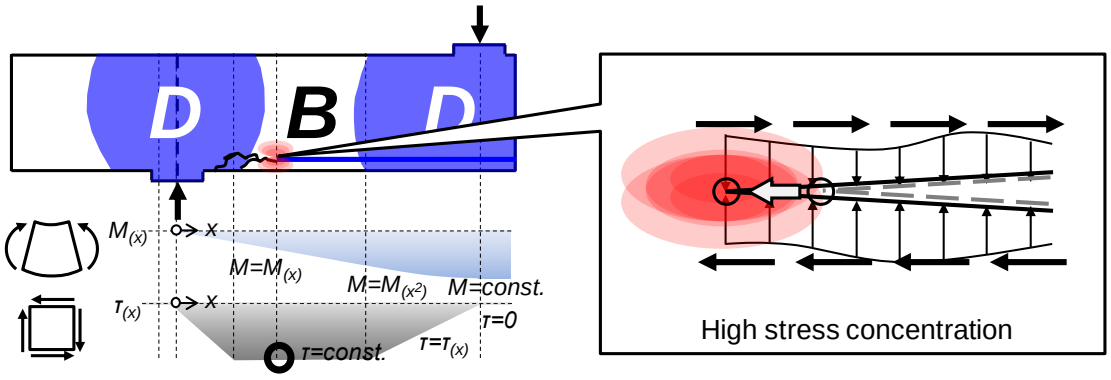

(b) Case that crack tip exists inside of B region

Figure 3.2 Prediction of stress concentration in D and B regions

region (Figure 3.2). In the *D* region, the cross sectional moment can be expressed as the quadratic function against the longitudinal coordinate due to contribution of vertical stress. The dimension of shear stress against the longitudinal coordinate decreases because the first deferential of moment represents the order of shear stress in longitudinal direction. Thus, it is expected that higher shear stress occurs in the *B* region and it is predicted that the higher shear stress causes the higher stress concentration at the position of crack tip. When the high stress concentration occurs, it is expected that the load carrying mechanism which is affected by stress fields is changed. Consequently, crack tip positions were changed as one of analytical parameters

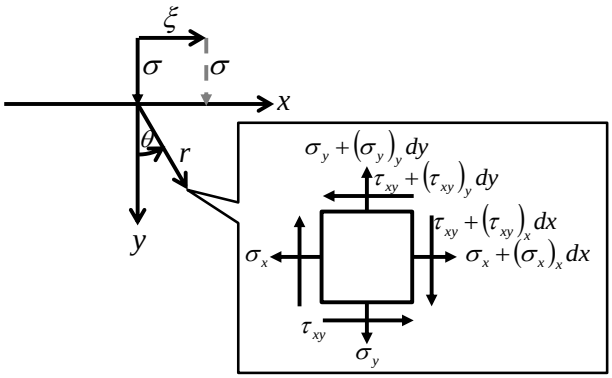

Figure 3.3 Definition of stress direction in half infinity elastic body

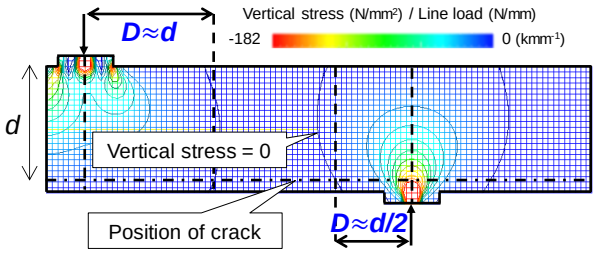

Figure 3.4 Definition of D region based on vertical stress distribution

based on *D* and *B* regions.

It was necessity to confirm the actual *D* region to decide the position of crack tip. The *D* region was defined based on the theory of elasticity as the region where the contribution of vertical stress cannot be neglected. The derivation method is described as follows.

The stresses in a two dimensional problem can be expressed as the following equations by using stress function $U_{(x,y)}$,

$$\sigma_{x(x,y)} = (U)_{yy} \tag{3.1}$$

$$\sigma_{y(x,y)} = (U)_{xx} \tag{3.2}$$

$$\tau_{xy(x,y)} = -(U)_{xy} \tag{3.3}$$

Where, $(U)_{x_i} = \partial_{x_i} U = \partial U / \partial x_i$, $\sigma_{x(x,y)}$: stress in longitudinal direction, $\sigma_{y(x,y)}$: stress in vertical direction, $\tau_{xy(x,y)}$: conjugate shear stress. When the relationships above are satisfied, the stress function also satisfies the following bi-harmonic equation.

$$\Delta\Delta U_{(x,y)} = \nabla^2\nabla^2 U_{(x,y)} = \left(\partial_{xx} + \partial_{yy}\right)^2 U_{(x,y)} = \left(\partial_{xx} + \partial_{yy}\right)\left(\sigma_x + \sigma_y\right) = 0 \tag{3.4}$$

By the transformation to polar coordinate system, *(3.4)* can be rewritten as the following equation.

$$\begin{aligned}\nabla^2\nabla^2 U_{(r,\theta)} = {} & \frac{1}{r^4}(U)_{\theta\theta\theta\theta} + \frac{2}{r^2}(U)_{rr\theta\theta} - \frac{2}{r^3}(U)_{r\theta\theta} + \frac{4}{r^4}(U)_{\theta\theta} \\ & + (U)_{rrrr} + \frac{2}{r}(U)_{rrr} - \frac{1}{r^2}(U)_{rr} + \frac{1}{r^3}(U)_r = 0\end{aligned} \tag{3.5}$$

Considering the stress field in a half infinity elastic body with vertical stress (Figure 3.3), the stress function can be set as,

$$U_{(r,\theta)} = r f_{(\theta)} \tag{3.6}$$

By substitution *(3.6)* into *(3.5)*,

$$(f)_{\theta\theta\theta\theta} - 2(f)_{\theta\theta} + 4(f)_{\theta\theta} + f = 0 \tag{3.7}$$

Thus,

$$U_{(r,\theta)} = r(C_1 \cos\theta + C_2 \sin\theta + C_3\theta \cos\theta + C_4\theta \sin\theta) \;\; C_i: a.c. \tag{3.8}$$

By the transformation to polar coordinate system, the stresses in polar coordinate can be written as,

$$\sigma_{r(r,\theta)} = \frac{1}{r}U_r + \frac{1}{r^2}U_{\theta\theta} \tag{3.9}$$

$$\sigma_{\theta(r,\theta)} = U_{rr} = 0 \tag{3.10}$$

$$\sigma_{r\theta(r,\theta)} = \frac{1}{r^2}U_\theta - \frac{1}{r}U_{r\theta} \tag{3.11}$$

Where, $\sigma_{r(r,\theta)}$: stress in r direction, $\sigma_{\theta(r,\theta)}$: stress in θ direction, $\sigma_{r\theta(r,\theta)}$: conjugate shear stress in polar coordinate.

From *(3.9)*,

$$\sigma_{r(r,\theta)} = \frac{2}{r}(C_4 \cos\theta - C_3 \sin\theta) \tag{3.12}$$

Boundary conditions are,

$$\sigma_{r(r,\theta)} = \sigma_{r(r,-\theta)} \tag{3.13}$$

$$\int_0^\infty \sigma_{r(r,\theta)} dy = \sigma \tag{3.14}$$

From *(3.13)* and *(3.14)*, $C_3 = 0$ and $C_4 = -\sigma/\pi$ are obtained respectively. Thus,

$$\sigma_{r(r,\theta)} = -\frac{2\sigma}{\pi r}\cos\theta \tag{3.15}$$

From the transformation of Cartesian coordinate system,

$$\sigma_{y(x,y)} = -\frac{2\sigma}{\pi}\frac{y^3}{(y^2+x^2)^2} \tag{3.16}$$

In case that the distance ξ is away from the origin shown in Figure 3.3, the vertical stress can be rewritten as,

$$\sigma_{y(x-\xi,y)} = -\frac{2\sigma}{\pi}\frac{y^3}{\{y^2+(x-\xi)^2\}^2} \tag{3.17}$$

The *D* region was defined as the region where $\sigma_{y(x,y)} < 0$ (negative value represents compressive side) was satisfied.

The distribution of $\sigma_{y(x,y)}$ is shown in Figure 3.4. The region where $\sigma_{y(x,y)} = 0$ at the position of crack in vertical direction was formed as half of effective depth away from the supporting point and effective depth away from the loading point. This region was defined as the *D* region in this study.

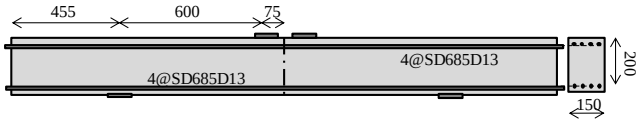

(a) N

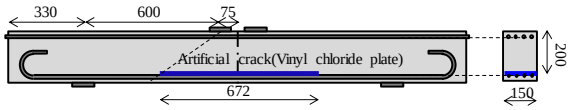

(c) B1

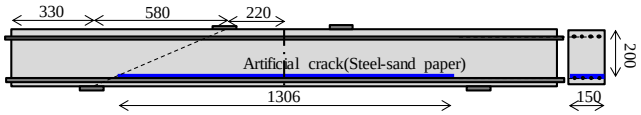

(b)B2S

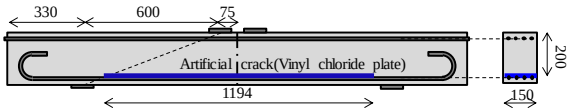

(d) B2

(*unit:* mm)

Figure 3.5 Shape and size of specimens

Table 3.1 Experimental cases

Name of specimens	Materials of artificial crack	Upper limit load ratio (%)	Upper limit load (kN)	Compressive strength of concrete (MPa)	Number of cycle at failure
N-100	—	100	86.8	39.2	1
B2S-100	Steel-sand paper		200.0	35.3	1
B1-100	Vinyl chloride plate		215.1	35.9	1
B1-74		74	160.0		1057
B1-33		33-37	70-80	40.2	1838900 (Non-failure)
B2-100		100	193.4	35.8	1
B2-72		72	140.0		22364
B2-38		38	73.0	40.2	30408 (Stopped)

*In case of *B1-33*, upper limit load was changed 70 kN – 80 kN at 1020990 cycle because the failure did not occur even after 1000000 cycles.

3.1.2. Details of experiment

a) Experimental cases

To grasp the macroscopic behavior of RC beams which have artificial crack along tensile rebars without stirrups, static and cyclic loading experiments were conducted.

The size and shape of specimens are shown in Figure 3.5. The *a/d* (shear span ratio) was set around 3.0 to make clear the load carrying mechanism of slender beams. Names of specimens represented the position of artificial crack which was inserted in the specimens to simulate severe state of corrosion crack and the magnitude of upper limit load ratio. All of the experimental cases are shown in Table 3.1. The first characters of *N, B1*and *B2* represented that sound, short crack and long crack whose tips existed inside *B* region respectively. The specimen had two types of the artificial crack made by composite materials of steel plate-sandpaper and vinyl chloride plate to confirm the effect of difference in the shear transfer on the crack surfaces. The specimen *B2S* had the composite type of artificial crack made by steel plate-sandpaper and other specimens had the artificial crack made by vinyl chloride plate. In the case of artificial crack made by steel plate-sandpaper, a sandpaper was pasted by epoxy adhesive on a steel plate whose thickness was 1.5 mm and the composite plate was arranged as the two plates face to face each other. In case of artificial crack made by vinyl chloride plate,

only one plate was arranged on the tensile rebars directly. As a result of the shearing test which is mentioned in the following section, the shear transfer of artificial crack made by steel plate-sandpaper was corresponding to that of the crack with 1.3 mm width by the shear transfer model which was proposed by the previous research[1]. The specimens were designed to fail in shear in sound state.

The Ordinary Portland Cement was used to make specimens. The compressive strengths at the time of experiment are shown in Table 3.1. The required properties of concrete were; maximum size of cores aggregate was 20 mm, slump was 12 cm, air content was 4.5±1.5 %. The experiments were conducted after 7 days sealing.

b) Loading condition

The static loading experiment and two types of cyclic loading experiments were conducted for each beam. After the diagonal crack occurred, the load carrying mechanism of the beam under cyclic loading might be changed because damage accumulating area can be change from the case without diagonal cracks. Thus, the upper limit loads were decided as the higher and lower load than the predicting equation of diagonal cracking load which was proposed by the previous research[2] (Table 3.1). In case of *B1-33*, upper limit load was changed 70kN to 80kN at 1020990 cycle because the failure did not occur even after 1000000 cycles.

The loading experiments were conducted under four-point bending condition. In case of static loading, the loading speed was fixed at 0.1 mm/sec for all specimens. Failure in static loading was decided as the maximum load of each beam. In case of cyclic loading, the same upper limit load was applied on each beam until failure. The lower limit load was fixed at 9.8 kN in all beams. Static loading was conducted when the load reached the target upper limit load, after that, the target upper limit load was applied under 0.3-0.5 Hz of loading frequency. The failure criteria under cyclic loading of each beam was decided as the middle span displacement of the beam reached the displacement at the static strength.

3.1.3. Details of analysis

a) Analytical cases

Fatigue analyses were conducted to make clear the effect of crack position after the validity of analytical model was confirmed. The FE analysis system which mentioned in **Chapter 2** was used in **Chapter 3**.

Shape and size of analytical models are shown in Figure 3.6. There were three types of *a/d* to confirm the effect of crack introducing positions which were governed by *D* and *B* regions. The analytical cases are shown in Table 3.2. The upper limit load ratios were changed at 100, 80, 60, 40 % of static strength. When the upper limit load ratio was 100 %, the loading

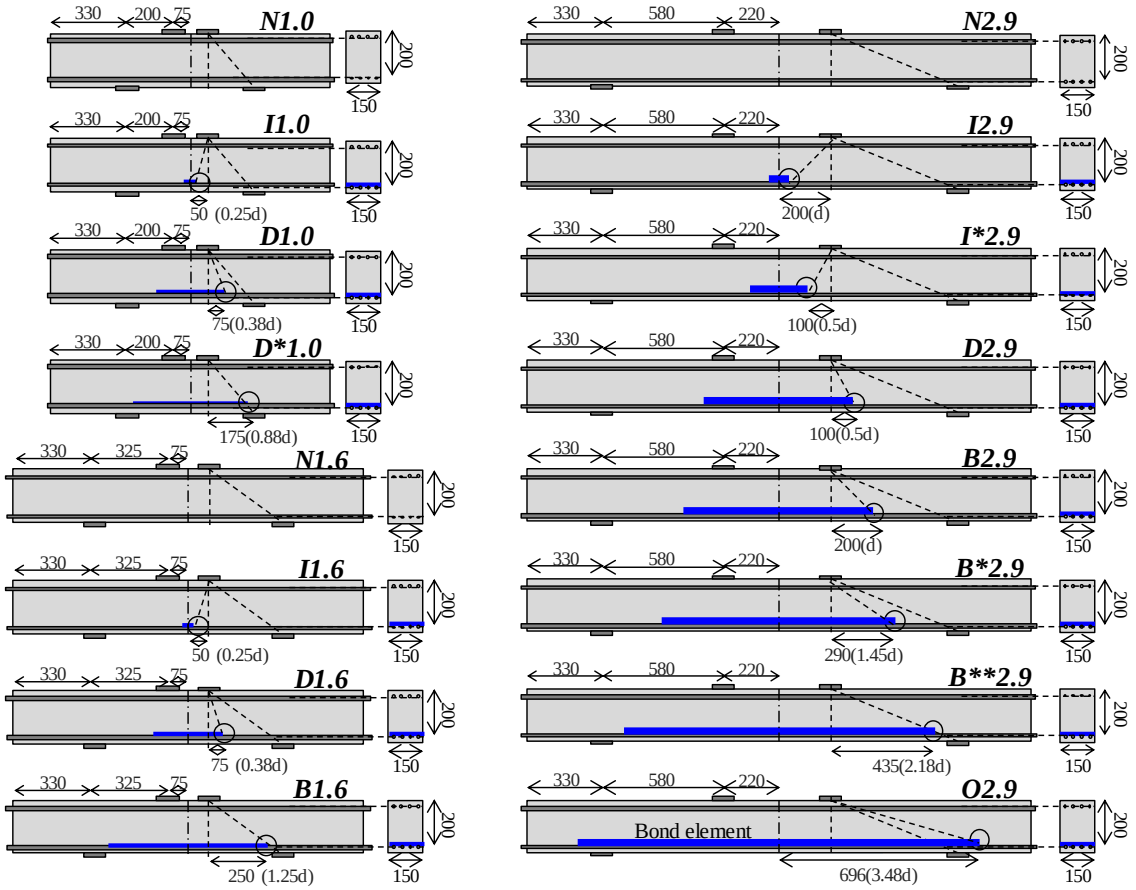

Figure 3.6 Shape and size of analytical models (unit: mm)

condition was similar to the static loading. In case of fixed upper limit load ratios, the magnitudes of upper limit load were changed. To confirm the effect of change in the upper limit load, the analytical case that 60 kN was set as the upper limit load was prepared. It was expected that the load carrying mechanism was changed by the magnitude of upper limit load. The compressive strength of concrete was set at 35 MPa constantly.

b) Property of analytical model

The bond elements were inserted in the analytical models to simulate slip behavior of artificial cracks. The properties of bond element were decided based on the elemental experiments as shown in Figure 3.7. There were mainly four modes to allow slipping and opening in the bond element; shear stiffness in opening and closing mode, and normal stiffness in opening and closing mode. *Mohr-Coulomb's* linear friction law was applied as the property of bond element based on the shear elemental experiment and compressive test. The shear elemental experiment allowed sliding of test surface made by the same materials as applied ones to analytical models of the beams with horizontal and vertical confined forces. As a result of the elemental experiment, the shear and normal stiffnesses in closing mode were obtained as 4.68 N/mm/mm^2 and 294 N/mm/mm^2 respectively. The value of shear stiffness in closing mode corresponded to

Table 3.2 Analytical cases

Name of specimens	Position of artificial crack	Static strength (kN)	Number of cycle at failure				
			Upper limit load ratio				Upper limit load
			100 %	80 %	60 %	40 %	60.0 kN
N1.0	-	365.5	1	4027	592777	112777781	5617777901 ↑
I1.0	Between loading points	345.6	1	5627	172777	115277781	5617777901 ↑
D1.0	*D* region	343.0	1	12652	567777	117777781	5617777901 ↑
*D*1.0*		343.7	1	12527	402777	107777781	5617777901 ↑
N1.6	-	111.8	1	1765277	13277777	432777781	17777777
I1.6	Between loading points	123.0	1	37777	172777	115277781	125277781
D1.6	*D* region	121.6	1	272777	13277777	427777781	122777781
B1.6	*B* region	163.9	1	11777	1165277	135277781	252777781
N2.9	-	89.8	1	577777	115277781	1580277801	117777781
I2.9	Between loading points	105.6	1	7777	115277781	1642777801	117777781
*I*2.9*		106.7	1	2752	115277781	1142777801	-
D2.9	*D* region	115.0	1	76	11902777	1017777801	187777781
B2.9	*B* region	109.5	1	577	17527777	1155277801	-
*B*2.9*		112.0	1	2677	105277781	2292777801	-
*B**2.9*		159.4	1	1764	562777	137777781	205277781
O2.9	Outside of shear span	105.3	1	27277	1665277	407777781	3727777

*The symbol ↑ represents that the beam did not fail after the cycle.

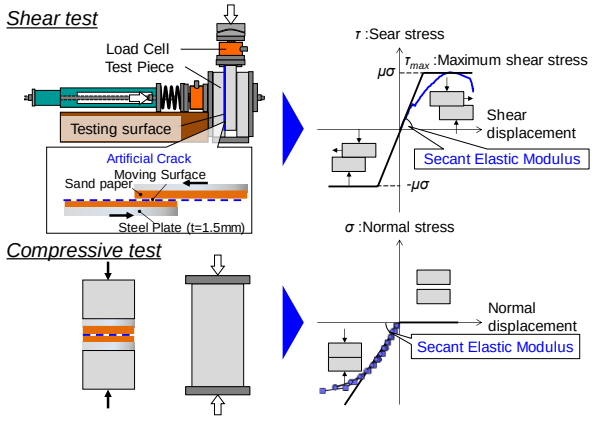

Figure 3.7 Outline of elemental experiments

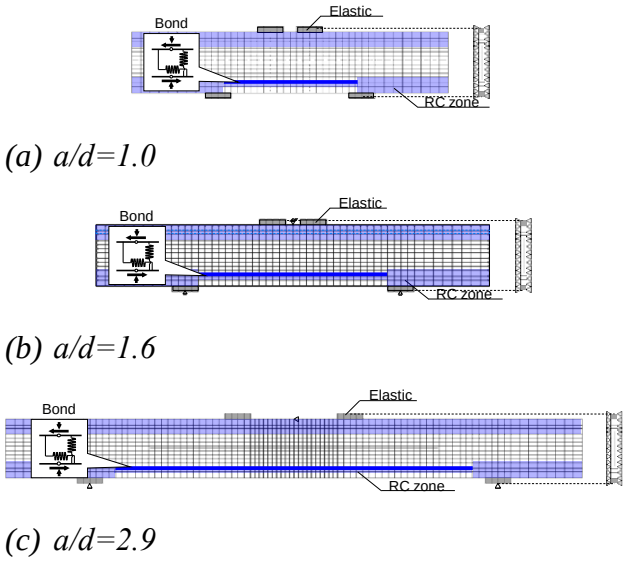

Figure 3.8 Analytical mesh models

that the crack of 1.3 mm width in the proposed shear model by the previous research[1]. The shear and normal stiffnesses in opening mode were set at 0 N/mm/mm^2 because in case of opening mode, the contact of crack surfaces never occurs. The stiffness was calculated as secant elastic modulus of stress-strain relationship. Accumulation of fatigue damage could be considered in concrete elements which were arranged around bond elements.

The analytical mesh models are shown in Figure 3.8. From consideration of symmetry, the elements were divided as aspect ratio was close to 1 in inner surface direction of the beams. The models were restricted in inner surface direction to analyze as the plane strain problem. The models were divided by 6 in beam width direction. The exponential curve was applied as

the tension softening behavior of elements. The index was calculated by volume of element and calculating equation of fracture energy which was proposed by *fib*[3]. In the reinforced concrete elements which has non-zero reinforced ratio, 0.4 was input as the value of index.

c) Loading condition

Static analyses were conducted under displacement control. The displacement speed was 0.06 mm/min. Fatigue analyses were conducted under loading control. The static load was applied until the load reached the target upper limit load. After that, the target upper limit load was applied on each beam under 1 Hz of loading frequency.

Failure in static analysis was decided as the load reached the maximum value. In case of fatigue analysis, the failure criterion of each beam was decided as the displacement reached the displacement of static strength.

3.2 Behavior under Static Loading

In this section, the effect of arch mechanism to the strength under static loading is explained based on static loading experiments and analytical result.

3.2.1. Macroscopic behavior in static loading experiments

The load deflection curve in each beam is shown in Figure 3.9. The calculated value of diagonal cracking load which was obtained by the predicting equation[2] is also shown in the figure. The static strength of *N* was almost the same as the predicted diagonal cracking load. On the other hand, cracked beams (*B2S, B1, B2*) showed about two times larger strength than that of *N*. The stiffness of *N* and *B1* was almost similar in the phase under predicted value of diagonal cracking load. The stiffness of *B2S* and *B2* was almost similar and these were lower than that of *N* and *B1*. It could be considered that the cracked beams (*B2S, B1, B2*) showed tied arch mechanism. To confirm the appearance of the tied arch mechanism, crack distribution map and strain distribution were focused.

The crack distribution map at the failure is shown in Figure 3.10. *N* showed typical diagonal cracking failure. In case of *B2S, B1,* and *B2*, bond splitting failure occurred after propagation of bending crack on the artificial crack surfaces. It was considered that load carrying mechanisms of *B2S, B1,* and *B2* could be regarded tied arch mechanisms. Especially, in case of *B1*, a horizontal crack propagated from the crack tip after the load reached the predicted diagonal cracking failure and the tendency of the load-deflection curve was close to *B2S* and *B2* (Figure 3.10 *(c)*). The diagonal cracks in case of *B1* occurred by buckling of compressive rebar due to the bond splitting.

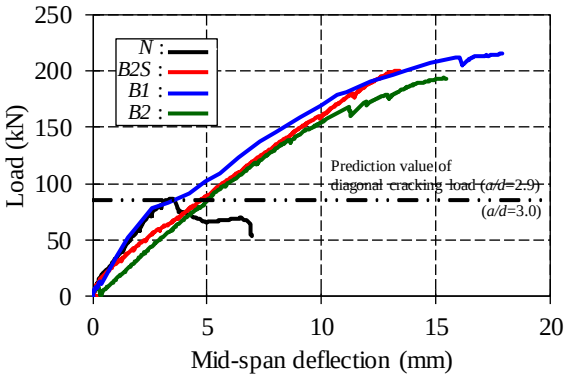

Figure 3.9 Load deflection curve

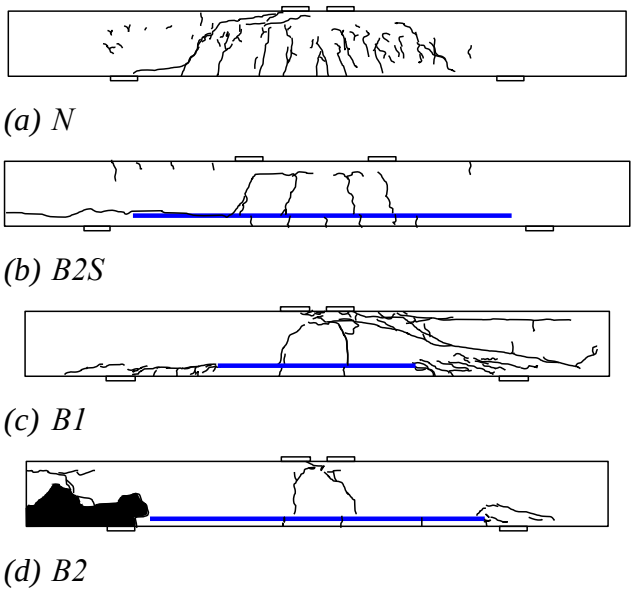

Figure 3.10 Crack distribution at failure

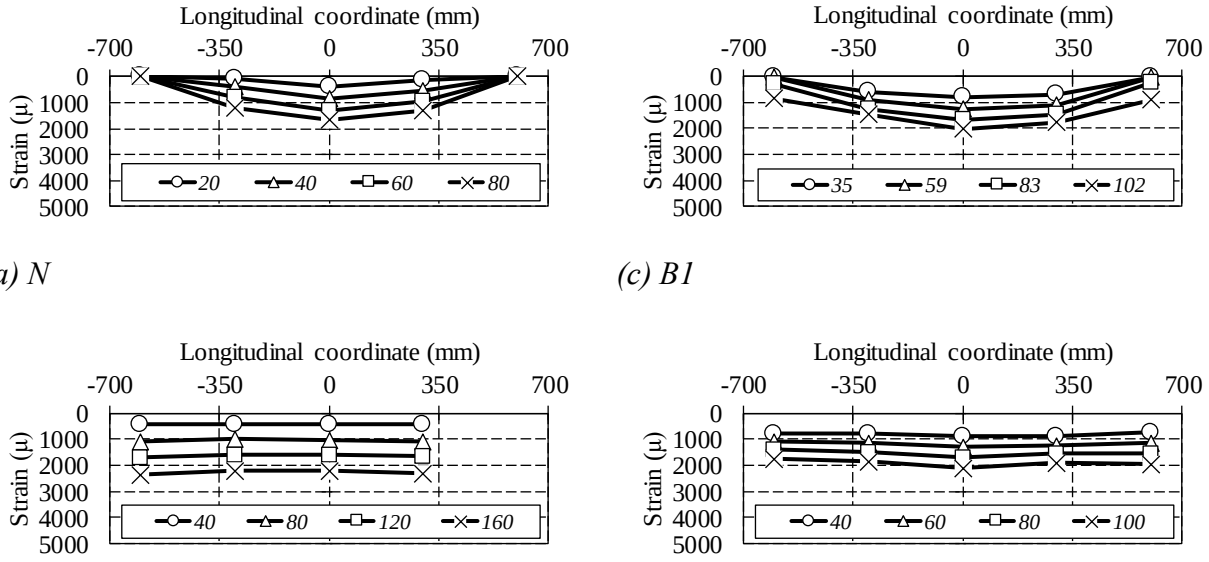

(a) N

(c) B1

(b) B2S

(d) B2

Figure 3.11 Strain distribution of tensile rebar in longitudinal direction

The strain distributions along tensile rebars in each beam are shown in Figure 3.11. The number in the figures means the magnitude of applied load (kN) at the time of measurement. If the strain distributes constantly, the beam shows tied arch mechanism as mentioned later. The bending deformation was confirmed in case of *N* because the magnitude of strain showed relatively high values with increase in the load (Figure 3.11 *(a)*).

In case of *B2S* and *B2*, the magnitudes of strains were almost constant regardless of applied load (Figure 3.11 *(b), (d)*). In case of *B1*, the tendency looks like bending behavior. However, the

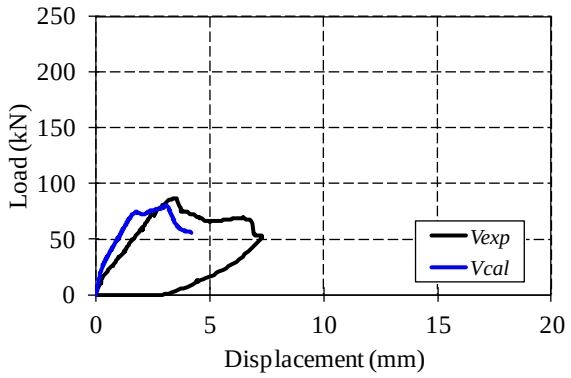

(a) N

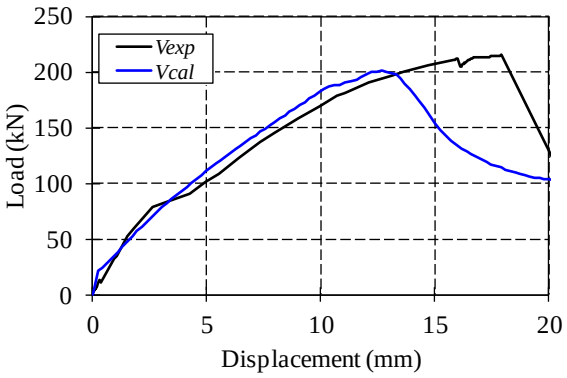

(c) B1

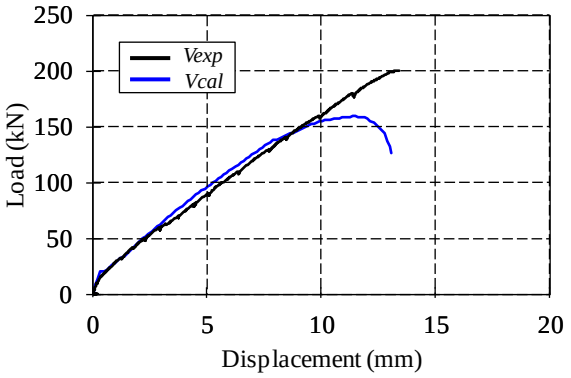

(b) B2S

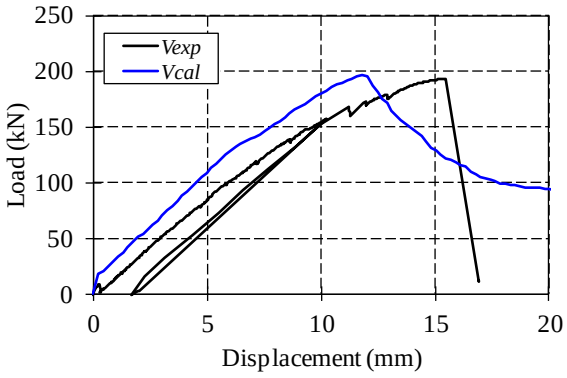

(d) B2

Figure 3.12 Reproducibility in load deflection curves

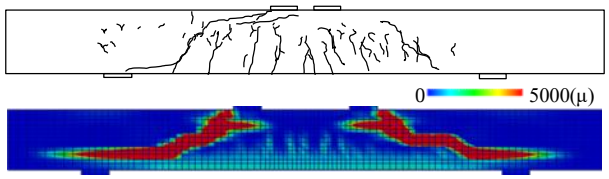

(a) N

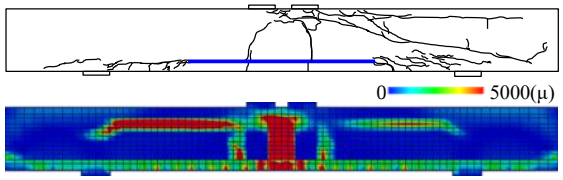

(c) B1

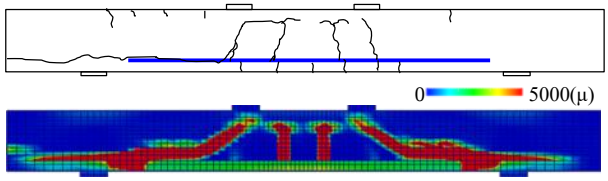

(b) B2S

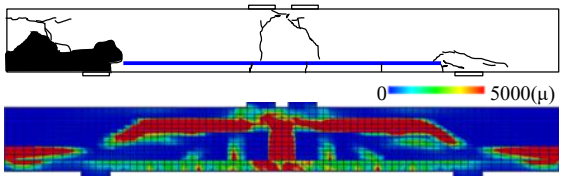

(d) B2

Figure 3.13 Reproducibility in strain distributions at failure

magnitude of strain at the ±600 mm showed higher value than that of *N* (Figure 3.11 *(c)*). This behavior represented that the magnitudes of strains were closed to be constant value. It is expected that the strain distribution behavior was caused by propagation of horizontal cracks because the tendency appeared after propagation of the cracks (after about 90 kN).

When the strain of rebar is constant value, this indicates that tensile force along the tensile rebar is almost constant value. When the tensile force of rebar became constant, the term of contributed load in beam mechanism V_b which was explained in **2.2** was canceled because $\partial C/\partial x = 0$ and $\partial T/\partial x = 0$ ($\because C = const., T = const.$). In this case, it is expected that the contributed load in arch mechanism V_a is predominant. Therefore, it is considered that the cracked beams (*B2S, B1, B2*) showed the tied arch mechanism.

3.2.2. Validity of analytical models

To confirm that the analytical model could reproduce the difference of the load carrying mechanism obtained by experimental results, static analyses were conducted. The reproducibility in the load deflection curves is shown in Figure 3.12. In the reproducing models of the *B1* and *B2*, the bond element as mentioned in the previous section was inserted to simulate the behavior of artificial cracks. The tendencies of load deflection curves which were obtained from analytical and experimental results were almost consistent in each beam. In case of cracked beams (Figure 3.12 *(b), (c), (d)*), increase in the static strength compared with the case of sound beam (Figure 3.12 *(a)*) was confirmed. Thus, it is considered that the increasing tendency of loads due to tied arch mechanism could be reproduced by these analytical models.

In addition, focused on the reproducibility in the strain distributions at failure shown in Figure 3.13, in case of *N*, propagation of diagonal crack at failure agreed well with the experimental result (Figure 3.13 *(a)*). The crack pattern at the time of failure was symmetry in the analysis, however the diagonal crack which reached top side of beam in one side was reached faster than another side. In case of *B2S*, *B1* and *B2,* the bending cracks which propagated on the crack surfaces, and bond splitting failure at the anchorages agreed well (Figure 3.13 *(b), (c), (d)*). Especially, it was confirmed that horizontal cracks propagated from the crack tips in case of *B1* (Figure 3.13 *(c)*). In case of *B1* and *B2,* propagations of cracks along compressive rebar due to bond splitting failure were also confirmed (Figure 3.13 *(c), (d)*). The reproducibility of tied arch mechanism was also confirmed in term of crack distribution. Because the cracked beams showed bond splitting failure at the anchorages which were connecting point of compressive arch rib and tensile rebar as a tendon.

In the both cases of experimental and analytical results, it could be confirmed that the tied arch mechanisms appeared in the cracked beams. Therefore, the validity of analytical model was confirmed, and fatigue analyses were conducted by using these analytical models.

3.2.3. Analytical consideration of load carrying mechanism of cracked RC beams

Before the fatigue analyses, appearance of arch mechanism in case of cracked beams was confirmed by using the decomposition method of load carrying mechanism which was described in **2.2**.

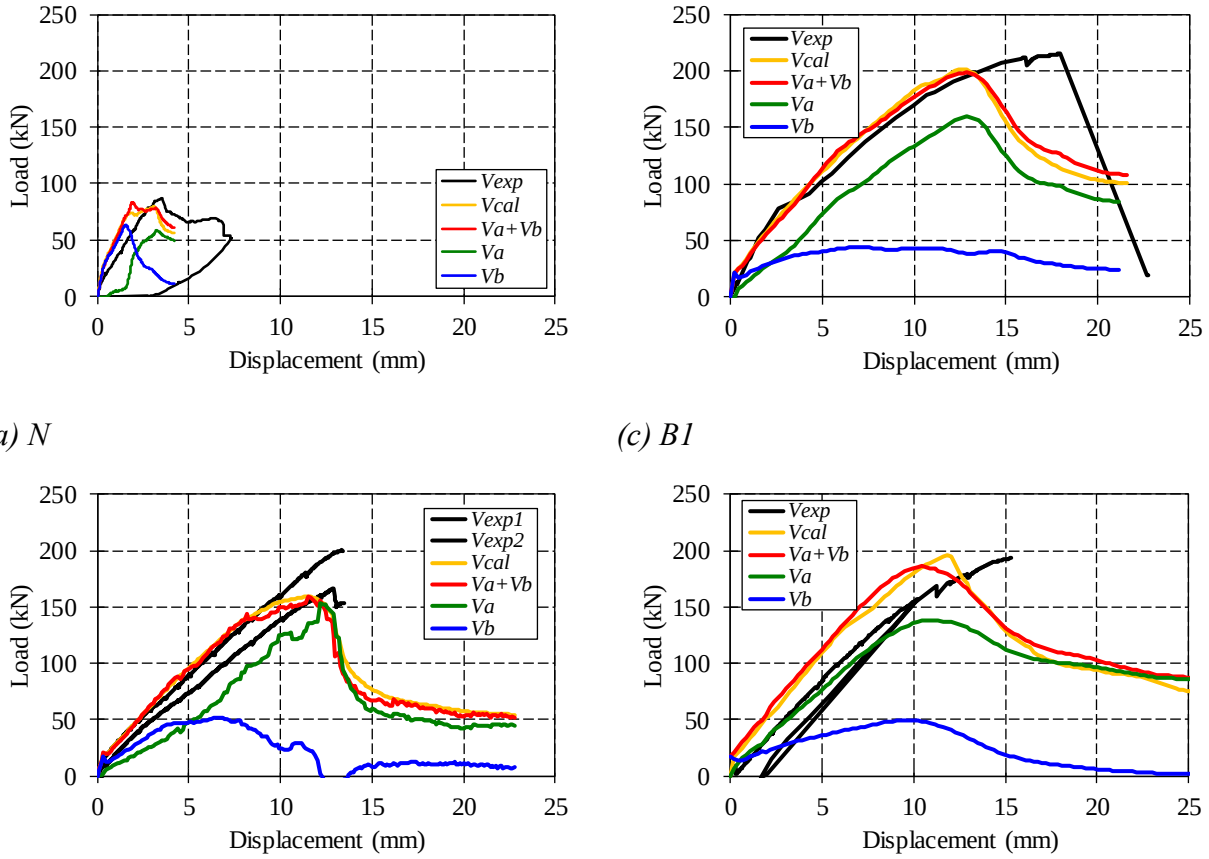

(a) N

(c) B1

(b) B2S

(d) B2

Figure 3.14 Contributed load of arch and beam mechanisms under static loading

Figure 3.14 shows the results of decomposition for each analytical result. The symbols in the figure represented V_{exp}: experimental load, V_{cal}: analytical load, V_a: calculated load of arch mechanism, V_b: calculated load of beam mechanism respectively. Summation of the calculated load of V_a and V_b showed good agreement with the analytical result. The validity of calculation results of V_a and V_b were confirmed. In case of *N*, arch mechanism appeared after loss of beam mechanism. On the other hand, in case of cracked beams *B2S, B1,* and *B2*, arch mechanism was predominant before ultimate failure of the beams. Therefore, it was confirmed that when the beam had cracks along tensile rebars, tied arch mechanism appeared and static strength was enhanced compared with sound beams. In addition, it is considered that in case of the beams in which crack tips exist inside of *B* region, arch mechanism was predominant.

3.3 Behavior under Cyclic Loading

In this section, effect of artificial crack length to fatigue resistibility of beams is discussed based on the result of cyclic loading experiments and results of fatigue analyses by using the analytical models whose validity was confirmed.

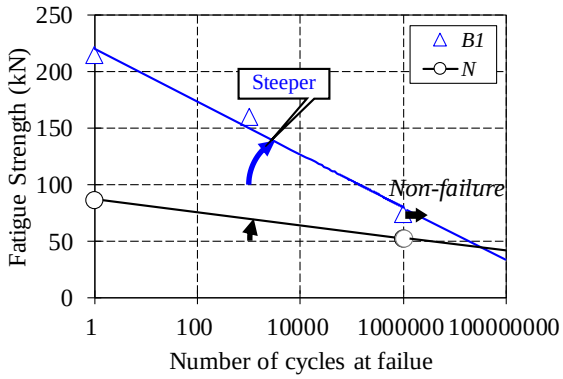

Figure 3.15 Change in fatigue strength against number of cycles at failure

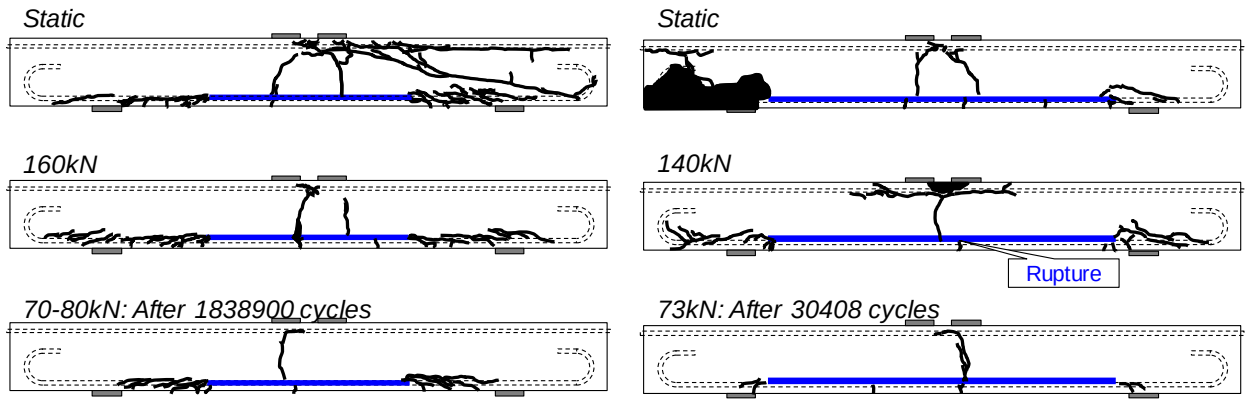

(a) B1 *(b) B2*

Figure 3.16 Comparison of failure mode at each upper limit load

3.3.1. Macroscopic behavior in fatigue experiments

Figure 3.15 shows the relationship between fatigue strength and number of cycles at failure. The fatigue strength represents the upper limit load which is applied until the failure of beams in this study. The logarithmic regression curves in each case were illustrated in the figure. The result of *B1* is illustrated instead of *B2* as the result of cracked beam because the load carrying mechanism under static loading was not changed remarkably. In case of *N*, the fatigue strength under 1000000 loading cycles was plotted based on result of previous study. Focused on the gradient of the regression curve, it was confirmed that the gradient in case of *B1* was steeper than that of *N*. This means that when relatively low cyclic load is applied on the beams which have crack tips inside B region, the fatigue life might be decreased compared with the sound beams. It was deduced that the fatigue resistibility of cracked beams which showed arch mechanism was lower than that of sound beams.

Figure 3.16 shows the crack distribution map at the time of cyclic loading was stopped. In case

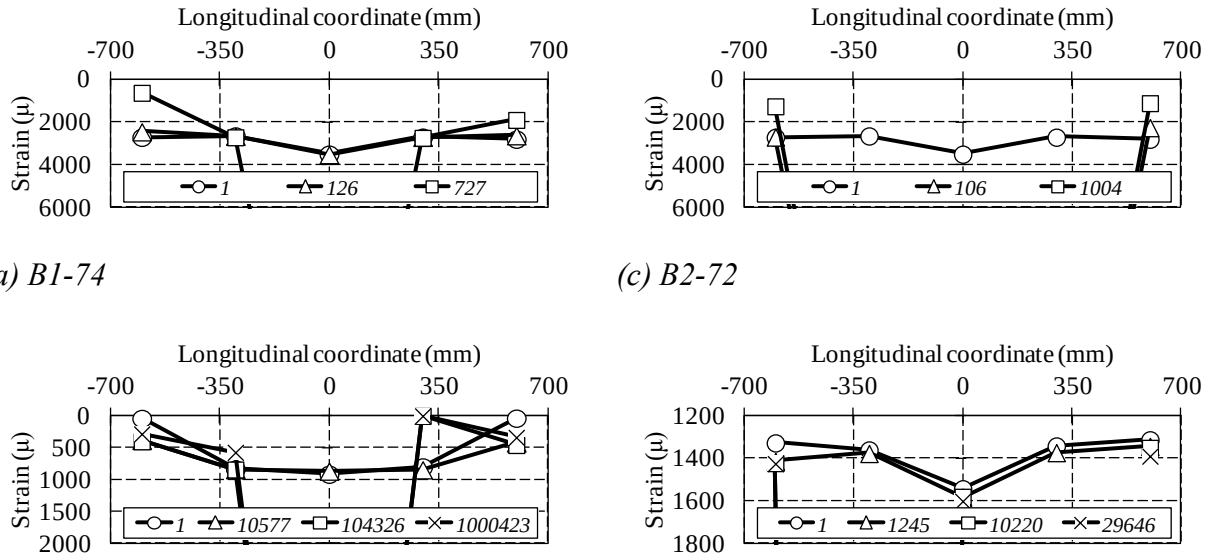

(a) B1-74

(c) B2-72

(b) B1-33

(d) B2-38

Figure 3.17 Strain distribution of tensile rebar under cyclic loading

of static loading, the cracked beams *B1-100* and *B2-100* failed in bond splitting mode. However, in case of cyclic loading, failures were caused by cyclic opening of bending cracks which propagated on the artificial crack surfaces regardless of magnitude of upper limit load. Especially, failure of *B2-72* was caused by rupture of tensile rebar at the middle span of the beam. In addition, in case of *B1-74* and *B1-33*, propagation of horizontal crack which was observed in case of static loading was confirmed. In case of *B1-33* and *B2-38*, cyclic loading was stopped at 1838900 and 30408 cycles respectively because extreme opening of bending cracks was observed.

Figure 3.17 shows the strain distribution along tensile rebars under cyclic loading. The number in these figures represents number of cycles at the time of measuring. The strains at the middle span in each beam could not be measured at 727, 57000, and 1000 cycles in *B1-74*, *B1-33* and *B2-72* respectively. Moreover, increase in strain at the middle span in each beam was confirmed with increase in the number of cycles.

From the crack distribution map which showed propagation of bending crack and tendencies of strain distributions which showed cyclic bending deformation, it was confirmed that the beams which had crack tips inside of *B* region represented bending fatigue failure in case of cyclic loading. It could be considered the reason of occurrence of bending fatigue failure was that large cyclic tensile force was transferred on the tensile rebar due to appearance of tied arch mechanism in case of cracked beams.

There is a possibility that the behavior is changed by difference in the position of artificial crack tips. From this view point, fatigue analyses were conducted to investigate the load carrying mechanism which was affected by the position of artificial crack tips.

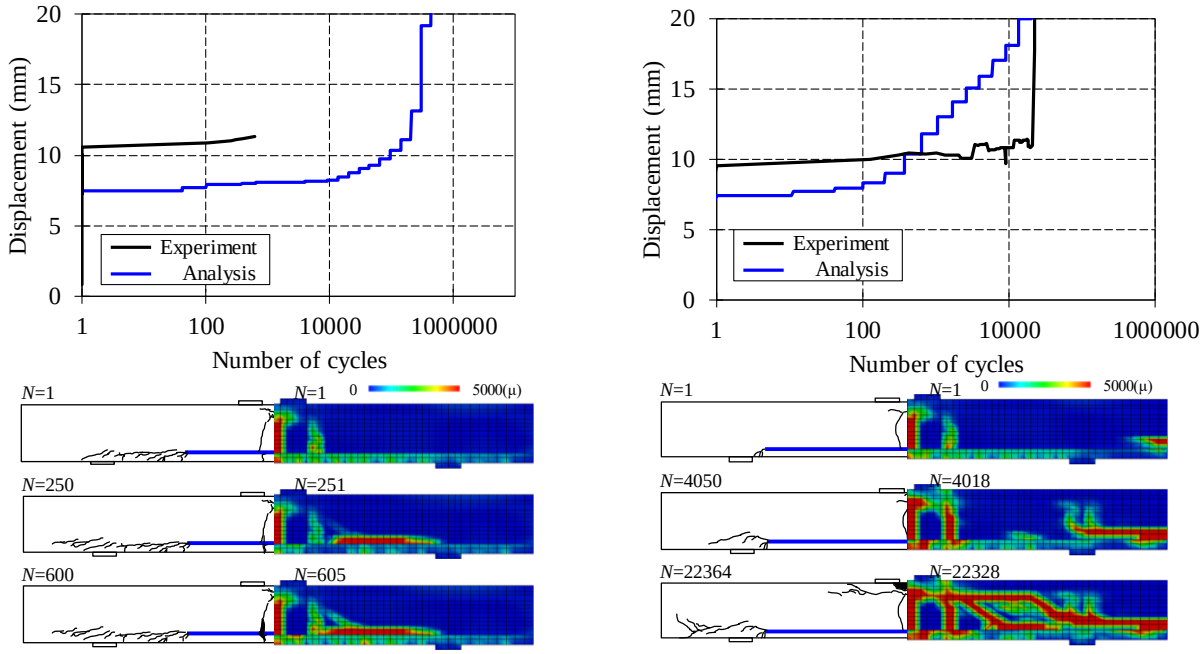

(a) B1-74 *(b) B2-72*

Figure 3.18 Reproducibility of displacement and strain distribution in fatigue

3.3.2. Macroscopic behavior in fatigue analysis

a) Validity of analytical model in fatigue analysis

Figure 3.18 shows analytical results of *B2-72* and *B1-74* to confirm the validity of fatigue analysis by using the same method to make analytical model as explained in the following section. The magnitude of displacement in the first part of the number of cycles almost agreed.

Focused on the strain and crack distribution, the tendency of propagation of bending cracks on the artificial crack surfaces and propagation of horizontal cracks could be reproduced in each analytical model.

Thus, it is considered that tied arch mechanism which appeared with propagation of horizontal cracks was reproduced by using this method. Consequently, fatigue analyses were conducted by using these analytical models in the target beams as shown in Figure 3.6.

b) Tendency of fatigue strength

Figure 3.19 shows the tendency of fatigue strength against number of cycles at failure. The one cycle in the number of the cycles at failure in the figure represents the number when the failure caused by static loading in this study.

In case of a/d=1.0, the static strengths and the tendencies of fatigue strength were not changed remarkably (Figure 3.19 *(a)*). It was considered that these tendencies were caused by predominance of compressive stress fields between loading points and supporting points. This

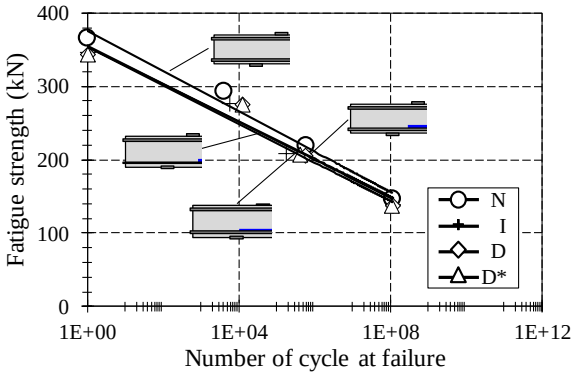

(a) a/d=1.0

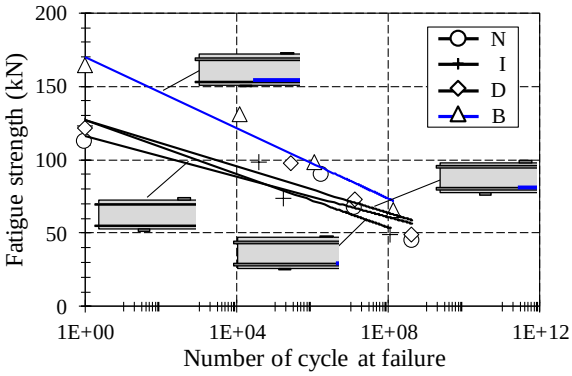

(b) a/d=1.6

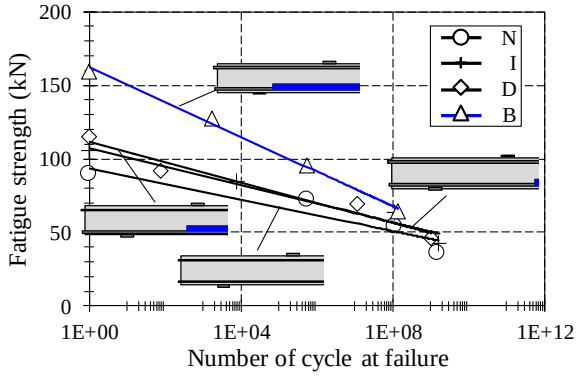

(c) a/d=2.9

Figure 3.19 Change in fatigue strength against number of cycles at failure

phenomenon was one of characters of the deep beam. In case of *a/d*=1.6 and 2.9, it was confirmed that the static strengths of *B1.6* and *B**2.9* were remarkably high due to tied arch mechanism compared with other beams (Figure 3.19 *(b), (c)*).

However, in the high cycle region, the fatigue strengths of *B1.6* and *B**2.9* were close to the strengths of other beams. These tendencies mean gradient of fatigue strengths were relatively high and the strengths were easy to drop against increase in the number of cycles.

When the fatigue strength was easy to drop, there was a possibility that fatigue life of cracked beams become shorter under lower cyclic load than that of sound beams. It was considered that this phenomenon was caused by accumulation of fatigue damage inside the beam.

From this viewpoint, the remained compressive strain was calculated as damage accumulating area by cyclic load.

c) Change in damage accumulating area

Figure 3.20 shows damage accumulating area under 40% upper limit load ratio and 60 kN upper limit load. The damage accumulating area corresponds to the remained minimum

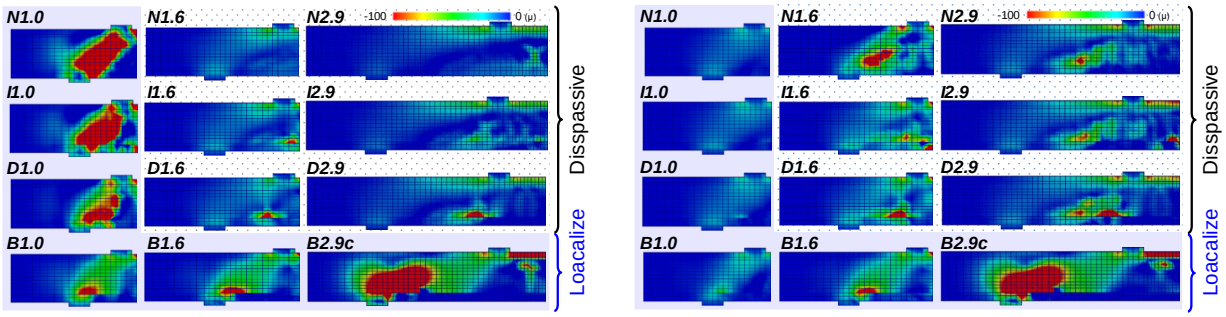

(a) 40 % *upper limit load ratio* *(b)* 60 kN *upper limit load*

Figure 3.20 Damage accumulating area (1 cycle to 777777 cycles)

(compressive) principal strain distribution from 1 cycle to the target cycle. In case of 40 % upper limit load ratio, the damage accumulating areas were affected by the magnitude of upper limit load. However, the damage accumulating areas were localized between loading points and supporting points regardless of upper limit load in case of the beams whose crack tips existed inside *B* region, showing relatively high gradient of fatigue strength curve.

It was considered that the damage accumulating area was changed by magnitude of cyclic compressive stress. In general, stress is distributed as the magnitude of stress at an arbitrary point is equals to averaged value of stress fields around the arbitrary point. In case of *a/d*=1.0, the compressive stress fields between loading and supporting points were predominant compared with the magnitude of stress at the crack tips. Thus, it can be considered that the area was not changed remarkably by change in the position of the crack tips. In case of *a/d*= 1.6 and 2.9, it is expected that magnitude of stress concentration at the crack tips was high compared with the stress between loading and supporting points. The stress fields were formed as the stress at the crack tips and the stress between loading and supporting points were averaged. As a result, in case of the beams whose crack tips existed near the stress field between loading and supporting points (crack tips existed inside *B* region,), the magnitude of stress was enhanced and relatively higher magnitude of stress field was localized in the area between loading and supporting points. If the stress field was averaged at another point, the stress was distributed dispersively. It is considered that the damage accumulating area was localized in the beam which had crack tips inside of *B* region due to the reason above.

3.3.3. Change in load carrying mechanism

a) Change in stress fields which contribute shape of load paths

To confirm the effect of stress distribution by change in the load carrying mechanism due to change in the position of crack tips, the load path was focused. The concept of load path was described in **Chapter 2**. The shape of load path is shown in Figure 3.21. In case of *a/d*=1.0, *B1.6* and *B**2.9*, the path showed linear shape as the line which connected to loading points and supporting points. These beams were corresponding to the beams whose damage

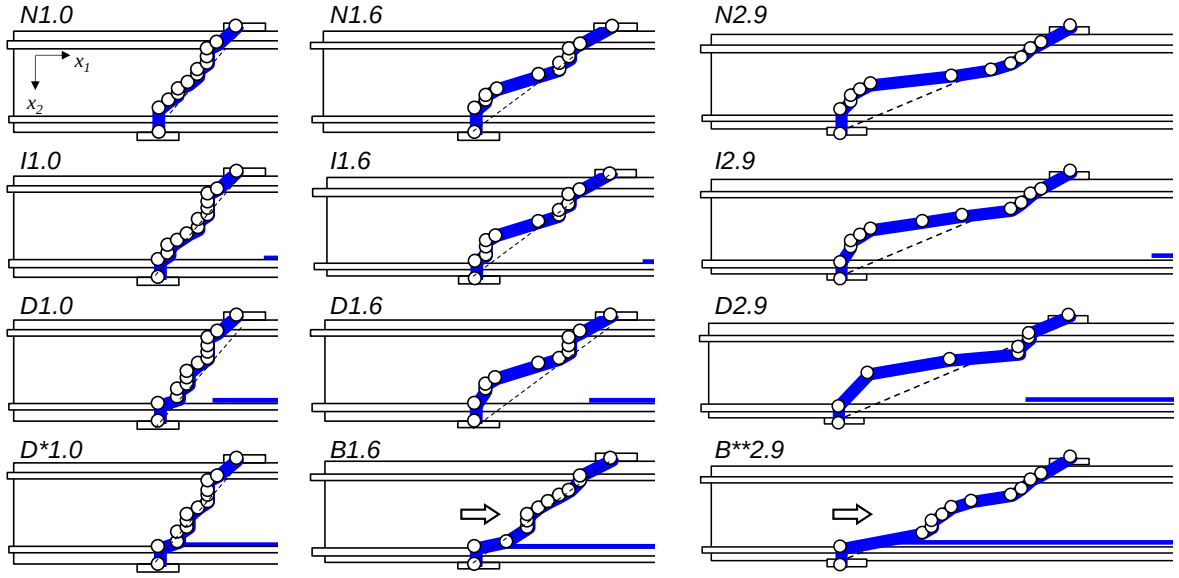

Figure 3.21 Shape of the load path (777777cycles)

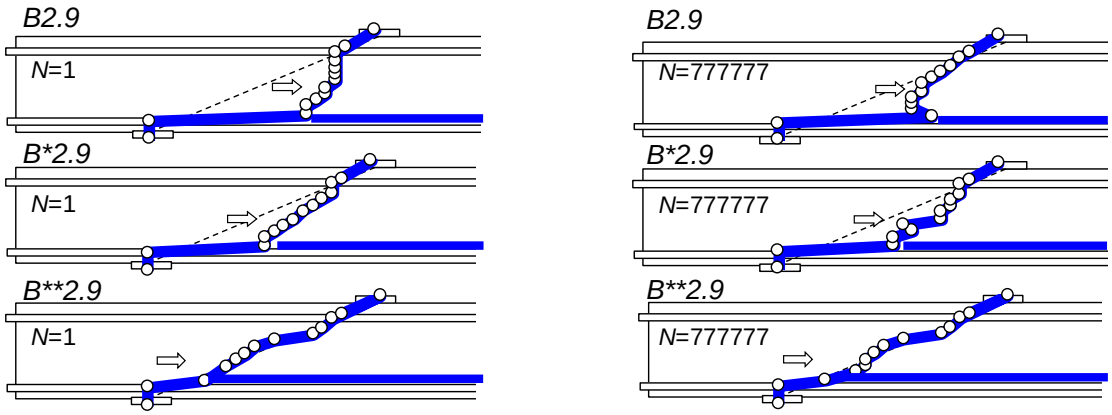

(a) N=1 *(b) N*=777777

Figure 3.22 Effect of cycles on shape of load path

accumulating areas were localized. Especially, in case of the beams whose crack tips existed inside *B* region, the path was attracted toward the position of crack tips. In other case of the beams whose crack tips existed inside of *B* region, this phenomenon was confirmed (Figure 3.22). It was confirmed that the shapes of load path were almost same in the case of *N*=1 and *N*=777777, and the paths were attracted toward the position of cracks tips. Therefore, it was found that the shapes were not affected with increase in the number of cycles (Figure 3.22). It is considered that this phenomenon was caused by change in the magnitude of stress concentration at the position of crack tips. In addition, the stress concentration was caused by shear deformation on the artificial cracks surface. Consequently, the shear stress distributions on the artificial cracks in longitudinal direction were focused.

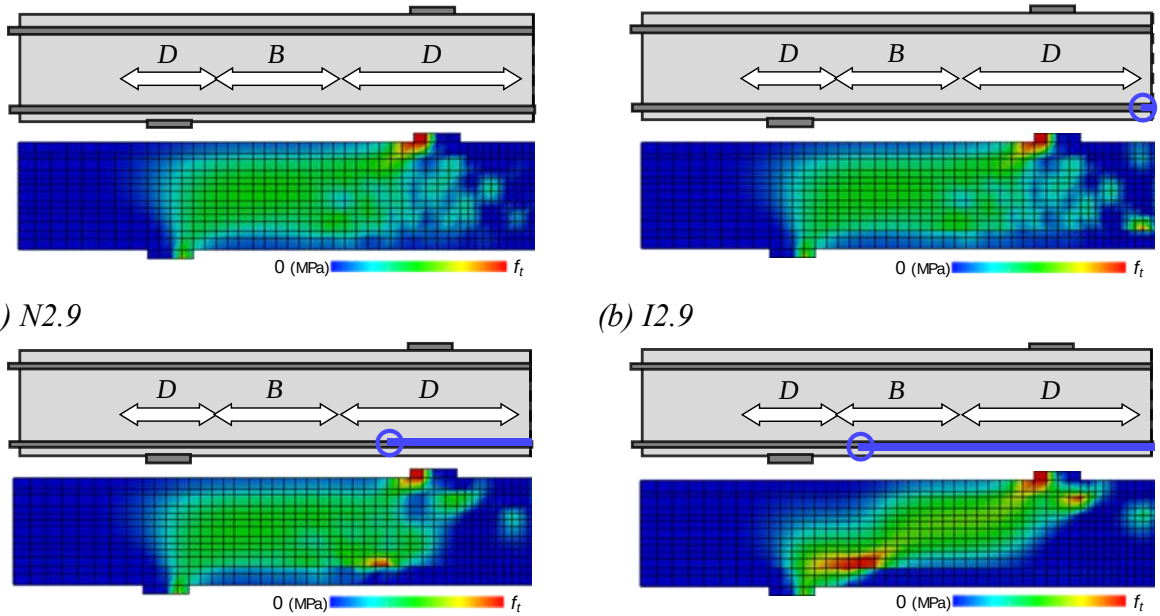

(a) N2.9 *(b) I2.9*

(c) D2.9 *(d) B2.9*

Figure 3.23 Shear stress distributions under 60 kN upper limit load

Figure 3.23 shows the shear stress distributions in case of *N*, *I*, *D* and *B*. The maximum range of the distribution is tensile strength of concrete (f_t). It could be confirmed that the distributions in case of *N*, *I*, *D* were not changed remarkably, however, the distribution in case of *B* was completely changed. In addition, it was confirmed that the stress concentration at the crack tip affected the stress distribution in the beams.

Figure 3.24 shows the shear stress distributions on the artificial cracks in longitudinal direction. The stress distributions at 1 cycle and 777777 cycles were presented. It was confirmed that the magnitude of stresses inside of *B* region was higher than that inside of *D* region in each case even though stress had scatters due to cyclic stress. This tendency corresponded to the hypothesis mentioned in *3.1.2*. It is considered that the stress was affected by contribution of vertical stress in *D* region. As a result, the magnitude of stress decreased inside of *D* region compared with that inside of *B* region.

In case of *I2.9* and *D2.9*, the magnitude of stress increased inside of *B* region and decreased inside *D* region with increase in the number of cycles. It is considered that these tendencies were caused by shear stress transfer which was caused by aggregate interlocking due to deformation of beams under cyclic loading.

In case of *B2.9*, *B*2.9* and *B**2.9* whose initial crack tips were inside of *B* region, it was confirmed that magnitude of the stresses was higher than that of *N2.9*, *I2.9* and *D2.9*. Especially, in case of *B**2.9* whose initial crack tips existed on the line which connected loading to supporting points, the peak value of the stress was the highest compared with other cases.

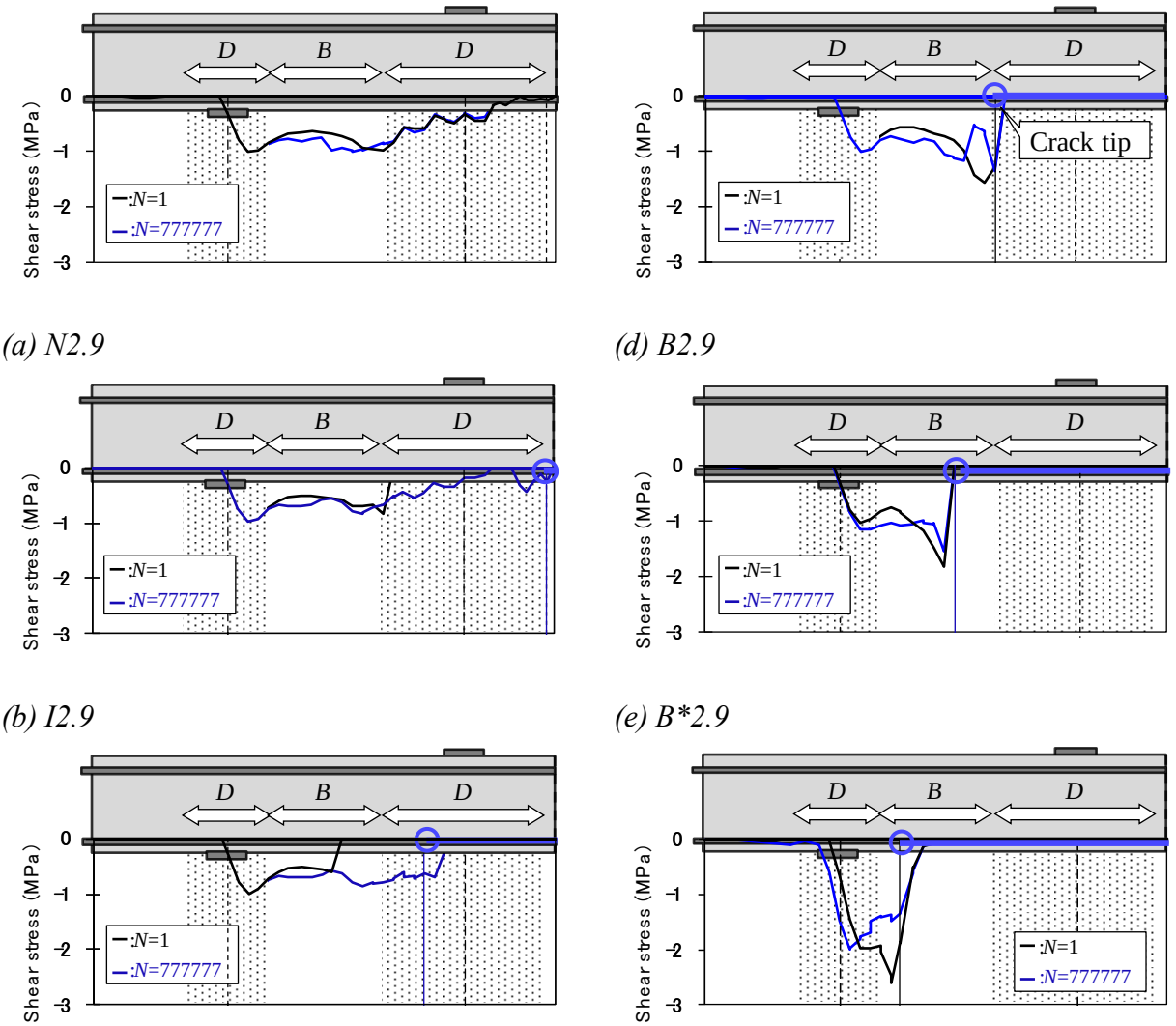

(a) N2.9

(d) B2.9

(b) I2.9

*(e) B*2.9*

(c) D2.9

*(f) B**2.9*

Figure 3.24 Shear stress distributions on artificial cracks in longitudinal direction

Moreover, the position of the peak value of stress which represented the position of crack tips moved the direction of supporting points. This phenomenon indicated that the horizontal crack propagated from the initial crack tips toward outside of the beam.

From the tendency that magnitude of stress at the crack tips inside of *B* region showed highest value regardless of number of cycles (Figure 3.24 *(d), (e), (f)*), it could be confirmed that the load path of the beams which had crack tips inside of *B* region was attracted toward the crack tips.

b) Change in the magnitude of arch and beam mechanisms

To confirm the relationship between shape of load path and load carrying mechanism, the contributed loads of arch and beam mechanisms under cyclic load were calculated.

The contributed loads of arch and beam mechanisms under 40% of upper limit load against

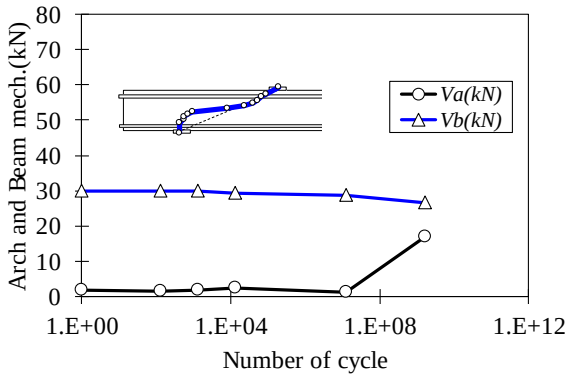

(a) N2.9

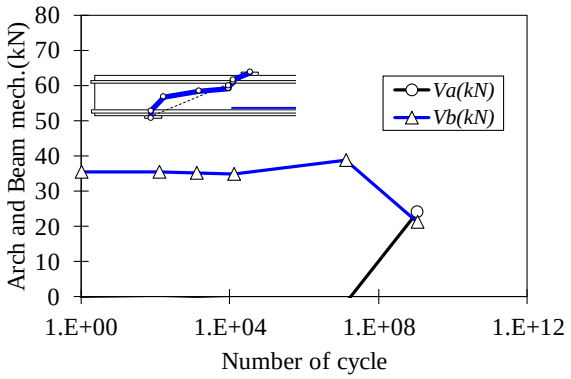

(c) D2.9

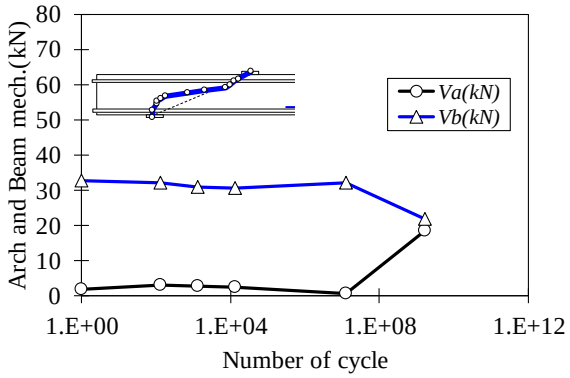

(b) I2.9

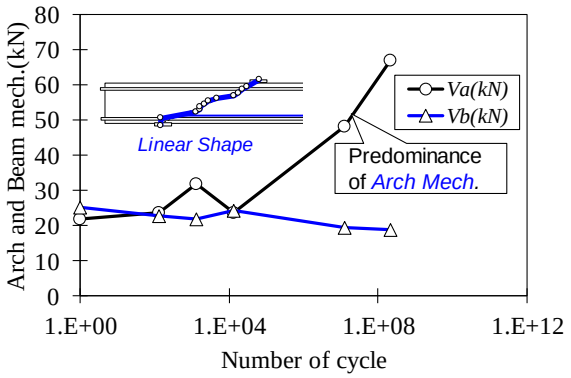

*(d) B**2.9*

Figure 3.25 Contributed load of arch and beam mechanisms against number of cycles

number of cycles are shown in Figure 3.25 and Figure 3.26 respectively. The shape of load path in each case is also shown in the figures.

The contributed load of arch mechanism increased at the time of failure in each case (Figure 3.25). In case of *B**2.9* whose load path showed linear shape, it was confirmed that magnitude of contributed load of arch mechanism was high compared with other beams. It could be deduced that when the shape of load path was linear, the arch mechanism was predominant. In addition, it was confirmed that the load carrying mechanism was not changed remarkably in case of *N2.9*, *I2.9* and *D2.9* whose shape of load path showed curvature shape.

Focused on the tendency of contributed load against number of cycles at failure, the arch mechanism was predominant against each fatigue strength (Figure 3.26). Especially, in case of *B**2.9* whose load path showed linear shape, it was confirmed that contribution ratio of arch mechanism was the highest in all cases. It can be considered the reason is that in case of *B**2.9*, magnitude of the stress between loading points and supporting points is enhanced due to high stress concentration at the position of crack tips.

Therefore, it was made clear that when the load path showed linear shape, arch mechanism

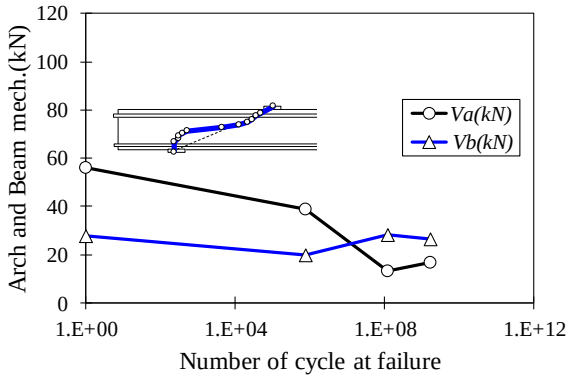

(a) N2.9

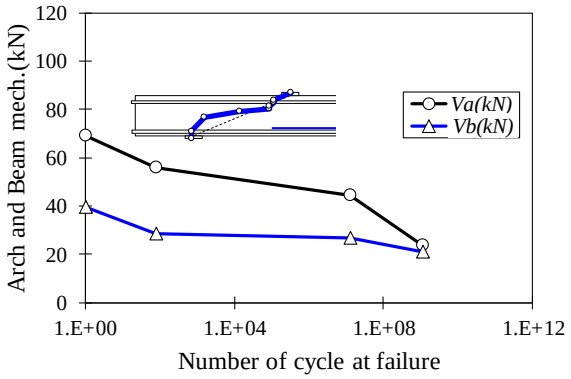

(c) D2.9

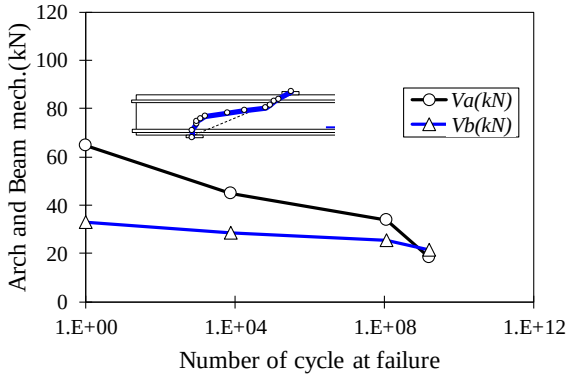

(b) I2.9

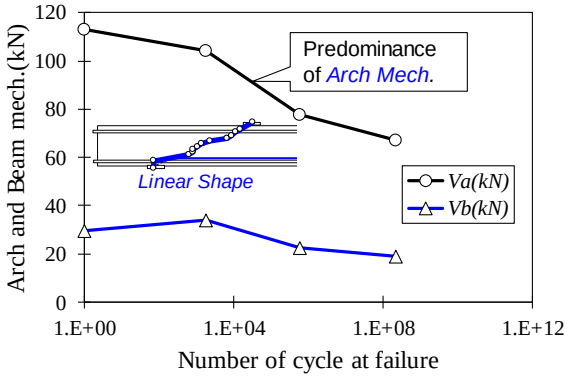

*(d) B**2.9*

Figure 3.26 Contributed load of arch and beam mechanisms against number of cycles at failure

was predominant. As a result, damage accumulating area was localized (Figure 3.20) and gradient of fatigue strength increased (Figure 3.19).

3.3.4. Crack propagating behavior

a) Effect of crack length

From the results of experiment and analysis, it was considered that the propagation of horizontal cracks was important to appear arch mechanism. The propagating behavior of horizontal cracks which was affected by the position of artificial crack tips is discussed based on the analytical results. Figure 3.27 shows maximum (tensile) principal strain distribution map in the case of static and fatigue loading. The range of strain was set as 0-5000 μ which represented about 0.1 mm crack opening width in vertical direction because the averaged FE size was about 20 mm. When the coalescence of the strain at the crack tips and the strain of diagonal crack in horizontal direction occurred, it was regarded that horizontal crack propagated.

Focused on the map, in case of static loading, horizontal crack propagated when the artificial

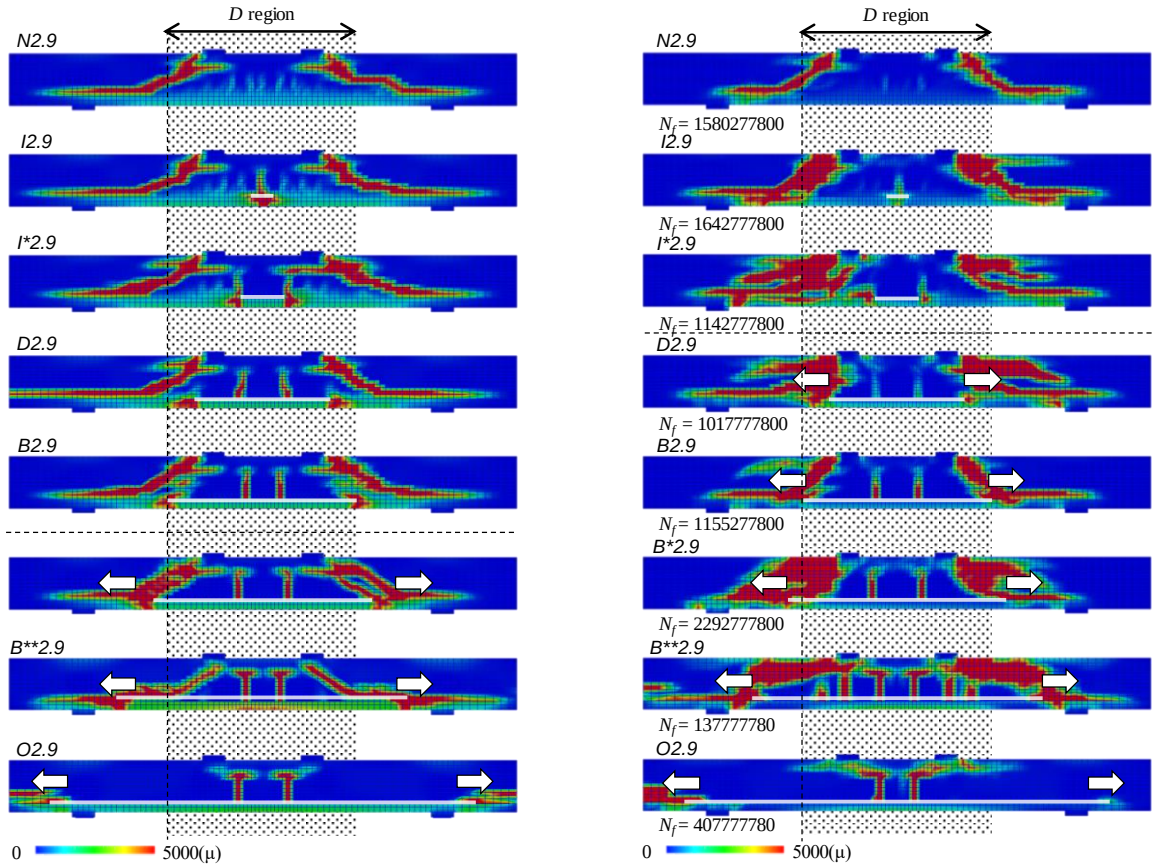

(a) Static loading *(b) Cyclic loading*

Figure 3.27 Maximum principal strain distribution at failure

crack length was longer than that of *B2.9*. On the other hand, in case of cyclic loading, horizontal crack propagated when the artificial crack length was longer than that of *I*2.9*. It was found that when the beams had the cracks inside of *D* region, the horizontal crack propagated under cyclic loading.

It is considered that horizontal crack propagated in the beams which had crack tips inside of *B* region due to high shear stress at the crack tips (Figure 3.25).

There is a possibility that relatively low shear stress which was acting on the crack tips inside of *D* region made the plastic region around the crack tips enough to propagate the horizontal cracks.

b) Evaluation of propagating behavior based on mode II stress intensity factors

It is considered that propagation of the horizontal cracks is characterized by shear (mode *II*) deformation because the propagation is caused by mode *II* opening crack. To estimate the area of plastic region which is main cause of propagation of horizontal crack, the mode *II* stress intensity factor[4],[5] at the crack tips was calculated. In general, the stress intensity factor which

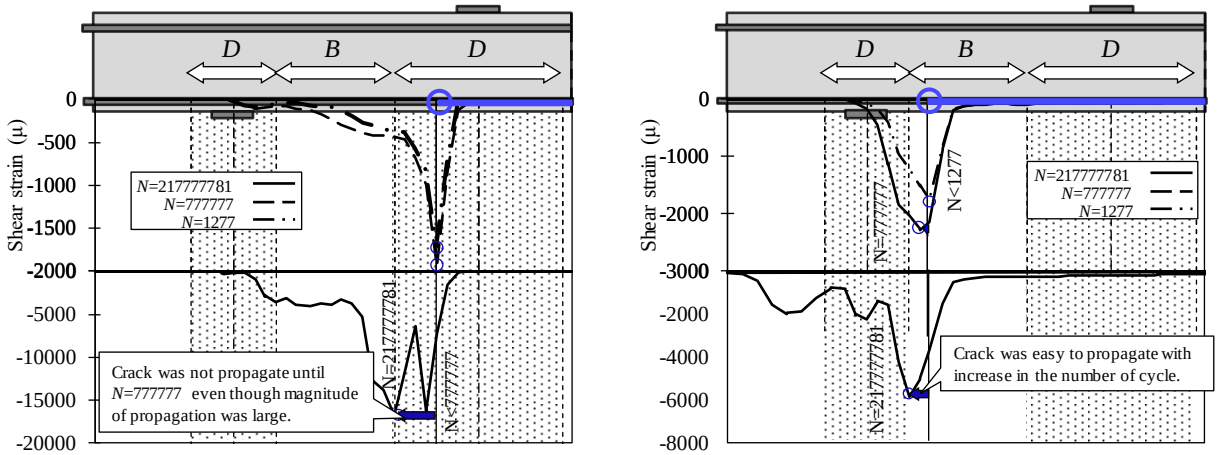

(a) D2.9 *(b) B**2.9*

Figure 3.28 Shear strain on artificial crack surfaces

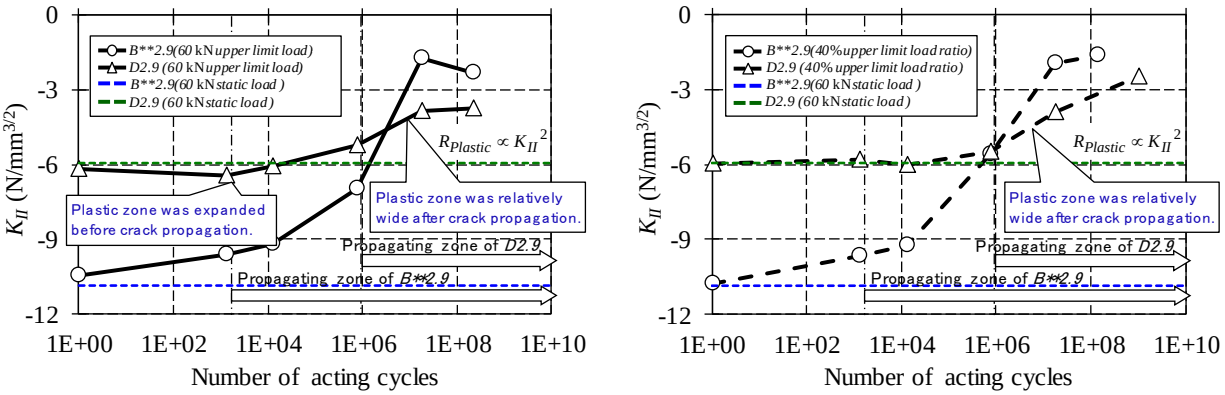

*(a) Under 60*kN *upper limit load* *(b) Under 40% upper limit load ratio*

Figure 3.29 Stress intensity factor in mode II deformation at the crack tips

is derived by theory of elasticity cannot apply for the concrete structures and materials. However, to grasp the tendency of stress concentration, the elastic stress intensity factor was applied in this study because the size of crack tip could be regarded enough to small against the beam size. The stress intensity factor detailed by using the following equation.

$$K_{II} = \tau_{xyII(r,\theta)}(2\pi r)^{1/2}\left\{\frac{1}{4}\left(\cos\frac{5}{2}\theta + 3\cos\frac{1}{2}\theta\right)\right\}^{-1} \qquad (3.18)$$

Where, K_{II}: stress intensity factor in mode *II* deformation, $\tau_{xyII(r,\theta)}$: shear stress at the crack tip in polar coordinate.

The origin of coordinate was set at the crack tips. The factor was derived by Eigen-function series expansion (*See.* **Appendix C**).

The stress intensity factor is related to magnitude of plastic region as follows.

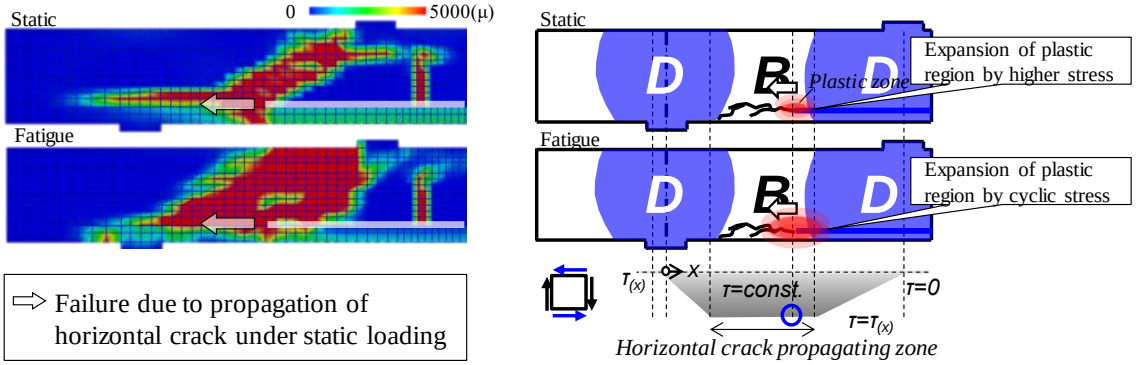

(a) In the case that crack tips exist inside of B region

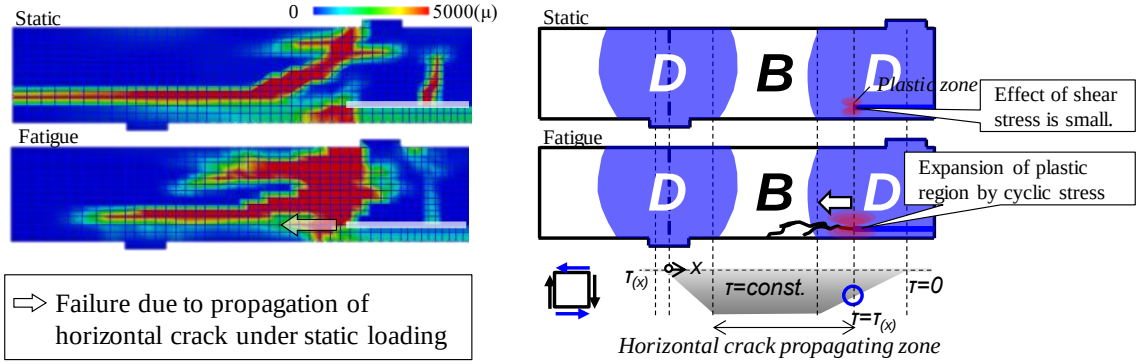

(b) In the case that crack tips exist inside of D region

Figure 3.30 Effect of difference in the plastic region at the crack tips

$$R_{Plastic} \propto {K_{II}}^2 \qquad (3.19)$$

Where, $R_{Plastic}$: plastic region at the crack tip.

In general, the peak strain occurs at the position where the stress concentration occurs. Thus, the position of crack tip was deduced based on shear strain on the artificial crack surfaces in longitudinal direction. The shear strain distribution under 60 kN upper limit load is illustrated in Figure 3.28. The shear strain was averaged value of nodal point of bond elements which were inserted at the position of artificial crack. From the peak value of strain distribution, it could be deduced that horizontal cracks propagated after 777777 and 1277 cycles in case of *D2.9* and *B**2.9* respectively because the peak value was moved after these cycles. In case of *D2.9*, the number of cycles before propagation of crack was larger than that of *B**2.9*, even though propagating length was longer than that of *B**2.9*.

The stress intensity factor in mode *II* deformation (K_{II}) is shown in Figure 3.29. There was a possibility that K_{II} was changed by magnitude of upper limit load, thus, the case of 40 % upper limit load ratio and 60 kN upper limit load are represented in the figure. However, no effect was confirmed regarding the magnitude of upper limit load. Consequently, in the following discussion, the case of 60 kN upper limit load was described. The K_{II} of the results in the static analyses at 60 kN is also shown in the figure.

Focused on the tendency of K_{II} before propagation of horizontal cracks which was deduced by Figure 3.28, the absolute value of K_{II} becomes relatively higher than that of *D2.9* in case of *B**2.9*. On the other hand, absolute value of K_{II} was larger than that of static loading before 12777 cycles in case of *D2.9*. Therefore, it could be considered that plastic region at the crack tips in case of *B**2.9* was always widely generated (Figure 3.30 *(a)*), however, the region in case of *D2.9* was wider than that of static before crack propagation (Figure 3.30 *(b)*).

Focused on the tendency in the region where less than 10^6 cycles, K_{II} of *D2.9* was lower than that of *B**2.9*. This fact represented that the crack was difficult to propagate in case of *D2.9* in initial region of acting cycles.

On the other hand, in the region where less than 10^7 cycles, K_{II} of *D2.9* was relatively higher than that of *B**2.9* after crack propagation. It could be considered that absolute value of K_{II} decreased after crack propagation due to strain energy release caused by crack propagation. In case of *D2.9* whose absolute value of K_{II} was relatively high after crack propagation, it could be affirmed that horizontal cracks were easy to propagate.

From the tendency of plastic region which was deduced by magnitude of K_{II}, it was confirmed that the reason why fatigue failure occurred after horizontal crack propagation even though the beam had the artificial crack tips inside of *D* region (Figure 3.27 *(b)*).

3.4 Evaluation of Load Carrying Mechanism Based on Strut and Tie Model

To propose a design scheme which considers change in stress fields due to existence of corrosion cracks, the method based on equivalent effective strength coefficient which was mentioned in **2.4** is described in this section. The details of calculation results are shown in Table 3.3. The equivalent effective strength coefficient was calculated by effective strut width and sine of effective strut angle based on the results of FE analysis.

3.4.1. Change in strut angle and width due to cyclic stress and artificial cracks

Figure 3.31 shows calculated sine of effective strut angle against crack ratio. Crack ratio was introduced to normalize crack length against shape of beam as shown in Figure 3.31. When the crack ratio takes 1, crack tips exist on the line which connects to supporting and loading points. Linear regression curves are shown in the figure against each case. The values of sine were not changed remarkably in each case of *a/d*, even though the sine had rather scatter around crack ratio of 1. In case that artificial crack was across the compressive strut, it is considered that stress transfer area was expanded by shear stress on the artificial cracks. However, the results mean that effect of crack length could be neglected versus principal stress distribution at the position of bottom side of the beams (*See. the calculating method in* **Chapter 2**). It could be considered

Table 3.3 Details of calculation results

Name of analytical models	Upper limit load (kN)	Upper limit load ratio (%)	Scale factor	Effective strut width (mm)	Sin of effective strut angle	Equivalent effective strength coefficient	Number of cycles at failure
N1.6-100	132.3	100	0.97	184	0.50	1.00	1
N1.6-90	118.8	90		185	0.48	0.92	32
N1.6-56	73.5	56		175	0.50	0.95	70277778
B1.6-100	163.9	100		189	0.48	0.96	1
B1.6-80	131.1	80		164	0.50	0.89	11777
B1.6-60	98.3	60		135	0.50	0.73	1165277
B1.6-40	65.6	40		117	0.52	0.69	135277781
N2.9-100	89.8	100	1.30	307	0.28	1.00	1
N2.9-80	71.8	80		259	0.28	0.71	577777
N2.9-60	53.9	60		348	0.28	0.79	115277781
N2.9-40	35.9	40		332	0.27	0.81	1580277801
*B*2.9-100*	112.0	100		218	0.28	0.88	1
*B*2.9-80*	89.6	80		236	0.29	0.84	2677
*B*2.9-60*	67.2	60		307	0.28	1.27	105277781
*B*2.9-40*	44.8	40		319	0.27	0.54	2292777801
*B**2.9-100*	159.4	100		236	0.28	1.16	1
*B**2.9-80*	127.5	80		331	0.30	1.01	1764
*B**2.9-60*	95.7	60		324	0.28	1.09	562777
*B**2.9-40*	63.8	40		183	0.29	1.08	137777781
O2.9-100	105.3	100		252	0.27	1.03	1
O2.9-80	84.3	80		157	0.28	1.02	27277
O2.9-60	63.2	60		229	0.33	0.67	1665277
O2.9-40	42.1	40		300	0.26	0.89	407777781

the reason was that the stress boundary at the bottom side of the beams which was required to calculate the sine was not affected by stress concentration at the artificial crack tip.

To confirm change in stress field due to cyclic loading the effective strut width was focused. Figure 3.32 shows effective strut width versus upper limit load ratio in case of *a/d*=1.6, 2.9. Linear regression curves are shown in each case. The blue line shows the case of *B1.6* and *B**2.9*. It was confirmed that all values of the strut width decreased by decrease in upper limit load ratio. In case of sound beam (*N1.6* and *N2.9*), the gradient was small compared with other cases. It is considered that the fact was caused by occurrence of wide damage accumulating area as shown in Figure 3.20, since the stress concentration did not occur. Especially, in case of *N1.6*, the gradient was remarkably small. Thus, it can be deduced that amount of decrement in the strut width was smaller in case of small *a/d* due to predominance of compressive stress fields. Moreover, in case of *B1.6* and *B**2.9*, the value of width was remarkably decreased. This tendency was corresponding to the localization of damage accumulating area which was shown in Figure 3.20. It was confirmed that the effect of localization of damage accumulating area remarkably appeared with decrease in effective compressive strut width.

3.4.2. Equivalent effective strength coefficient

For the quantitative consideration of the load carrying mechanism, this study focused equivalent effective strength coefficient. Figure 3.33 shows calculated equivalent effective strength coefficient based on the sine and width of effective strut. Linear regression curves are shown in

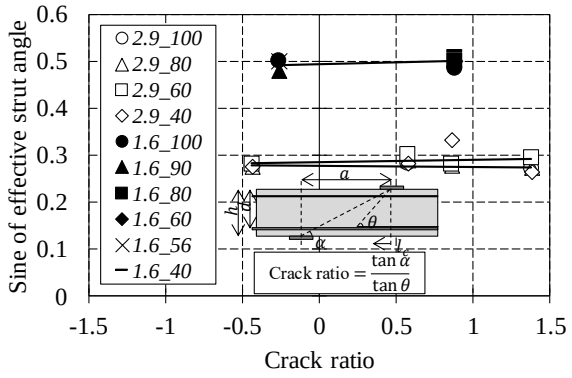

Figure 3.31 Sine of effective strut angle

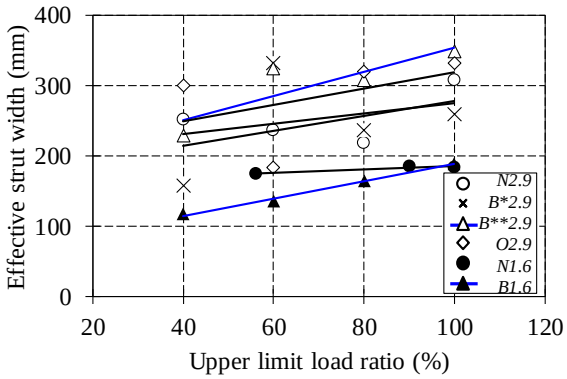

Figure 3.32 Width of effective strut

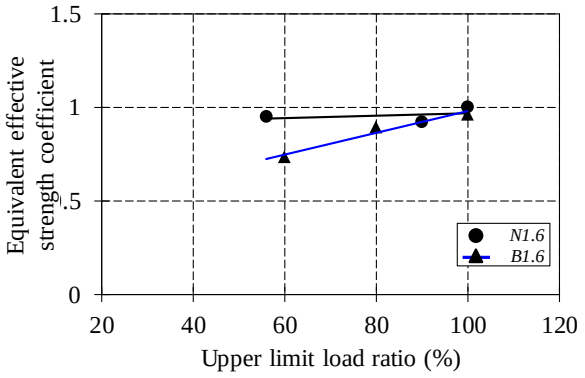

(a) a/d=1.6

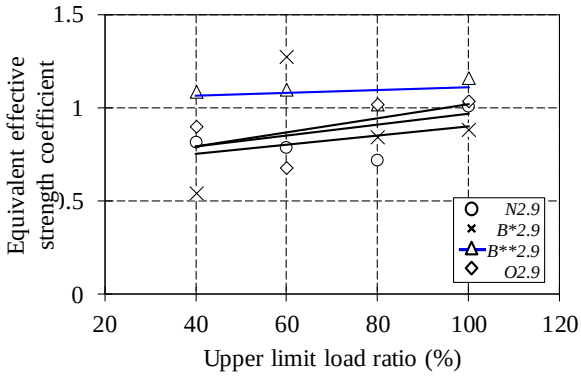

(b) a/d=2.9

Figure 3.33 Equivalent effective strength coefficient

the figure. It was confirmed that the coefficient was mainly affected by compressive strut width. However, the coefficient showed almost constant value in the case of *B**2.9*. It could be considered that this tendency was caused by the sine of strut angle as shown in Figure 3.31, because in case of *B**2.9* whose crack ratio took nearly one, the value of sine was high. The coefficient was proportional to square of the sine, therefore, it is considered that the equivalent effective strength coefficient was easy to affect the magnitude of the sine. Focused on the case of *B1.6*, it was confirmed that the gradient of equivalent effective strength coefficient was the highest in all cases. Thus, it is considered that there is a possibility that damage accumulation in compressive strut of cracked beams should be considered in the case of small *a/d*.

The calculated equivalent effective strength coefficients were exceeded 0.4. The value (0.4) was defined as the minimum value of the effective strength coefficient in the design code. Therefore, it can be considered that the safety of cracked structure under cyclic loading is secured when the design is conducted in the most dangerous side with the range of this study.

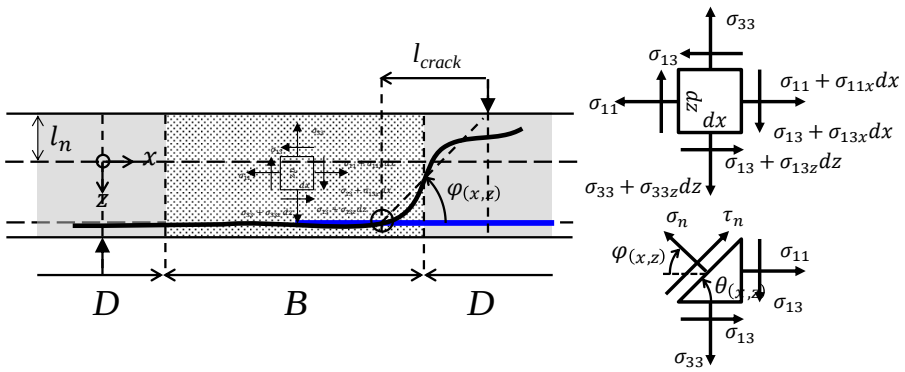

Figure 3.34 Definitions regarding position of crack occurrence

3.5 Proposal of Prediction Methods of Fatigue Life and Crack Position

If the crack propagating position and remaining fatigue life of cracked RC beams can be predicted, a suitable maintenance method can be established. This section describes the proposed methods to predict fatigue life and crack position of cracked beams.

The load carrying mechanism of the beams which had artificial cracks along tensile rebars was governed by the crack which was generated on the artificial crack surfaces. If the occurrence of cracks which propagated on the actual corrosion crack surfaces, failure position of structural members can be deduced from the position of corrosion crack, the position of loading points, and shape of structural members.

In addition, it is known that the strut and tie model as load carrying model is effective for the case that *a/d* is less than 3.0[6],[7]. If the failure positions of cracked beams are able to be predicted, verification position for failure can be limited as the member of the strut and tie model.

The verification in the phase of maintenance for each member in strut and tie model can be conducted based on the previous research regarding the fatigue life of compressive concrete and tensile rebar.

The prediction method of crack position based on the theory of elasticity and the prediction method of fatigue life based on the strut and tie model are explained in the following sub sections.

3.5.1. Prediction method of crack propagating position

a) Assumption

It is expected that the effect of crack width of real corrosion surface can be regarded as the difference of shear transfer on the ideal corrosion surface.

The method to predict the starting point of critical crack which affects for failure directly based on the theory of elasticity including the effect of difference in the shear transfer on corrosion crack width is explained.

Figure 3.34 shows the definitions regarding position of crack occurrence. From the experimental and analytical knowledge, the following assumption can be introduced.

i. Critical crack which affects the failure of beams propagated immediately at the same time of the occurrence.

ii. Crack angle coincides with the minimum principal stress angle.

iii. The generated cracks on the artificial crack surface propagates to the loading point.

b) Derivation

From the assumption *i*, the elastic solution is available. From the assumption ii, the crack angle can be written as follows.

$$\varphi_{(x,z)} = \frac{\pi}{2} - \frac{1}{2}\tan^{-1}\frac{\sigma_{13}}{\sigma_{33} - \sigma_{11}} \tag{3.20}$$

From the equilibrium condition in horizontal direction, the relationship between the normal stress in longitudinal direction and shear stress written as follows.

$$\frac{\partial \sigma_{11(x,z)}}{\partial x} + \frac{\partial \sigma_{13(x,z)}}{\partial z} = 0 \tag{3.21}$$

The normal stress in longitudinal direction can be expressed as,

$$\sigma_{11(x,z)} = \frac{M_{(x)}}{I} z = \frac{Px}{I} z \tag{3.22}$$

Where, $M_{(x)}$: cross sectional moment, I: moment of inertia of area in cross section, P: acting force. Substituting *(3.22)* into *(3.21)*, *(3.21)* becomes a separable variable differential equation.

The equation can be solved under the boundary condition: $\sigma_{13(x,-l_n)} = 0$, $\sigma_{13(x,h-l_n)} = 0$. Thus,

$$\sigma_{13(x,z)} = \frac{P}{2I}\left(\frac{h^2}{4} - z^2\right) \tag{3.23}$$

Substituting *(3.23)* and $\sigma_{33} = 0$ ($\because$In *B* region, the vertical stress can be neglected.) into *(3.20)*, the crack angle can be rewritten as follows.

$$\varphi_{(x,z)} = \frac{\pi}{2} - \frac{1}{2}\tan^{-1}\frac{z^2 - h^2/4}{xz} \tag{3.24}$$

On the other hand, from the assumption *iii*, the crack occurrence potion can be expressed as follows.

$$l_{\text{Crack}} = \frac{h/2 + z}{\tan\left\{\frac{\pi}{2} - \frac{1}{2}\tan^{-1}\frac{z^2 - h^2/4}{xz}\right\}} \tag{3.25}$$

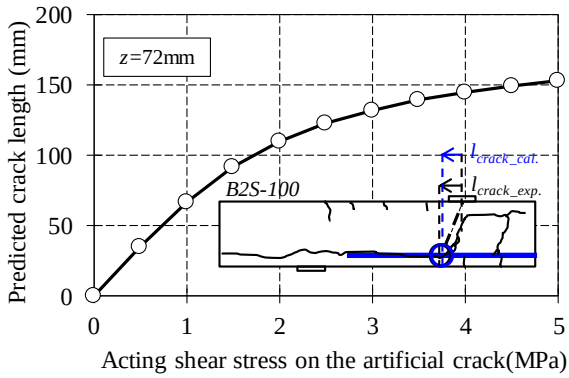

Figure 3.35 Predicted crack length

l_{Crack} must satisfy $l_{\mathrm{Crack}} = a - x$.

If the beam has corrosion cracks, l_{Crack} can be rewritten as follows by using acting shear stress on the crack surfaces.

$$l_{\mathrm{Crack}} = \frac{h/2 + z}{\tan\left\{\frac{\pi}{2} - \frac{1}{2}\tan^{-1}\frac{2I\hat{\sigma}_{13(x,z)}}{Pxz}\right\}} \tag{3.26}$$

Where, $\hat{\sigma}_{13(x,z)}$: shear stress on the corrosion crack surfaces.

c) Result of prediction

Figure 3.35 shows prediction result of crack position which was obtained by substitution of acting shear stress on the artificial crack surfaces in case of *B2S-100*. The shear stress was obtained from the elemental experiment which was shown in Figure 3.7. It was confirmed that the predicted point well agreed with experimental result. And, the calculated value was close to be zero when the acting shear stress became zero. It means that if corrosion crack width is wide as there is no shear transfer, the crack propagates from directly below the loading points. In this case, the failure behavior is close to be flexural failure.

In case of static loading, relatively good accuracy was obtained. However, there is necessity to expand the applicable range to the case of fatigue.

3.5.2. Prediction method of fatigue life of cracked RC beams

a) Applicability of strut and tie model

In general, the calculating formula of strength based on strut and tie model has high accuracy in case of $a/d < 3.0$ whose load carrying mechanism is governed by D region, compared with the formula based on the equilibrium condition of cross sectional forces. It is considered that the prediction equation of fatigue life based on the assumption that failure of compressive part

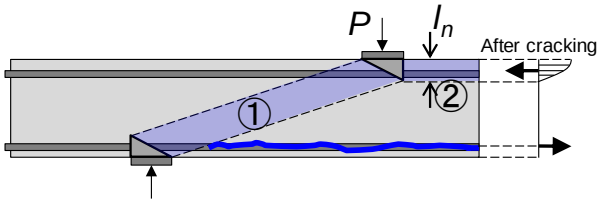

Figure 3.36 Definition of number of members in strut and tie model

in strut tie model is governed by the compressive fatigue strength of concrete as the material properties is able to be derived.

This subsection describes one of the method to predict fatigue life of cracked RC beams based on the strut tie model and fatigue strength property of sound concrete. The *B2-38* was treated as the prediction example. The effect of corrosion crack can be considered as the change in verification position of the failure which is determined by using the prediction method of failure position.

b) Derivation of upper limit stress ratio of sound concrete

According to the previous research[8], it was confirmed that the upper limit stress ratio of sound concrete in 2000000 cycles was 62.8%. Thus, the upper limit stress of sound concrete at the compressive failure can be given as follows, based on the assumption that fatigue life obeys logarithmic normal distribution.

$$R = \frac{0.372}{\log 2 + 6} \log N + 1 \qquad (3.27)$$

Where, R: upper limit stress ratio, N: number of cycles at failure.

c) Derivation of strength at compressive failure in compressive side

It is important to decide the compressive strut width in strut and tie model. There are a lot of researches to discuss about the decision of compressive strut width. A good accuracy was obtained from the result of previous research[9] under the assumption that compressive stress distribution in the cross section of the strut was similar to that of ultimate bending condition. From this view point, assumed that the strut width was same as the height of neutral axis in ultimate bending condition, the strength of strut can be obtained.

This section discusses about failure position 2 as shown in Figure 3.36 in the strut and tie model as an example. The strength caused by the failure position 2 is follows.

$$F_{f2} = 0.68 f_c b l_n \qquad (3.28)$$

Where, F_{f2}: strength caused by the failure position 2, b: beam width, l_n: height of neutral axis.

The acting force in compressive strut at the failure position 2 can be obtained as follows.

$$F_2 = \frac{P}{a/d} \tag{3.29}$$

Where, F_2: acting force in compressive strut at the failure position 2, P: acting load in a shear span, a: shear span, d: effective depth.

From *(3.28)* and *(3.29)*, failure load caused by the failure position 2 can be obtained as follows.

$$P_{f2} = \frac{0.68 f_c b l_n}{a/d} = C_2 f_c \tag{3.30}$$

Where, P_{f2}: failure load at the failure position 2, C_2: mode factor. The mode factor characterizes change in the verification point.

Figure 3.37 shows the compressive failure load at the failure position 2 based on *(3.30)* and the experimental load when the compressive strain at the failure position 2 reached typical ultimate compressive strain (3500 μ). The calculation result showed good accuracy even though the calculation values rather high compared with the experimental value.

d) Derivation of number of cycles at compressive failure

The acting compressive stress of concrete under upper limit load is expressed by the following equation.

$$f_{cmax} = \frac{P_{max}}{C_2} \tag{3.31}$$

Where, f_{cmax}: acting compressive stress of concrete under upper limit load. The stress ratio R is,

$$R = \frac{f_{cmax}}{f_c} \tag{3.32}$$

Substituting *(3.27)*, *(3.30)*, *(3.31)* into *(3.32)*, the following equation can be obtained.

$$\frac{f_{cmax}}{f_c} = \frac{P_{max}}{P_{f2}} = \frac{0.372}{\log 2 + 6} \log N + 1 \tag{3.33}$$

Therefore, the number of cycles at compressive failure at the failure position 2 can be derived as follows:

$$N_{f2} = e^{\left\{\left(1 - \frac{P_{max}}{C_2 f_c}\right)\frac{\ln 2 + 6 \ln 10}{0.372}\right\}} \tag{3.34}$$

The mode factor of compressive concrete C_i(i=1,2) is constant in each compressive failure mode.

Thus, *(3.34)* can be expanded to each failure mode. The number of cycles at compressive

failure in each compressive failure mode is given as follows:

$$N_{fi} = e^{\left\{\left(1-\frac{P_{max}}{C_i f_c}\right)\frac{\ln 2+6\ln 10}{0.372}\right\}} \quad (3.35)$$

Where, C_i(i=1,2): mode factor of compressive concrete in each failure mode. Modes 1 and 2 are the failure mode that is corresponding to diagonal compressive failure and shear compressive failure respectively. The prediction equation in the case of tensile failure of rebar can be derived based on other function of stress ratio by using the same derivation method as mentioned above.

e) *General derivation*

In general, the stress ratio of each material can be given as the following logarithmic formula.

$$R_j = A_j \ln N_j + B_j \quad (3.36)$$

Where, R_j *(j=1,2,...,number of materials)*: stress ratio in each material, A_j, B_j :coefficients which determine the material properties.

The failure load in each member is given as follows:

$$P_{fi} = C_i f_j \quad (3.37)$$

Where, P_{fi}: failure load in each member, C_i*(i=1,2,...,number of failure mode)*: mode factor, f_j*(j=1,2,...,number of materials)*: strength of each material.

Substituting *(3.37)* into *(3.36)*,

$$\frac{P_{max}}{P_{fi}} = A_j \ln N_j + B_j \quad (3.38)$$

Thus, number of cycles at failure in the structural member is obtained as follows:

$$N_f = \min\left[N_{fj} = e^{\left\{\left(\frac{P_{max}}{C_i f_j}-B_j\right)A_j{}^{-1}\right\}}\right] \quad (3.39)$$

Where, N_f: number of cycles at failure in the structural member, N_{fj}: number of cycles at failure in each material and failure mode.

f) Validity of predicting equation

To confirm the validity of prediction equation, the compressive strain at the failure position 2 which was derived from *(3.34)* and compressive strain of *B2-38* were compared.

The following assumptions were introduced to derive the compressive strain.

i. Compressive strain obeys logarithmic normal distribution.

ii. Compressive failure occurs when the compressive strain reaches 3500 μ.

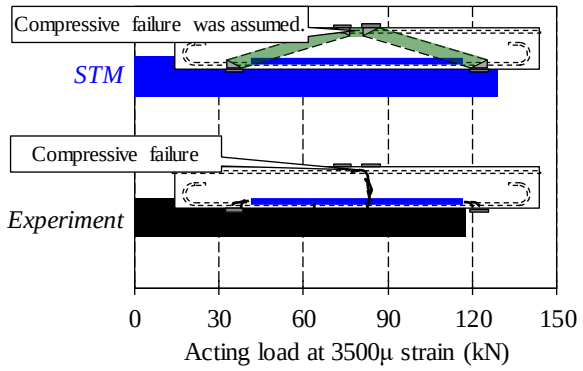

Figure 3.37 Accuracy of strut and tie model

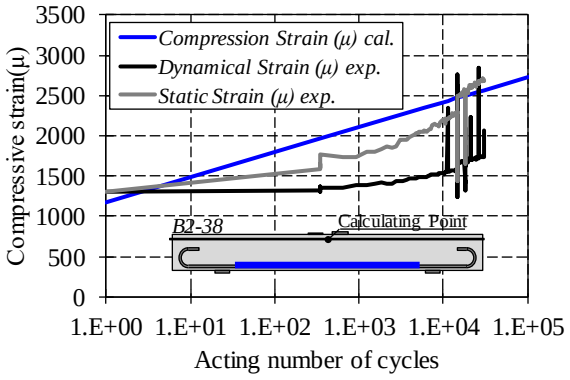

Figure 3.38 Accuracy of strut and tie model

The compressive strain can be given as follows:

$$\varepsilon_c = \frac{\varepsilon_{cf} - \varepsilon_{in}}{\log N_{f2}} \log N + \varepsilon_{in} \qquad (3.40)$$

Where, ε_{cf}: 3500 μ, ε_{in}: initial strain under target upper limit load based on elastic solution, N_{f2}: number of cycles at compressive failure at the failure position 2 which was derived from *(3.34)*. The ε_{in} can be given as follows.

$$\varepsilon_{in} = \frac{P_{max} ah}{2EI} \qquad (3.41)$$

Where, P_{max}: target upper limit load, a: shear span, h: beam height, E: Young's modulus of concrete, I: moment of inertia of area in cross section.

Figure 3.38 shows the tendency of compressive strain against number of acting cycles based on the calculation with experimental result. The effect of inertia force in experimental loading frequency cannot be neglected. Thus, the value of compressive strain was modified by using dynamic elastic modulus instead of static elastic modulus. It was confirmed that the increasing tendency almost agreed with the experimental result.

It is considered that this fact was a result that existence of artificial crack changed the failure mode of the beam; diagonal cracking failure to shear compressive failure. A possibility that the load carrying mechanism and fatigue life of the cracked RC beams was explained by using the strut and tie model could be deduced was shown.

3.6 Summary of Chapter 3

This chapter described that macroscopic behavior of cracked RC beams without stirrups.

To make clear the mechanism, cyclic loading experiments and FE analyses were conducted by

using the specimens which had different length of artificial cracks. The experimental results indicated that the load carrying mechanism was governed by tied arch mechanism due to horizontal cracks which propagated from the artificial crack tips regardless of loading conditions. In case of the beams whose static strength was enhanced due to the tied arch mechanism, the number of cycles at failure was the same as the sound beam under the cyclic load of 40% upper limit load ratio. It was demonstrated that the reason was localization of relative damage accumulation area caused by linearization of the load path. The analytical results showed that the linearization occurred by stress concentration around the position of crack tips which existed inside of *B* region. It was made clear that when the crack tips existed inside of *D* region, horizontal crack was easy to propagate with increase in the number of loading cycles.

To expand the fundamental knowledge as mentioned above into the design code, the methods to predict of failure position and fatigue life based on the strut and tie model were proposed. As a result of calculation of equivalent effective strength coefficient, it was confirmed that the effective strut width decreased with decrease in upper limit load ratio even though there was no effect of artificial crack length on the effective strut angle in case of the beams which showed arch mechanism predominantly. This fact corresponded to localization of damage accumulating area. In addition, it was confirmed that the safety of cracked structures under cyclic loading was secured when the design was conducted in the most dangerous side in the present design code.

The prediction method of position of crack starting point based on the theory of elasticity showed good agreement with the experimental result. A possibility that the crack starting position could be estimated by inputting the shear transfer which was changed by actual corrosion crack width was shown.

The prediction method of fatigue life for compressive failure mode showed also good agreement with the experimental result by modifying based on dynamic elastic modulus. The prediction equation was derived by the experimental result of fatigue life and static strength of the strut and tie model. A possibility that the load carrying mechanism of the beams which had a crack along tensile rebars in the shear span was explained by using the strut and tie model could be deduced was shown.

References in Chapter 3

[1] Yamada, K., Aoyagi, M.: Shear Transfer on the Crack Surface, *Proceedings of JCI 2nd Colloquium on Shear Analysis of RC Structures*, pp.19-28, 1983.9.

[2] Niwa, J., Yamada, K., Yokozawa, K., Okamura, H.: Revaluation of the Equation for Shear Strength of Reinforced Concrete Beams without Web Reinforcement, *Journal of Japan Society of Civil Engineers*, Vol.372, No.5, pp.167-176, 1986.8.

[3] federation internationale du beton (fib): fib Model Code for Concrete Structures 2010, 2010.

[4] Schlaich, J., Schafer, K., Jennewein, M.: Toward a Consistent Design of Structural Concrete, *PCI Journal*, Vol.32, pp.74-150, 1987.5-6.

[5] ACI Committee 318: Building Code Requirements for Structural Concrete and Commentary ACI 318-08, pp.379-393, 2008.2.

[6] Tada, H., Paris, P. C., Irwin, G. R. : The Stress Analysis of Cracks Handbook, *Del Research Co.*, 1973.

[7] Liebowitz, H., et al. : FRACTURE, Mathematical Fundamentals, Vol.2, *Academic Press*, 1968.

[8] Matsushita, H., Tokumitsu, Y.: A Study on Compressive Fatigue Strength of Concrete Considered Survival Probability, *Proceedings of the Japan Society of Civil Engineers*, Vol.284, pp.127-138, 1979.4. (in Japanese)

[9] Tanaka, Y., Kishi, T., Maekawa, K.: Strength Evaluation Method of RC Beams without Shear Reinforcement after Shear Cracking, *Proceedings of the Japan Concrete Institute*, Vol.26, No.2, pp.949-954, 2004. (in Japanese)

CHAPTER 4
BEHAVIOR OF RC BEAMS MODELED BY ARTIFICIAL CRACK WITH STIRRUPS

This chapter describes the effect of stirrup under cyclic loading in the cracked RC beams. To make clear the effect of stirrup, cyclic loading experiments and FE analyses were conducted by using the beams which had different length of artificial cracks and stirrup. As a result of static analyses, it was confirmed that the dowel action of stirrup reduced the contribution of arch mechanism, even though the effect of the dowel action to the load carrying mechanism was relatively small in the static experiment. As a result of cyclic loading experiments and FE analyses, it was confirmed that fatigue life in the high cycle region was increased in case of the beam with stirrup due to reduction of absorbing energy of arch mechanism by the dowel action of stirrup.

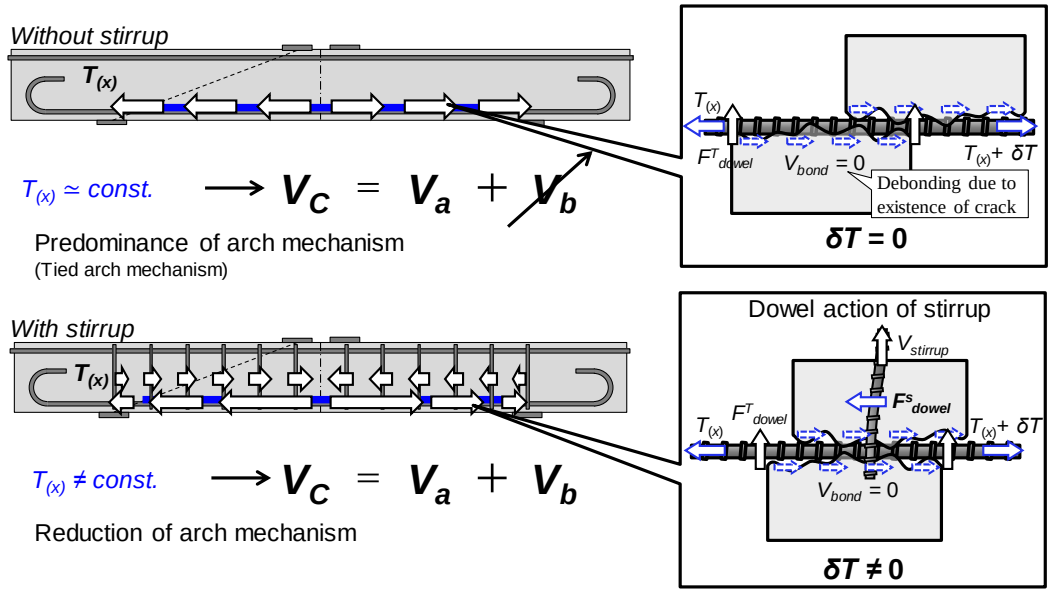

Figure 4.1 Hypothesis regarding the effect of stirrups

4.1 Hypothesis regarding the Effect of Stirrups

This section describes experimental and analytical set up to make clear the effect of stirrup in the cracked RC beams based on hypothesis which is obtained from **Chapter 3**.

4.1.1. Hypothesis

In the **Chapter 3**, it was made clear that the strain distributions of rebar in the beams which had the artificial crack along tensile rebar showed constant value due to tied arch mechanism. It is considered that the tied arch mechanism appears when the contributed load of beam mechanism can be neglected. The constant distribution of strain represents tensile force which transferred on the tensile rebar shows almost constant value. When the tensile force became constant, the term of contributed load in beam mechanism V_b which was mentioned **2.2** was canceled because $\partial C/\partial x = 0$ and $\partial T/\partial x = 0$ $(\because C = const., T = const.)$. This fact was confirmed in **Chapter 3** in case of the beams without stirrup.

When the beam had stirrup, the strain distribution along tensile rebar was not constant value due to dowel action of stirrup (Figure 4.1) because $\partial C/\partial x \neq 0$ and $\partial T/\partial x \neq 0$ $(\because C \neq const., T \neq const.)$. However, the contributed load of concrete V_C in each beam must be same because shape of beam was same in ideal condition.

Thus, the relationship of contributed load of arch and beam mechanism could be expressed as follows,

$$V_C = V_{Ca0} + V_{Cb0} = V_{CaR} + V_{CbR} \qquad (4.1)$$

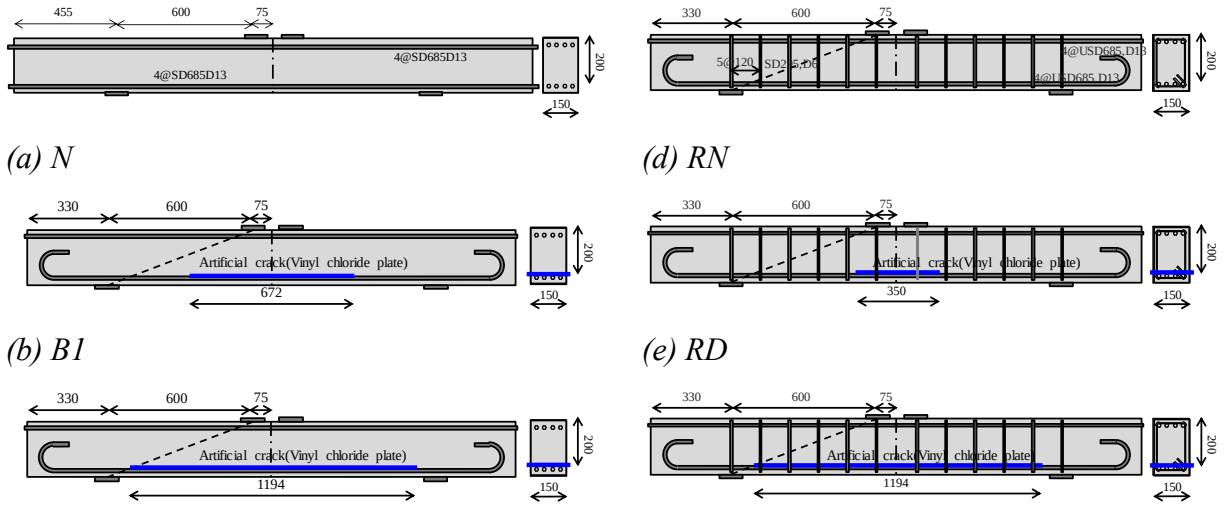

Figure 4.2 Size and shape of specimens

Table 4.1 Experimental cases

Name of specimens	Positions of artificial crack	Upper limit load ratio (%)	Upper limit load (kN)	Failure displacement (mm)	Number of cycle at failure
N-100	—	100	86.8	3.54	1
B1-100	*B* region	100	215.1	17.93	1
B1-74		74	160.0		1057
B1-35		33-37	70-80		1838900 (Non-failure)
B2-100		100	193.4	15.33	1
B2-72		72	140.0		22364
B2-38		38	73.0		30408 (Stopped)
RN-100	-	100	165.8	7.81	1
RN-78		78	130.0		854
RD-100	*D* region	100	182.3	10.13	1
RD-71		71	130.0		6121
RD-44		44	80.0		205690
RB-100	*B* region	100	185.5	14.81	1
RB-86		86	160.0		1717
RB-49		43-51	80.0-95.0		298785

*In case of *B1-33*, upper limit load was changed 70 kN - 80 kN at 1020990 cycle.
*In case of *RB-49*, upper limit load was changed 80 kN - 95 kN at 76530 cycle.

Where, V_{Ca0}: contributed load of arch mechanism in concrete without stirrup, V_{Cb0}: contributed load of beam mechanism in concrete without stirrup, V_{CaR}: contributed load of arch mechanism in concrete with stirrup, V_{CbR}: contributed load of beam mechanism in concrete with stirrup.

When the crack existed inside of the beams which showed tied arch mechanism, $V_{Cb0} = 0$ should be satisfied. Therefore, $V_{Ca0} > V_{CaR}$. Form this relationship, it can be deduced that existence of stirrup reduces the arch mechanism. Also, it was confirmed that when the beams showed tied arch mechanism, the fatigue strength was easy to decrease in **Chapter 3**.

There is a possibility that when the contribution of arch mechanism is decrease, the fatigue strength become difficult to decrease. To confirm this hypothesis, cyclic loading experiment and FE analysis were conducted.

Table 4.2 Analytical cases

Name of specimens	Positions of artificial crack	Upper limit load ratio (%)	Upper limit load (kN)	Failure displacement (mm)	Number of cycles at failure
N-100	-	100	80.3	3.12	1
N-80		80	64.3		280513344
N-60		60	48.2		4778702150
N-40		40	32.1		176389815025
RN-100		100	161.1	8.04	1
RN-80		80	128.9		9435877
RN-60		60	96.7		900195183
RN-40		40	64.5		21036301239
RD-100	*D* region	100	170.0	8.21	1
RD-80		80	136.0		4428238
RD-60		60	102.0		5285646600
RD-40		40	68.0		110091481225
RB-100	*B* region	100	186.4	12.25	1
RB-80		80	149.1		139216
RB-60		60	111.8		6392857
RB-40		40	74.6		917410459
B1-100		100	201.2	12.68	1
B1-80		80	161.0		282394
B1-60		60	120.7		19937753
B1-40		40	80.5		5713702160
B1-100		100	196.4	11.80	1
B2-80		80	157.1		100
B2-60		60	117.8		2999317
B2-40		40	78.6		19937753
RN-130kN	-	81	130.0	8.04	13828759
RD-80kN	*D* region	47	80.0	8.21	4428238
RB-160kN	*B* region	86	160.0	12.25	203
RB-92kN		49	92.0		59641262
B2-140kN		71	140.0	11.80	380

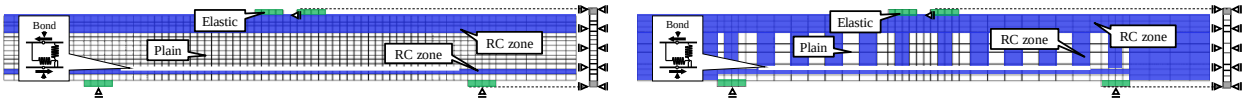

(a) Without stirrup *(b) With stirrup*

Figure 4.3 Analytical mesh model

Table 4.3 Properties of bond elements

	Closure mode (N/mm/mm^2)		*Opening mode* (N/mm/mm^2)		*Frictional coefficient*
	Normal direction	*Shear direction*	*Normal direction*	*Shear direction*	
Property of vinyl chloride plate	2450	4.68	0	0	0.1
Property of vinyl chloride plate with stirrup	294	4.68	0	9.8	1.4

4.1.2. Outline of experiment

The size and shape of specimens which treat in this section are shown in Figure 4.2. The *a/d* (shear span ratio) was set around 3.0 to compare the behavior with the beam without stirrups. The SD295 D6 (deformed rebar) was used as the stirrup in all specimens. The name of specimen represented; the position of artificial crack which was inserted in the specimens to simulate severe state of corrosion crack, and existence of stirrups. The artificial cracks were made by vinyl

chloride plate as mentioned **Chapter 3**. The interference between artificial crack and stirrup was avoided by making holes in the artificial crack. The *N* represented sound beam. The *D* and *B* represented that position of artificial crack tips existed inside *D* and *B* region respectively. The initial part of the name *R* represented existence of stirrup. The specimens *RN*, *RD* and *RB* had the artificial cracks. The specimens were designed as fail in shear in sound state.

All of experimental cases are shown in Table 4.1. Upper limit loads were decided by magnitude of the predicted diagonal cracking load which was proposed by previous research[1]. The number in the name of specimens represented the magnitude of upper limit load ratio. The upper limit loads were changed 70 to 80 kN at 1020990 cycles in case of *B1-33* and 80 to 95 kN at 76530 cycles in case of *RB-49* respectively because of time limitation of experiments.

The loading experiments were conducted under four-point bending condition. In case of static loading, the loading speed was fixed in around 0.1 mm/sec in each specimen. Failure in static loading was decided as the load reached the static strength of each beam. In case of cyclic loading, constant upper limit load was applied on each beam until failure. Lower limit load was fixed in 9.8 kN in all beams. Static loading was conducted when the load reached at the target upper limit load, after that, the target upper limit load was applied under 0.3-0.5 Hz of loading frequency. The failure condition of each beam was defined as the condition when the displacement reached at the displacement of static strength.

The Ordinary Portland Cement was used to make specimens. The compressive strengths at the time of experiment are under 50MPa (25-41MPa). The required properties of concrete were; maximum size of cores aggregate was 20 mm, slump was 12 cm, air content was 4.5±1.5 %. The experiments were conducted after 7 days sealing.

4.1.3. Outline of analysis

The analytical cases are shown in Table 4.2. The analytical targets were same with the cases of experiment as shown in Figure 4.2. To confirm the macroscopic behavior under cyclic loading, the upper limit load ratios were changed at 100, 80, 60, 40 % respectively. To confirm the validity of analytical model, *RN-130kN*, *RD-80kN*, *RB-160kN* and *B2-140kN* were analyzed under constant upper limit load.

The analytical mesh models are shown in Figure 4.3. There are two types of analytical models for the case with and without stirrup. From consideration of symmetry, the elements were divided as aspect ratio close to 1 in inner surface direction of the beams. The models were restricted in inner surface direction to analyze as the plane strain problem. The models were divided by 6 in beam width direction. The exponential curve was applied as the tension softening behavior of elements and the index was calculated by volume of element and calculating equation of fracture energy which was proposed by *fib*[2] as mentioned **Chapter 3**. The bond elements were inserted

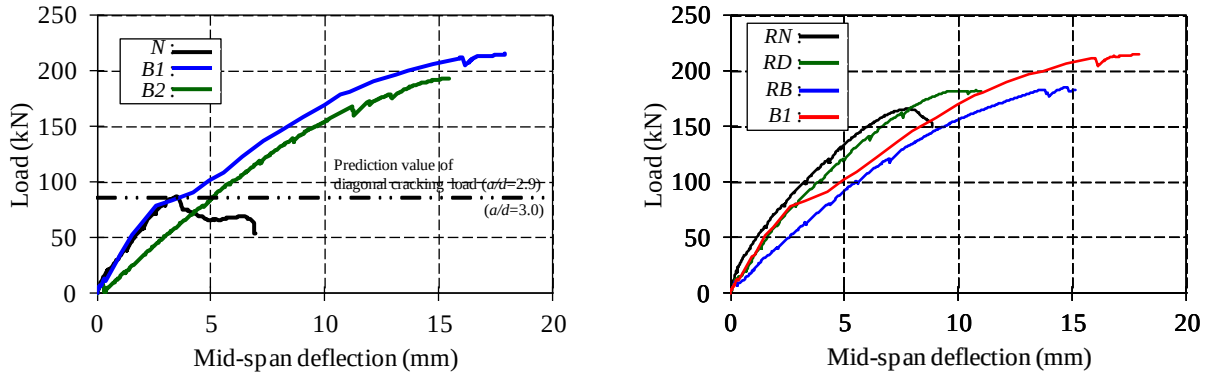

(a) Without stirrup *(b) With stirrup*

Figure 4.4 Load deflection curve

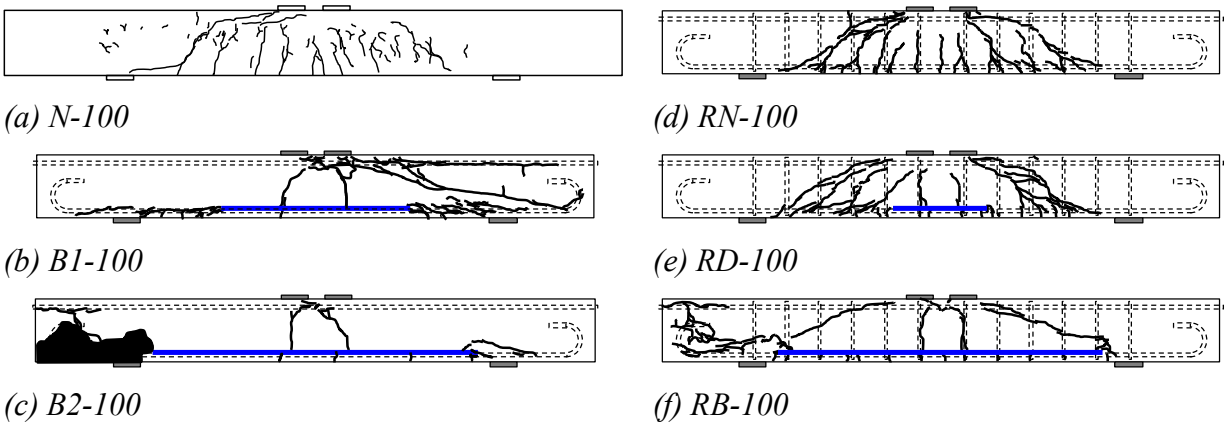

(a) N-100 *(d) RN-100*

(b) B1-100 *(e) RD-100*

(c) B2-100 *(f) RB-100*

Figure 4.5 Crack distribution map at the time of failure

in the analytical models to simulate the slipping behavior of artificial cracks. In case without stirrup, the bond elements were penetrated in longitudinal direction of beams. The part of concrete on the bond elements was expressed as element could not slip. In case with stirrup, the elements were only installed the position of artificial cracks in experiment. The element properties were defined by sensitivity analysis as mentioned later. The existence of stirrup was expressed by introducing the high stiffness and the high friction coefficient on the bond elements compared with the case of no stirrup. The sensitivity analyses were conducted as the load deflection curve of analytical result coincided with experimental result as mentioned following section. As a result of the sensitivity analysis, the properties of bond elements were obtained as shown in Table 4.3. In case with stirrup, the property of bond element was stiffer than that of the case without stirrup. This fact represents dowel action of stirrup.

Static analyses were conducted under displacement control. The displacement speed was 0.06 mm/min. Fatigue analyses were conducted under loading control. The static load was applied during that the load was under target upper limit load. After that, target upper limit load was applied on each beam under 1 Hz of loading frequency.

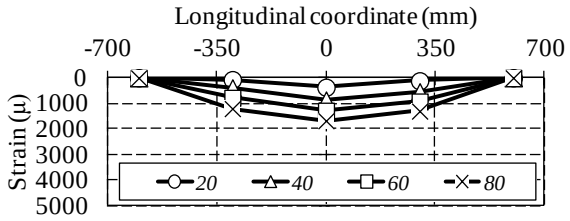

(a) N-100

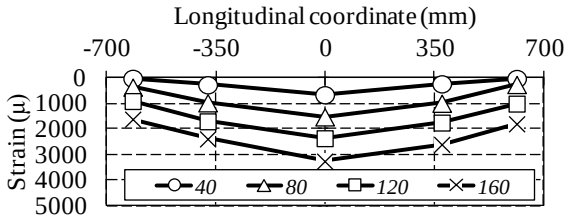

(d) RN-100

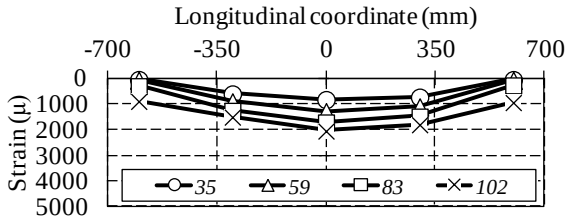

(b) B1-100

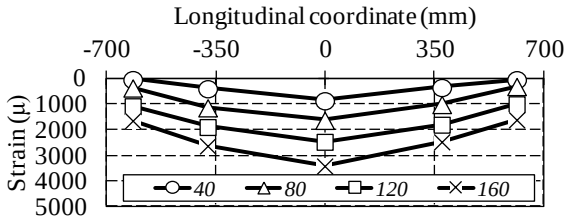

(e) RD-100

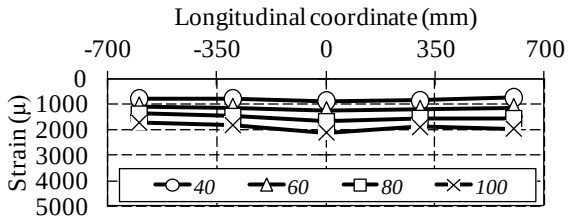

(c) B2-100

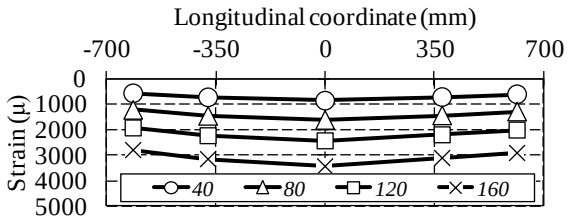

(f) RB-100

Figure 4.6 Strain of tensile rebar

4.2 Behavior under Static Loading

This section describes the effect of stirrup under static loading. To grasp the behaviors, results of static loading experiments and static analyses are explained.

4.2.1. Macroscopic behavior in static loading experiments

The load defection curves in each case are shown in Figure 4.4. In the case without stirrup, the cracked beams showed high strength due to tied arch mechanism (Figure 4.4 *(a)*) as mentioned in **Chapter 3**. It could be regarded that the load carrying mechanism of the beams *B1-100* which had short artificial crack and *B2-100* which had long artificial crack were same mechanism due to propagation of horizontal crack. Thus, compared with the case with stirrup and *B1-100* as representative beam without stirrup, the strengths of the case with stirrup (*RN-100*, *RD-100*, *RB-100*) were lower than that of *B1-100* (Figure 4.4 *(b)*). There is a possibility that strengths in

cases with stirrup were smaller than that of the case without stirrup by reduction of arch mechanism due to dowel action of stirrup.

The static strength of *RN-100* was almost same with the predicted strength 147.0 kN which was derived based on truss theory. In case of cracked beams with stirrup, it was confirmed that the strength showed higher value than that of *RN-100*. It was considered that the increase in the strength was caused by tied arch mechanism even though contribution of the arch mechanism was decreased by existence of stirrup. The stiffness of *RD-100* was higher than that of *RB-100*. The reason was that the slip on the artificial cracks of *RD-100* which had shorter crack was prevented by surrounding concrete of artificial crack compared with the case of *RB-100*.

The crack distribution maps at the time of failure are shown in Figure 4.5. *N-100*, *RN-100* and *RD-100* showed diagonal cracking failure (Figure 4.5 *(a), (d), (e)*). On the other hand, *B1-100*, *B2-100* and *RB-100* which had long artificial crack showed bond splitting failure (Figure 4.5 *(b),(c),(f)*). It could be deduced that the bond splitting failure was caused by appearance of arch mechanism. From these results, it could be deduced that beam mechanism was predominance in case of *N-100*, *RN-100* and *RD-100*. Especially, the horizontal crack which propagated at the crack tip was not observed in case of *RD-100*. It could be considered the cause was that low stress concentration occurred at the position of crack tips inside *D* region compared with other cases as mentioned **Chapter 3**. In addition, this phenomenon was caused by the dowel action of stirrup which contributed to prevent slipping of artificial crack surface.

Focused on the strain distribution along tensile rebar as shown in Figure 4.6, the bending behavior in case of *N-100*, *RN-100* and *RD-100*were confirmed (Figure 4.6 *(a), (d), (e)*). On the other hand, the tendency of strain showed almost constant value in case of *B1-100*, *B2-100* and *RB-100* (Figure 4.6 *(b),(c),(f)*). Especially, in case of *B2-100* and *RB-100* (Figure 4.6 *(c),(f)*), the strain distributed consistently after bending crack occurred. It could be deduced that *B2-100* and *RB-100* showed arch mechanism. However, the actual contributed load of arch mechanism was unknown. To investigate the actual contributed load in each mechanism, the FE analyses were conducted.

4.2.2. Validity of analytical models

Before the investigation, the validity of analytical models was confirmed. The reproducibility of load deflection curves in each case are shown in Figure 4.7. It was confirmed that the initial stiffness and peak load in each case were good agreement with experimental results in each case. Especially, in case of the beam with stirrup, the load deflection curves were coincided well with experimental result except post peak behavior. It was considered that one of the reasons of the good agreement in case with stirrup was installing method of bond element. Because in case of the beam with stirrup whose bond elements were not penetrated in horizontal direction completely. As a result, the slip behaviors of the artificial crack surface were rather close to actual

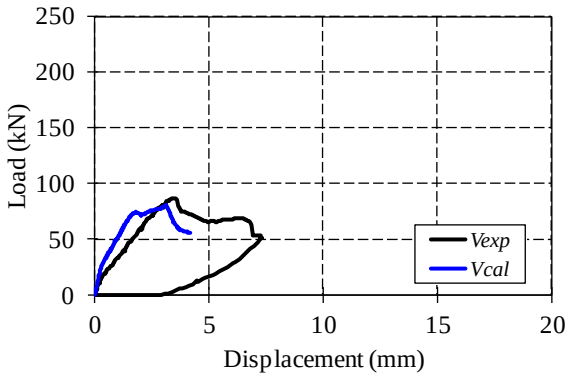

(a) N-100

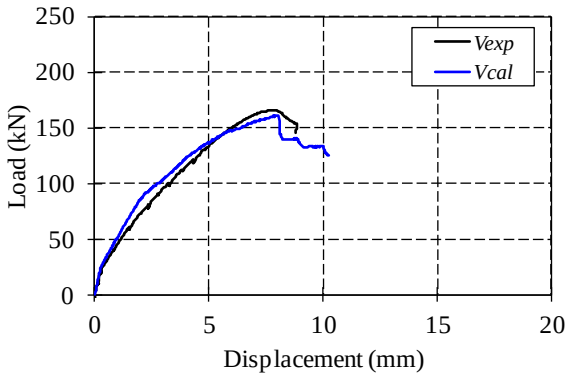

(d) RN-100

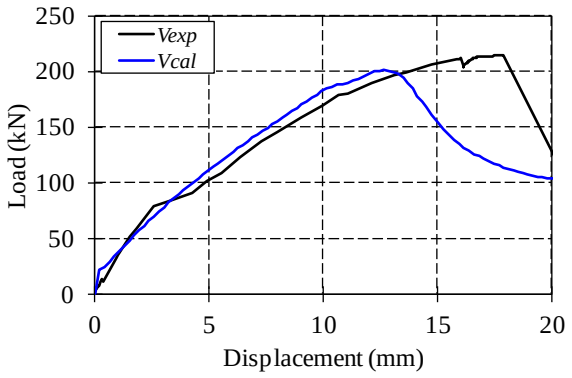

(b) B1-100

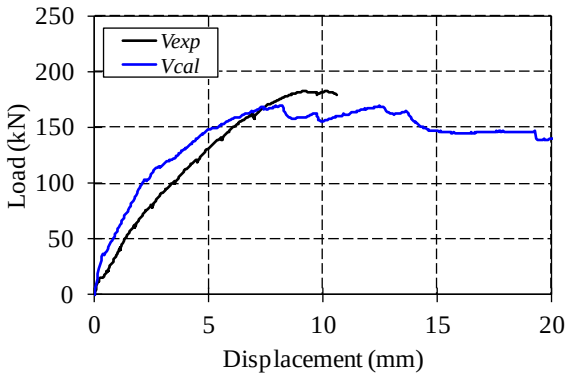

(e) RD-100

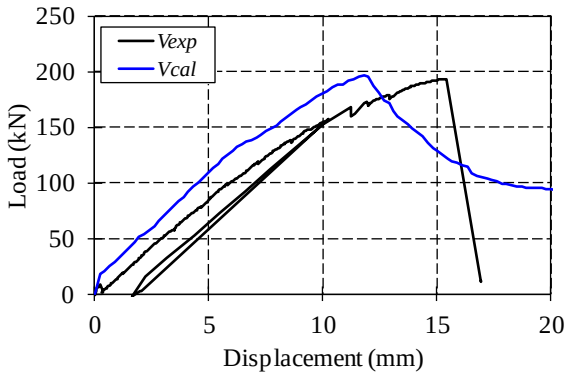

(c) B2-100

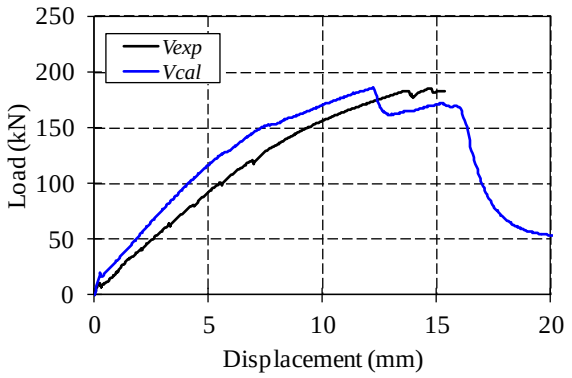

(f) RB-100

Figure 4.7 Reproducibility of load deflection curves

behaviors which were observed by experiments.

Focused on the maximum (tensile) principal strain distribution map as shown in Figure 4.8, it was confirmed that the strain distributions were almost coincide with experimental crack distribution enough to explain the failure mode. In case of *N-100*, *RN-100* and *RD-100* (Figure 4.8 *(a),(d),(e)*), the diagonal cracks at failure were reproduced. In addition, in case of *B1-100*, *B2-100* and *RB-100* (Figure 4.8 *(b),(c),(f)*), the bond splitting failure and propagated crack along

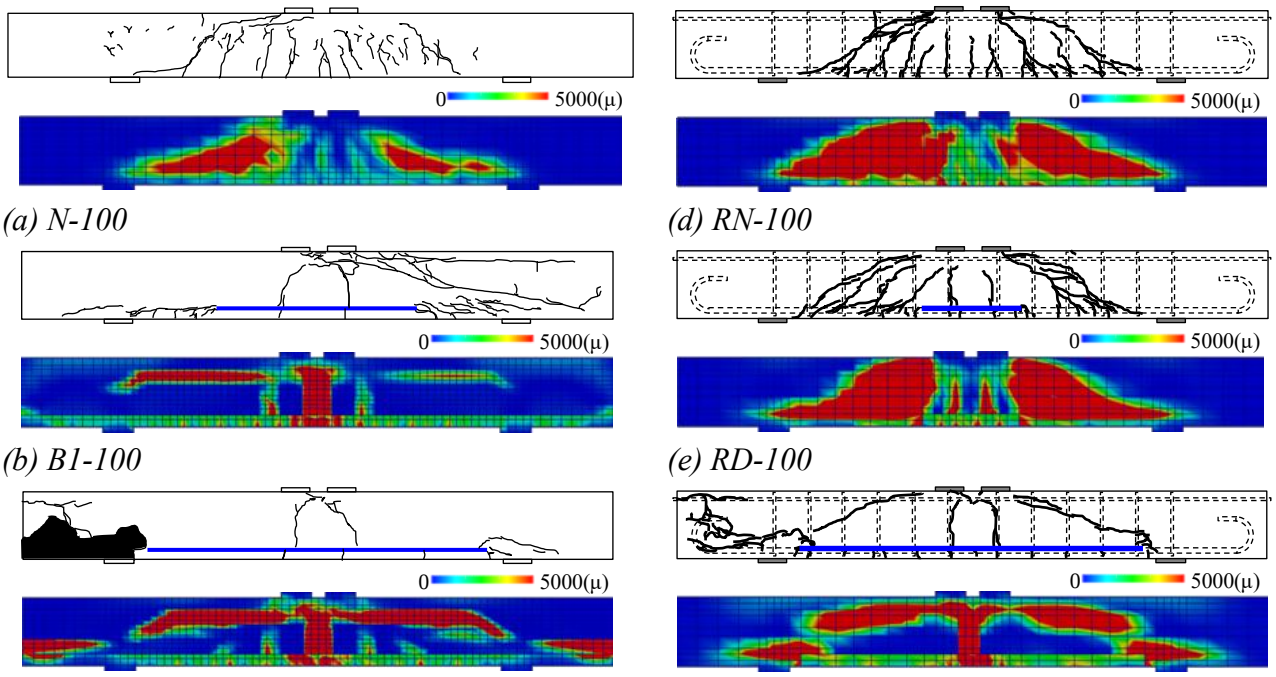

(a) N-100 *(d) RN-100*

(b) B1-100 *(e) RD-100*

(c) B2-100 *(f) RB-100*

Figure 4.8 Reproducibility of crack distribution at the time of failure

compressive rebar were reproduced. It could be deduced that appearance of arch mechanism was reproduced in case of *B1-100*, *B2-100* and *RB-100*.

From the tendency of load deflection and maximum principal strain distribution, it could be regarded that the validity of analytical model was enough to reproduce the load carrying mechanism. Thus, the contributed load of arch and beam were calculated from these analytical results based on the decomposition method as mentioned **2.2**.

4.2.3. Effect of stirrups under static loading

From the result of static analysis, the contributed load of arch and beam mechanism was calculated to confirm the tendency of load carrying mechanism which was observed in the experiments. The decomposition results of load carrying mechanism are shown in Figure 4.9. The black, orange and red line shows experimental, analytical and calculated results respectively. It was confirmed that these three lines were almost coincide with each other. Thus, validity of calculating procedure was confirmed.

Also, the blue and green lines represent contributed load of beam and arch mechanism respectively. Focused on the result of *N-100*, it was confirmed that beam mechanism was predominance near the peak load, after that, arch mechanism appeared just before ultimate failure of the beam. This tendency is fundamental behavior of the RC beam (Figure 4.9 *(a)*).

In case of *B1-100* and *B2-100* which had no stirrup, it was confirmed that the mechanism was almost similar. The arch mechanism was predominance compared with sound beam because of

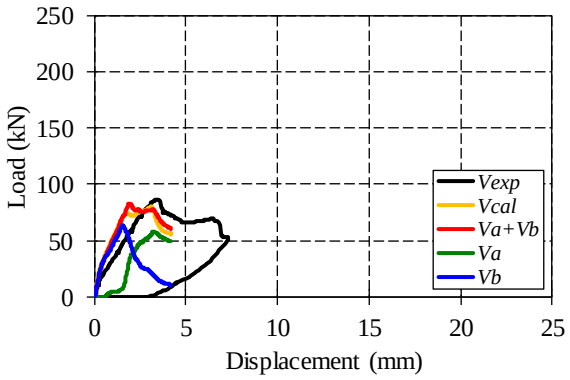

(a) N-100

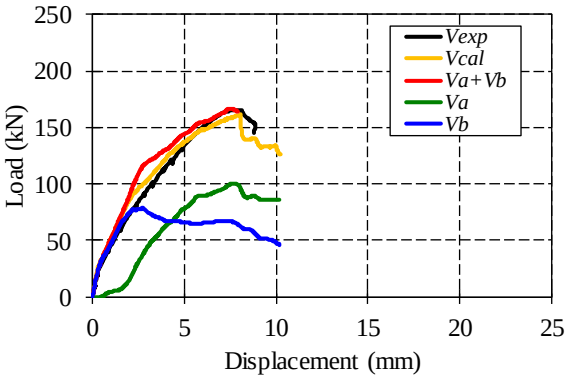

(d) RN-100

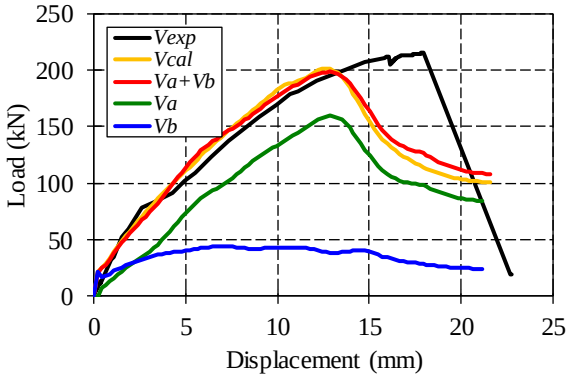

(b) B1-100

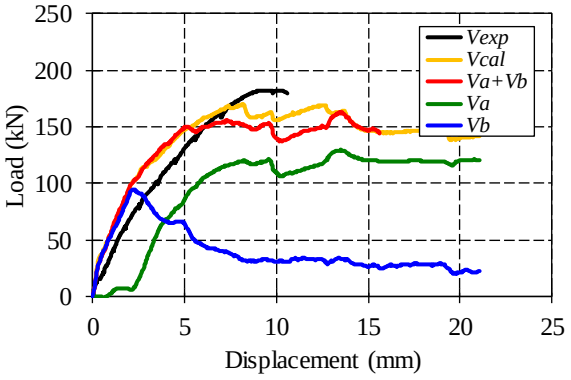

(e) RD-100

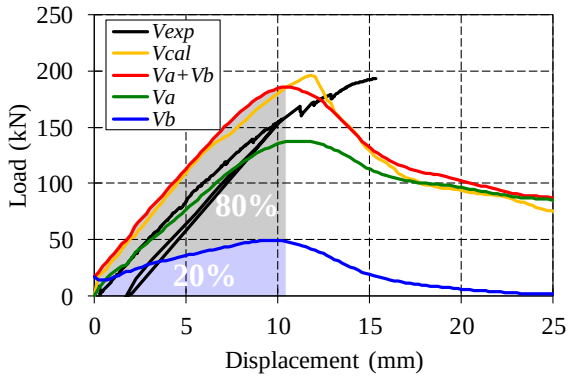

(c) B2-100

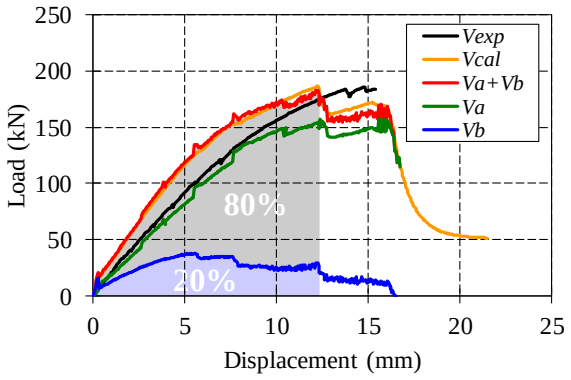

(f) RB-100

Figure 4.9 Decomposition results of load carrying mechanism

propagation of horizontal cracks (Figure 4.9 *(b), (c)*).

Focused on the result of *RN-100*, beam mechanism was kept after the failure of the beam and the arch mechanism appeared before ultimate failure of the beam (Figure 4.9 *(d)*). From comparison with the tendency of arch mechanism in case of the *N-100*, it is considered that the keeping of beam mechanism was caused by contribution of stirrup because the stirrups contributed the appearance of truss mechanism which was one of the beam mechanisms.

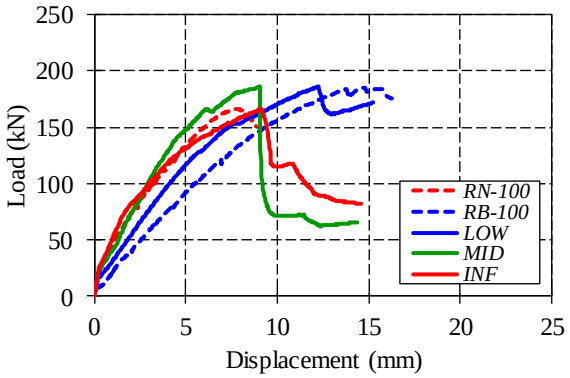

(a) Load deflection curve

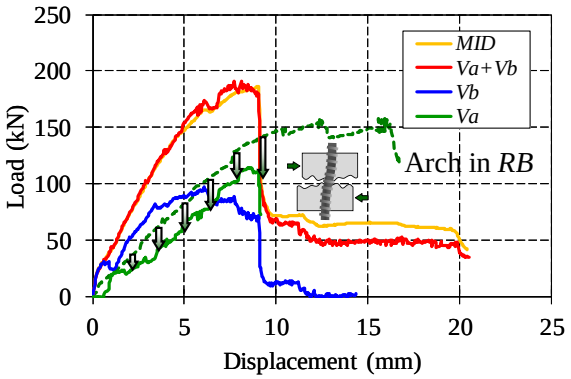

(c) Each mechanism in case of MID

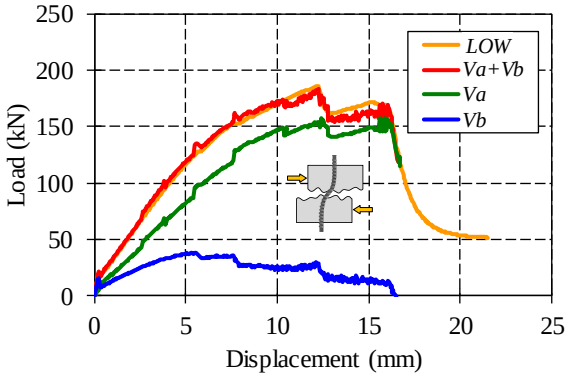

(b) Each mechanism in case of LOW

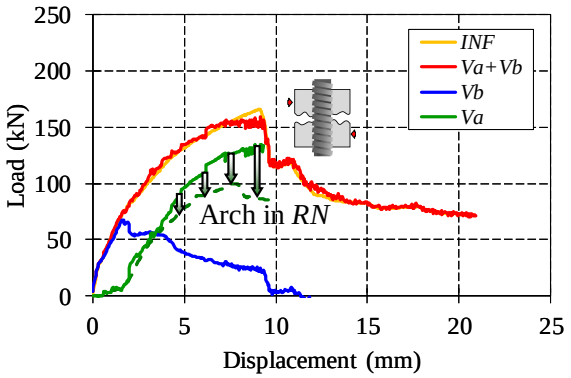

(d) Each mechanism in case of INF

Figure 4.10 Effect of magnitude of shear transfer to arch mechanism

In case of *RD-100*, the similar mechanism with the case of *RN-100* was confirmed (Figure 4.9 *(e)*). This tendency represented that the crack inside *D* region did not affect the load carrying mechanism of the RC beam. It is considered that the reason was that magnitude of stress concentration at the crack tip was relatively lower compared with that of *B* region. The difference of magnitude of stress concentration was confirmed in the **3.3**. However, there is a possibility that the relatively lower stress concentration affects to the load carrying mechanism in case of fatigue due to cyclic stress at the crack tips as mentioned in **3.3**.

In case of *RB-100*, the contributed load of arch mechanism was predominance (Figure 4.9 *(f)*). Focusing on the energy absorption before the peak load in case of *RB-100* and *B2-100* to identify the effect of stirrup, the absorbed energy of arch and beam were approximate 80 and 20 % respectively in both case of *RB-100* and *B2-100*. It was confirmed that no remarkable effect of stirrup in case of cracked beams whose artificial crack length was same. There was a possibility that the magnitude of shear transfer on the artificial crack surface was not remarkably change only in case of the experiments because small diameter of stirrup was installed inside of the specimens.

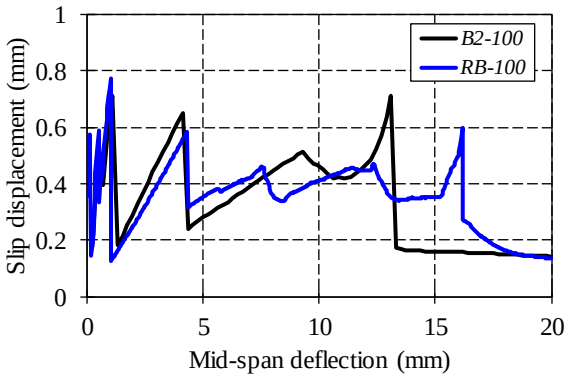

Figure 4.11 Slip displacement at the middle part of shear span

It is considered that the shear transfer on the artificial crack surface is increased by remarkable appearance of dowel action of stirrup, and that the dowel action is enhanced by increase in the diameter of stirrup. To confirm the effect of change in the shear transfer on the artificial crack surface as the existence of thicker diameter stirrup, sensitivity analysis for the shear transfer was conducted. The results of sensitivity analysis were shown in Figure 4.10. The name of analytical results *LOW*, *MID* and *INF* represents the difference of shear transfer. The *LOW* was the result of reproducing analysis of *RB-100* whose shear stiffness on the artificial crack surface in closing mode was 478 N/mm/mm^2. The shear and normal stiffnesses in closing and opening mode of *MID* were 1000000 and 2500 N/mm/mm^2 respectively to simulate middle shear transfer between the case *LOW* and *INF*. The friction coefficient was inputted 50 to reproduce higher shear transfer than that of *LOW*. The shear and normal stiffnesses in closing and opening mode of *INF* were 999999999 N/mm/mm^2 to prevent sliding on the artificial crack surface completely.

The load deflection curves of the analytical and experimental results were shown in Figure 4.10 *(a)*. It could be confirmed that when the shear transfer became high, the analytical result was close to be the results of *RN-100*. This fact represented that when the diameter of stirrup become larger, the behavior of the beams was close to be the behavior of sound beam.

Focusing on the change in contributed load of arch and beam mechanism in each case, the contributed load of arch mechanism in case of *MID* decreased compared with the case of *LOW* (Figure 4.10 *(b), (c)*). It was also confirmed that in case of *INF*, the change in arch and beam mechanisms became similar tendency compared with the case of reproducing analysis in *RN*. It was proved that when the shear transfer became larger, contributed load of arch mechanism decreased.

There is a necessity to identify that the decrease in the contributed load of arch mechanism was caused by increase in the shear transfer on the artificial crack surface as the dowel action as mentioned in 4.1.1.

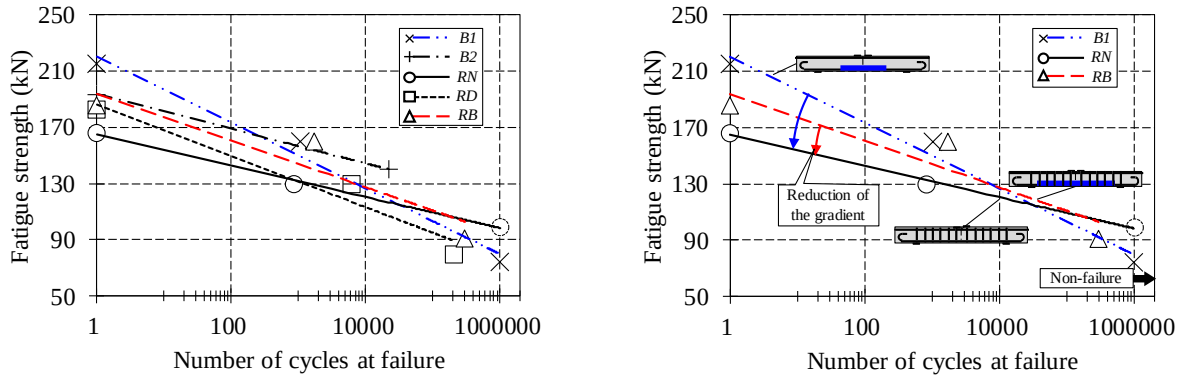

(a) All case *(b) RN, B1 and RB*

Figure 4.12 Fatigue strength against number of cycles at failure

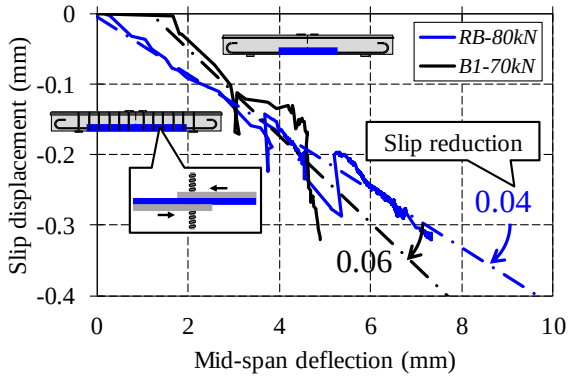

Figure 4.13 Slip displacement on the artificial crack surface

To confirm the dowel action of stirrup, focused on the slip displacement of artificial crack at the middle part of shear span as shown in Figure 4.11, it could be confirmed that magnitude of slip displacement of *RB-100* was reduced compared with that of *B2-100*. These behaviors were caused by the properties of bond element which represented the dowel action of stirrup.

It was confirmed that the dowel action of stirrup which contributed to increase in the shear transfer on the artificial crack surface decreased contribution of arch mechanism in the static analysis. However, in the experimental case, the difference of shear transfer which was caused by diameter of stirrup did not affect remarkably to the behavior of the cracked beams with relatively small diameter of stirrup.

4.3 Behavior under Cyclic Loading

This section describes the effect of stirrup under cyclic loading. To grasp the behaviors, results of

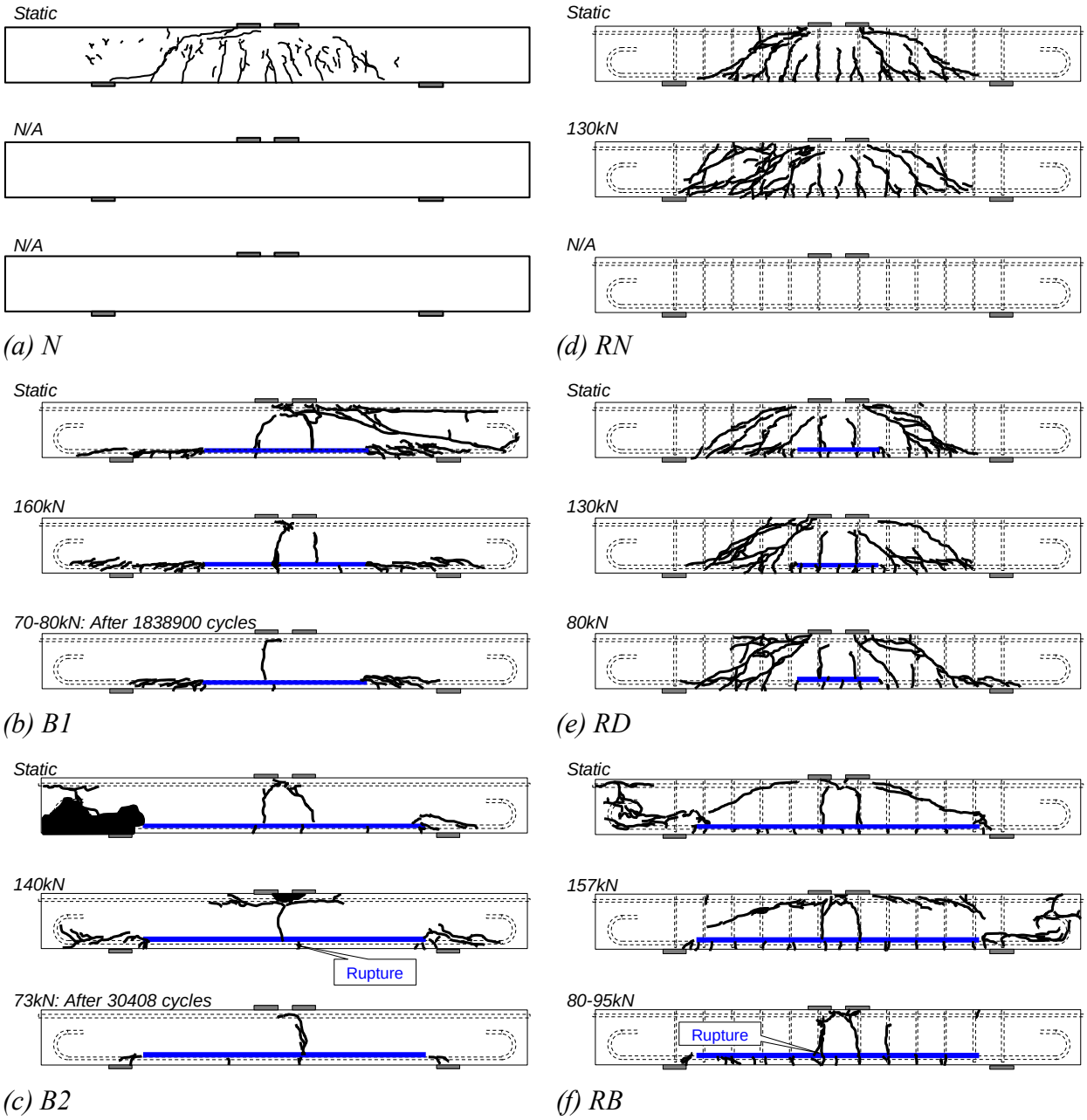

Figure 4.14 Crack distribution map at failure

cyclic loading experiments and fatigue analyses are explained.

4.3.1. Macroscopic behavior in cyclic loading experiments

The fatigue strength against number of cycles in each case with regression line were shown in Figure 4.12. The fatigue strength represented applied upper limit load which was acting on the beam until failure. The one cycle in the number of the cycles at failure in the figure represents the number when the failure caused by static loading in this study. In case of *B1-35* and *RB-49*, the fatigue strength was calculated as weighted averaging by acting cycle, that is, the contribution

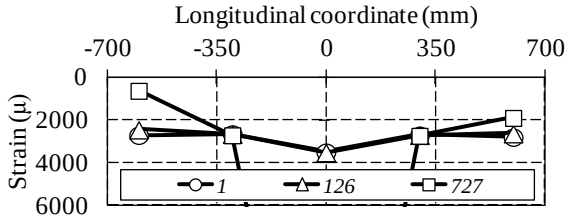

(a) B1-74

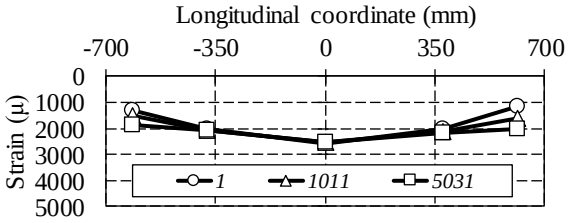

(e) RD-71

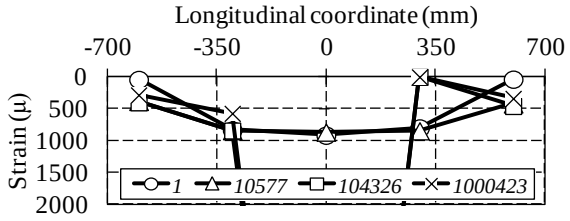

(b) B1-33

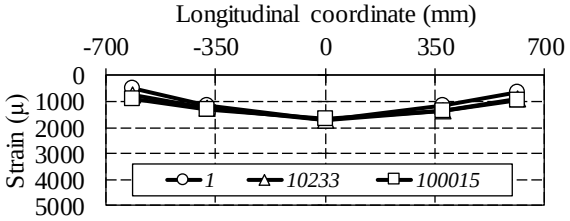

(f) RD-44

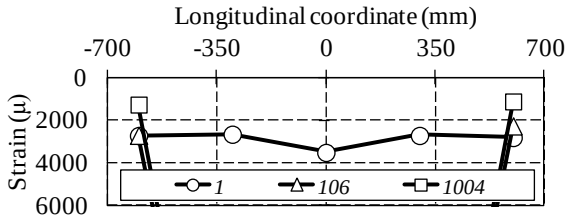

(c) B2-72

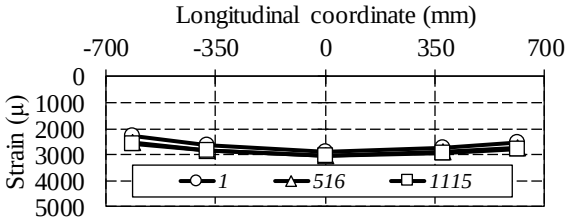

(g) RB-86

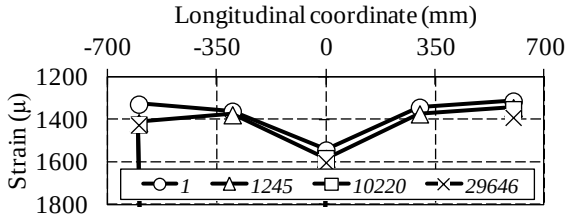

(d) B2-38

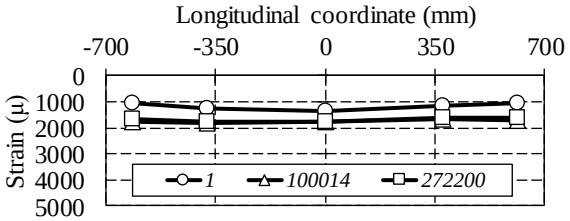

(h) RB-49

Figure 4.15 Strain of tensile rebar

of upper limit load for the fatigue strength was proportional to the number of cycles. In case of *N*, the predicted value of fatigue strength at the 1000000 cycles was shown in the Figure 4.12 based on the result of previous research[2]. The experimental result of *RN-78* was on the line of predicted value of fatigue strength. This tendency was corresponding to previous knowledge that 60 % of fatigue strength appeared at the 1000000 cycles[2].

Focused on the tendency of fatigue strength in each beam, it was confirmed that the fatigue strength of cracked beams showed higher value in the low cycle region, however, the strength showed lower value in the high cycle region compared with sound beam (Figure 4.12 *(a)*). It

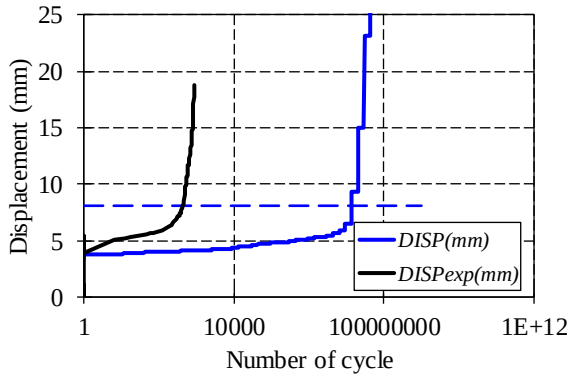

(a) RN-130kN

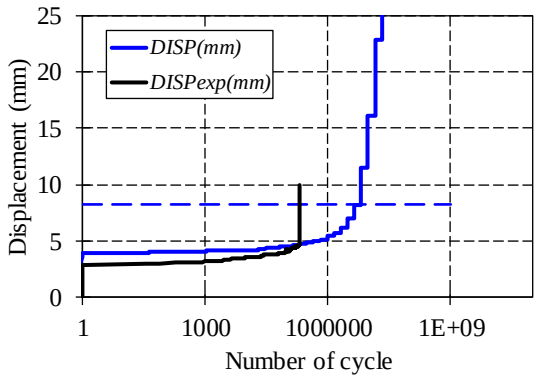

(b) RD-80kN

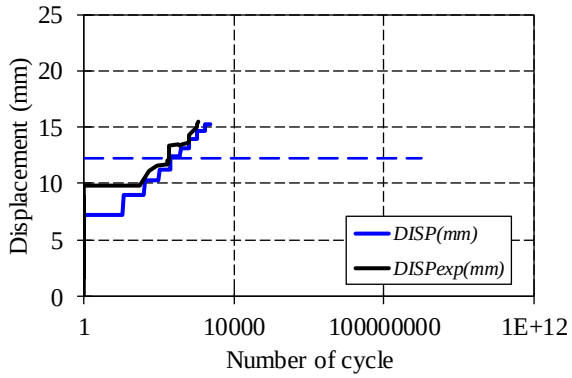

(c) RB-160kN

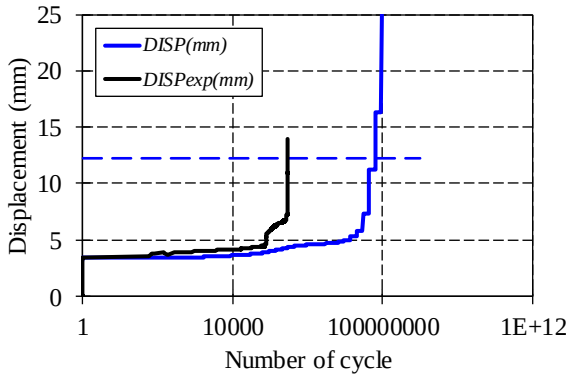

(d) RB-92kN

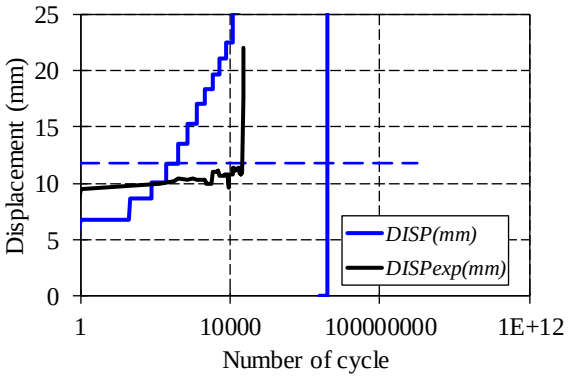

(e) B2-140kN

Figure 4.16 Reproducibility of displacement

could be regarded as the load carrying mechanism of *B1* was same with *B2* from the Figure 4.9 *(b), (c)*. Consequently, focused on the tendency of fatigue strength of *RN*, *B1* and *RB* to identify the effect of stirrup in cracked beams (Figure 4.12 *(b)*), the gradient of regression line in fatigue strength against the number of cycles at failure of *B1* was highest value and *RB* was medium value. The magnitude of gradient could be deduced from the logarithmic regression curve which was also shown in Figure 4.12. The gradient represented the resistibility of fatigue. If the gradient showed large value, the beam was easy to fail under low upper limit load. In other word,

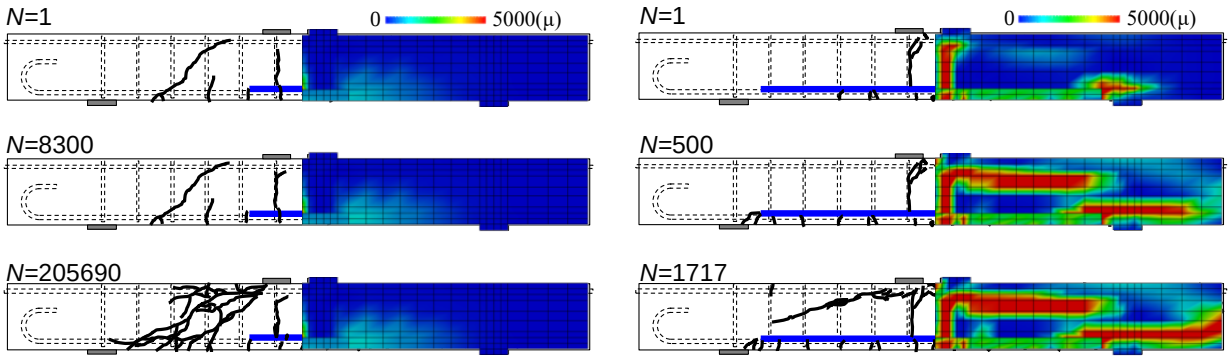

(a) RD-80kN *(b) RB-160kN*

Figure 4.17 Reproducibility of crack distribution

if the gradient was small, the fatigue resistance was high. Therefore, it could be deduced that the fatigue resistance was improved by existence of stirrup even though the fatigue strengths had scatter.

The slip displacement on the artificial crack at the middle shear span against the middle span deflection of the beam in case of *B1-35* and *RB-49* are shown in Figure 4.13. The legalistic regression curve in each case were shown in the figure as dashed line. It was confirmed that the gradient of regression line in case of *RB-49* was lower value than that of *B1-35*. The gradient represented resistibility of slipping. It could be considered that the resistibility of slipping in case of *RB-49* which had stirrup was higher compared with that of *B1-35*. Therefore, it was confirmed that existence of stirrup enhanced the resistibility due to dowel action of stirrup and fatigue resistance was improved by dowel action of stirrup.

The crack distribution map at the time of failure in each loading condition were shown in Figure 4.14. The failure mode in each case was not changed obviously against change in the magnitude of upper limit load. In case of *N*, *RN* and *RD* showed diagonal cracking failure in each upper limit load (Figure 4.14 *(a), (d), (e)*). In these cases, bending crack was propagated, then diagonal crack was propagated. It was considered that there was no effect of existence of crack inside *D* region because of lower stress concentration at the position of crack tips and dowel action of stirrup. On the other hand, in case of *B1*, *B2* and *RB* showed bending fatigue failure in each upper limit load. The failure was caused by cyclic opening of bending crack on the artificial crack surface (Figure 4.14 *(a), (d), (e)*). Especially, in case of *B2-72* and *RB-49*, failure due to rupture of tensile rebar occurred (Figure 4.14 *(c), (f)*). It could be deduced that the cyclic stress which was acting on the tensile rebar was mainly affected the failure behavior of the beams, because failure was caused by rupture of the rebar. There is a possibility that when the beam fails by bending crack, the stirrup does not contribute to support vertical force, because the bending cracks do not across the stirrup.

The strain distributions along tensile rebar against acting cycle in each cycle are shown in the

Figure 4.15. In case of *B1-74*, *B1-33*, *B2-72* and *B2-38*, the strain at the middle span had not measured after the cyclic loading was started (Figure 4.15 *(a), (b), (c), (d)*). It was deduced that the cyclic stress which was acting on the middle span of tensile rebar was mainly affected to the failure mode as shown in Figure 4.14*(a), (b), (c)*. In case of *RD-71*, *RD-44*, the tendencies of strain distribution were not changed remarkably against increase in the cycles (Figure 4.15 *(e), (f)*). However, the magnitude of strain distribution of middle span was relatively high. Thus, it could be considered that the bending behavior was shown in these cases. In case of *RB-86* and *RB-49*, the strain showed constant value in each cycle even though the magnitude was not remarkably changed by increase in the cycles (Figure 4.15 *(g), (h)*).

The qualitative evaluation of the load carrying mechanism from the strain distribution could be conducted. However, there is a necessity to conduct quantitative evaluation of the load carrying mechanism which was deduced from the experimental result. To apply the decomposition method of load carrying mechanism, the FE analysis was conducted.

4.3.2. Validity of analytical models

Before the analytical investigation, the validity of analytical models under cyclic loading was confirmed. The properties of bond element which was installed to simulate the behavior of the artificial crack were decided based on the sensitively analysis. As a result, stiffer property of the bond element in case with stirrup mentioned in Table 4.3 was obtained compared with that of the case without stirrup. This stiffer property represented the dowel action of stirrup.

The reproduced results of displacements were shown in Figure 4.16. The dashed line represents failure displacements in each case. It could be confirmed that the beams showed brittle failure because magnitude of displacement suddenly increased. Focused on the analytical results, the tendency of brittle failure and initial displacement could be reproduced even though the displacements in high cycle region were not coincided.

The maximum principal strain distribution and the crack distribution map against acting cycle in case of *RD-80kN* and *RB-160kN* were shown in Figure 4.17 as the representative case. It was confirmed that in case of *RD-80kN*, the propagation of bending crack and diagonal crack was confirmed, also in case of *RB-160kN*, propagation of bond splitting cracks and horizontal cracks along compressive rebar were confirmed. From these tendencies, it could be regarded that the analytical models showed good agreement with the experimental result in the viewpoint of reproducibility of the load carrying mechanism.

Therefore, the fatigue analysis was conducted by using these analytical models and decomposition method was applied for the analytical results because it is considered that these analytical models can reproduce the load carrying mechanism of cracked RC beams.

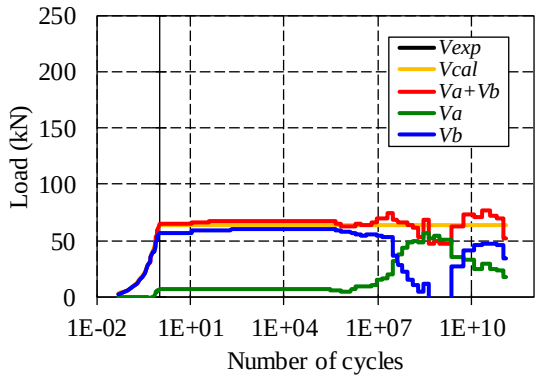

(aa) N-80

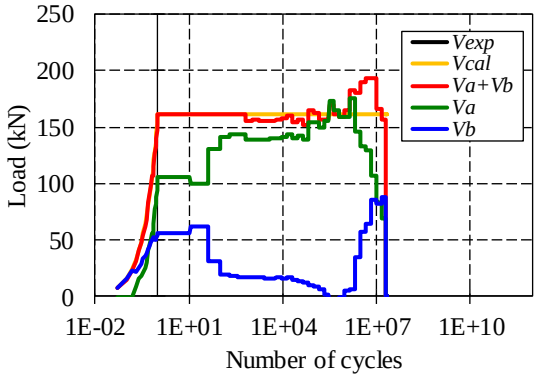

(ba) B1-80

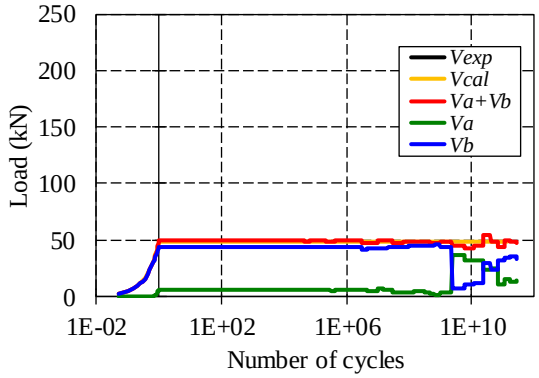

(ab) N-60

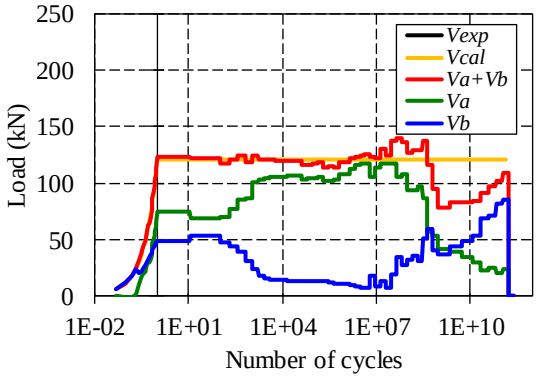

(bb) B1-60

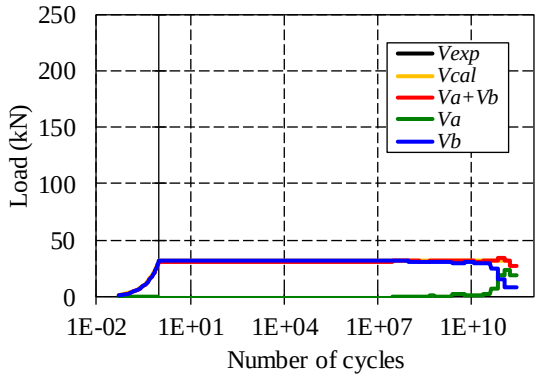

(ac) N-40

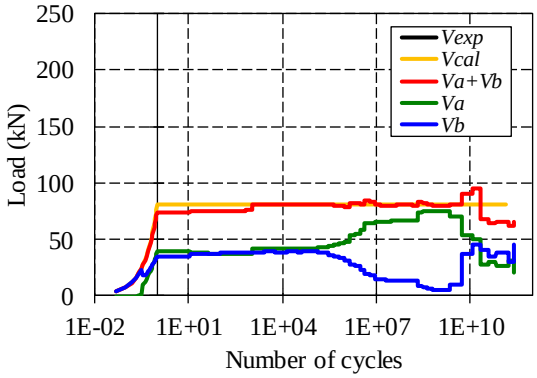

(bc) B1-40

Figure 4.18 Tendencies of load carrying mechanism against number of acting cycles

4.3.3. Change in contributed load under cyclic loading

The contributed load of arch and beam mechanism in each case were calculated by using the analytical model as mentioned in previous section.

The tendencies of maximum value of contributed load in the load carrying mechanism against acting cycle of all cases are shown in Figure 4.18. The sum of calculated load (red line) almost

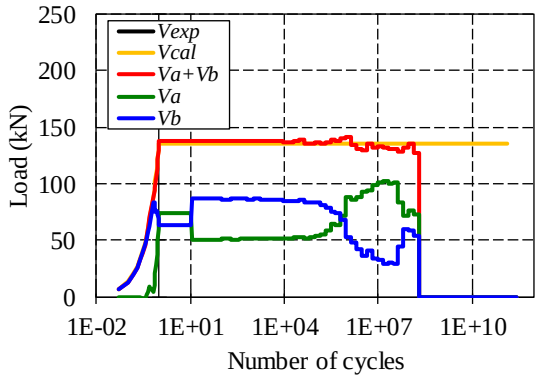

(ea) RD-80

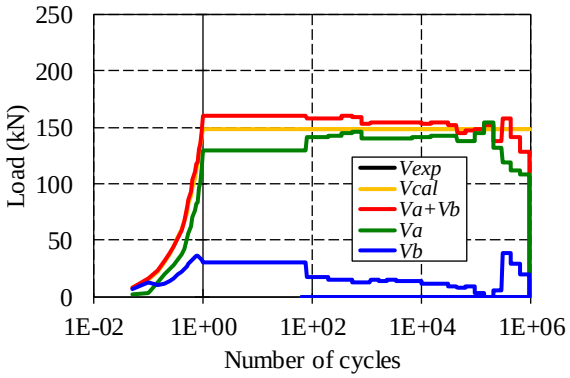

(fa) RB-80

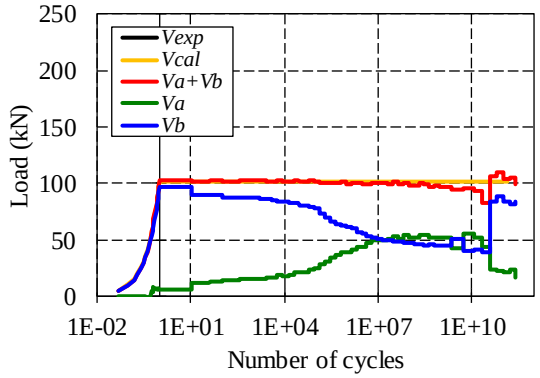

(eb) RD-60

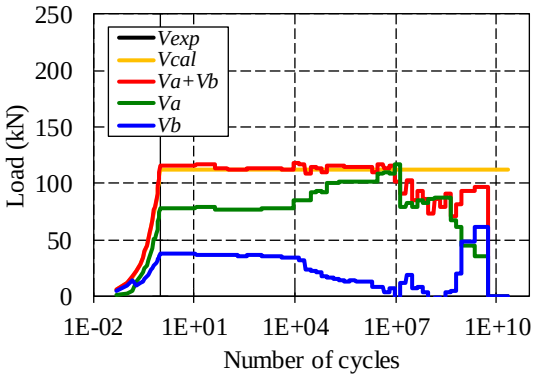

(fb) RB-60

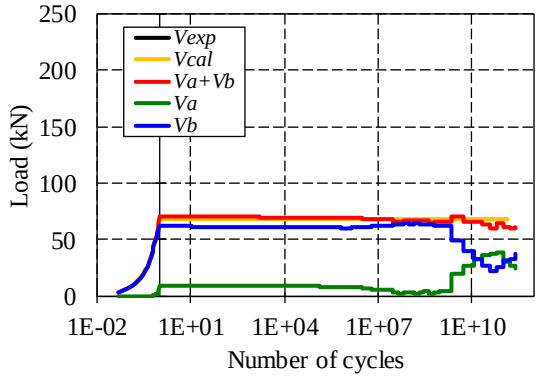

(ec) RD-40

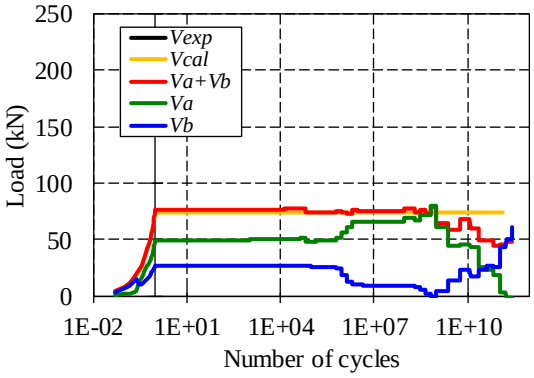

(fc) RB-40

Figure 4.18 Tendencies of load carrying mechanism against number of acting cycles

agreed with the target upper limit load in each case (orange line) even though large scatter occurred in high cycle region. The contributed load of arch mechanism in each case showed increase tendency by increase in the number of acting cycles. However, when the relatively small upper limit load was applied, the contributing ratio was difficult to change. In addition, at the first time that applied load reached the upper limit load, the contributing ratio of arch and beam mechanism was not remarkably changed with the case of static loading. In case of the beam whose contributing ratio of arch became high under the high level of the static load, the tendency

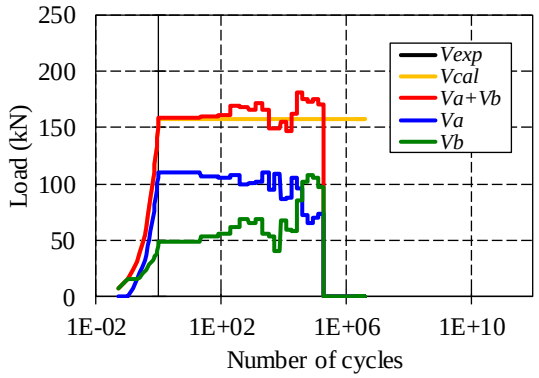

(ca) B2-80

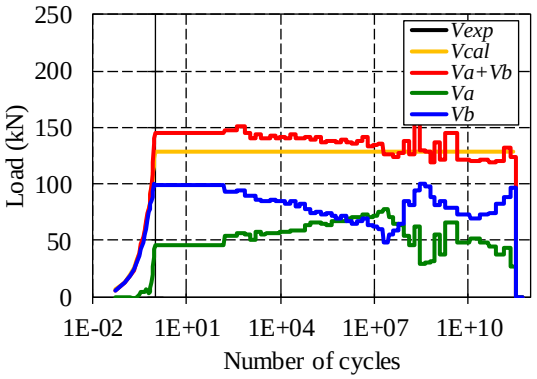

(da) RN-80

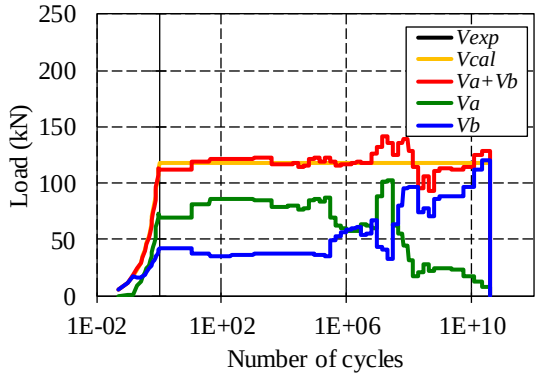

(cb) B2-60

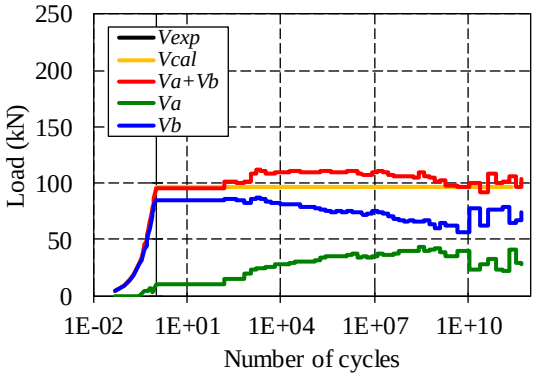

(db) RN-60

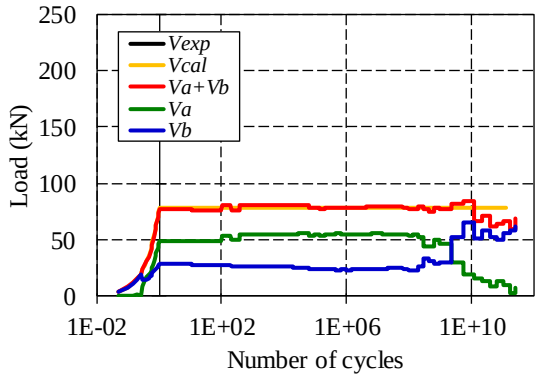

(cc) B2-40

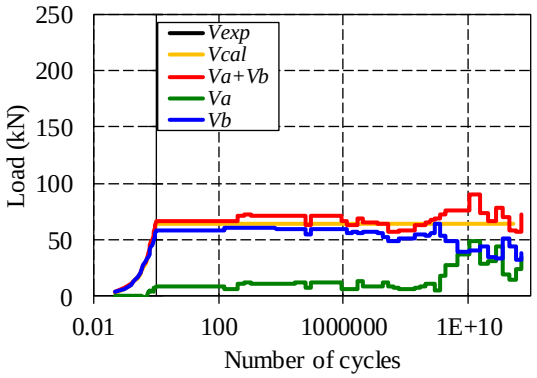

(dc) RN-40

Figure 4.18 Tendencies of load carrying mechanism against number of acting cycles

that the arch mechanism was easy to appear under high upper limit load was confirmed.

Normally, the arch mechanism was predominance just before ultimate failure of the beam except the cracked case. This fact represented that the arch mechanism was predominance under high upper limit load. In addition, it was confirmed that the arch mechanism decreased fatigue resistance as mentioned **Chapter 3**. Therefore, it could be considered that the fatigue life in low cycle region shown in the Figure 4.12 was decreased by high contribution of acting arch

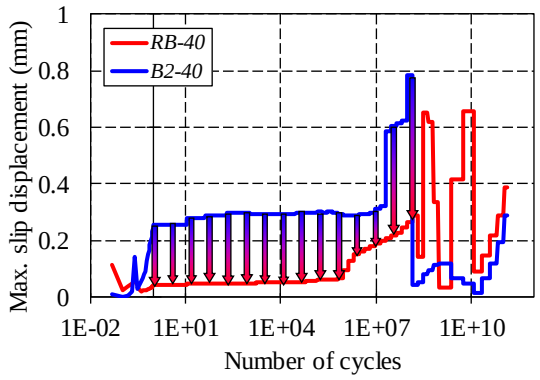

Figure 4.19 Maximum slip displacement against number of acting cycles

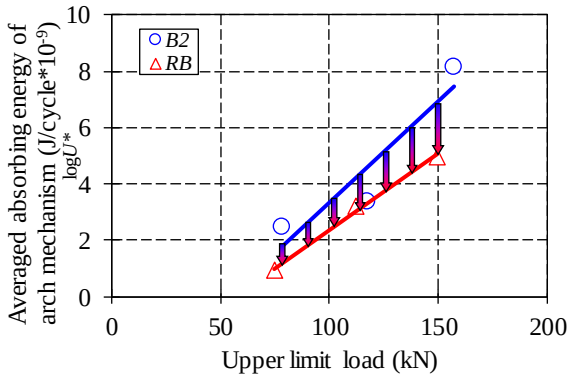

Figure 4.20 Averaged absorbing energy of arch mechanism in B2 and RB

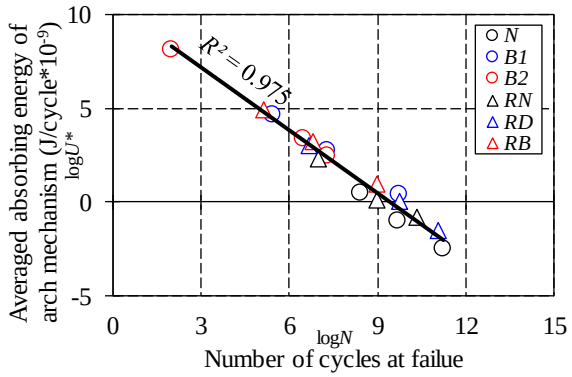

Figure 4.21 Averaged absorbing energy of arch mechanism against number of cycles at failure

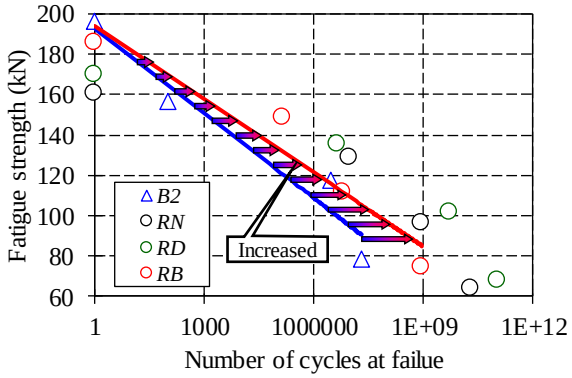

Figure 4.22 Relationship between fatigue strength and number of cycles at failure in analysis

mechanism.

It is expected that the contributed load of arch mechanism is decreased by the dowel action of stirrup as mentioned in previous parts. To confirm the effect of stirrup under cyclic loading, the slip displacements on the artificial crack surface at the mid shear span in case of *RB-40* and *B2-40* under almost same upper limit load were focused. The displacement against number of acting cycles is shown in Figure 4.19. It is confirmed that the magnitude of displacement was decreased in case of *RB-40* compared with the case of *B2-40*. This phenomenon was caused by the large shear transfer on the artificial crack surface which simulated large dowel action of stirrup in case of *RB-40*. It could be confirmed that the dowel action of stirrup was able to express by using this analytical model.

To confirm the reduction of arch mechanism due to the dowel action, amount of absorbing energy of arch mechanism until the ultimate failure of the beam was calculated. The absorbing energy of arch mechanism was calculated by following equation.

$$U_a^* = \frac{1}{N_f}\int_0^{u_f} V_{a(u)}^{max}\,du \qquad (4.2)$$

Where, U_a^*: absorbing energy of arch mechanism per one cycle until the ultimate failure, N_f: number of cycles at failure, u_f: failure displacement, $V_{a(u)}^{max}$: maximum contributing load of arch mechanism in each cycle.

Figure 4.20 shows absorbing energy of arch mechanism per one cycle until the ultimate failure in case of *RB-40* and *B2-40*. The absorbing energy in case of *RB-40* was decreased compared with the case of *B2-40* regardless of magnitude of applied upper limit load. It was confirmed that contribution of arch mechanism was remarkably decreased by dowel action of stirrup under cyclic loading.

There is a possibility that the number of cycles at failure of the beams could be explained by magnitude of absorbing energy of arch mechanism regardless of corrosion crack position, applied load and existence of stirrup. From this view point, relationship between absorbing energy of arch mechanism per one cycle and number of cycles at failure was focused.

Figure 4.21 shows the absorbing energy of arch mechanism per one cycle against number of cycles at failure. The regression curve with determinant coefficient was also illustrated in the figure. The determinant coefficient was calculated by following equation.

$$R^2 = \frac{\{\sum(U_i - \overline{U})\,(U_{ai}^* - \overline{U}_{ai}^*)\}^2}{\sum(U_i - \overline{U})^2 \sum(U_{ai}^* - \overline{U}_{ai}^*)^2} \qquad (4.3)$$

Where, U_i: data set of regression curve, $\overline{U}$: averaged value in the data set of regression curve, U_{ai}^*: data set of the absorbing energy, $\overline{U}_{ai}^*$: averaged value in the data set of the absorbing energy.

From the figure, it was confirmed that the absorbing energy and number of cycles at failure in each beam had higher correlation regardless of corrosion crack position, applied load and existence of stirrup. From these results above, it could be considered that fatigue life in case of *RB* in each fatigue strength was increased compared with *B2* due to decrease in the absorbing energy of arch mechanism by dowel action of stirrup (Figure 4.12). Figure 4.22 shows relationships between fatigue strength and number of cycle at failure in analytical results. The increase in the fatigue life in case of *RB* was observed both cases in experimental and analytical results as shown in Figure 4.12 and Figure 4.22.

It was proved that the absorbing energy of arch mechanism contributed to decrease the fatigue resistance and the contribution could be reduced by introducing the stirrup, and that the reduction of absorbing energy occurred under cyclic loading, even if the effect of dowel action of stirrup was relatively small under static loading. These results can be obtained from decomposition method of arch and beam mechanisms based on experimental results which is explained in **Appendix D**.

4.4 Summary of Chapter 4

This chapter described the effect of stirrup under cyclic loading in the cracked RC beams. To make clear the effect of stirrup, cyclic loading experiments and FE analyses were conducted by using the beams which had different length of artificial cracks and stirrup.

As a result of static loading experiments, in case of sound beam and the beam which had the artificial crack inside *D* region, the failure mode showed diagonal cracking failure. On the other hand, in case of the beam which had the artificial crack inside *B* region, the failure mode showed bond splitting failure. It represented that the effect of crack inside of *D* region could be neglected. As a result of experiments, effect of stirrup to the load carrying mechanism was small. However, from the results of sensitively analysis for the shear transfer on the artificial crack surface which simulate effect of dowel action of stirrup, it was confirmed that the dowel action of stirrup was contributed to decrease arch mechanism. When the dowel action of stirrup was increased, the load carrying mechanism of the cracked beam became similar mechanism with the sound beam.

As a result of cyclic loading experiments, it was confirmed that when the beams had stirrup, the fatigue life was increased in each fatigue strength compared with the case without stirrup. From the results of FE analyses, the fatigue life in each fatigue strength in case of the beam which had artificial crack inside B region with stirrup was increased. It was proved that the reason was reduction of energy absorption in the arch mechanism until ultimate failure of the beam due to dowel action of stirrups, even if the effect of dowel action was relatively small under static loading. Moreover, it was confirmed that there was high correlation between the energy absorption of the arch mechanism and number of cycles at failure.

References in Chapter 4

[1] Niwa, J., Yamada, K., Yokozawa, K., Okamura, H.: Revaluation of the Equation for Shear Strength of Reinforced Concrete Beams without Web Reinforcement, *Journal of Japan Society of Civil Engineers*, Vol.372, No.5, pp.167-176, 1986.8.

[2] Higai, T.: Fundamental Study on Shear Failure of Reinforced Concrete Beams, *Proceedings of the Japan Society of Civil Engineers*, Vol.279, pp.113-126, 1978.11. (in Japanese)

CHAPTER 5
BEHAVIOR OF RC BEAMS WITH REAL CORROSION CRACKS

This chapter describes the behavior of RC beams with real corrosion cracks. From the knowledge, validity of reproducing method of the load carrying mechanism of corroded beams by using artificial crack is discussed. To confirm the validity, corrosion acceleration test and cyclic loading experiment were conducted. The rebar corrosion cracks were introduced in the center of span to make similar condition with the case of the beams which had artificial crack. The corrosion ratio was defined as 20 and 50 % in case of the beam with and without stirrup respectively. As a result of the cyclic loading experiment, rupture of tensile rebar occurred regardless of the crack reproducing method. From the tendencies of displacement and crack distribution of the cracked beams with and without stirrup, it was confirmed that the load carrying mechanism of the corroded beams could be simulated by introducing the artificial cracks.

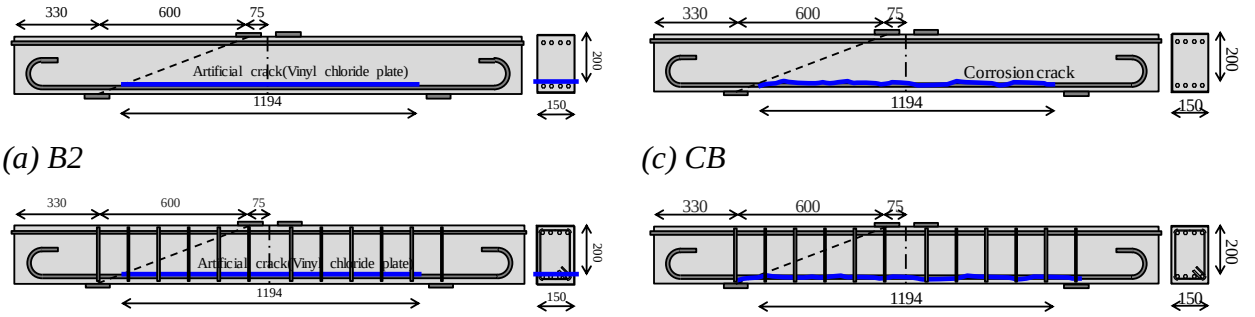

(a) B2 *(c) CB*

(b) RB *(d) CRB* (unit: mm)

Figure 5.1 Shape and size of specimens

Table 5.1 Experimental cases

Name of specimens	Upper limit load ratio (%)	Upper limit load (kN)	Failure displacement (mm)	Real mass loss (%)	Number of cycles at failure
B2-72	72	140.0	15.33	-	22364
RB-49	43-51	80-95	14.81	-	298785
CB	-	15.0	15.33	50	72241
CRB	-	80.0	14.81	20	4891

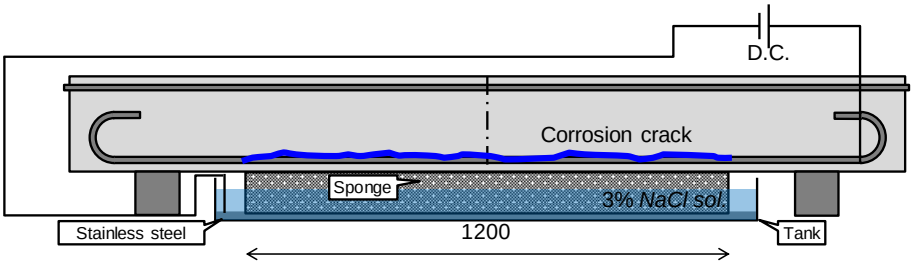

Figure 5.2 Set up of corrosion acceleration test

5.1 Outline of Experiment

To confirm that the beams which had artificial cracks could simulate the behavior of the beams which had real corrosion cracks, the corrosion acceleration test and cyclic loading experiments were conducted. This section describes the experimental procedures of corrosion acceleration test and cyclic loading experiments.

5.1.1. Experimental cases

The shape and size of specimens are shown in Figure 5.1. The shape of the beam was same in all cases. *B2-72* and *CB* were the case without stirrups and *RB-49* and *CRB* case were with stirrups. The shear span ratio *a/d* was fixed as 3.0. *B2-72* and *RB-49* had artificial cracks inside of *B* region where the arch mechanism became predominance. The corrosion cracks were inserted in the *CB* and *CRB* cases. The length of corrosion cracks was same in *B2-72* and

RB-49. The specimens were designed to fail in shear in sound state.

The details of experimental cases are shown in Table 5.1. In case of *B2-72* and *CB*, the upper limit load was decided as the load when the bending crack reached the position of compressive rebar. In case of *RB-49* and *CRB*, the upper limit load was decided as almost same as the predicted value of diagonal cracking load in sound state. The target mass loss of *CB* and *CRB* was decided to assume the severe state of actual corrosion. The corrosion of rebar was caused by corrosion acceleration test.

Figure 5.2 shows the setup of corrosion acceleration test. The corrosion rate can be accelerated electrically in this test. To introduce the corrosion crack with the target length, the sponge with 3% sodium chloride (NaCl) solution was attached on the bottom surface of the beam. The stainless steel was used as the cathode of electric circuit.

5.1.2. Evaluating method of corrosion ratio

The current applying time was decided based on Faraday's law. The method is explained in the following part.

The weight loss of rebar can be expressed as follows:

$$W = \alpha IT \tag{5.1}$$

Where, W: weight loss of rebar (g), α: constant which was obtained by the previous research[1] (0.766), I: current (A), T: current applying time (h).

The corrosion ratio can be expressed as follows:

$$C = \frac{m - m_c}{m} \tag{5.2}$$

Where, C: corrosion ratio, m: unit mass of rebar per 1 cm (g), m_c: unit mass of corroded rebar per 1 cm (g).

The weight loss of rebar can be rewritten as follows:

$$W = (m - m_c)l_c = mCl_c = \rho_s A_s C l_c \tag{5.3}$$

Where, l_s: corroded length of rebar, ρ_s: density of rebar, A_s: cross sectional area of rebar.

Substituting *(5.3)* into *(5.1)*,

$$T = \frac{\rho_s A_s C l_c}{\alpha I} \tag{5.4}$$

From the relationship between current and the applying time in *(5.4)*, the current applying time was decided. When the predicted corrosion ratio reached the target value as shown in Table 5.1. The corrosion acceleration test was stopped. The change in the corrosion ratio in *CB* and

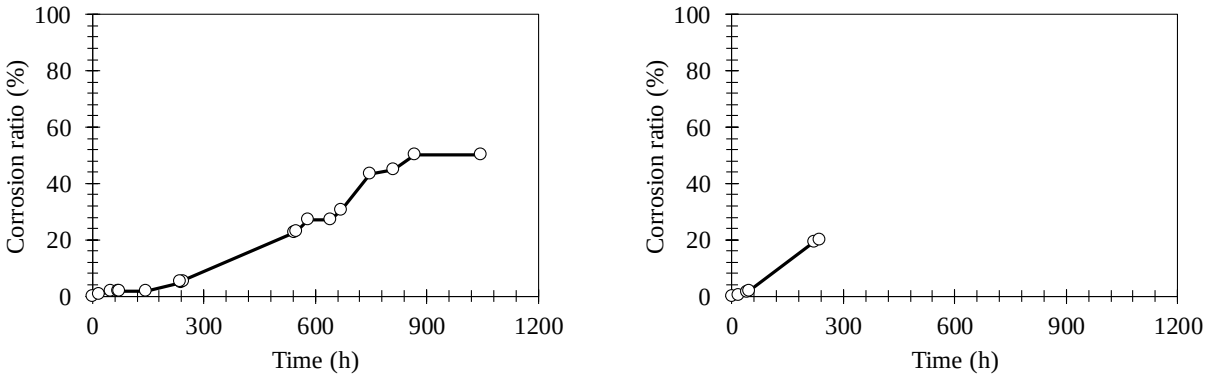

(a) CB *(b) CRB*

Figure 5.3 Change in corrosion ratio

CRB is shown in Figure 5.3.

5.1.3. Loading conditions

The loading experiments were conducted under the same condition mentioned in the previous chapters. The experiments were conducted under four-point bending condition. The constant upper limit load was applied on each beam until failure. The lower limit load was fixed at 9.8 kN in all beams. Static loading was conducted when the load reached the target upper limit load, after that, the target upper limit load was applied under 0.3-0.5 Hz of loading frequency. The failure criteria of each beam were decided as the displacement reached the displacement at the static strength of *B2* and *RB* as shown in Table 5.1.

5.2 Surface Appearance of Specimens

Surface appearance of specimens after corrosion acceleration test is shown in Figure 5.4. In case of *CB*, the cracks were concentrated in one side (Figure 5.4 *(a)*). The most severe condition was observed on the bottom surface. It could be considered that the expansion pressure was released mainly on the bottom surface. The red hatching part represents where the concreate was spalled off. The position was also concentrated only in one side. Thus, it could be deduced that rupture of tensile rebar occurred at this position even though the averaged crack width in vertical direction was approximately 0.9 mm. This width represented severe condition of corrosion.

On the other hand, focused on the surface appearance in case of *CRB*, it could be confirmed that the most severe state of corrosion cracks appeared also on the bottom of the beam (Figure 5.4 *(b)*). The horizontal cracks along tensile rebar which was shown in case of *CB* was not observed. It could be considered that the reason of this tendency was decrease in the cracking pressure due

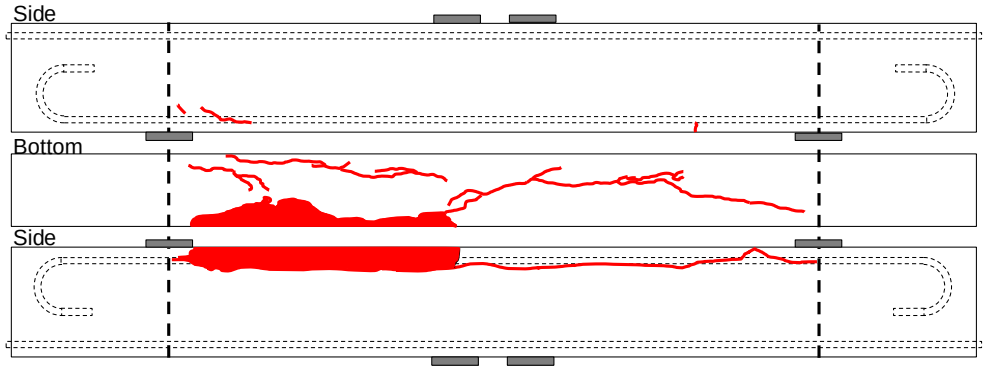

(a) CB

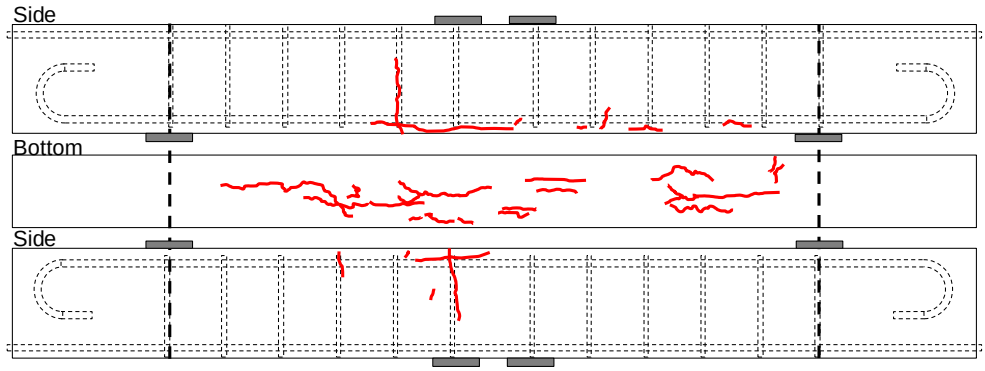

(b) CRB

Figure 5.4 Surface appearance of specimens after corrosion acceleration test

to the vertical crack which propagated along the stirrups. Actually, the vertical crack along the stirrups was observed, thus, it was confirmed that corrosion crack was relatively distributed since the expansion pressure was released by opening of the vertical crack.

In the both cases, the horizontal crack along tensile rebar did not penetrate in lateral direction (beam width direction). This condition was different from the condition of the artificial cracks used in this study. However, it can be considered that the tensile stress which is transferred on the tensile rebars becomes almost constant because the bonding stress between rebars and concrete was completely lost due to the corrosion cracks on the bottom side of the beam. Since the beam failed in the rupture of tensile rebar mentioned later. If the bond between concrete and rebar was completely lost, tensile force of rebar became constant, and tied arch mechanism appeared (*See.* **Chapter 3**). There was a possibility that this condition made tied arch mechanism which was observed in case of artificial cracks. Therefore, the cyclic loading experiments were conducted by using these corroded beams.

5.3 Crack Propagating Behavior

The change in displacement in each case are shown in Figure 5.5. It was confirmed that the

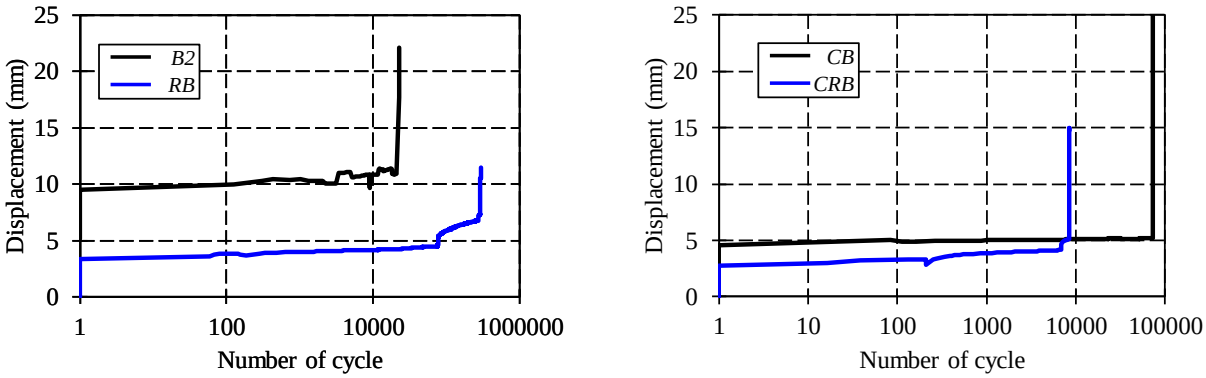

(a) With artificial cracks *(b) With corrosion cracks*

Figure 5.5 Change in mid span displacement

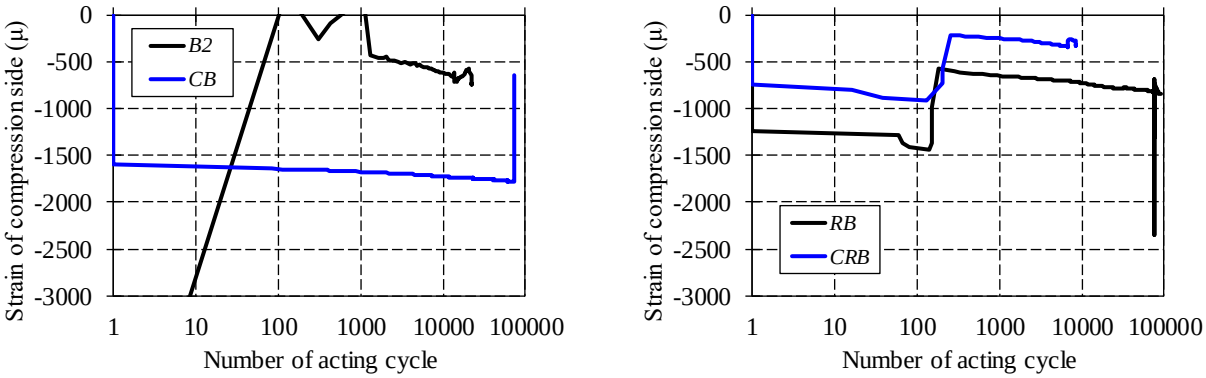

(a) Without stirrup *(b) With stirrup*

Figure 5.6 Strain of concrete at mid span in compressive side

beam showed brittle failure because the magnitude of displacement suddenly increased just before the failure. The failure was caused by rupture of tensile rebar as mentioned later.

Focused on the compressive strain of concrete at the mid span (Figure 5.6), in case of *B2* and *CB*, it was confirmed that the compressive failure of concrete did not occur before the failure of beams because the magnitude of strain did not reach 3500 μ which was typical compressive failure strain of concrete (Figure 5.6 *(a)*). Also, in case of *RB* and *CRB*, it was confirmed that the compressive failure of concrete did not occur before the failure. In addition, increase in the strains around 100 cycles were observed in each case because magnitude of the upper limit loads in both case was almost same (Figure 5.6 *(b)*).

The crack distribution map of corroded beams is shown in Figure 5.7. In case of *CB*, the bending cracks appeared in the phase of static loading until the upper limit load. After cyclic loading was started, the horizontal crack propagated along compressive rebars. The failure occurred by rupture of tensile rebar at mid span with spalling of concrete around tensile rebars

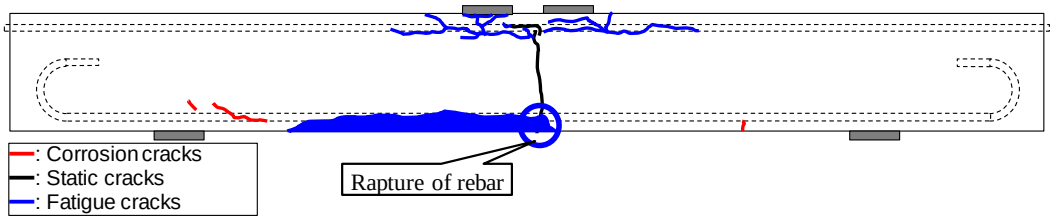

(a) CB

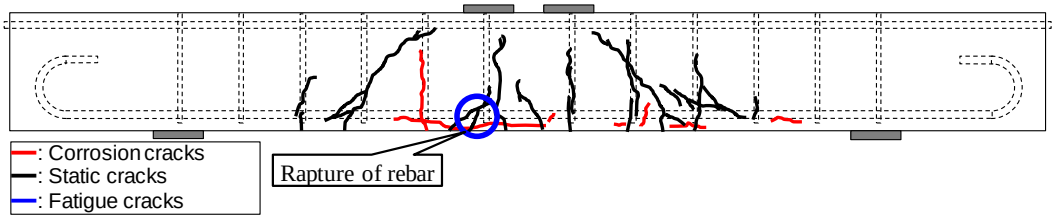

(b) CRB

Figure 5.7 Crack distribution map of corroded beams

due to cyclic opening of bending cracks at the circle point in Figure 5.7 *(a)*.

In case of *CRB*, the bending cracks and diagonal cracks appeared in the phase of static loading until the upper limit load. Contrary to the case of *CB*, the propagation of cracks due to cyclic loading was not observed. Finally, the failure occurred by rupture of tensile rebar at the mid span due to cyclic opening of bending cracks at the circle point in Figure 5.7 *(b)*.

5.4 Validity of Reproducing Method of Load Carrying Mechanism by Artificial Crack

Comparisons of crack distributions with the beams which had artificial crack and corrosion crack are shown in Figure 5.8. It was confirmed that the crack distribution maps of each case almost agreed.

In case of *B2*, the failure occurred due to rupture of tensile rebar at the circle point in Figure 5.8 *(a)* with the propagation of bond splitting crack at the anchorages. Also, the propagation tendency of bending crack was almost same as the case of *CB*. From the tendencies of propagation of bending cracks and rupture of tensile rebar with propagation of horizontal crack along compressive rebar, it was considered that the load carrying mechanisms of *B2* and *CB* were almost same even though propagation tendency of bond splitting crack was different. Therefore, it could be considered that the tied arch mechanisms appeared in case of *CB* and *B2*.

In case of *RB*, the failure occurred due to rupture of tensile rebar at the circle point in the Figure 5.8 *(b)*. This failure mode was similar with the case of *CRB*. However, the propagation of

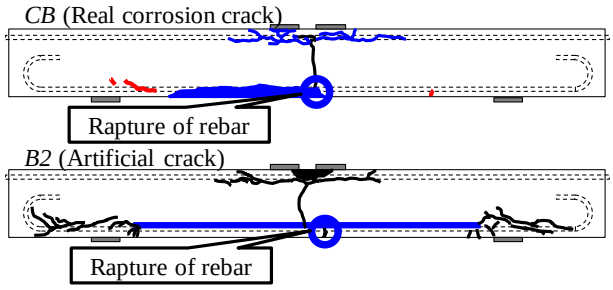

(a) Without stirrup

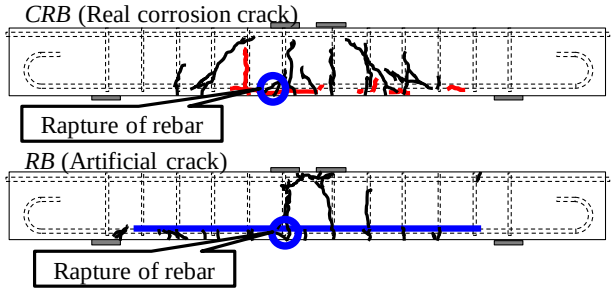

(b) With stirrup

Figure 5.8 Comparisons of crack distribution

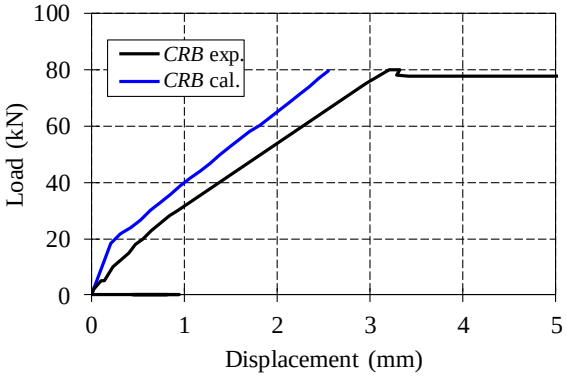

(a) Load deflection curve

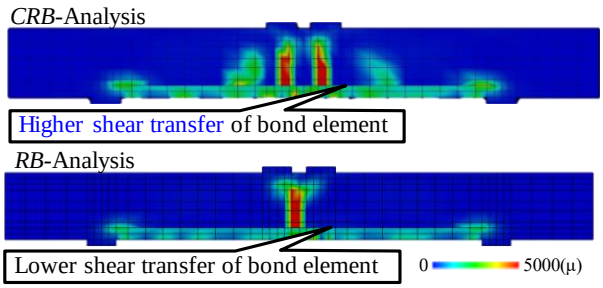

(b) Maximum principal strain map

Figure 5.9 Results of sensitivity analysis

diagonal cracks which was observed in case of *CRB* was different from the case of *RB*. It was considered that this reason was the remaining bond stress between concrete and rebar at the middle position of shear span in the phase of static loading. The existence of remaining bond stress could be deduced from the phenomena that the corrosion crack did not continuously occur in horizontal direction on the bottom surface as shown in Figure 5.4 *(b)*. It could be considered that the rupture of tensile rebar occurred due the bond stress disappeared with increase in the cycles. Therefore, it could be considered that the load carrying mechanism of *CRB* and *RB* were same. From the change in the displacement and crack distribution, it can be considered that the load carrying mechanism of the corroded beams can be simulated by introducing the artificial cracks.

To confirm that the behavior of the beam which has corrosion cracks can be reproduced by the behavior of the beam which has artificial crack in case of *CRB*, sensitivity analysis by using the analytical model which was mentioned in **Chapter 4** was conducted.

Figure 5.9 shows the results of sensitivity analysis against property of bond element which was installed to reproduce the behavior of artificial crack. The stiffer bond property compared with the case of *RB* was applied in the analytical model of *CRB*. The properties of bond elements in case of *RB* are follows; the shear stiffness in closing mode: 4.7 N/mm/mm^2, The shear stiffness

in opening mode: 0.0 N/mm/mm^2, the normal stiffness in closing mode: 294.0 N/mm/mm^2, the normal stiffness in opening mode: 0.0 N/mm/mm^2, the friction coefficient: 1.4. The properties of bond elements in case of *CRB* are follows; the shear stiffness in closing mode: 9.8 N/mm/mm^2, The shear stiffness in opening mode: 19.6 N/mm/mm^2, the normal stiffness in closing mode: 5880.0 N/mm/mm^2, the normal stiffness in opening mode: 19.6 N/mm/mm^2, the friction coefficient: 1000.

The load deflection curve of *CRB* in case of analytical and experimental results are almost agree in each case (Figure 5.9 *(a)*). It was considered that reason why initial stiffness of analytical result was larger than that of experimental result was caused by reduction of bond stress between concrete and rebar in case of experiment. Focused on the maximum principal strain map in case of *CB* and *CRB*, the diagonal crack which was observed in experiment occurred in case of only *CRB* (Figure 5.9 *(b)*). It could be deduced that the occurrence of diagonal cracks was caused by stiffer bond property which was installed to explain the remaining bond stress between concrete and rebar.

Therefore, it could be confirmed that the behavior of the beam which has corrosion cracks can be reproduced by the behavior of the beam which has artificial crack.

5.5 Summary of Chapter 5

This chapter described the behavior of the RC beams which had real corrosion crack along tensile rebar. The corrosion cracks were installed by corrosion acceleration test. The corrosion ratio was defined 20 and 50 % against the case of the beam with and without stirrup respectively. As a result of surface appearance, in case without stirrup, the corrosion crack along tensile rebar in severe condition was observed. In case with stirrup, the corrosion crack along tensile rebar was not observed due to release of cracking pressure with occurrence of vertical cracks along stirrups.

To discuss the validity of reproducing method of the load carrying mechanism by artificial crack, cyclic loading experiment was conducted. As a result of cyclic loading experiment, it was confirmed that the all beams failed in rupture of tensile rebar regardless of crack reproducing method. From the change in the displacement and crack distribution, it was confirmed that the load carrying mechanism of the corroded beams and the beams with artificial cracks showed the tied arch mechanism.

References in Chapter 5

[1] Sato, T., Hikida, M., Kurachi, H., Kobayashi, K.: Comparison of the Effect of Rebar Corrosion to the Shape of Corrosion due to Electric Corrosion Acceleration and Salt Content, *Proceedings of the Japan Concrete Institute*, Vol.31, No.1, pp.1063-1068, 2009. (in Japanese)

CHAPTER 6
CONCLUSIONS

This chapter describes conclusions and recommendations of this study. The part describes the main conclusions of this study and the summary of the results in each chapter. From these conclusions, the recommendations for next researches are described.

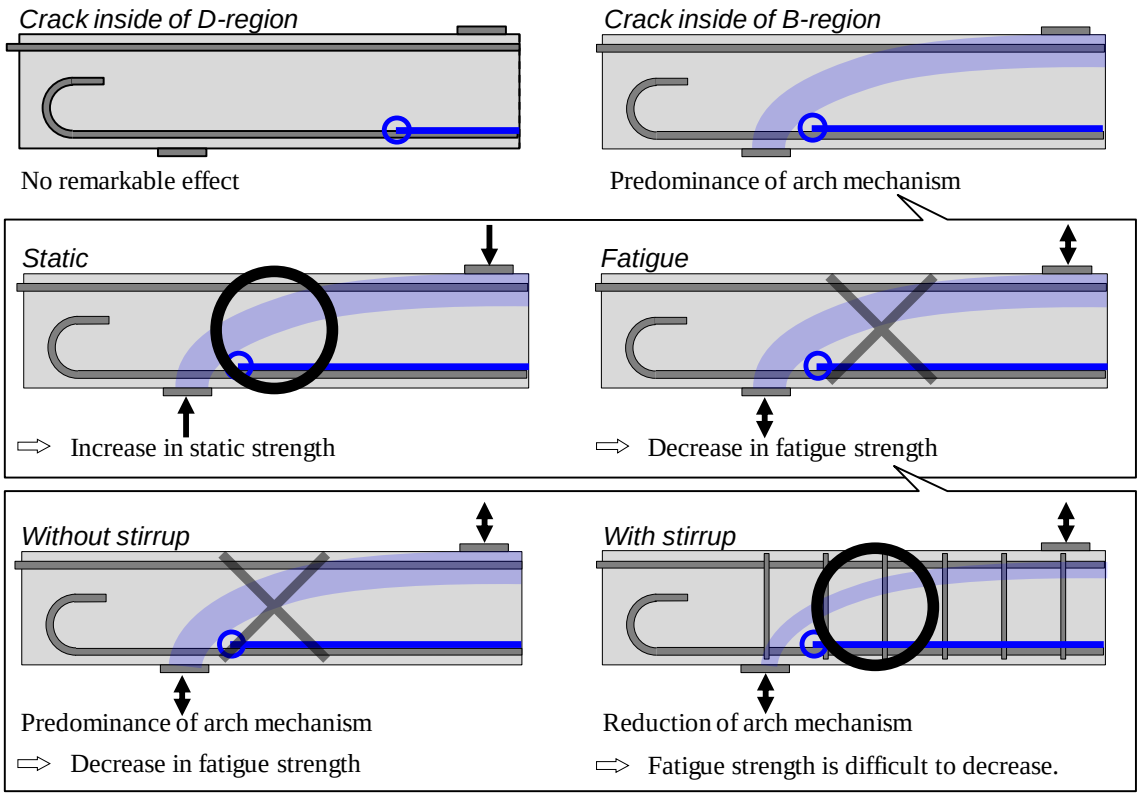

Figure 6.1 Conceptual figure of main conclusion

6.1 Conclusions

To make clear the load carrying mechanism of RC beams which had corrosion crack along tensile rebars, cyclic loading experiment and FE analysis were conducted. The main conclusions (*See.* Figure 6.1) of this study are as follows:

i) When the corrosion crack tips existed inside of the *B* region of RC beams which had a corrosion crack along tensile rebars, the arch mechanism was predominant due to higher stress concentration of the crack tips.

ii) When the corrosion crack tips existed inside of the *D* region of RC beams which had a corrosion crack along tensile rebars, the load carrying mechanism was similar with the sound beams because the effect of stress concentration at the crack tips was small enough to neglect.

iii) Contribution ratios of arch and beam mechanism were not changed against acting number of cycles remarkably even though the ratios depended on the magnitude of upper limit load of cyclic loading.

iv) When the arch mechanism was predominant, the number of cycles at failure became easy to

decrease due to localization of damage accumulating area even though static strength was enhanced compared with sound beam.

v) The existence of stirrups contributed to decrease in the arch mechanism due to dowel action of stirrups on the corrosion crack surfaces.

vi) When the beams had a corrosion cracks along tensile rebar, the fatigue strength of the beam which had stirrups was hardly to decrease compared with the beam without stirrups.

vii) The predominance of arch mechanism could be represented by the phenomena that the load path shows linear shape on the path connected to loading points to supporting points because of stress concentration at the crack tips inside *B* region.

The details of conclusions in each chapter were summarized in the following section.

Chapter 1 explained the background, objective and methodology of this research based on previous review. **Chapter 1** mentioned a necessity to make clear the shear fatigue load carrying mechanism of RC beam with corrosion cracks due to increase in the deteriorated infrastructures. As a result of investigation of previous research, it was decided that this research investigated the effect of corrosion cracks along tensile rebar in shear span and the effect of stirrup in the *a/d* =1.0, 1.6 and 2.9.

Chapter 2 described description methods of the load carrying mechanism. The methods were obtained from FE analysis which was developed by the previous researches. It was described that the constitutive law of the FE analysis was suitable to explain the fatigue behavior of cracked RC beams. The decomposition method of load carrying mechanism was proposed to express the mechanism systematically. The calculating method was developed in this research. Arch and beam mechanisms which represented the contribution for external force by compressive strut truss mechanism respectively were calculated from the stress distribution of the beam in longitudinal direction. The concept of the load path was introduced to visualize these mechanisms. The concept and calculating method was proposed in this research. The load path was defined as a ridge line of the minimum principal stress distribution of the beams. By using this concept, stress flow could be expressed more obviously. The equivalent effective strength coefficient was introduced to apply change in the load carrying mechanism based on the assumption that the mechanism mainly affected by the existence of corrosion cracks and cyclic stress in the beams. The coefficient could be calculated by change in effective strut width and effective strut angle in the strut and tie model. These concepts were applied to describe the load carrying mechanism in the following chapters.

The load carrying mechanism of RC beams without stirrups was made clear in **Chapter 3**. To make clear the mechanism, cyclic loading experiments and FE analyses were conducted by using the specimens which had different length of artificial cracks. The length of artificial crack was

decided based on the area where the vertical stress contribution existed. The experimental results indicated that the load carrying mechanism was governed by tied arch mechanism due to horizontal cracks which propagated from artificial crack tips regardless of loading conditions. In case of the beams whose static strength was enhanced due to the tied arch mechanism, the number of cycles at failure was almost the same as the sound beam under the cyclic load of 40% upper limit load ratio. It was demonstrated that the reason was localization of relative damage accumulation area caused by linearization of the load path. The analytical results showed that the linearization occurred by stress concentration at the position of crack tips which existed inside of *B* region. It was made clear that when the crack tips existed inside of *D* region, the horizontal crack was easy to propagate with increase in the number of loading cycles.

To expand the fundamental knowledge as mentioned above for the design code, the methods to predict of failure position and fatigue life based on the strut and tie model were proposed. As a result of calculation of equivalent effective strength coefficient, it was confirmed that the effective strut width decreased against decrease in upper limit load ratio even though there were no effect of artificial crack length on effective strut angle in case of the beams which showed the arch mechanism predominantly. This fact corresponded to localization of damage accumulating area. In addition, it was confirmed that the calculated values of all cases were higher than most dangerous side in the present design code.

The prediction method of position of crack starting point based on the theory of elasticity showed good agreement with experimental result. A possibility that the crack starting position could be estimate by inputting the shear transfer which was changed by actual corrosion crack width was shown.

The prediction method of fatigue life for compressive failure mode showed also good agreement with experimental result by modification of the elastic modulus based on dynamic elastic modulus. The prediction equation was derived by experimental results of fatigue life and static strength of the strut and tie model. A possibility was shown that the load carrying mechanism of the beams which had a crack along tensile rebars in the shear span was explained by using the strut and tie model and fatigue life could be deduced.

The effect of stirrups under cyclic loading in the cracked RC beams was made clear in **Chapter 4**. To make clear the effect of stirrups, cyclic loading experiments and FE analyses were conducted by using the beams which had different length of artificial cracks with and without stirrups.

As a result of static loading experiments, in case of sound beam and the beam which had the artificial crack inside *D* region, the failure mode showed diagonal cracking failure. On the other hand, in case of the beam which had the artificial crack inside *B* region, the failure mode showed bond splitting failure. It represented that the effect of crack inside of *D* region could be neglected.

As a result of experiments, effect of stirrup to the load carrying mechanism was small. However, from the results of sensitively analysis for the shear transfer on the artificial crack surface which simulate effect of dowel action of stirrup, it was confirmed that the dowel action of stirrup was contributed to decrease arch mechanism. When the dowel action of stirrup was increased, the load carrying mechanism of the cracked beam became similar mechanism with the sound beam.

As a result of cyclic loading experiments, it was confirmed that when the beams had stirrup, the fatigue life was increased in each fatigue strength compared with the case without stirrup. From the results of FE analyses, the fatigue life in each fatigue strength in case of the beam which had artificial crack inside B region with stirrup was increased. It was proved that the reason was reduction of energy absorption in the arch mechanism until ultimate failure of the beam due to dowel action of stirrups, even if the effect of dowel action was relatively small under static loading. Moreover, it was confirmed that there was high correlation between the energy absorption of the arch mechanism and number of cycles at failure.

The validity of reproducing method of the behavior of corroded beams by using artificial crack was confirmed in **Chapter 5**. To confirm the validity, corrosion acceleration test and cyclic loading experiment were conducted. The rebar corrosion cracks were introduced at the center of span to compare the load carrying behavior with the case of artificial cracks. The mass losses of rebars were defined as 20 and 50 % against the case of the beam with and without stirrups respectively. As a result of cyclic loading experiment, rupture of tensile rebar occurred regardless of the crack reproducing methods. From the tendencies of displacement and crack distribution, it was confirmed that the load carrying mechanism of the corroded beams could be simulated by introducing the artificial cracks used in this study.

6.2 Recommendations for Future Researches

The conclusions above were obtained from the experimental and analytical results which treated the beams with corrosion cracks along tensile rebars inside of the shear span. There is a possibility that the different conclusions are derived if the target beams have maldistributed corrosion cracks along tensile, compressive rebars and stirrups.

It is deduced that when the short corrosion crack exists only inside the shear span, a diagonal crack is easy to propagate. In this case, the fatigue life is easy to drop because localization of cyclic strain at the position of stirrups. On the other hand, it is also deduced that the localization of strain can be reduced by corrosion crack which existed along stirrups. Thus, there is a necessity of investigation of effect of corrosion crack position. Moreover, if the shear reinforcement ratio and strength of stirrups increase, it is considered that the dowel action of stirrup is enhanced, and that the contribution of arch mechanism is decreased efficiency even

though the corrosion crack exists inside of *B* region. Therefore, there is a necessity of investigation of effect of shear reinforcement ratio and strength of stirrups as a future work.

The results of this study gave convictions that the load carrying mechanism of deteriorated RC beams is completely made clear by investigating these effects and the steadily accumulation of the knowledge leads establishment of suitable maintenance method for the deteriorated infrastructures and sustainable future.

APPENDIX. A
PROGRAMING CODE ON THE CALCULATION METHOD OF ARCH AND BEAM MECHANISM

The programing code of decomposition method of the load carrying mechanism mentioned in **Chapter 2** based on *Visual Basic* is denoted in this appendix. The calculation methods were separated in the case with and without bond elements.

A.1 The procedure in the case without BOND elements

A.1.1 Form

```
VERSION 5.00
Begin {C62A69F0-16DC-11CE-9E98-00AA00574A4F} UserForm1
   Caption         =   "UserForm1"
   ClientHeight    =   1845
   ClientLeft      =   45
   ClientTop       =   375
   ClientWidth     =   4485
   OleObjectBlob   =   "UserForm1.frx":0000
   StartUpPosition =   1  'Center of owner form
End
Attribute VB_Name = "UserForm1"
Attribute VB_GlobalNameSpace = False
Attribute VB_Creatable = False
Attribute VB_PredeclaredId = True
Attribute VB_Exposed = False

Private Sub CommandButton1_Click()

        Call Main

End Sub

Private Sub Label1_Click()

End Sub

Private Sub UserForm_Click()

End Sub
```

A.1.2 Main procedure

```
Attribute VB_Name = "Module1"
Rem ==========================================================================================================================================

Sub Auto_Open()

        UserForm1.Show (vbModeless)

End Sub

Rem ==========================================================================================================================================

Sub Main()

Dim m, n, i, j, k As Double
Dim Ci, Mi, ygi, yi, xi, Si As Double
Dim yj, xj, xji, yjj, Sjj, Sji, Num_nod As Double
Dim e, ne, nb, yb, a, b, lbok, h, t, d, c, l, s, inc As Double
Dim Arch_Mech, Beam_Mech As Double
Dim varFileName As Variant

MsgBox "Coded by Yuta Yamada 2015" & vbCrLf & "yamada.y.av@m.titech.ac.jp", vbInformation, "Credit"

Rem Input=====================================================================================================================================

Num_nod = Application.InputBox("Number of nodal points?", "Input the number of nodal points", "940", , , , , 1)
ne = Application.InputBox("Number of elements in vertical direction?", "Input the number of elements", "12", , , , , 1)
nb = Application.InputBox("Number of elements in perpendicular to longitudinal direction?", "Input the number of elements", "6", , , , , 1)
yb1 = Application.InputBox("The position of BOND elements in vertical direction?(mm)", "Input the position of elements", "0", , , , , 1)
yb2 = Application.InputBox("The position of BOND elements in vertical direction?(mm)", "Input the position of elements", "0", , , , , 1)
a = Application.InputBox("Shear span?(mm)", "Input shear span", "600", , , , , 1)                                    'Shear span
d = Application.InputBox("Effective depth?(mm)", "Input effective depth", "200", , , , , 1)                         'Effective depth
lbok = Application.InputBox("Anchorage length?(mm)", "Input anchorage length", "330", , , , , 1)                   'Anchorage length
ll = Application.InputBox("Interval of loading points?(mm)", "Input Interval of loading points", "150", , , , , 1)  'Interval of loading points
h = Application.InputBox("Hight of the beam?(mm)", "Input beam hight", "230", 1)                                    'Beam hight
t = Application.InputBox("Thickness of the loading plates?(mm)", "Input thickness of the loading plates", "20", , , , , 1)  'Thickness of the loading plates
bw = Application.InputBox("Width of the loading plates?(mm)", "Input width of the loading plates", "100", , , , , 1)  'Width of the loading plates
b = Application.InputBox("Beam width?(mm)", "Input beam width", "150", , , , , 1)                                   'Beam width
c = h - d                                                                                                           'Covering depth
l = lbok + a
s = lbok + a - 25 - 1

Rem ==========================================================================================================================================

Method = Application.InputBox("Method?", "Selection of methods", "0 or Other key", , , , , 1)
inc = Application.InputBox("Increment?", "Input increment for calculation of resultant force(mm)", "1", , , , , 1)

Rem ==========================================================================================================================================

i = 0

Range(Cells(1, 1), Cells(9999, 9999)).ClearContents

varFileName = Application.GetOpenFilename(FileFilter:="vtu file(*.vtu),*.vtu", Title:="Slect vtu file", MultiSelect:=True)

For Each FileName In varFileName

        i = i + 1
        Worksheets(1).Cells(i + 2, 1) = i

        Call Open_Paste(Num_nod, FileName)

        Application.ScreenUpdating = False

Rem ==========================================================================================================================================

                If Method = 0 Or Method = 9999 Then

                        Call Cal_Arch_and_Truss_Mech_Comp_Tens(e, ne, nb, yb1, yb2, a, b, lbok, ll, h, t, bw, d, c, l, s, inc, Method)

                        Arch_Mech = Worksheets(1).Cells(1, 7)
                        Beam_Mech = Worksheets(1).Cells(1, 10)
                        Shear_Force = Worksheets(1).Cells(1, 13)

                        Worksheets(1).Cells(i + 1, 16) = Arch_Mech
                        Worksheets(1).Cells(i + 1, 17) = Beam_Mech
                        Worksheets(1).Cells(i + 1, 18) = Shear_Force

                        Worksheets(1).Cells(i + 1, 19) = FileName

                Else

                        Call Cal_Arch_and_Truss_Mech_Comp(e, ne, nb, yb, a, b, lbok, ll, h, t, bw, d, c, l, s, inc, Method)

                        Arch_Mech = Worksheets(1).Cells(1, 7)
                        Beam_Mech = Worksheets(1).Cells(1, 10)
                        Shear_Force = Worksheets(1).Cells(1, 13)
```

```
87
88                              Worksheets(1).Cells(i + 1, 16) = Arch_Mech
89                              Worksheets(1).Cells(i + 1, 17) = Beam_Mech
90                              Worksheets(1).Cells(i + 1, 18) = Shear_Force
91
92                              Worksheets(1).Cells(i + 1, 19) = FileName
93
94                      End If
95
96                      If i > 60 Then
97
98                              Application.GoTo Cells(i + 1 - 55, 16), True
99
100                     End If
101
102             Application.ScreenUpdating = True
103
104     Next
105
106     Rem ================================================================================================================================================================
107
108             Worksheets(1).Cells(1, 16) = "Va"
109             Worksheets(1).Cells(1, 17) = "Vb"
110             Worksheets(1).Cells(1, 19) = "Ver.1.05"
111             Worksheets(1).Cells(1, 2) = "NODE"
112             Worksheets(1).Cells(2, 2) = "N/A"
113             Worksheets(1).Cells(2, 3) = "Y(mm)"
114             Worksheets(1).Cells(2, 4) = "Z(mm)"
115             Worksheets(1).Cells(2, 5) = "Stress-YY(MPa)"
116
117             Range(Cells(2, 16), Cells(i + 1, 17)).Select
118
119     End Sub
120
121     Rem ================================================================================================================================================================
122
123     Sub Open_Paste(ByVal Num_nod As Integer, ByVal FileName As Variant)
124
125     Dim buf0, buf1, buf1_xyz, Str As String
126
127     Range(Cells(3, 2), Cells(9999, 6)).ClearContents
128
129     'Open "H:¥01. VTU Data¥10. Effect of Shear Reinforcement¥Main¥SRB¥vtu¥result-00020.vtu" For Input As #i
130     Open FileName For Input As #1
131
132             For j = 1 To 500000
133
134                     Line Input #1, buf0
135
136                             If InStr(1, buf0, "STRESS-YY(MPa)") <> 0 Then
137
138                                     For k = 1 To Num_nod + 1
139
140                                             Line Input #1, buf0
141
142                                             Worksheets(1).Cells(k + 2 - 1, 5) = buf0
143
144                                     Next k
145
146                             End If
147
148                             If InStr(1, buf0, "/PointData") <> 0 Then
149
150                                     For k = 1 To Num_nod + 2
151
152                                             Line Input #1, buf0
153
154                                                     'If IsNumeric(buf0) Then
155
156                                                             For ii = 0 To UBound(Split(buf0, "       "))
157
158                                                                     buf1 = Split(buf0, "       ")
159
160                                                                     Worksheets(1).Cells(k, ii + 1) = buf1(ii)
161
162                                                             Next ii
163
164                                                     'End If
165
166                                     Next k
167
168                             End If
169
170                     If EOF(1) = True Then
171
172                             Exit For
173
174                     End If
175
```

```
176             Next j
177
178     Close #1
179
180     End Sub
181
182     Rem ==========================================================================================================================================================
183
184     Sub Cal_Arch_and_Truss_Mech_Comp_Tens(ByVal e As Double, ByVal ne As Double, ByVal nb As Double, ByVal yb1 As Double, ByVal yb2 As Double, ByVal a As Double, _
185     ByVal b As Double, ByVal lbok As Double, ByVal ll As Double, ByVal h As Double, ByVal t As Double, ByVal bw As Double, ByVal d As Double, ByVal c As Double, _
186     ByVal l As Double, ByVal s As Double, ByVal inc As Double, ByVal Method As Integer)
187
188     Rem Data Sort=================================================================================================================================================
189
190     Range(Cells(3, 6), Cells(9999, 14)).ClearContents
191     n = Application.WorksheetFunction.Count(Range("E4:E9999"))
192
193             For i = 1 To n
194
195                     NA = Worksheets(1).Cells(i + 2, 2)
196                     yi = Worksheets(1).Cells(i + 2, 4)
197
198                             If NA <> 0 Then
199
200                                     Range(Cells(i + 2, 2), Cells(i + 2, 5)).ClearContents
201
202                             End If
203
204                             If yi = yb1 Or yi = yb2 Then
205
206                                     Range(Cells(i + 2, 2), Cells(i + 2, 5)).ClearContents
207
208                             End If
209
210                             If yi = 0 Then
211
212                                     Range(Cells(i + 2, 2), Cells(i + 2, 5)).ClearContents
213
214                             End If
215
216                             If yi = h + 2 * t Then
217
218                                     Range(Cells(i + 2, 2), Cells(i + 2, 5)).ClearContents
219
220                             End If
221
222             Next i
223
224
225     Call Sort1(n)
226
227     Rem ==========================================================================================================================================================
228
229     n = Application.WorksheetFunction.Count(Range("E4:E9999"))
230     Ci = 0
231     Ti = 0
232     Mi = 0
233     Mti = 0
234
235             For i = 2 To n
236
237                     xh = Worksheets(1).Cells(i + 2 - 1, 3)
238                     yh = Worksheets(1).Cells(i + 2 - 1, 4)
239                     Sh = Worksheets(1).Cells(i + 2 - 1, 5)
240
241                     xi = Worksheets(1).Cells(i + 2, 3)
242                     yi = Worksheets(1).Cells(i + 2, 4)
243                     Si = Worksheets(1).Cells(i + 2, 5)
244
245                     xj = Worksheets(1).Cells(i + 2 + 1, 3)
246                     yj = Worksheets(1).Cells(i + 2 + 1, 4)
247                     Sj = Worksheets(1).Cells(i + 2 + 1, 5)
248
249                     dxi = xi - xh
250                     dyi = yi - yh
251                     dSi = Si - Sh
252
253                     dx = xj - xi
254                     dy = yj - yi
255                     dS = Sj - Si
256
257                     If xi > lbok + a And xi <= lbok + a + ll Then
258
259                             GoTo Continue
260
261                     End If
262
263     Rem Resultant compressive force===============================================================================================================================
264
```

```
265                         If dx = 0 And xi > 0 And xi <= lbok + a Then 'lbok + 2 * a + ll Then
266
267                                 If xi <> 0 And 0.5 * (Sj + Si) * dy < 0 Then
268
269                                         Ci = Ci + 0.5 * (Sj + Si) * dy * b / nb
270
271                                 End If
272
273                                 If xi <> 0 And 0.5 * (Sj + Si) * dy > 0 Then
274
275                                         Ti = Ti + 0.5 * (Sj + Si) * dy * b / nb
276
277                                 End If
278
279                         End If
280
281     Rem Position of the neutral axis=============================================================================================================
282
283                         If dyi < 0 Then
284
285                                 Rimin = 1E+20
286
287                                 For j = i To i + ne
288
289                                         xji = Worksheets(1).Cells(j + 2, 3)
290                                         yji = Worksheets(1).Cells(j + 2, 4)
291                                         Sji = Worksheets(1).Cells(j + 2, 5)
292
293                                         xjj = Worksheets(1).Cells(j + 2 + 1, 3)
294                                         yjj = Worksheets(1).Cells(j + 2 + 1, 4)
295                                         Sjj = Worksheets(1).Cells(j + 2 + 1, 5)
296
297                                         dxj = xjj - xji
298                                         dyj = yjj - yji
299
300                                         Ri = Abs(0.5 * (Sjj + Sji) * dyj * b / nb)
301
302                                         If Ri < Rimin Then
303
304                                                 yn = 0.5 * (yjj + yji)
305                                                 Rimin = Ri
306
307                                         End If
308
309                                 Next j
310
311                         End If
312
313     Rem Position of the center of gravity========================================================================================================
314
315                         If dyi < 0 Then
316
317                                         For y = t To h + t Step inc
318
319                                                 For j = i To i + ne
320
321                                                         xji = Worksheets(1).Cells(j + 2, 3)
322                                                         yji = Worksheets(1).Cells(j + 2, 4)
323                                                         Sji = Worksheets(1).Cells(j + 2, 5)
324
325                                                         xjj = Worksheets(1).Cells(j + 2 + 1, 3)
326                                                         yjj = Worksheets(1).Cells(j + 2 + 1, 4)
327                                                         Sjj = Worksheets(1).Cells(j + 2 + 1, 5)
328
329                                                         dxj = xjj - xji
330                                                         dyj = yjj - yji
331
332                                                                 If dxj = 0 And dyj > 0 And 0.5 * (Sjj + Sji) * dyj < 0 Then
333
334                                                                         Mi = Mi + 0.5 * (Sjj + Sji) * dyj * b / nb * (y - 0.5 * (yjj + yji))
335
336                                                                                 If Mi > 0 Then
337
338                                                                                         ygj = y - yn
339                                                                                         Exit For
340
341                                                                                 End If
342
343                                                                 End If
344                                                 Next j
345
346                                                 For j = i To i + ne
347
348                                                         xji = Worksheets(1).Cells(j + 2, 3)
349                                                         yji = Worksheets(1).Cells(j + 2, 4)
350                                                         Sji = Worksheets(1).Cells(j + 2, 5)
351
352                                                         xjj = Worksheets(1).Cells(j + 2 + 1, 3)
353                                                         yjj = Worksheets(1).Cells(j + 2 + 1, 4)
```

```
                                                Sjj = Worksheets(1).Cells(j + 2 + 1, 5)

                                                dxj = xjj - xji
                                                dyj = yjj - yji

                                                        If dxj = 0 And dyj > 0 And 0.5 * (Sjj + Sji) * dyj > 0 Then

                                                                Mti = Mti + 0.5 * (Sjj + Sji) * dyj * b / nb * (y - 0.5 * (yjj + yji))

                                                                        If Mti < 0 Then

                                                                                ygtj = yn - y
                                                                                Exit For

                                                                        End If

                                                        End If

                                        Next j

                                        Mi = 0
                                        Mti = 0

                                Next y

                        End If

Rem Output Shear Strength of Arch and Truss Mech=============================================================================================================

                        If dx <> 0 And xi > 0 And xi <= lbok + a Then 'lbok + 2 * a + ll Then

                                Worksheets(1).Cells(2, 6) = "Ci"
                                Worksheets(1).Cells(2, 7) = "ygi"
                                Worksheets(1).Cells(2, 8) = "dC"
                                Worksheets(1).Cells(2, 9) = "dyg"
                                Worksheets(1).Cells(2, 10) = "dx"

                                Worksheets(1).Cells(2, 11) = "Ti"
                                Worksheets(1).Cells(2, 12) = "ygti"
                                Worksheets(1).Cells(2, 13) = "dT"
                                Worksheets(1).Cells(2, 14) = "dygt"
                                Worksheets(1).Cells(2, 15) = "yn"


                                Worksheets(1).Cells(1, 6) = "Va="
                                Worksheets(1).Cells(1, 8) = "kN"

                                Worksheets(1).Cells(1, 9) = "Vb="
                                Worksheets(1).Cells(1, 11) = "kN"

                                Worksheets(1).Cells(1, 12) = "V="
                                Worksheets(1).Cells(1, 14) = "kN"

                                Worksheets(1).Cells(i + 2, 6) = Ci
                                Worksheets(1).Cells(i + 2, 11) = Ti

                                Cij = Ci
                                dC = Cij - Cii
                                dyg = ygj - ygi

                                Tij = Ti
                                dT = Tij - Tii
                                dygt = ygtj - ygti

                                If Method = 9999 Then

                                        Vaci = (Ci) * (dyg) / dx + Vaci
                                        Vbci = (ygj) * (dC) / dx + Vbci
                                        Vati = (Ti) * (dygt) / dx + Vati
                                        Vbti = (ygti) * (dT) / dx + Vbti

                                        Worksheets(1).Cells(1, 20) = "Developer edition"

                                Else

                                        Vaci = (Ci) * (dyg) / dx
                                        Vbci = (ygj) * (dC) / dx
                                        Vati = (Ti) * (dygt) / dx
                                        Vbti = (ygti) * (dT) / dx

                                End If

                                Worksheets(1).Cells(i + 2, 7) = ygj
                                Worksheets(1).Cells(i + 2, 8) = dC
                                Worksheets(1).Cells(i + 2, 9) = dyg
                                Worksheets(1).Cells(i + 2, 10) = dx

                                Worksheets(1).Cells(i + 2, 12) = ygtj
                                Worksheets(1).Cells(i + 2, 13) = dT
```

```
443                                 Worksheets(1).Cells(i + 2, 14) = dygt
444                                 Worksheets(1).Cells(i + 2, 15) = yn
445
446                                 Worksheets(1).Cells(i + 1, 7) = -(Vaci - Vati) * nb / 1000 * 2
447                                 Worksheets(1).Cells(i + 1, 10) = -(Vbci - Vbti) * nb / 1000 * 2
448
449                                         If dx <> 0 And xi > lbok + (bw / 2 + d / 4) And xi <= lbok + a - (bw / 2 + d / 4) Then
450
451                                                 Numsum = Numsum + 1
452
453                                                 If Method = 9999 Then
454
455                                                         Va = -(Vaci - Vati) * nb / 1000 * 2
456                                                         Vb = -(Vbci - Vbti) * nb / 1000 * 2
457
458                                                 Else
459
460                                                         Va = -(Vaci - Vati) * nb / 1000 * 2 + dVa
461                                                         Vb = -(Vbci - Vbti) * nb / 1000 * 2 + dVb
462
463                                                 End If
464
465                                                 Worksheets(1).Cells(1, 7) = Va / Numsum
466                                                 Worksheets(1).Cells(1, 10) = Vb / Numsum
467                                                 Worksheets(1).Cells(1, 13) = (Va + Vb) / Numsum
468
469                                                 Worksheets(1).Cells(1, 18) = Numsum
470
471                                                 dVa = Va
472                                                 dVb = Vb
473
474                                         End If
475
476                                 Cii = Cij
477                                 ygi = ygj
478                                 Ci = 0
479
480                                 Tii = Tij
481                                 ygti = ygtj
482                                 Ti = 0
483
484                         End If
485
486         Continue:
487
488                 Next i
489
490                 Vai = 0
491                 Vbi = 0
492                 Vati = 0
493                 Vbti = 0
494
495         End Sub
496
497         Rem ===========================================================================================================================================
498
499         Sub Cal_Arch_and_Truss_Mech_Comp(ByVal e As Double, ByVal ne As Double, ByVal nb As Double, ByVal yb As Double, ByVal a As Double, ByVal b As Double, _
500         ByVal lbok As Double, ByVal ll As Double, ByVal h As Double, ByVal t As Double, ByVal bw As Double, ByVal d As Double, ByVal c As Double, ByVal l As Double, _
501         ByVal s As Double, ByVal inc As Double, ByVal Method As Integer)
502
503         Rem Data Sort=================================================================================================================================================
504
505         Range(Cells(3, 6), Cells(9999, 10)).ClearContents
506         n = Application.WorksheetFunction.Count(Range("E4:E9999"))
507
508                 For i = 1 To n
509
510                         NA = Worksheets(1).Cells(i + 2, 2)
511                         yi = Worksheets(1).Cells(i + 2, 4)
512
513                                 If NA <> 0 Then
514
515                                         Range(Cells(i + 2, 2), Cells(i + 2, 5)).ClearContents
516
517                                 End If
518
519                                 If yi = yb Then
520
521                                         Range(Cells(i + 2, 2), Cells(i + 2, 5)).ClearContents
522
523                                 End If
524
525                                 If yi = 0 Then
526
527                                         Range(Cells(i + 2, 2), Cells(i + 2, 5)).ClearContents
528
529                                 End If
530
531                                 If yi = h + 2 * t Then
```

```
532
533                                 Range(Cells(i + 2, 2), Cells(i + 2, 5)).ClearContents
534
535                         End If
536
537         Next i
538
539
540     Call Sort1(n)
541
542     Rem ==========================================================================================================================================================
543
544     n = Application.WorksheetFunction.Count(Range("E4:E9999"))
545     Ci = 0
546     Mi = 0
547     Mmin = e
548
549         For i = 2 To n
550
551                 xh = Worksheets(1).Cells(i + 2 - 1, 3)
552                 yh = Worksheets(1).Cells(i + 2 - 1, 4)
553                 Sh = Worksheets(1).Cells(i + 2 - 1, 5)
554
555                 xi = Worksheets(1).Cells(i + 2, 3)
556                 yi = Worksheets(1).Cells(i + 2, 4)
557                 Si = Worksheets(1).Cells(i + 2, 5)
558
559                 xj = Worksheets(1).Cells(i + 2 + 1, 3)
560                 yj = Worksheets(1).Cells(i + 2 + 1, 4)
561                 Sj = Worksheets(1).Cells(i + 2 + 1, 5)
562
563                 dxi = xi - xh
564                 dyi = yi - yh
565                 dSi = Si - Sh
566
567                 dx = xj - xi
568                 dy = yj - yi
569                 dS = Sj - Si
570
571                 If xi > lbok + a And xi <= lbok + a + ll Then
572
573                         GoTo Continue
574
575                 End If
576
577     Rem Resultant compressive force=======================================================================================================================
578
579                         If dx = 0 And xi > 0 And xi <= lbok + a Then 'lbok + 2 * a + ll Then
580
581                                 If xi <> 0 And 0.5 * (Sj + Si) * dy < 0 Then
582
583                                         Ci = Ci + 0.5 * (Sj + Si) * dy
584
585                                 End If
586
587                         End If
588
589     Rem Position of the neutral axis======================================================================================================================
590
591                         If dyi < 0 Then
592
593                                 Rimin = 1E+20
594
595                                 For j = i To i + ne
596
597                                         xji = Worksheets(1).Cells(j + 2, 3)
598                                         yji = Worksheets(1).Cells(j + 2, 4)
599                                         Sji = Worksheets(1).Cells(j + 2, 5)
600
601                                         xjj = Worksheets(1).Cells(j + 2 + 1, 3)
602                                         yjj = Worksheets(1).Cells(j + 2 + 1, 4)
603                                         Sjj = Worksheets(1).Cells(j + 2 + 1, 5)
604
605                                         dxj = xjj - xji
606                                         dyj = yjj - yji
607
608                                         Ri = Abs(0.5 * (Sjj + Sji) * dyj * b / nb)
609
610                                         If Ri < Rimin Then
611
612                                                 yn = 0.5 * (yjj + yji)
613                                                 Rimin = Ri
614
615                                         End If
616
617                                 Next j
618
619                         End If
620
```

```
Rem Position of the center of gravity=============================================================================================================================

                        If dyi < 0 Then

                                For y = t To h + t Step inc

                                        For j = i To i + ne

                                                xji = Worksheets(1).Cells(j + 2, 3)
                                                yji = Worksheets(1).Cells(j + 2, 4)
                                                Sji = Worksheets(1).Cells(j + 2, 5)

                                                xjj = Worksheets(1).Cells(j + 2 + 1, 3)
                                                yjj = Worksheets(1).Cells(j + 2 + 1, 4)
                                                Sjj = Worksheets(1).Cells(j + 2 + 1, 5)

                                                dxj = xjj - xji
                                                dyj = yjj - yji

                                                        If dxj = 0 And dyj > 0 And 0.5 * (Sjj + Sji) * dyj < 0 Then

                                                                Mi = Mi + 0.5 * (Sjj + Sji) * dyj * b / nb * (y - 0.5 * (yjj + yji))

                                                                        If Mi > 0 Then

                                                                                ygj = y - yn
                                                                                Exit For

                                                                        End If

                                                        End If

                                        Next j

                                        Mi = 0
                                        Mmin = e

                                Next y

                        End If

Rem Output Shear Strength of Arch and Truss Mech=================================================================================================================

                        If dx <> 0 And xi > 0 And xi <= lbok + a Then 'lbok + 2 * a + ll Then

                                Worksheets(1).Cells(2, 6) = "Ci"
                                Worksheets(1).Cells(2, 7) = "ygi"
                                Worksheets(1).Cells(2, 8) = "dC"
                                Worksheets(1).Cells(2, 9) = "dyg"
                                Worksheets(1).Cells(2, 10) = "dx"
                                Worksheets(1).Cells(2, 15) = "yn"

                                Worksheets(1).Cells(1, 6) = "Va="
                                Worksheets(1).Cells(1, 8) = "kN"

                                Worksheets(1).Cells(1, 9) = "Vb="
                                Worksheets(1).Cells(1, 11) = "kN"

                                Worksheets(1).Cells(1, 12) = "V="
                                Worksheets(1).Cells(1, 14) = "kN"

                                Worksheets(1).Cells(i + 2, 6) = Ci

                                Cij = Ci
                                dC = Cij - Cii
                                dyg = ygj - ygi

                                Worksheets(1).Cells(i + 2, 7) = ygj
                                Worksheets(1).Cells(i + 2, 8) = dC
                                Worksheets(1).Cells(i + 2, 9) = dyg
                                Worksheets(1).Cells(i + 2, 10) = dx
                                Worksheets(1).Cells(i + 2, 15) = yn

                                        If dx <> 0 And xi > lbok + (bw / 2 + d / 4) And xi <= lbok + a - (bw / 2 + d / 4) Then

                                                Numsum = Numsum + 1

                                                Vai = (Ci) * (dyg) / dx
                                                Vbi = (ygj) * (dC) / dx

                                                Va = -(Vai) * nb / 1000 * 2 + dVa
                                                Vb = -(Vbi) * nb / 1000 * 2 + dVb

                                                Worksheets(1).Cells(1, 7) = Va / Numsum
                                                Worksheets(1).Cells(1, 10) = Vb / Numsum
                                                Worksheets(1).Cells(1, 13) = (Va + Vb) / Numsum

                                                Worksheets(1).Cells(1, 17) = Numsum
```

```
                                                dVa = Va
                                                dVb = Vb

                                        End If

                                Cii = Cij
                                ygi = ygj
                                Ci = 0

                        End If

Continue:

        Next i

        Vai = 0
        Vbi = 0

End Sub

Rem ===========================================================================================================================================================

Sub Sort1(ByVal n As Double)

        Worksheets(1).Range(Cells(3, 2), Cells(n, 5)) _
        .Sort Key1:=Worksheets(1).Cells(3, 3), order1:=xlAscending

End Sub
```

A.2 The procedure in the case with BOND elements

A.2.1 Form

```
VERSION 5.00
Begin {C62A69F0-16DC-11CE-9E98-00AA00574A4F} UserForm1
   Caption         =   "UserForm1"
   ClientHeight    =   1845
   ClientLeft      =   45
   ClientTop       =   375
   ClientWidth     =   4485
   OleObjectBlob   =   "UserForm1.frx":0000
   StartUpPosition =   1  'CenterOwner
End
Attribute VB_Name = "UserForm1"
Attribute VB_GlobalNameSpace = False
Attribute VB_Creatable = False
Attribute VB_PredeclaredId = True
Attribute VB_Exposed = False


Private Sub CommandButton1_Click()

        Call Main

End Sub

Private Sub Label1_Click()

End Sub

Private Sub UserForm_Click()

End Sub
```

A.2.2 Main procedure

```
Attribute VB_Name = "Module1"
Rem ==========================================================================================================================================

Sub Auto_Open()

        UserForm1.Show (vbModeless)

End Sub

Rem ==========================================================================================================================================

Sub Main()

Dim m, n, i, j, k As Double
Dim Ci, Mi, ygi, yi, xi, Si As Double
Dim yj, xj, xji, yjj, Sjj, Sji, Num_nod As Double
Dim e, ne, nb, yb, a, b, lbok, h, t, d, c, l, s, inc As Double
Dim Arch_Mech, Beam_Mech As Double
Dim varFileName As Variant

MsgBox "Coded by Yuta Yamada 2015" & vbCrLf & "yamada.y.av@m.titech.ac.jp", vbInformation, "Credit"

Rem Input control and beam shape==============================================================================================================

Num_nod = Application.InputBox("Number of nodal points?", "Input the number of nodal points", "940", , , , , 1)
ne = Application.InputBox("Number of elements in vertical direction?", "Input the number of elements", "12", , , , , 1)
nb = Application.InputBox("Number of elements in perpendicular to longitudinal direction?", "Input the number of elements", "6", , , , , 1)
yb1 = Application.InputBox("The position of removal BOND elements in vertical direction?(mm)", "Input the position of elements 1", "0", , , , , 1)
yb2 = Application.InputBox("The position of removal BOND elements in vertical direction?(mm)", "Input the position of elements 2", "0", , , , , 1)
a = Application.InputBox("Shear span?(mm)", "Input shear span", "600", , , , , 1)                                    'Shear span
d = Application.InputBox("Effective depth?(mm)", "Input effective depth", "200", , , , , 1)                          'Effective depth
lbok = Application.InputBox("Anchorage length?(mm)", "Input anchorage length", "330", , , , , 1)                    'Anchorage length
ll = Application.InputBox("Interval of loading points?(mm)", "Input interval of loading points", "150", , , , , 1)  'Interval of loading points
h = Application.InputBox("Hight of the beam?(mm)", "Input beam hight", "230", 1)                                     'Beam hight
t = Application.InputBox("Thickness of the loading plates?(mm)", "Input thickness of the loading plates", "20", , , , , 1)  'Thickness of the loading plates
bw = Application.InputBox("Width of the loading plates?(mm)", "Input width of the loading plates", "100", , , , , 1)  'Width of the loading plates
b = Application.InputBox("Beam width?(mm)", "Input beam width", "150", , , , , 1)                                    'Beam width
c = h - d                                                                                                            'Covering depth
l = lbok + a
s = lbok + a - 25 - 1

Rem ==========================================================================================================================================

Method = Application.InputBox("Method?", "Selection of methods", "0 or Other key", , , , , 1)
inc = Application.InputBox("Increment?", "Input increment for calculation of resultant force(mm)", "1", , , , , 1)

Rem ==========================================================================================================================================

i = 0

Range(Cells(1, 1), Cells(9999, 9999)).ClearContents

varFileName = Application.GetOpenFilename(FileFilter:="vtu file(*.vtu),*.vtu", Title:="Slect vtu file", MultiSelect:=True)

For Each FileName In varFileName

        i = i + 1
        Worksheets(1).Cells(i + 2, 1) = i

        Call Open_Paste(Num_nod, FileName)

        Application.ScreenUpdating = False

Rem ==========================================================================================================================================

                If Method = 0 Then

                        Call Cal_Arch_and_Truss_Mech_Comp_Tens(e, ne, nb, yb1, yb2, a, b, lbok, ll, h, t, bw, d, c, l, s, inc)

                        Arch_Mech = Worksheets(1).Cells(1, 7)
                        Beam_Mech = Worksheets(1).Cells(1, 10)
                        Shear_Force = Worksheets(1).Cells(1, 13)

                        Worksheets(1).Cells(i + 1, 16) = Arch_Mech
                        Worksheets(1).Cells(i + 1, 17) = Beam_Mech
                        Worksheets(1).Cells(i + 1, 18) = Shear_Force

                        Worksheets(1).Cells(i + 1, 19) = FileName

                End If

                If Method <> 0 Then

                        Call Cal_Arch_and_Truss_Mech_Comp(e, ne, nb, yb, a, b, lbok, ll, h, t, bw, d, c, l, s, inc)

                        Arch_Mech = Worksheets(1).Cells(1, 7)
                        Beam_Mech = Worksheets(1).Cells(1, 10)
```

```
88                              Shear_Force = Worksheets(1).Cells(1, 13)
89
90                              Worksheets(1).Cells(i + 1, 16) = Arch_Mech
91                              Worksheets(1).Cells(i + 1, 17) = Beam_Mech
92                              Worksheets(1).Cells(i + 1, 18) = Shear_Force
93
94                              Worksheets(1).Cells(i + 1, 19) = FileName
95
96                      End If
97
98                      If i > 60 Then
99
100                             Application.GoTo Cells(i + 1 - 55, 16), True
101
102                     End If
103
104             Application.ScreenUpdating = True
105
106     Next
107
108     Rem ==========================================================================================================================================================
109
110             Worksheets(1).Cells(1, 16) = "Va"
111             Worksheets(1).Cells(1, 17) = "Vb"
112             Worksheets(1).Cells(1, 19) = "Ver.1.07"
113             Worksheets(1).Cells(1, 2) = "NODE"
114             Worksheets(1).Cells(2, 2) = "N/A"
115             Worksheets(1).Cells(2, 3) = "Y(mm)"
116             Worksheets(1).Cells(2, 4) = "Z(mm)"
117             Worksheets(1).Cells(2, 5) = "Stress-YY(MPa)"
118
119             Range(Cells(2, 16), Cells(i + 1, 17)).Select
120
121     End Sub
122
123     Rem ==========================================================================================================================================================
124
125     Sub Open_Paste(ByVal Num_nod As Integer, ByVal FileName As Variant)
126
127     Dim buf0, buf1, buf1_xyz, Str As String
128
129     Range(Cells(3, 2), Cells(9999, 6)).ClearContents
130
131     'Open "H:¥01. VTU Data¥10. Effect of Shear Reinforcement¥Main¥SRB¥vtu¥result-00020.vtu" For Input As #i
132     Open FileName For Input As #1
133
134             For j = 1 To 500000
135
136                     Line Input #1, buf0
137
138                             If InStr(1, buf0, "STRESS-YY(MPa)") <> 0 Then
139
140                                     For k = 1 To Num_nod + 1
141
142                                             Line Input #1, buf0
143
144                                             Worksheets(1).Cells(k + 2 - 1, 5) = buf0
145
146                                     Next k
147
148                             End If
149
150                             If InStr(1, buf0, "/PointData") <> 0 Then
151
152                                     For k = 1 To Num_nod + 2
153
154                                             Line Input #1, buf0
155
156                                                     'If IsNumeric(buf0) Then
157
158                                                             For ii = 0 To UBound(Split(buf0, "       "))
159
160                                                                     buf1 = Split(buf0, "       ")
161
162                                                                     Worksheets(1).Cells(k, ii + 1) = buf1(ii)
163
164                                                             Next ii
165
166                                                     'End If
167
168                                     Next k
169
170                             End If
171
172                     If EOF(1) = True Then
173
174                             Exit For
175
176                     End If
```

```
177
178             Next j
179
180     Close #1
181
182     End Sub
183
184     Rem ==========================================================================================================================================================
185
186     Sub Cal_Arch_and_Truss_Mech_Comp_Tens(ByVal e As Double, ByVal ne As Double, ByVal nb As Double, ByVal yb1 As Double, ByVal yb2 As Double, ByVal a As Double, _
187     ByVal b As Double, ByVal lbok As Double, ByVal ll As Double, ByVal h As Double, ByVal t As Double, ByVal bw As Double, ByVal d As Double, ByVal c As Double, _
188     ByVal l As Double, ByVal s As Double, ByVal inc As Double)
189
190     Rem Data Sort=================================================================================================================================================
191
192     Range(Cells(3, 6), Cells(9999, 14)).ClearContents
193     n = Application.WorksheetFunction.Count(Range("E4:E9999"))
194
195             For i = 1 To n
196
197                     NA = Worksheets(1).Cells(i + 2, 2)
198                     yi = Worksheets(1).Cells(i + 2, 4)
199
200                             If NA <> 0 Then
201
202                                     Range(Cells(i + 2, 2), Cells(i + 2, 5)).ClearContents
203
204                             End If
205
206                             If yi = yb1 Or yi = yb2 Then
207
208                                     Range(Cells(i + 2, 2), Cells(i + 2, 5)).ClearContents
209
210                             End If
211
212                             If yi = 0 Then
213
214                                     Range(Cells(i + 2, 2), Cells(i + 2, 5)).ClearContents
215
216                             End If
217
218                             If yi = h + 2 * t Then
219
220                                     Range(Cells(i + 2, 2), Cells(i + 2, 5)).ClearContents
221
222                             End If
223
224             Next i
225
226
227     Call Sort1(n)
228
229     Rem ==========================================================================================================================================================
230
231     n = Application.WorksheetFunction.Count(Range("E4:E9999"))
232     Ci = 0
233     Ti = 0
234     Mi = 0
235     Mti = 0
236
237             For i = 2 To n
238
239                     xh = Worksheets(1).Cells(i + 2 - 1, 3)
240                     yh = Worksheets(1).Cells(i + 2 - 1, 4)
241                     Sh = Worksheets(1).Cells(i + 2 - 1, 5)
242
243                     xi = Worksheets(1).Cells(i + 2, 3)
244                     yi = Worksheets(1).Cells(i + 2, 4)
245                     Si = Worksheets(1).Cells(i + 2, 5)
246
247                     xj = Worksheets(1).Cells(i + 2 + 1, 3)
248                     yj = Worksheets(1).Cells(i + 2 + 1, 4)
249                     Sj = Worksheets(1).Cells(i + 2 + 1, 5)
250
251                     dxi = xi - xh
252                     dyi = yi - yh
253                     dSi = Si - Sh
254
255                     dx = xj - xi
256                     dy = yj - yi
257                     dS = Sj - Si
258
259                     If xi > lbok + a And xi <= lbok + a + ll Then
260
261                             GoTo Continue
262
263                     End If
264
265     Rem Resultant compressive force===============================================================================================================================
```

```
266
267                         If dx = 0 And xi > 0 And xi <= lbok + a Then
268
269                                 If xi <> 0 And 0.5 * (Sj + Si) * dy < 0 Then
270
271                                         Ci = Ci + 0.5 * (Sj + Si) * dy * b / nb
272
273                                 End If
274
275                                 If xi <> 0 And 0.5 * (Sj + Si) * dy > 0 Then
276
277                                         Ti = Ti + 0.5 * (Sj + Si) * dy * b / nb
278
279                                 End If
280
281                         End If
282
283     Rem Position of the neutral axis=============================================================================================================================
284
285                         If dyi < 0 Then
286
287                                 Rimin = 1E+20
288
289                                 For j = i To i + ne
290
291                                         xji = Worksheets(1).Cells(j + 2, 3)
292                                         yji = Worksheets(1).Cells(j + 2, 4)
293                                         Sji = Worksheets(1).Cells(j + 2, 5)
294
295                                         xjj = Worksheets(1).Cells(j + 2 + 1, 3)
296                                         yjj = Worksheets(1).Cells(j + 2 + 1, 4)
297                                         Sjj = Worksheets(1).Cells(j + 2 + 1, 5)
298
299                                         dxj = xjj - xji
300                                         dyj = yjj - yji
301
302                                         Ri = Abs(0.5 * (Sjj + Sji) * dyj * b / nb)
303
304                                         If Ri < Rimin Then
305
306                                                 yn = 0.5 * (yjj + yji)
307                                                 Rimin = Ri
308
309                                         End If
310
311                                 Next j
312
313                         End If
314
315     Rem Position of the center of gravity========================================================================================================================
316
317                         If dyi < 0 Then
318
319                                         For y = t To h + t Step inc
320
321                                                 For j = i To i + ne
322
323                                                         xji = Worksheets(1).Cells(j + 2, 3)
324                                                         yji = Worksheets(1).Cells(j + 2, 4)
325                                                         Sji = Worksheets(1).Cells(j + 2, 5)
326
327                                                         xjj = Worksheets(1).Cells(j + 2 + 1, 3)
328                                                         yjj = Worksheets(1).Cells(j + 2 + 1, 4)
329                                                         Sjj = Worksheets(1).Cells(j + 2 + 1, 5)
330
331                                                         dxj = xjj - xji
332                                                         dyj = yjj - yji
333
334                                                                 If dxj = 0 And dyj > 0 And 0.5 * (Sjj + Sji) * dyj < 0 Then
335
336                                                                         Mi = Mi + 0.5 * (Sjj + Sji) * dyj * b / nb * (y - 0.5 * (yjj + yji))
337
338                                                                                 If Mi > 0 Then
339
340                                                                                         ygj = y - t - c
341                                                                                         'ygj = y - yn ' Introduction of neutral axis
342                                                                                         Exit For
343
344                                                                                 End If
345
346                                                                 End If
347                                                 Next j
348
349                                                 For j = i To i + ne
350
351                                                         xji = Worksheets(1).Cells(j + 2, 3)
352                                                         yji = Worksheets(1).Cells(j + 2, 4)
353                                                         Sji = Worksheets(1).Cells(j + 2, 5)
354
```

```
                                        xjj = Worksheets(1).Cells(j + 2 + 1, 3)
                                        yjj = Worksheets(1).Cells(j + 2 + 1, 4)
                                        Sjj = Worksheets(1).Cells(j + 2 + 1, 5)

                                        dxj = xjj - xji
                                        dyj = yjj - yji

                                                If dxj = 0 And dyj > 0 And 0.5 * (Sjj + Sji) * dyj > 0 Then

                                                        Mti = Mti + 0.5 * (Sjj + Sji) * dyj * b / nb * (y - 0.5 * (yjj + yji))

                                                                If Mti < 0 Then

                                                                        ygtj = y - t - c
                                                                        'ygtj = yn - y ' Introduction of neutral axis
                                                                        Exit For

                                                                End If

                                                End If

                                    Next j

                                    Mi = 0
                                    Mti = 0

                                Next y

                        End If

Rem Output Shear Strength of Arch and Truss Mech=============================================================================================================

                        If dx <> 0 And xi > 0 And xi <= lbok + a Then

                                Worksheets(1).Cells(2, 6) = "Ci"
                                Worksheets(1).Cells(2, 7) = "ygi"
                                Worksheets(1).Cells(2, 8) = "dC"
                                Worksheets(1).Cells(2, 9) = "dyg"
                                Worksheets(1).Cells(2, 10) = "dx"

                                Worksheets(1).Cells(2, 11) = "Ti"
                                Worksheets(1).Cells(2, 12) = "ygti"
                                Worksheets(1).Cells(2, 13) = "dT"
                                Worksheets(1).Cells(2, 14) = "dygt"
                                Worksheets(1).Cells(2, 15) = "yn"


                                Worksheets(1).Cells(1, 6) = "Va="
                                Worksheets(1).Cells(1, 8) = "kN"

                                Worksheets(1).Cells(1, 9) = "Vb="
                                Worksheets(1).Cells(1, 11) = "kN"

                                Worksheets(1).Cells(1, 12) = "V="
                                Worksheets(1).Cells(1, 14) = "kN"

                                Worksheets(1).Cells(i + 2, 6) = Ci
                                Worksheets(1).Cells(i + 2, 11) = Ti

                                Cij = Ci
                                dC = Cij - Cii
                                dyg = ygj - ygi

                                Tij = Ti
                                dT = Tij - Tii
                                dygt = ygtj - ygti

                                Vaci = (Ci) * (dyg) / dx
                                Vbci = (ygj) * (dC) / dx
                                Vati = (Ti) * (dygt) / dx
                                Vbti = (ygti) * (dT) / dx

                                Worksheets(1).Cells(i + 2, 7) = ygj
                                Worksheets(1).Cells(i + 2, 8) = dC
                                Worksheets(1).Cells(i + 2, 9) = dyg
                                Worksheets(1).Cells(i + 2, 10) = dx

                                Worksheets(1).Cells(i + 2, 12) = ygtj
                                Worksheets(1).Cells(i + 2, 13) = dT
                                Worksheets(1).Cells(i + 2, 14) = dygt
                                Worksheets(1).Cells(i + 2, 15) = yn

                                Worksheets(1).Cells(i + 1, 7) = -(Vaci + Vati) * nb / 1000 * 2
                                Worksheets(1).Cells(i + 1, 10) = -(Vbci + Vbti) * nb / 1000 * 2

                                        If dx <> 0 And xi > lbok + (bw / 2 + d / 4) And xi <= lbok + a - (bw / 2 + d / 4) Then

                                                Numsum = Numsum + 1

```

```
                                        Va = -(Vaci + Vati) * nb / 1000 * 2 + dVa
                                        Vb = -(Vbci + Vbti) * nb / 1000 * 2 + dVb

                                        Worksheets(1).Cells(1, 7) = Va / Numsum
                                        Worksheets(1).Cells(1, 10) = Vb / Numsum
                                        Worksheets(1).Cells(1, 13) = (Va + Vb) / Numsum

                                        Worksheets(1).Cells(1, 18) = Numsum

                                        dVa = Va
                                        dVb = Vb

                                End If

                        Cii = Cij
                        ygi = ygj
                        Ci = 0

                        Tii = Tij
                        ygti = ygtj
                        Ti = 0

                End If

Continue:

        Next i

End Sub

Rem ============================================================================================================================================================

Sub Cal_Arch_and_Truss_Mech_Comp(ByVal e As Double, ByVal ne As Double, ByVal nb As Double, ByVal yb As Double, ByVal a As Double, ByVal b As Double, _
ByVal lbok As Double, ByVal ll As Double, ByVal h As Double, ByVal t As Double, ByVal bw As Double, ByVal d As Double, ByVal c As Double, ByVal l As Double, _
ByVal s As Double, ByVal inc As Double)

Rem Data Sort=================================================================================================================================================

Range(Cells(3, 6), Cells(9999, 10)).ClearContents
n = Application.WorksheetFunction.Count(Range("E4:E9999"))

        For i = 1 To n

                NA = Worksheets(1).Cells(i + 2, 2)
                yi = Worksheets(1).Cells(i + 2, 4)

                        If NA <> 0 Then

                                Range(Cells(i + 2, 2), Cells(i + 2, 5)).ClearContents

                        End If

                        If yi = yb Then

                                Range(Cells(i + 2, 2), Cells(i + 2, 5)).ClearContents

                        End If

                        If yi = 0 Then

                                Range(Cells(i + 2, 2), Cells(i + 2, 5)).ClearContents

                        End If

                        If yi = h + 2 * t Then

                                Range(Cells(i + 2, 2), Cells(i + 2, 5)).ClearContents

                        End If

        Next i


Call Sort1(n)

Rem ============================================================================================================================================================

n = Application.WorksheetFunction.Count(Range("E4:E9999"))
Ci = 0
Mi = 0
Mmin = e

        For i = 2 To n

                xh = Worksheets(1).Cells(i + 2 - 1, 3)
                yh = Worksheets(1).Cells(i + 2 - 1, 4)
                Sh = Worksheets(1).Cells(i + 2 - 1, 5)

                xi = Worksheets(1).Cells(i + 2, 3)
```

```
533                     yi = Worksheets(1).Cells(i + 2, 4)
534                     Si = Worksheets(1).Cells(i + 2, 5)
535
536                     xj = Worksheets(1).Cells(i + 2 + 1, 3)
537                     yj = Worksheets(1).Cells(i + 2 + 1, 4)
538                     Sj = Worksheets(1).Cells(i + 2 + 1, 5)
539
540                     dxi = xi - xh
541                     dyi = yi - yh
542                     dSi = Si - Sh
543
544                     dx = xj - xi
545                     dy = yj - yi
546                     dS = Sj - Si
547
548                     If xi > lbok + a And xi <= lbok + a + ll Then
549
550                             GoTo Continue
551
552                     End If
553
554     Rem Resultant compressive force=============================================================================================================================
555
556                             If dx = 0 And xi > 0 And xi <= lbok + a Then 'lbok + 2 * a + ll Then
557
558                                     If xi <> 0 And 0.5 * (Sj + Si) * dy < 0 Then
559
560                                             Ci = Ci + 0.5 * (Sj + Si) * dy
561
562                                     End If
563
564                             End If
565
566     Rem Position of the neutral axis============================================================================================================================
567
568                             If dyi < 0 Then
569
570                                     Rimin = 1E+20
571
572                                     For j = i To i + ne
573
574                                             xji = Worksheets(1).Cells(j + 2, 3)
575                                             yji = Worksheets(1).Cells(j + 2, 4)
576                                             Sji = Worksheets(1).Cells(j + 2, 5)
577
578                                             xjj = Worksheets(1).Cells(j + 2 + 1, 3)
579                                             yjj = Worksheets(1).Cells(j + 2 + 1, 4)
580                                             Sjj = Worksheets(1).Cells(j + 2 + 1, 5)
581
582                                             dxj = xjj - xji
583                                             dyj = yjj - yji
584
585                                             Ri = Abs(0.5 * (Sjj + Sji) * dyj * b / nb)
586
587                                             If Ri < Rimin Then
588
589                                                     yn = 0.5 * (yjj + yji)
590                                                     Rimin = Ri
591
592                                             End If
593
594                                     Next j
595
596                             End If
597
598     Rem Position of the center of gravity=======================================================================================================================
599
600                             If dyi < 0 Then
601
602                                             For y = t To h + t Step inc
603
604                                                     For j = i To i + ne
605
606                                                             xji = Worksheets(1).Cells(j + 2, 3)
607                                                             yji = Worksheets(1).Cells(j + 2, 4)
608                                                             Sji = Worksheets(1).Cells(j + 2, 5)
609
610                                                             xjj = Worksheets(1).Cells(j + 2 + 1, 3)
611                                                             yjj = Worksheets(1).Cells(j + 2 + 1, 4)
612                                                             Sjj = Worksheets(1).Cells(j + 2 + 1, 5)
613
614                                                             dxj = xjj - xji
615                                                             dyj = yjj - yji
616
617                                                                     If dxj = 0 And dyj > 0 And 0.5 * (Sjj + Sji) * dyj < 0 Then
618
619                                                                             Mi = Mi + 0.5 * (Sjj + Sji) * dyj * b / nb * (y - 0.5 * (yjj + yji))
620
621                                                                                     If Mi > 0 Then
```

```
622
623                                                                     ygj = y '- yn
624                                                                     Exit For
625
626                                                                 End If
627
628                                                             End If
629
630                                         Next j
631
632                                         Mi = 0
633                                         Mmin = e
634
635                                     Next y
636
637                         End If
638
639     Rem Output Shear Strength of Arch and Truss Mech=============================================================================================================
640
641                         If dx <> 0 And xi > 0 And xi <= lbok + a Then
642
643                                 Worksheets(1).Cells(2, 6) = "Ci"
644                                 Worksheets(1).Cells(2, 7) = "ygi"
645                                 Worksheets(1).Cells(2, 8) = "dC"
646                                 Worksheets(1).Cells(2, 9) = "dyg"
647                                 Worksheets(1).Cells(2, 10) = "dx"
648                                 Worksheets(1).Cells(2, 15) = "yn"
649
650                                 Worksheets(1).Cells(1, 6) = "Va="
651                                 Worksheets(1).Cells(1, 8) = "kN"
652
653                                 Worksheets(1).Cells(1, 9) = "Vb="
654                                 Worksheets(1).Cells(1, 11) = "kN"
655
656                                 Worksheets(1).Cells(1, 12) = "V="
657                                 Worksheets(1).Cells(1, 14) = "kN"
658
659                                 Worksheets(1).Cells(i + 2, 6) = Ci
660
661                                 Cij = Ci
662                                 dC = Cij - Cii
663                                 dyg = ygj - ygi
664
665                                 Worksheets(1).Cells(i + 2, 7) = ygj
666                                 Worksheets(1).Cells(i + 2, 8) = dC
667                                 Worksheets(1).Cells(i + 2, 9) = dyg
668                                 Worksheets(1).Cells(i + 2, 10) = dx
669                                 Worksheets(1).Cells(i + 2, 15) = yn
670
671                                     If dx <> 0 And xi > lbok + bw / 2 And xi <= lbok + a - bw / 2 Then
672
673                                         Numsum = Numsum + 1
674
675                                         Vai = (Ci) * (dyg) / dx
676                                         Vbi = (ygj) * (dC) / dx
677
678                                         Va = -(Vai) * nb / 1000 * 2 + dVa
679                                         Vb = -(Vbi) * nb / 1000 * 2 + dVb
680
681                                         Worksheets(1).Cells(1, 7) = Va / Numsum
682                                         Worksheets(1).Cells(1, 10) = Vb / Numsum
683                                         Worksheets(1).Cells(1, 13) = (Va + Vb) / Numsum
684
685                                         Worksheets(1).Cells(1, 17) = Numsum
686
687                                         dVa = Va
688                                         dVb = Vb
689
690                                     End If
691
692                                 Cii = Cij
693                                 ygi = ygj
694                                 Ci = 0
695
696                         End If
697
698     Continue:
699
700             Next i
701
702             Vai = 0
703             Vbi = 0
704
705     End Sub
706
707     Rem =============================================================================================================================================
708
709     Sub Sort1(ByVal n As Double)
710
```

```
711                 Worksheets(1).Range(Cells(3, 2), Cells(n, 5)) _
712                 .Sort Key1:=Worksheets(1).Cells(3, 3), order1:=xlAscending
713
714         End Sub
```

APPENDIX. B
PROGRAMING CODE ON THE CALCULATION METHOD OF LOAD PATH

The programing code on calculation method of the Load Path mentioned in *Chapter 2* based on *Visual Basic* is denoted in this appendix.

B.1 Form

```
VERSION 5.00
Begin {C62A69F0-16DC-11CE-9E98-00AA00574A4F} UserForm1
   Caption         =   "UserForm1"
   ClientHeight    =   1845
   ClientLeft      =   45
   ClientTop       =   375
   ClientWidth     =   4485
   OleObjectBlob   =   "CLP_UserForm1_Ver.1.02.frx":0000
   StartUpPosition =   1  ' Center of owner form
End
Attribute VB_Name = "UserForm1"
Attribute VB_GlobalNameSpace = False
Attribute VB_Creatable = False
Attribute VB_PredeclaredId = True
Attribute VB_Exposed = False

Private Sub CommandButton1_Click()

        Call Main

End Sub

Private Sub UserForm_Click()

End Sub
```

B.2 Main procedure

```
Attribute VB_Name = "Module1"
Rem ==========================================================================================================================================

Sub Auto_Open()

        UserForm1.Show (vbModeless)

End Sub

Rem ==========================================================================================================================================

Sub Main()

Dim m, n, i, j, k As Double
Dim Ci, Mi, ygi, yi, xi, Si As Double
Dim yj, xj, xji, yjj, Sjj, Sji, Num_nod As Double
Dim e, ne, nb, yb, a, b, lbok, h, t, d, c, l, s, inc As Double
Dim varFileName As Variant
Dim sheeti, Sheet1 As Worksheet

MsgBox "Coded by Yuta Yamada 2015" & vbCrLf & "yamada.y.av@m.titech.ac.jp", vbInformation, "Credit"

Rem Selection of calculation method ==========================================================================================================

Cal_method = 1 'Application.InputBox("Please select calculation Method.(0=grad(S), 1=min(dS))", "Selection of calculation Method", "(0 or 1)", , , , , 1)
Eva_method = 1 'Application.InputBox("Please select evaluation Method.(0=Sum of Length, 1=RSS)", "Selection of evaluation Method", "(0 or 1)", , , , , 1)

        If Cal_method * Eva_method > 1 Or Cal_method < 0 Or Eva_method < 0 Then

                MsgBox "Please input 1 or 0.", vbAboutretryIgnore, "Error"
                Exit Sub

        End If

Rem Input ====================================================================================================================================

Num_nod = Application.InputBox("Number of nodal points?", "Input the number of nodal points", "2028", , , , , 1)
yb = Application.InputBox("Please input the position of BOND elements in vertical direction?(mm)", "Input the position of elements", "58.84,60", , , , , 1)
a = Application.InputBox("Shear span?(mm)", "Input shear span", "580,600", , , , , 1)                                    'Shear span
d = Application.InputBox("Effective depth?(mm)", "Input effective depth", "200", , , , , 1)                              'Effective depth
lbok = Application.InputBox("Anchorage length?(mm)", "Input anchorage length", "330", , , , , 1)                        'Anchorage length
h = Application.InputBox("Hight of the beam?(mm)", "Input beam hight", "230", 1)                                         'Beam height
t = Application.InputBox("Thickness of the loading plates?(mm)", "Input thickness of the loading plates", "20", , , , , 1)  'Thickness of loading plates
b = Application.InputBox("Beam width?(mm)", "Input beam width", "150", , , , , 1)                                       'Beam width
c = h - d                                                                                                               'Bottom cover depth
l = lbok + a                                                                                                            'Span
s = lbok + a - 25 - 1

Rem ==========================================================================================================================================

i_file = 0

varFileName = Application.GetOpenFilename(FileFilter:="vtu file(*.vtu),*.vtu", Title:="Slect vtu file", MultiSelect:=True)

For Each FileName In varFileName

        i_file = i_file + 1

        Set sheeti = Worksheets(i_file)
        sheeti.Activate

        Call Open_Paste(i_file, Num_nod, FileName)

        Application.ScreenUpdating = False

Rem ==========================================================================================================================================

                'If Cal_method = 0 Then

                        'Call LP0(Num_nod, a, b, lbok, h, t, l, s)

                'End If

                If Cal_method = 1 Then

                        Call LP(i_file, yb, Num_nod, a, b, lbok, h, t, l, s)

                        Worksheets(i_file).Cells(1, 1) = FileName

                End If

        Application.ScreenUpdating = True

        Worksheets(i_file).Cells(1, 2) = "NODE"
        Worksheets(i_file).Cells(2, 2) = "N/A"
        Worksheets(i_file).Cells(2, 3) = "Y(mm)"
```

```
87              Worksheets(i_file).Cells(2, 4) = "Z(mm)"
88              Worksheets(i_file).Cells(2, 5) = "ThrSTRESS(MPa)"
89              Worksheets(i_file).Cells(2, 6) = "Load Path"
90
91      Next
92
93      Rem ===========================================================================================================================================================
94
95              Set Sheet1 = Worksheets(1)
96
97              Sheet1.Activate
98              Range(Cells(1, 1), Cells(1, 1)).Select
99
100     End Sub
101
102     Rem ===========================================================================================================================================================
103
104     Sub Open_Paste(ByVal i_file As Integer, ByVal Num_nod As Integer, ByVal FileName As Variant)
105
106     Dim buf0, buf1, buf1_xyz, Str As String
107
108     Range(Cells(3, 2), Cells(9999, 6)).ClearContents
109
110     Open FileName For Input As #1
111
112             For j = 1 To 500000
113
114                     Line Input #1, buf0
115
116                             If InStr(1, buf0, "ThrSTRESS(MPa)") <> 0 Then
117
118                                     For k = 1 To Num_nod + 1
119
120                                             Line Input #1, buf0
121
122                                             Worksheets(i_file).Cells(k + 2 - 1, 5) = buf0
123
124                                     Next k
125
126                             End If
127
128                             If InStr(1, buf0, "/PointData") <> 0 Then
129
130                                     For k = 1 To Num_nod + 2
131
132                                             Line Input #1, buf0
133
134                                                     'If IsNumeric(buf0) Then
135
136                                                             For ii = 0 To UBound(Split(buf0, "       "))
137
138                                                                     buf1 = Split(buf0, "       ")
139
140                                                                     Worksheets(i_file).Cells(k, ii + 1) = buf1(ii)
141
142                                                             Next ii
143
144                                                     'End If
145
146                                     Next k
147
148                             End If
149
150                     If EOF(1) = True Then
151
152                             Exit For
153
154                     End If
155
156             Next j
157
158     Close #1
159
160     End Sub
161
162     Rem ===========================================================================================================================================================
163
164     Sub LP(ByVal i_file As Integer, ByVal yb As Double, ByVal Num_nod As Integer, ByVal a As Integer, ByVal d As Integer, ByVal lbok As Integer, ByVal h As Integer,
165     ByVal t As Integer, ByVal l As Integer, ByVal s As Integer)
166
167             For i = 1 To Num_nod
168
169                     xi = Worksheets(i_file).Cells(i + 2, 2)
170                     yi = Worksheets(i_file).Cells(i + 2, 3)
171                     zi = Worksheets(i_file).Cells(i + 2, 4)
172                     Si = Worksheets(i_file).Cells(i + 2, 5)
173
174                             If xi <> 0 Or zi = yb Or zi = 0 Or yi > a + lbok Then
175
```

```
176                                 Range(Cells(i + 2, 2), Cells(i + 2, 5)).ClearContents
177
178                             End If
179
180             Next i
181
182     Call Sort1(i_file, Num_nod)
183
184     Rem ================================================================================================================================================
185
186             For i = 1 To Num_nod
187
188                     yi = Worksheets(i_file).Cells(i + 2, 3)
189                     zi = Worksheets(i_file).Cells(i + 2, 4)
190                     Si = Worksheets(i_file).Cells(i + 2, 5)
191
192                     yj = Worksheets(i_file).Cells(i + 2 + 1, 3)
193                     zj = Worksheets(i_file).Cells(i + 2 + 1, 4)
194                     Sj = Worksheets(i_file).Cells(i + 2 + 1, 5)
195
196                     dy = yj - yi
197                     dz = zj - zi
198                     ds = Sj - Si
199
200                     If dy <> 0 Then
201
202                     Gradi = ds / dy
203
204                             If dz = 0 Then
205
206                                     If Gradi * Grad > 0 Then
207
208                                             Worksheets(i_file).Range(Cells(i + 2, 2), Cells(i + 2, 5)).ClearContents
209
210                                     End If
211
212                                     'Worksheets(i_file).Cells(i + 2, 6) = Gradi * 10 ^ 6
213                                     Grad = Gradi
214
215                             End If
216
217                     End If
218
219             Next i
220
221     Call Sort1(i_file, Num_nod)
222
223     Rem ================================================================================================================================================
224
225             For i = 1 To Num_nod
226
227                     yi = Worksheets(i_file).Cells(i + 2, 3)
228                     zi = Worksheets(i_file).Cells(i + 2, 4)
229                     Si = Worksheets(i_file).Cells(i + 2, 5)
230
231                             If yi = lbok And zi = t Then
232
233                                     Ssup = Si
234                                     Worksheets(i_file).Cells(i + 2, 6) = yi
235
236                             End If
237
238                             If yi = a + lbok And zi = t + h Then
239
240                                     Worksheets(i_file).Cells(i + 2, 6) = yi
241
242                             End If
243
244             Next i
245
246     Rem ================================================================================================================================================
247
248     Slp = Ssup
249     dSlpmin = 999
250
251             For i = 1 To Num_nod
252
253                     yii = Worksheets(i_file).Cells(i + 2, 3)
254                     zii = Worksheets(i_file).Cells(i + 2, 4)
255
256                     yij = Worksheets(i_file).Cells(i + 2 + 1, 3)
257                     zij = Worksheets(i_file).Cells(i + 2 + 1, 4)
258
259                     dzi = zij - zii
260
261                             If dzi > 0 Then
262
263                                     For j = i + 1 To Num_nod
264
```

```
                                        yji = Worksheets(i_file).Cells(j + 2, 3)
                                        zji = Worksheets(i_file).Cells(j + 2, 4)
                                        zjj = Worksheets(i_file).Cells(j + 2 + 1, 4)

                                        Sji = Worksheets(i_file).Cells(j + 2, 5)

                                        dzj = zjj - zji
                                        dSlpj = Slp - Sji

                                                If dzj > 0 Then

                                                        Exit For

                                                End If

                                                If Abs(dSlpmin) > Abs(dSlpj) Then

                                                        dSlpmin = dSlpj

                                                End If

                                Next j

                                For j = i + 1 To Num_nod

                                        yji = Worksheets(i_file).Cells(j + 2, 3)
                                        zji = Worksheets(i_file).Cells(j + 2, 4)
                                        zjj = Worksheets(i_file).Cells(j + 2 + 1, 4)

                                        Sji = Worksheets(i_file).Cells(j + 2, 5)

                                        dSlpj = Slp - Sji

                                                If dSlpj = dSlpmin Then

                                                        Slp = Sji
                                                        Worksheets(i_file).Cells(j + 2, 6) = yji
                                                        dSlpmin = 999
                                                        Exit For

                                                End If

                                Next j

                        End If

        Next i

End Sub

Rem ===========================================================================================================================================================

Sub Sort1(ByVal i_file As Integer, ByVal Num_nod As Double)

        Range(Cells(3, 2), Cells(Num_nod, 5)) _
        .Sort Key1:=Worksheets(i_file).Cells(3, 4), order1:=xlAscending, _
              Key2:=Worksheets(i_file).Cells(3, 3), order2:=xlAscending

End Sub
```

APPENDIX. C
DERIVATION OF STRESS INTENSITY FACTORS IN EIGEN FUNCTION SERIES EXPANSION

When a region Γ is taken smaller as an analytical region compared with a region of elastic body, the stress intensity factors that are governed by shear stress is derived based on Eigen-function Series Expansion. The stress intensity factors are introduced in the discussion regarding the stress field near the crack tip. A derivation method based on Eigen-function Series Expansion by using Goursat's stress function is mentioned in this appendix.

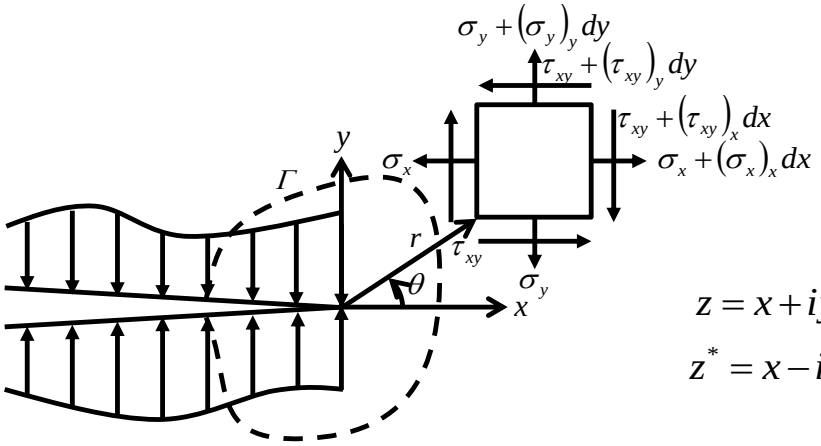

Figure A.1 Definition of analytical region and direction of the stresses

C.1 Governing Equation in Theory of Elasticity

In the theory of elasticity, the stress field near the crack tip is governed by singular stress field. The magnitude of stress near the crack tip becomes infinity. From this fact, the theory of elasticity is beyond the application range to discuss the stress field near the crack tip. To discuss the stress field near the crack tip, the stress intensity factor is introduced. The formula of this factor is expressed as a multiplication of a stress in an arbitrary position and a function regarding the position. The crack propagating condition and magnitude of plastic region near the crack tip can be discussed by introduction of the stress intensity factor.

To derive the stress intensity factor, consider a two dimensional analytical region as shown in Figure A.1. The stresses in each direction can be expressed in the following equations by using stress function $U_{(x,y)}$,

$$\sigma_{x(x,y)} = (U)_{yy} \tag{A.1}$$

$$\sigma_{y(x,y)} = (U)_{xx} \tag{A.2}$$

$$\tau_{xy(x,y)} = -(U)_{xy} \tag{A.3}$$

Where, $(U)_{x_i} = \partial_{x_i} U = \partial U / \partial x_i$. When the relationships above are satisfied, the stress function is also satisfied the following bi-harmonic equation,

$$\Delta\Delta U_{(x,y)} = \nabla^2 \nabla^2 U_{(x,y)} = \left(\partial_{xx} + \partial_{yy}\right)^2 U_{(x,y)} = \left(\partial_{xx} + \partial_{yy}\right)\left(\sigma_x + \sigma_y\right) = 0 \tag{A.4}$$

The stresses around crack tip are governed by the following boundary condition.

$$\begin{cases} \sigma_{y(r,\pm\pi)} = 0 \\ \tau_{xy(r,\pm\pi)} = 0 \\ \tau_{xy(0,\theta)} = \infty \end{cases} \tag{A.5}$$

C.2 Shear Stress in Goursat's Stress Function

To express the shear stress as shown in *(A.6)*, Goursat's stress function as shown in *(A.7)* is introduced.

$$\tau_{xy(x,y)} = K_i f_{(r,\theta)} \quad (A.6)$$

$$U_{(x,y)} = \mathrm{Re}\{z^* \varphi_{(z)} + \chi_{(z)}\} \quad (A.7)$$

Where, K_i: stress intensity factor, $f_{(r,\theta)}$: a function regarding an arbitrary position, z^*: conjugate complex numbers.

For convenience in calculation, to make the same form as in the phase of Eigen-function expansion in linear summation terms of *(A.7)*, the following function is introduced.

$$\chi_{(z)} = \int \psi_{(z)} dz \quad (A.8)$$

From the *(A.8)*, *(A.7)* can be rewrite as follows.

$$U_{(x,y)} = x\mathrm{Re}\varphi_{(z)} + y\mathrm{Im}\varphi_{(z)} + \mathrm{Re}\int \psi_{(z)} dz \quad (A.9)$$

By substituting *(A.9)* into *(A.3)*, and by applying Cauchy-Riemann relationship, the shear stress can be obtained as follows.

$$\tau_{xy(r,\theta)} = r\cos\theta\left(\mathrm{Im}\varphi_{(z)}\right)_{zz} - r\sin\theta\left(\mathrm{Re}\varphi_{(z)}\right)_{zz} + \left(\mathrm{Im}\psi_{(z)}\right)_{z} \quad (A.10)$$

C.3 Derivation of the Stress Function

For expression of stress function $U_{(x,y)}$ in Eigen-function expansion, $\varphi_{(z)}$ and $\psi_{(z)}$ can be assumed as follows due to satisfaction of the orthogonality.

$$\varphi_{(z)} = \sum_n A_n z^{\lambda_n} \quad (A.11)$$

$$\psi_{(z)} = \sum_n B_n z^{\lambda_n} \quad (A.12)$$

Where, $A_n = \mathrm{Re}A_n + i\mathrm{Im}A_n$, $B_n = \mathrm{Re}B_n + i\mathrm{Im}B_n$, λ_n: Eigen-values.

Therefore,

$$\begin{cases} \left(\mathrm{Re}\varphi_{(z)}\right)_z = \sum_n \lambda_n r^{\lambda_n-1}(\mathrm{Re}A_n \cos(\lambda_n-1)\,\theta - \mathrm{Im}A_n \sin(\lambda_n-1)\,\theta\,) \\ \left(\mathrm{Im}\varphi_{(z)}\right)_z = \sum_n \lambda_n r^{\lambda_n-1}(\mathrm{Re}A_n \sin(\lambda_n-1)\,\theta + \mathrm{Im}A_n \cos(\lambda_n-1)\,\theta\,) \\ \left(\mathrm{Re}\psi_{(z)}\right)_z = \sum_n \lambda_n r^{\lambda_n-1}(\mathrm{Re}B_n \cos(\lambda_n-1)\,\theta - \mathrm{Im}B_n \sin(\lambda_n-1)\,\theta\,) \\ \left(\mathrm{Im}\psi_{(z)}\right)_z = \sum_n \lambda_n r^{\lambda_n-1}(\mathrm{Re}B_n \sin(\lambda_n-1)\,\theta + \mathrm{Im}B_n \cos(\lambda_n-1)\,\theta\,) \end{cases} \quad (A.13)$$

$$\begin{cases} \left(\mathrm{Re}\varphi_{(z)}\right)_{zz} = \sum_n \lambda_n(\lambda_n-1) r^{\lambda_n-2}(\mathrm{Re}A_n \cos(\lambda_n-2)\,\theta - \mathrm{Im}A_n \sin(\lambda_n-2)\,\theta\,) \\ \left(\mathrm{Im}\varphi_{(z)}\right)_{zz} = \sum_n \lambda_n(\lambda_n-1) r^{\lambda_n-2}(\mathrm{Re}A_n \sin(\lambda_n-2)\,\theta + \mathrm{Im}A_n \cos(\lambda_n-2)\,\theta\,) \\ \left(\mathrm{Re}\psi_{(z)}\right)_{zz} = \sum_n \lambda_n(\lambda_n-1) r^{\lambda_n-2}(\mathrm{Re}B_n \cos(\lambda_n-2)\,\theta - \mathrm{Im}B_n \sin(\lambda_n-2)\,\theta\,) \\ \left(\mathrm{Im}\psi_{(z)}\right)_{zz} = \sum_n \lambda_n(\lambda_n-1) r^{\lambda_n-2}(\mathrm{Re}B_n \sin(\lambda_n-2)\,\theta + \mathrm{Im}B_n \cos(\lambda_n-2)\,\theta\,) \end{cases} \quad (A.14)$$

C.4 Determination of Eigen-values

Substituting *(A.13)* and *(A.14)* into *(A.10)*,

$$\begin{aligned} \tau_{xy(r,\theta)} = \sum_n \lambda_n r^{\lambda_n-1}\{&(\lambda_n-1)\mathrm{Re}A_n \cos\theta \sin(\lambda_n-2)\,\theta \\ &+(\lambda_n-1)\mathrm{Im}A_n \cos\theta \cos(\lambda_n-2)\,\theta \\ &-(\lambda_n-1)\mathrm{Re}A_n \sin\theta \cos(\lambda_n-2)\,\theta \\ &+(\lambda_n-1)\mathrm{Im}A_n \sin\theta \sin(\lambda_n-2)\,\theta \\ &+\mathrm{Re}B_n \sin(\lambda_n-1)\,\theta + \mathrm{Im}B_n \cos(\lambda_n-1)\,\theta\} \end{aligned} \quad (A.15)$$

From the boundary condition *(A.5)* , by substituting $\tau_{xy(r,\pm\pi)} = 0$ into *(A.15)*,

$$\begin{pmatrix} \sin\lambda_n\pi & \cos\lambda_n\pi \\ -\sin\lambda_n\pi & \cos\lambda_n\pi \end{pmatrix} \begin{pmatrix} -\mathrm{Re}A_n(\lambda_n-1) - \mathrm{Re}B_n \\ -\mathrm{Im}A_n(\lambda_n-1) - \mathrm{Im}B_n \end{pmatrix} = 0 \quad (A.16)$$

$(-\mathrm{Re}A_n(\lambda_n-1) - \mathrm{Re}B_n \quad -\mathrm{Im}A_n(\lambda_n-1) - \mathrm{Im}B_n)^T \neq 0$ in *(A.16)*,

$$\begin{vmatrix} \sin\lambda_n\pi & \cos\lambda_n\pi \\ -\sin\lambda_n\pi & \cos\lambda_n\pi \end{vmatrix} = \sin 2\lambda_n\pi = 0 \quad (A.17)$$

Thus,

$$\lambda_n = \frac{n}{2} \quad (\mathrm{n} = 1, 2, 3, \ldots, \infty) \tag{A.18}$$

C.5 Decision of Undetermined Coefficient

To eliminate $\mathrm{Re}B_n$ and $\mathrm{Im}B_n$ in *(A.15)*, by substituting λ_n=1/2 (n=1) into *(A.16)*, $\mathrm{Re}B_n$ can be obtained as follows,

$$\mathrm{Re}B_n = \frac{1}{2}\mathrm{Re}A_n \tag{A.19}$$

$\mathrm{Im}B_n$ cannot be determined by *(A.16)*. The boundary condition *(A.5)* , $\sigma_{y(r,\pm\pi)} = 0$ must be required to derive $\mathrm{Im}B_n$.

By substituting *(A.9)* into *(A.2)*, and by applying Cauchy-Riemann relationship, the vertical stress can be obtained as follows.

$$\sigma_{y(r,\theta)} = 2\left(\mathrm{Re}\varphi_{(z)}\right)_z + r\cos\theta\left(\mathrm{Re}\varphi_{(z)}\right)_{zz} + r\sin\theta\left(\mathrm{Im}\varphi_{(z)}\right)_{zz} + \left(\mathrm{Re}\psi_{(z)}\right)_z \tag{A.20}$$

Substituting *(A.13)* and *(A.14)* into *(A.20)*,

$$\begin{aligned}\sigma_{y(r,\theta)} = \sum_n \lambda_n r^{\lambda_n - 1}\{&2\mathrm{Re}A_n\cos(\lambda_n - 1)\theta - 2\mathrm{Im}A_n\sin(\lambda_n - 1)\theta \\ &+(\lambda_n - 1)\mathrm{Re}A_n\cos\theta\cos(\lambda_n - 2)\,\theta - (\lambda_n - 1)\mathrm{Im}A_n\cos\theta\sin(\lambda_n - 2)\,\theta \\ &+(\lambda_n - 1)\mathrm{Re}A_n\sin\theta\sin(\lambda_n - 2)\,\theta + (\lambda_n - 1)\mathrm{Im}A_n\sin\theta\cos(\lambda_n - 2)\,\theta \\ &+\mathrm{Re}B_n\cos(\lambda_n - 1)\,\theta - \mathrm{Im}B_n\sin(\lambda_n - 1)\,\theta\}\end{aligned} \tag{A.21}$$

Substituting $\sigma_{y(r,\pm\pi)} = 0$ as a boundary condition and λ_n=1/2 (n=1) into *(A.21)*,

$$\mathrm{Im}B_n = -\frac{3}{2}\mathrm{Im}A_n \tag{A.22}$$

C.6 Derivation of Mode *I* and Mode *II* Stress Intensity Factor

Substituting *(A.19)* and *(A.22)* into *(A.15)*, we can determine the shear stress.

$$\begin{aligned}\tau_{xy(r,\theta)} = \frac{1}{2}\sum_n nr^{\frac{n}{2}-1}\Big[&\mathrm{Re}A_n\left\{\left(\frac{n}{2} - 1\right)\sin\left(\frac{n}{2} - 3\right)\theta + \frac{1}{2}\sin\left(\frac{n}{2} - 1\right)\theta\right\} \\ &+\mathrm{Im}A_n\left\{\left(\frac{n}{2} - 1\right)\cos\left(\frac{n}{2} - 3\right)\theta - \frac{3}{2}\cos\left(\frac{n}{2} - 1\right)\theta\right\}\Big]\end{aligned} \tag{A.23}$$

Set stress intensity factors in Mode *I* and *II* as follows,

$$\begin{Bmatrix} \mathrm{Re}A_n \\ \mathrm{Im}A_n \end{Bmatrix} = \begin{pmatrix} K_I \\ -K_{II} \end{pmatrix} (2\pi)^{-1/2} \tag{A.24}$$

(A.23) must be satisfied with the boundary condition $\tau_{xy(0,\theta)} = \infty$ *(A.5)*. The stable solution is only in the case of λ_n=1/2 (n=1). *(A.23)* can be rewritten as follows,

$$\tau_{xy(r,\theta)} = (2\pi)^{-1/2} \left\{ K_I \frac{1}{4} \left(\sin\frac{5}{2}\theta - \sin\frac{1}{2}\theta \right) + K_{II} \frac{1}{4} \left(\cos\frac{5}{2}\theta + 3\cos\frac{1}{2}\theta \right) \right\} \tag{A.25}$$

(A.25) is written in linear summation formula. This fact is corresponding that superposition principle can be applied to elastic bodies.

Therefore,

$$K_I = \tau_{xyI(r,\theta)} (2\pi r)^{1/2} \left\{ \frac{1}{4} \left(\sin\frac{5}{2}\theta - \sin\frac{1}{2}\theta \right) \right\}^{-1} \tag{A.26}$$

$$K_{II} = \tau_{xyII(r,\theta)} (2\pi r)^{1/2} \left\{ \frac{1}{4} \left(\cos\frac{5}{2}\theta + 3\cos\frac{1}{2}\theta \right) \right\}^{-1} \tag{A.27}$$

The equations above were introduced in **Chapter 3** to deduce the area of plastic zone at the crack tips.

APPENDIX. D
DECOMPOSITION METHOD OF ARCH AND BEAM MECHANISMS BASED ON EXPERIMENTAL RESULTS

This appendix proposes the decomposition method of arch and beam mechanisms of RC beams based on experimental results. By using the concept which was described in **Chapter 2**, the contribution ratios of arch and beam mechanism can be calculated by strain distribution of rebar in each loading step. The validity of calculation is explained based on analytical results in **Chapter 4**.

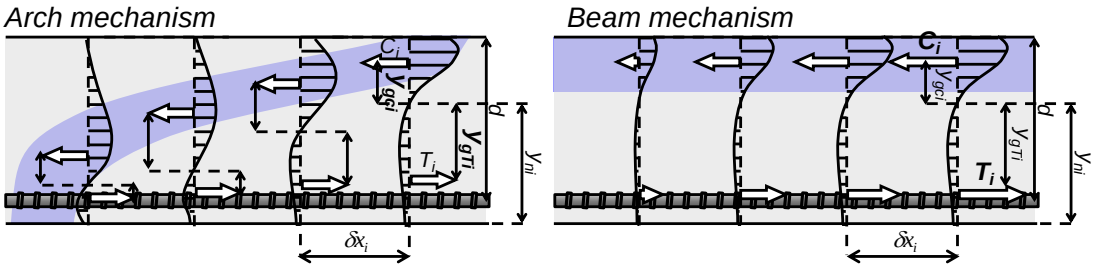

Cross sectional moment

$$M_{(x,t)} = C_{(x,t)}\, y_{gC(x,t)} + T_{(x,t)}\, y_{gT(x,t)}$$

Application of chain law

Cross sectional shear force

$$V_{(x,t)} = C_{(x,t)}\frac{\partial}{\partial x} y_{gC(x,t)} + T_{(x,t)}\frac{\partial}{\partial x} y_{gT(x,t)}$$

Contribution of arch mechanism

$$+ y_{gC(x,t)}\frac{\partial}{\partial x} C_{(x,t)} + y_{gT(x,t)}\frac{\partial}{\partial x} T_{(x,t)}$$

Contribution of beam mechanism

Figure D.1 Definition of arch and beam mechanisms

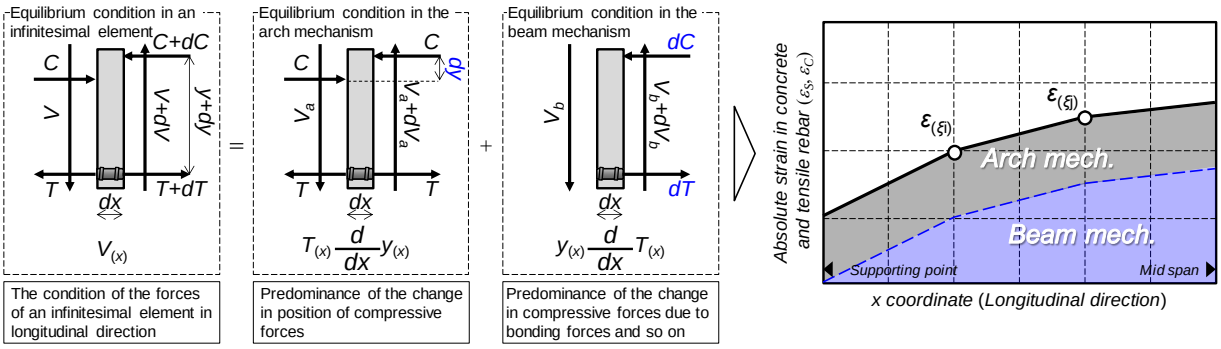

Figure D.2 Physical meaning of arch and beam mechanisms

D.1 Physical meaning of arch and beam mechanisms

To propose the decomposition method of arch and beam mechanisms, this section considers the physical meaning of arch and beam mechanisms again. Figure D.1 shows definition of arch and beam mechanisms. The contributed loads of arch and beam mechanisms could be obtained to apply the chain law of differential to the cross sectional moment as mentioned in **Chapter 2**. The contributed loads of arch and beam mechanisms can be expressed by the equation as shown in Figure D.1. However, the contributed loads of arch and beam mechanisms were difficult to obtain from the experimental results based on the equations, because this equation needed to measure the stress distribution of concrete in entire region of the RC beams.

Focused on the equilibrium condition of forces of free body on infinitesimal element, the equilibrium conditions to establish the equations are shown in Figure D.2. The conditions in case without the effect of change in the position of tensile forces are illustrated in the figure for the simplified consideration. From these conditions, it can be confirmed that the constant part of cross sectional forces contribute to establish the arch mechanism, and the different part of cross sectional forces contribute to establish the beam mechanism. In general, appearance of cross sectional forces can be regarded as appearance of the rebar strain distribution. This means that the constant part of strain of rebar in longitudinal direction contributes to establish the arch mechanism, and the different part of strain of rebar in longitudinal direction contributes to establish the beam mechanism. Therefore, it can be considered that the contributed ratios of arch and beam mechanisms might be calculated based on rebar strain distribution.

D.2 Decomposition method of arch and beam mechanisms

D.2.1 The method based on differential equations

For the calculation of contributed ratios of arch and beam mechanisms, the decomposition method based on differential equations which is illustrated Figure D.3 *(a)* is one of the effective methods.

From the definition of arch and beam mechanisms without the effect of change in the position of tensile forces, the contributed loads could be represented as following equations.

$$V_{a(x)} = T_{(x)} \frac{dy_{(x)}}{dx} \quad (D.1)$$

$$V_{b(x)} = y_{(x)} \frac{dT_{(x)}}{dx} \quad (D.2)$$

Where, V_a, V_b: contributed loads of arch and beam mechanisms,

When the contributed ratios of each mechanisms were introduced, the V_a and V_b could be given as follows.

$$V_{a(x)} = V_{(x)} P_a \quad (D.3)$$

$$V_{b(x)} = V_{(x)} P_b \quad (D.4)$$

Where, P_a, P_b: contributed ratios of arch and beam mechanisms, V: shear force.

Moreover, the cross sectional moment could be given as follows under the 4 points bending condition.

$$M_{(x)} = V_{(x)} x = T_{(x)} y_{(x)} \quad (D.5)$$

From the coalescing of *(D.1)* to *(D.5)*, following differential equations can be obtained.

$$\frac{dy_{(x)}}{dx} - \frac{P_a}{x} y_{(x)} = 0 \quad (D.6)$$

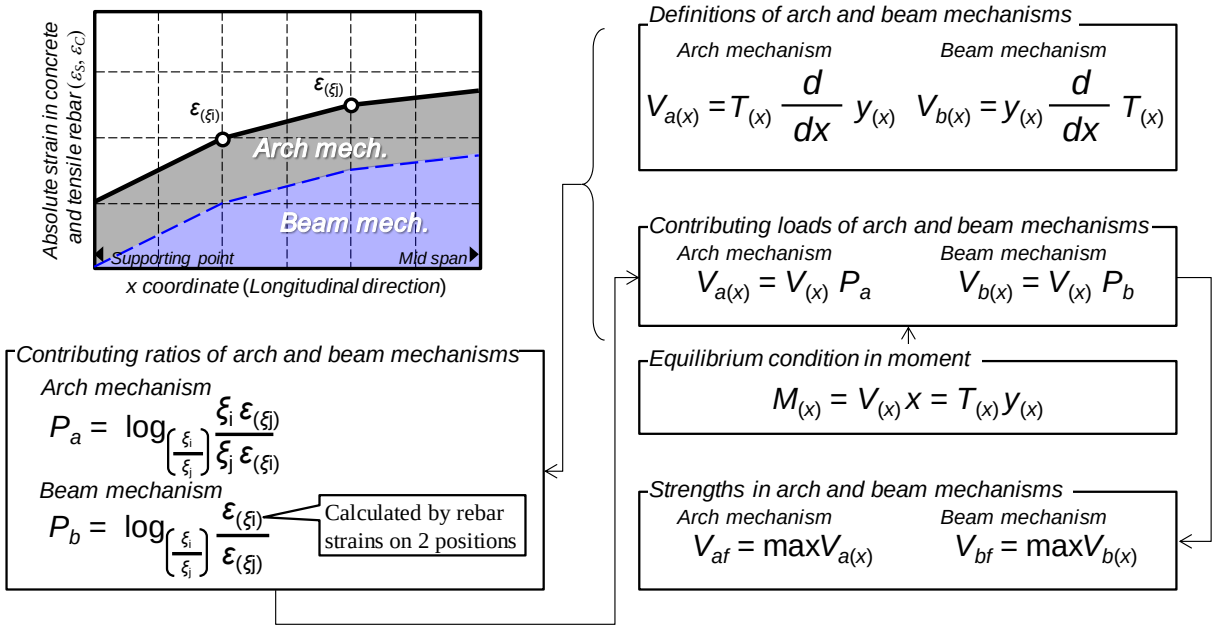

(a) The concept based on differential equations

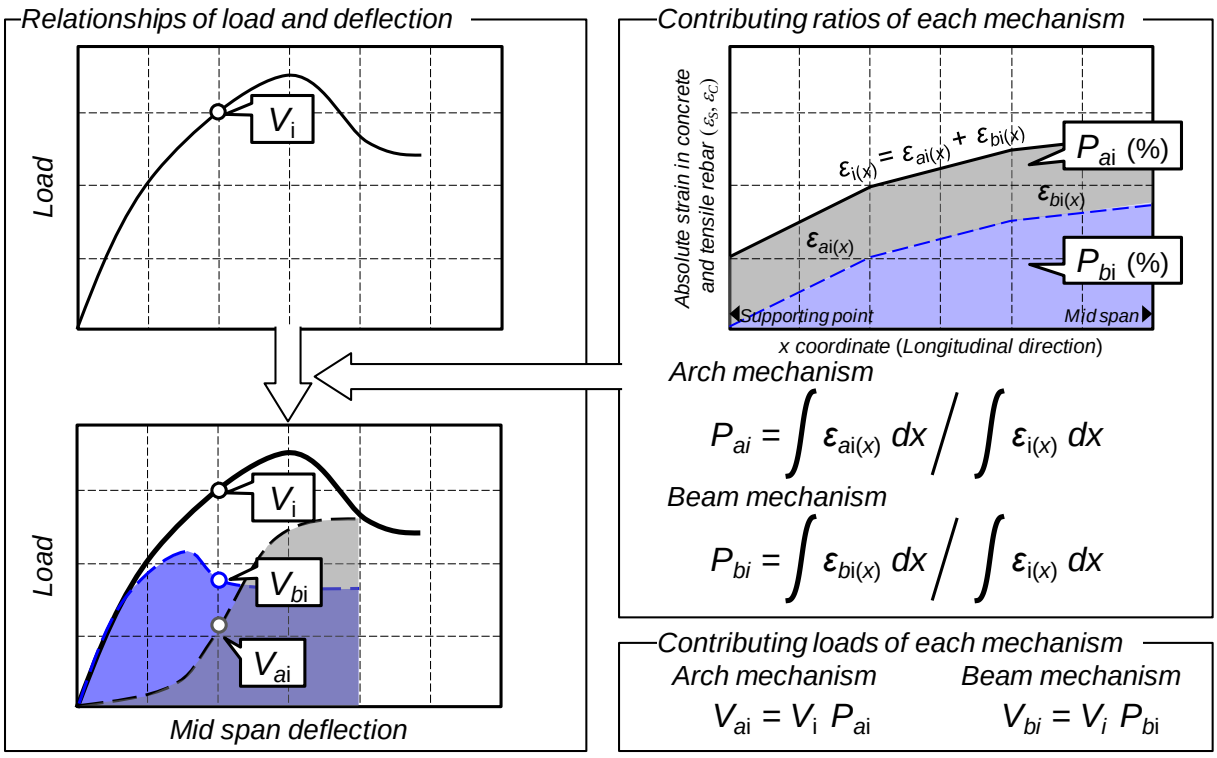

(b) The concept based on strain integral

Figure D.3 Concept of calculation

$$\frac{dT_{(x)}}{dx} - \frac{P_b}{x} T_{(x)} = 0 \qquad (D.7)$$

Solve the equations, we can get following solutions.

$$y_{(x)} = y_{(\xi)} \left(\frac{x}{\xi}\right)^{P_a} \tag{D.8}$$

$$T_{(x)} = T_{(\xi)} \left(\frac{x}{\xi}\right)^{P_b} \tag{D.9}$$

Where, ξ: longitudinal coordinate. The *(D.8)* and *(D.9)* hold for any ξ. Thus,

$$P_a = \log_{\left(\frac{\xi_i}{\xi_j}\right)} \left(\frac{y_{(\xi_i)}}{y_{(\xi_j)}}\right) \tag{D.10}$$

$$P_b = \log_{\left(\frac{\xi_i}{\xi_j}\right)} \left(\frac{T_{(\xi_i)}}{T_{(\xi_j)}}\right) \tag{D.11}$$

Where, $i \neq j$.

In general, the cross sectional area and the elastic modulus of rebars are constant in longitudinal direction. Therefore, *(D.10)* and *(D.11)* can be rewrite as following equations.

$$P_a = \log_{\left(\frac{\xi_i}{\xi_j}\right)} \left(\frac{\xi_i \varepsilon_{(\xi_j)}}{\xi_j \varepsilon_{(\xi_i)}}\right) \tag{D.12}$$

$$P_b = \log_{\left(\frac{\xi_i}{\xi_j}\right)} \left(\frac{\varepsilon_{(\xi_i)}}{\varepsilon_{(\xi_j)}}\right) \tag{D.13}$$

Where, ε: strain of the rebar in longitudinal direction.

From *(D.12)* and *(D.13)*, it could be confirmed that the contributed ratios of each mechanism could be derived by 2 points of strains of rebar. However, there were assumptions that the RC beams subjected to 4 points bending condition and that the effect of change in the positions of tensile forces could be neglected for deriving the proposed method above.

To expand applicable range of the decomposition method based of experimental results, the generalized method based on strain integral was proposed.

D.2.2 The method based on strain integral

If the external force makes the strain distribution, it can be regarded that the strain distribution makes the force on the RC beam. From this consideration, this study proposed the method to calculate the contributed loads of arch and beam mechanisms based on the rebar strain distribution and the applied force on the RC beam.

The concept of calculation is shown in Figure D.3 *(b)*. If the *i* th load in the load deflection curve was obtained and the rebar strain distribution at the same time was also obtained as shown in Figure

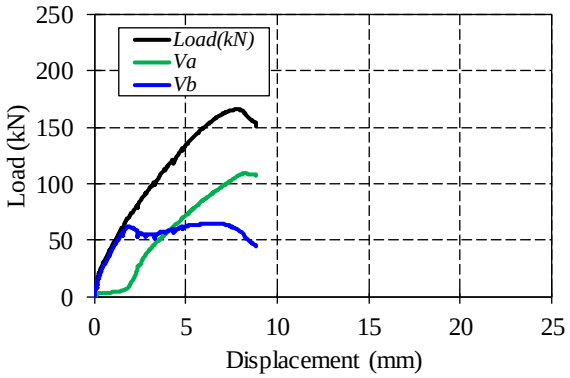

(a) RN in experiment

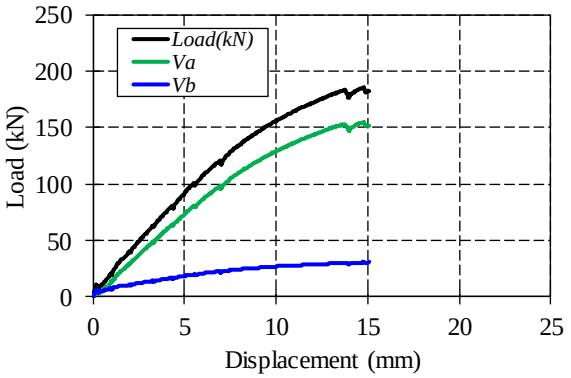

(c) RB in experiment

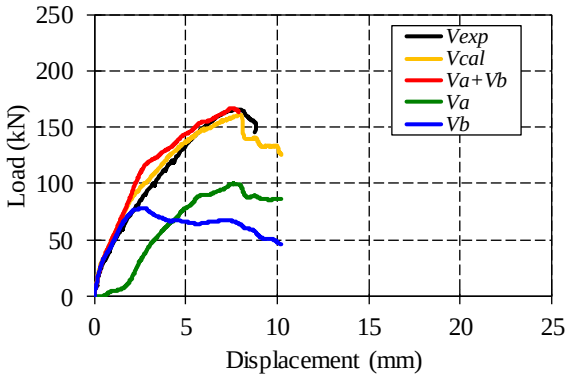

(b) RN in analysis

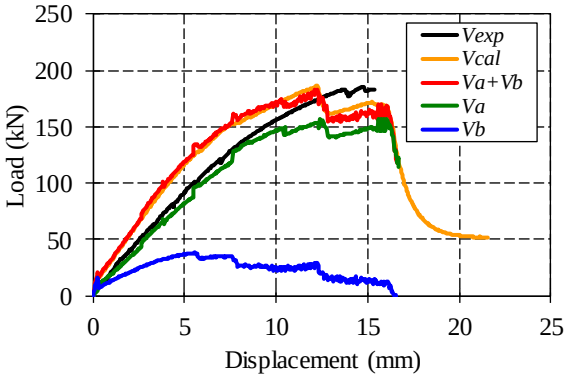

(d) RB in analysis

Figure D.4 Comparison with the analytical results

D.3 *(b)*, the *i* th contributed ratios of arch and beam mechanisms can be calculated as the percentage of entire area of contributed part of arch and beam mechanism against the closing area of actual strain distribution. That is,

$$P_{ai} = \int \varepsilon_{ai(x)} dx \Big/ \int \varepsilon_{i(x)} dx \qquad (D.14)$$

$$P_{bi} = \int \varepsilon_{bi(x)} dx \Big/ \int \varepsilon_{i(x)} dx \qquad (D.15)$$

Where, P_{ai}, P_{bi}: i th contributed ratios of arch and beam mechanisms, $\varepsilon_{ai}, \varepsilon_{bi}$: strain distribution caused by arch and beam mechanism, ε_i: total strain distribution which is obtained by experiment, x: longitudinal coordinate in the RC beam. ε_{ai} can be regarded as the non-zero strain at the supporting points of the beams.

After the calculation of the contributed ratio, the *i* th contributed loads of arch and beam mechanisms can be obtained as multiplication of the *i* th load and contributed ratios. That is,

$$V_{ai} = V_i P_{ai} \qquad (D.16)$$

$$V_{bi} = V_i P_{bi} \qquad (D.17)$$

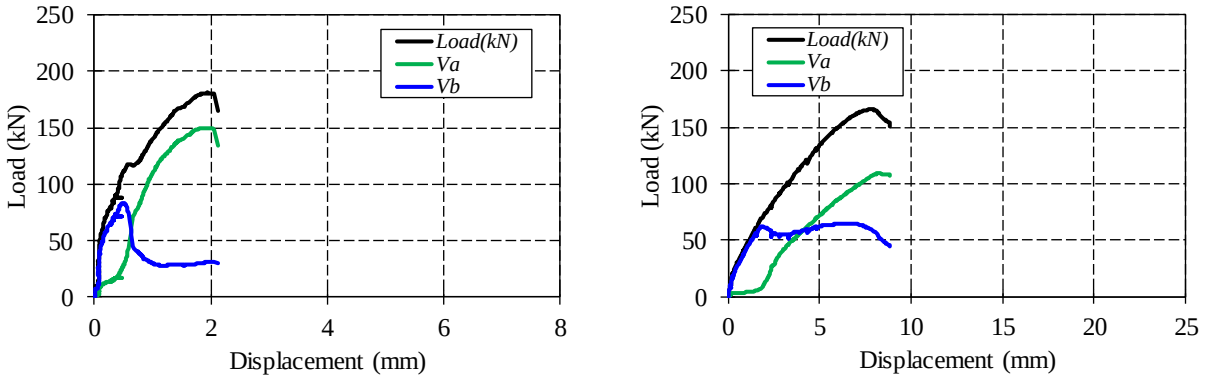

(a) a/d =1.6 without stirrup *(b) a/d =3.0 with stirrup (RN)*

Figure D.5 Comparison with the results of a/d=1.6 and 3.0

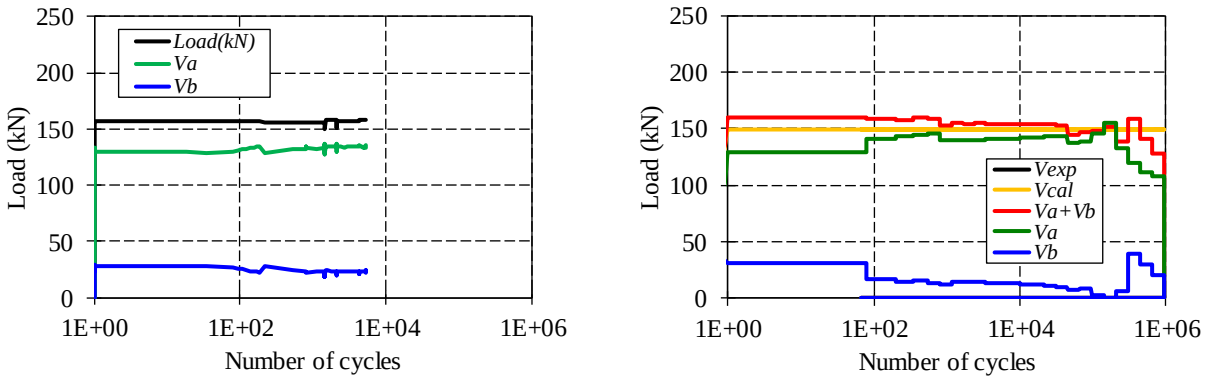

(a) Experiment *(b) Analysis*

Figure D.6 Comparison under fatigue loading (RB)

Where, V_{ai}, V_{bi}: i th contributed loads of arch and beam mechanisms, V_i: i th load in the load deflection curve.

D.3 Validity confirmation

The application of this method and comparison with the analytical results are shown in Figure D.4. The target beams are *RN* (sound beam) and *RB* (with artificial crack) as mentioned in **Chapter 4**. The changes in the arch and beam mechanisms are similar with the analytical results, and the predominance of the contributed load in arch mechanism was confirmed in case of *RB*.

Figure D.5 shows the changes in arch and beam mechanism of the sound beams in *a/d*=1.6 and 3.0 based on previous experimental results. The shape and rebar ratio in the cross section are same in both cases. It was confirmed that the contributed load in arch mechanism in case of *a/d*=1.6 (short

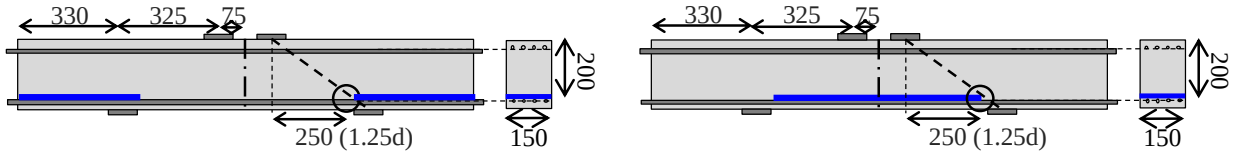

(a) A1.6 *(b) B1.6*

Figure D.7 Shape of specimens in previous study (*a/d*=1.6)

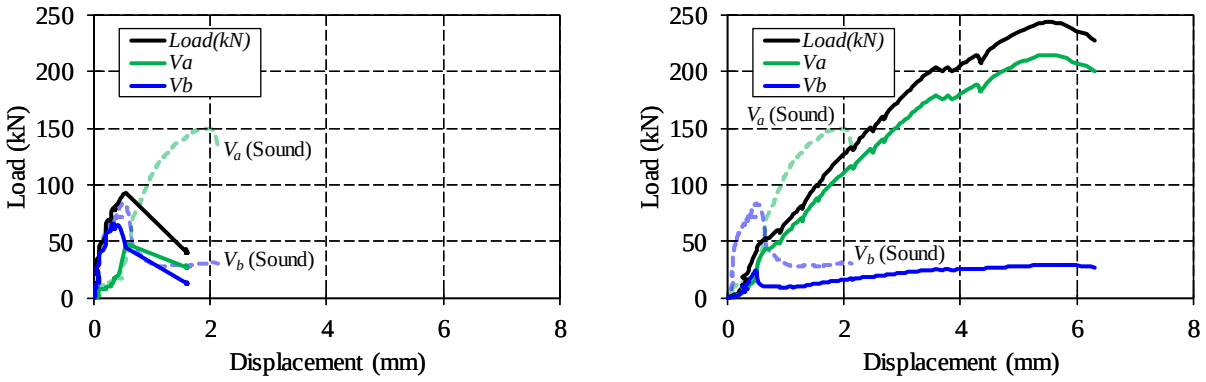

(a) A1.6 *(b) B1.6*

Figure D.8 Contributing load of arch and beam mechanism in case of *a/d*=1.6

beam) was higher than that of *a/d*=3.0 (slender beam). These results indicated that load carrying mechanism in case of *a/d*=1.6 was mainly governed by arch mechanism, and this results corresponded the previous knowledge.

Figure D.6 shows the changes in arch and beam mechanism under fatigue loading of *RB*. The upper limit loads in case of experiment and analysis are almost same. The analytical result was mentioned in **Chapter 4**. The same trend against number of acting cycles could be confirmed in both cases.

From comparisons above, the validity of calculating method by using experimental results was confirmed under static and fatigue loading.

D.4 Application

To make clear the effect of artificial crack positions, the method mentioned above was applied to the experimental results of previous study. The shapes of the beams are shown in Figure D.7. The shape of *B1.6* and properties of the artificial cracks were same with the case which was mentioned in **Chapter 3**. The *A1.6* had the artificial cracks at the anchorage parts of the beam. The application results are shown in Figure D.8. In case of *A1.6,* the contributed loads of arch and beam mechanisms were suddenly decreased at the ultimate failure of the beam regardless of change in the mechanisms

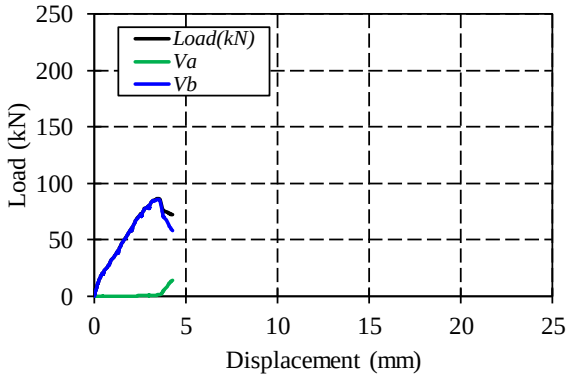

(a) N

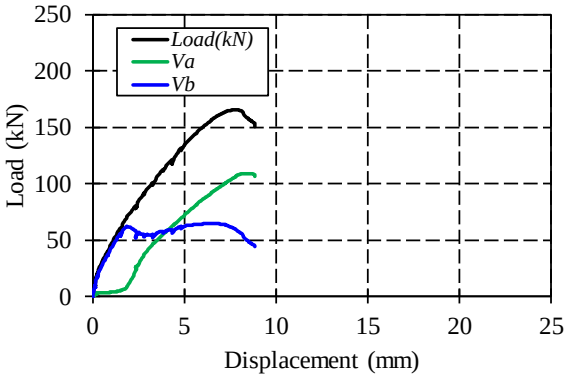

(d) RN

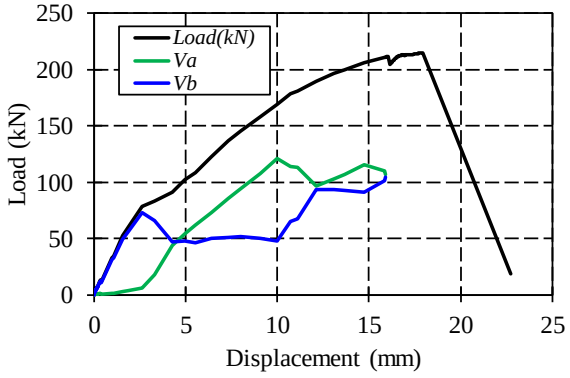

(b) B1

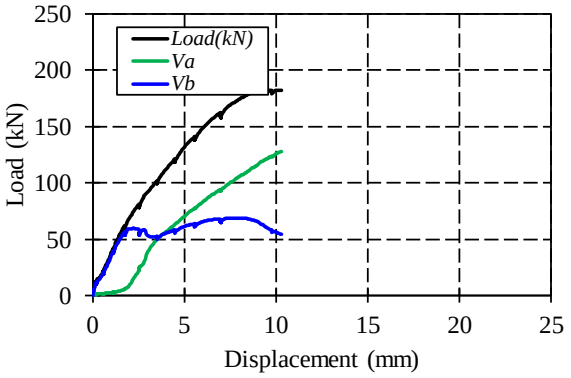

(e) RD

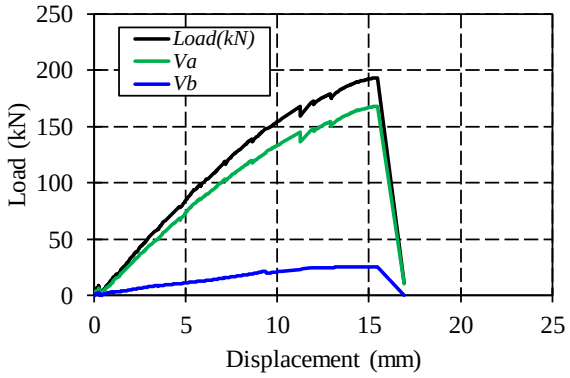

(c) B2

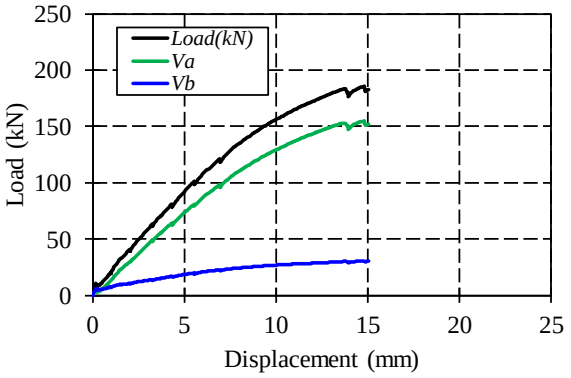

(f) RB

Figure D.9 Contributing load of arch and beam mechanism in case of *a/d*=3.0

compared with the case of sound beam (Figure D.5 *(a)*). In case of *B1.6*, the contributed load of arch mechanism was predominant from the initial loading. Thus, it was confirmed that the increase in the static strength due to predominance of arch mechanism was caused by only the artificial crack which exist inside the shear span in case of *a/d=1.6*.

Figure D.9 shows the contributed loads of arch and beam mechanisms based on the experimental

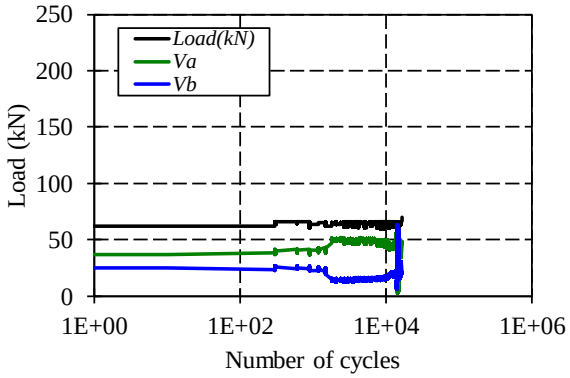

(a) A1.6

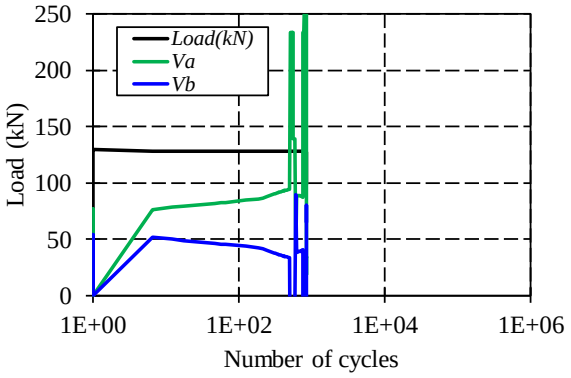

(b) RN

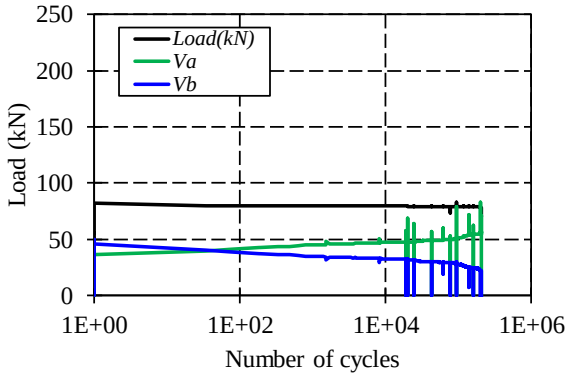

(c) RD under low upper limit load

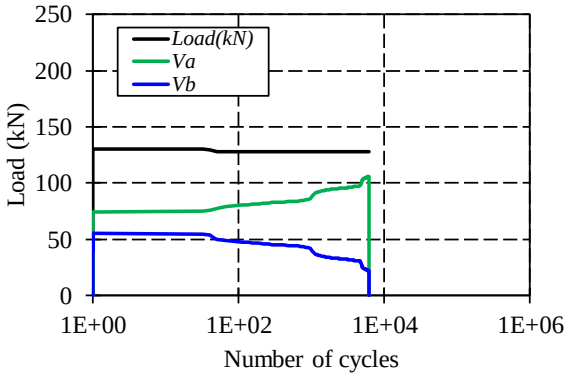

(d) RD under high upper limit load

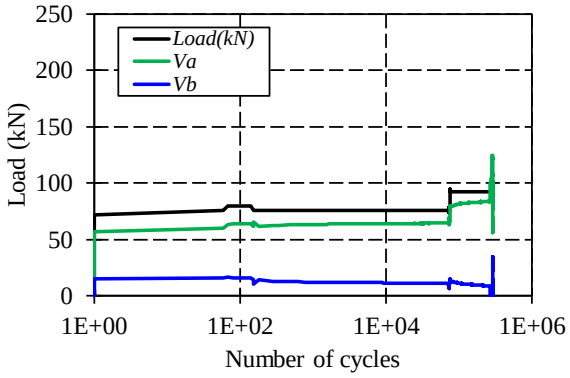

(e) RB under low upper limit load

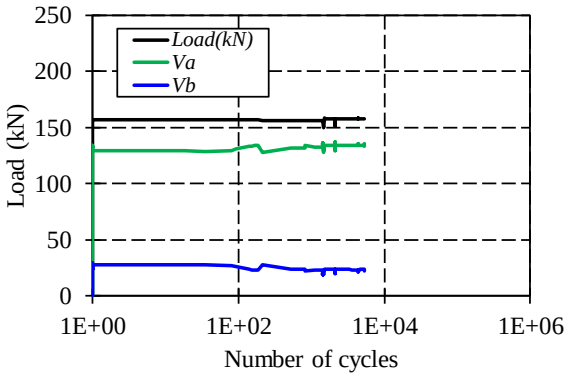

(f) RB under high upper limit load

Figure D.10 Contributing load of arch and beam mechanism under fatigue load

results mentioned in **Chapter 4**. Focused on the result of the case without stirrup, the predominance of arch mechanism was confirmed in case of *B1* and *B2* compared with the result of *N*, even though the reliability of the calculation results in case *N* and *B1* were low because the measured data of rebar strain had large scatter (Figure D.9 *(a), (b), (c)*). Focused on the result of the case with stirrup, the mechanisms were not changed remarkably in case of *RN* and *RD*. Thus, it was confirmed that the effect of artificial crack tips inside of *D* region was not contributed to the change in the load carrying mechanism (Figure D.9 *(d), (e)*). Also, in case of *RB*, the predominance of arch mechanism was

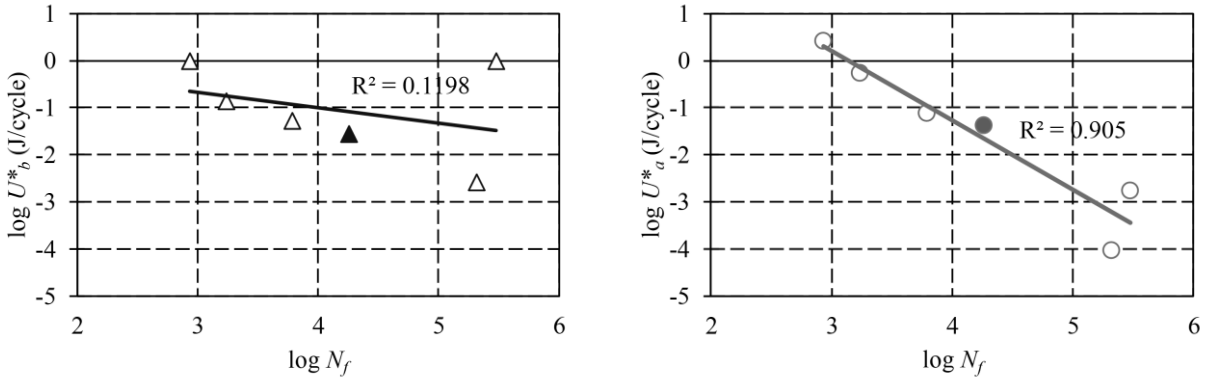

(a) Averaged energy of beam mechanism *(b) Averaged energy of Arch mechanism*

Figure D.11 Averaged absorbing energy of arch mechanism against number of cycles at failure

confirmed (Figure D.9 *(f)*). To confirm the effect of stirrup, focused on the results of *B2* and *RB,* the contribution of arch mechanism in case of *RB* with stirrup was slightly low compared with case of *B2*. However, the change in the tendency was not confirmed obviously because the effect of dowel action of stirrup was relatively low. These results were corresponded to the results which were obtained from analytical result mentioned in **Chapter 4**.

Figure D.10 shows the contributed loads of arch and beam mechanisms under fatigue load. The contributed load of arch mechanism was increased in high cycle region regardless of *a/d*, position of artificial cracks and magnitude of upper limit loads.

Figure D.11 shows absorbing energy of arch and beam mechanism per one cycle until the ultimate failure mentioned in **Chapter 4**. The data set of *RN*, *RD*, *RB* and *A1.6* were include in this figure. *B1* and *B2* were not illustrated in this figure because of large scatter. The solid dots show the result of *A1.6*. From these figures, the averaged energy of arch mechanism was suitable to explain the number of cycle at failure regardless of *a/d*, position of artificial cracks and magnitude of upper limit loads. These results were also corresponded to the results which were obtained from analytical result mentioned in **Chapter 4**.

Application and validity of the decomposition method of arch and beam mechanism based on experimental results were indicated.

謝辞

主査の岩波光保教授には，研究開始当初から常に親切なご指導を賜った．研究者としての道を歩む筆者の根幹に，先生の指導方針や哲学が強く影響していると感じる．ここに厚く御礼申し上げる．

副査の二羽淳一郎教授，廣瀬壮一教授，佐々木栄一准教授，千々和伸浩准教授にも多大なご助言を賜った．二羽淳一郎教授には，コンクリートのせん断に関して数多のご助言を賜ってきた．ここに深くお礼申し上げる．廣瀬壮一教授には，審査のみならず講義を通じて解析学に関する知見をご教授いただいた．ここに深くお礼申し上げる．佐々木栄一准教授には，疲労に関して論文の研鑽に不可欠な数多のご意見を賜った．ここに深くお礼申し上げる．千々和伸浩准教授には，実験や解析の方法を含めて，広範に渡りご助言を賜った．先生の研究に対する姿勢からも学ぶものが多かった．ここに深くお礼申し上げる．

研究室生活では，秘書の林葉庫さんをはじめ，学生からも多大なご支援をいただいた．ここに深くお礼申し上げる．また，英語での論文執筆やプレゼンテーションに際し，ご助言をいただいた留学生の皆さんの存在も大きかった．ここにお礼申し上げる．

最後に，博士課程への進学に際し，支援をしていただいた両親にも感謝を述べたい．

山田　雄太